JOURNAL OF RESEARCH

OF THE U.S. GEOLOGICAL SURVEY

JANUARY–FEBRUARY 1974
VOLUME 2, NUMBER 1

Scientific notes and summaries of investigations in geology, hydrology, and related fields

U.S. DEPARTMENT OF THE INTERIOR

UNITED STATES DEPARTMENT OF THE INTERIOR
ROGERS C. B. MORTON, Secretary
GEOLOGICAL SURVEY
V. E. McKelvey, Director

For sale by the Superintendent of Documents, U.S. Government Printing Office, Washington, DC 20402. Order by SD Catalog No. JRGS. Annual subscription rate $15.50 (plus $3.75 for foreign mailing). Single copy $2.75. Make checks or money orders payable to the Superintendent of Documents.

Send all subscription inquiries and address changes to the Superintendent of Documents at the above address.

Purchase orders should not be sent to the U.S. Geological Survey library.

Library of Congress Catalog-card No. 72-600241.

The Journal of Research is published every 2 months in Washington, D.C., by the U.S. Geological Survey. It contains papers by members of the Geological Survey and their professional colleagues on geologic, hydrologic, topographic, and other scientific and technical subjects.

Correspondence and inquiries concerning the Journal (other than subscription inquiries and address changes) should be directed to the Journal of Research, Publications Division, U.S. Geological Survey, National Center, Reston, VA 22092.

Papers for the Journal should be submitted through regular Division publication channels.

The Secretary of the Interior has determined that the publication of this periodical is necessary in the transaction of the public business required by law of this Department. Use of funds for printing this periodical has been approved by the Director of the Office of Management and Budget through February 11, 1975.

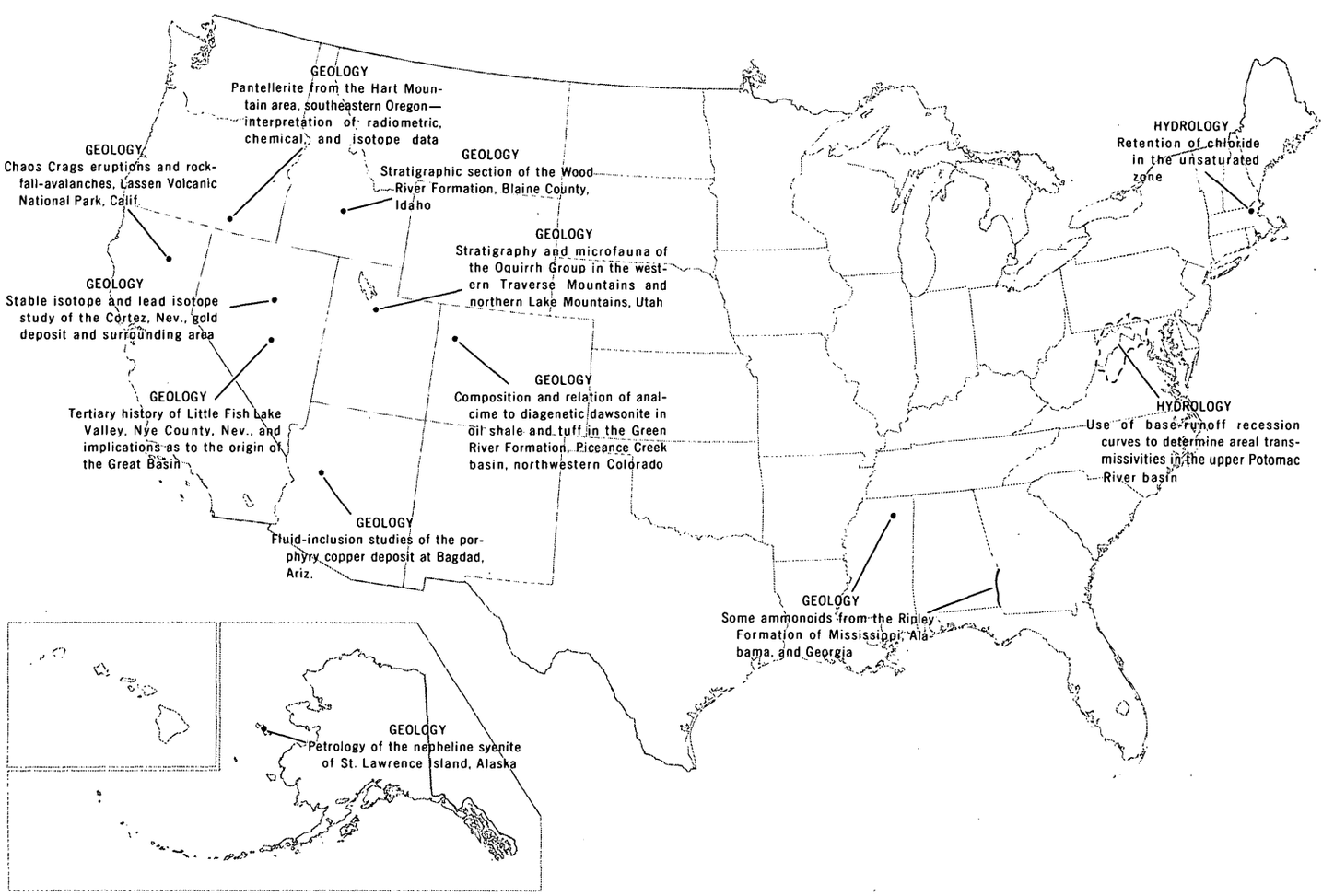

GEOGRAPHIC INDEX TO ARTICLES

See "Contents" for articles concerning areas outside the United States and articles without geographic orientation.

JOURNAL OF RESEARCH

of the

U.S. Geological Survey

Vol. 2 No. 1 Jan.-Feb. 1974

CONTENTS

ABBREVIATIONS

A	ampere
Å	angstrom
ADP	ammonium dihydrogen phosphate
b.y.	billion years
°C	degree Celsius
cal	calorie
C.I.	color index
CIPW	Cross, Iddings, Pirsson, and Washington
cm	centimeter
cm^3	cubic centimeter
d	day
diam	diameter
F.D.&C.	Food, Drug, and Cosmetic [dye]
ft	foot
ft^2	square foot
ft^3	cubic foot
g	gram
h	hour
in.	inch
K	kelvin
kg	kilogram
km	kilometer
km^2	square kilometer
km^3	cubic kilometer
kV	kilovolt
l	liter
ln	logarithm (natural)
log	logarithm (common)
m	meter
m^2	square meter
m^3	cubic meter
MA	megampere
mg	milligram
mGal	milligal
mi	mile
mi^2	square mile
min	minute
ml	milliliter
mm	millimeter
mo	month
mol	mole
m.y.	million years
µg	microgram
µm	micrometer
nm	nanometer
PDB	Peedee belemnite
pH	measure of hydrogen ion activity
p/m	part per million
s	second
SMOW	standard mean ocean water
wt	weight
yd^3	cubic yard
yr	year

Jour. Research U.S. Geol. Survey
Vol. 2, No. 1, Jan.-Feb. 1974, p. 1—6

LUNAR HIGHLANDS VOLCANISM—IMPLICATIONS FROM LUNA 20 AND APOLLO 16

By H. G. WILSHIRE, D. E. WILHELMS, and K. A. HOWARD,
Menlo Park, Calif.

Abstract.—Highlands materials sampled at the Apollo 16 and Luna 20 sites represent units of distinctive morphology that are widespread on the lunar nearside. Samples from the Apollo 16 site represent hilly and furrowed materials of the Descartes highlands and Cayley Formation. Materials were collected by Luna 20 from terrain resembling the Descartes terrain. Most photogeologic interpretations of these units favored volcanic origins, but the samples fail to support this interpretation. Luna 20 soil fragments are mainly glassy microbreccia with lithic inclusions of fine-grained hornfels; less than 3 percent of the fragments have textures of volcanic rocks, and most of these are likely crystalline products of impact melting. Apollo 16 soils formed on ejecta derived from a plutonic anorthosite-norite-troctolite suite. The similarity of Luna 20 soils indicates that these too formed as regolith on ejecta of anorthosite-norite-troctolite composition. Interpretation of the samples from the two locations now suggests that hilly and furrowed terrains, previously thought to be of volcanic origin, are impact ejecta; in view of the plutonic nature of the source rocks and their extensive fusion and metamorphism, it is likely that the ejecta were derived from multiring basins. At one point, the Apollo 16 site, the Cayley Formation is composed of basin ejecta.

Apollo 16 and Luna 20 have provided tests for the hypothesis that Imbrian or late pre-Imbrian volcanism was an important process in the lunar highlands (Trask and McCauley, 1972). There are several distinctive regional terrain types or stratigraphic units in the highlands that have been difficult to explain by known impact processes and for which volcanic origins were proposed (McCauley and Wilhelms, 1971; Wilhelms and McCauley, 1971; Trask and McCauley, 1972). The Apollo 16 mission was designed to sample the two most distinctive of these—light-plains materials (Cayley Formation) and hilly and furrowed material (of the Descartes highlands). Most of the returned samples, which are predominantly nonvolcanic breccias, have been assigned to the light plains, as reported by AFGIT (Apollo Field Geology Investigation Team, 1973). Whether the adjacent hilly and furrowed material was actually sampled is uncertain (AFGIT, 1973) but seems likely. Luna 20 sampled terrain that partly resembles the hilly and furrowed Descartes highlands (Olson and Wilhelms, 1974) in an area lacking Cayley materials. In this paper we discuss the geologic setting and lithologic comparisons of materials at the two highland sites and the implications of these comparisons for highland volcanism.

Acknowledgments.—This work was done under NASA contracts W-13,130 and T-4738A. We are particularly indebted to C. A. Hodges for discussion of many points relevant to this paper and to P. R. Brett and W. R. Muehlberger for critical reviews of the manuscript. We thank R. E. Sabala and J. W. Shervais for their assistance with the illustrations. Wilshire examined the samples in Albuquerque, N. Mex., with the kind permission of Klaus Keil and assistance of Martin Prinz.

APOLLO 16 SITE

Units exposed at the Apollo 16 site (fig. 1) represent the Cayley Formation (a level-surfaced material that partly fills highland basins, Wilhelms and McCauley, 1971) and two facies of the Descartes highlands materials (Milton, 1968; Hodges, 1972a). The southernmost facies of Descartes material appears to partly fill the crater Descartes (Milton, 1968) and has a pronounced furrowed texture that was interpreted to result from coalescing volcanic domes or elongate vents (Milton, 1968, 1972; Hodges, 1972b). The northern facies is less distinctive and is cut by Imbrium sculpture (Hodges, 1972a; Wilhelms, 1973).

The question of whether either of the facies of Descartes materials were sampled in addition to Cayley Formation remains unanswered, partly because rock types at the site lack clearly distinctive differences and because Cayley debris was ejected from South Ray crater onto the sampled area of Stone Mountain (AFGIT, 1973). Stations 4 and 5 are located low on the slopes of Stone Mountain in the southern facies of Descartes material (AFGIT, 1973). Some of the samples probably represent the southern Descartes material unless the South Ray ejecta deposit is much thicker than expected. Calculation of the average thickness of South Ray ejecta by G. E. Ulrich (written commun., 1973) suggests that a maximum of 5 cm could occur this far from South Ray crater; hence, the underlying Descartes material was probably sampled.

North Ray crater, whose ejecta were sampled extensively, penetrates 200 m deep into a low ridge that rises above the

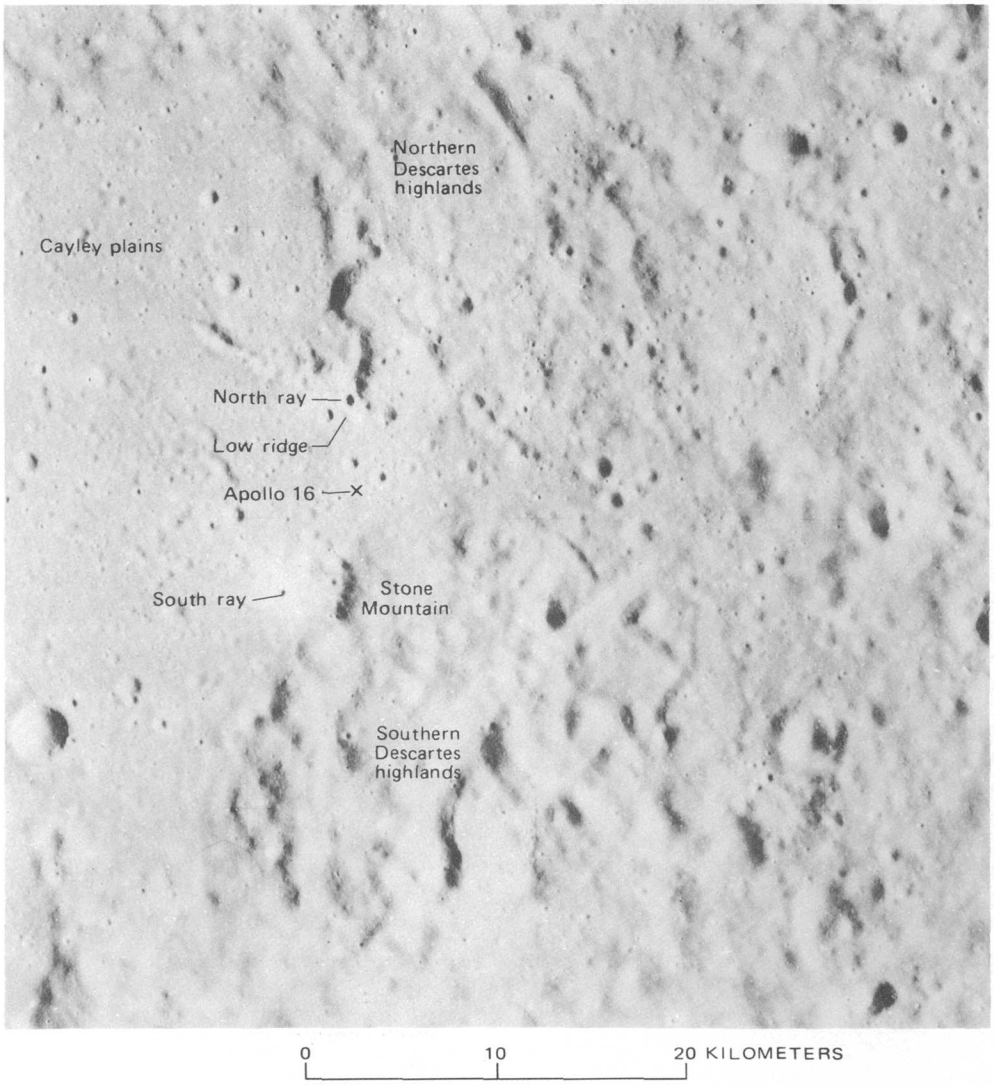

Figure 1.—The Apollo 16 (Descartes) site. The Descartes highlands are hilly and furrowed terrain. Apollo 16 panoramic photograph 4623.

Cayley plains and is adjacent to the northern part of the Descartes highlands (fig. 1). Photographs obtained during the Apollo 16 mission show that this ridge is topographically more like the adjacent Descartes highlands than the Cayley surface. Accordingly, much or all of the material ejected from North Ray crater likely represents Descartes material.

Considering the likelihood that both facies of the Descartes highlands material were sampled as well as the Cayley Formation, the lithologic differences between larger samples of them must be subtle, and their source rocks similar (Wilshire and others, 1973). However, Ulrich (1973) has found systematic differences in proportions of clasts and matrix of otherwise similar breccias between the Cayley plains material and North Ray crater ejecta.

LUNA 20 SITE

Luna 20 landed at lat 3°32′ N., long 56°33′ E., on the southern rim of the Crisium multiringed basin just west of the crater Apollonius C (Vinogradov, 1972). Olson and Wilhelms (1974) included the area of the landing site (fig. 2), before its position was known, in the unit "hilly and pitted material of irregular microrelief," which they described as "aggregates of closely spaced, moderately fresh looking, irregular to subcircular craters, pits, and furrows and minor hills." Prior to the acquisition of Apollo 15 photography, the area was mapped by Wilhelms and McCauley (1971) simply as undivided terra material. Thus this terrain forms a hilly and furrowed province (fig. 3) grossly similar to that at Descartes or that northwest of

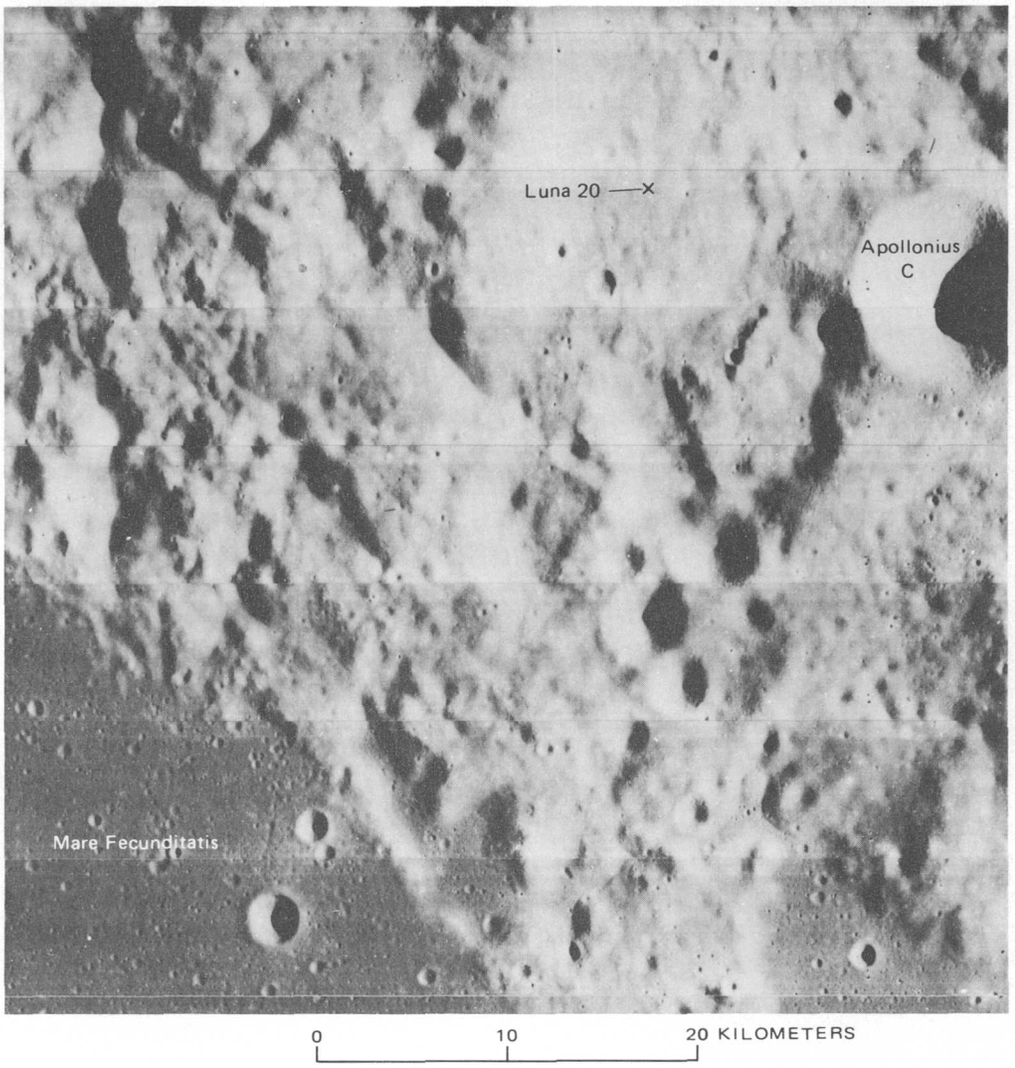

Figure 2.—The Luna 20 site, located from Vinogradov's (1972) coordinates plotted on U.S. Air Force ACIC Lunar Chart LAC 62. The highlands here are hilly and furrowed, but not so distinctively as the Descartes highlands. Lunar Orbiter I photograph M33.

Mare Humorum (Wilhelms and McCauley, 1971; Trask and McCauley, 1972). Fractures are suggested by the linearity of many furrows. The furrows and pits could be interpreted as volcanic vents, collapse features, faults, or alternatively, secondary impact craters. In the immediate vicinity of the Luna 20 site, the furrows are rather indistinct. About 30 km to the west the unit becomes more distinctive, consisting of small domical hills and large intervening fracturelike linear furrows. Hilly, pitted, and furrowed terrain continues in the terra around the west half of Mare Crisium. Similar hilly terra, but without conspicuous pits and furrows, occurs at the Apollo 17 landing site (Scott and Pohn, 1972; Scott and others, 1972) where it is called "sculptured hills." Because of their continuity with this terrain, we would expect the materials at the Luna 20 site to be representative of the hilly and furrowed province. However, the materials may be atypical of this province, as suggested by the indistinctness of the furrows here.

The similarity of the Luna 20 topography to the Descartes highlands has added significance because no Cayley Formation occurs in the vicinity of the Luna 20 site, so that the Cayley is not the source of the rocks sampled. Hence, lithologic similarity of Apollo 16 and Luna 20 samples, described in the following section, lends credence to our view that Cayley and Descartes units at the Apollo 16 site are lithologically the same.

PETROLOGIC COMPARISON OF APOLLO 16 AND LUNA 20 SAMPLES

Petrochemical data show the broad compositional similarity of materials at the Luna 20 and Apollo 16 sites (Vinogradov,

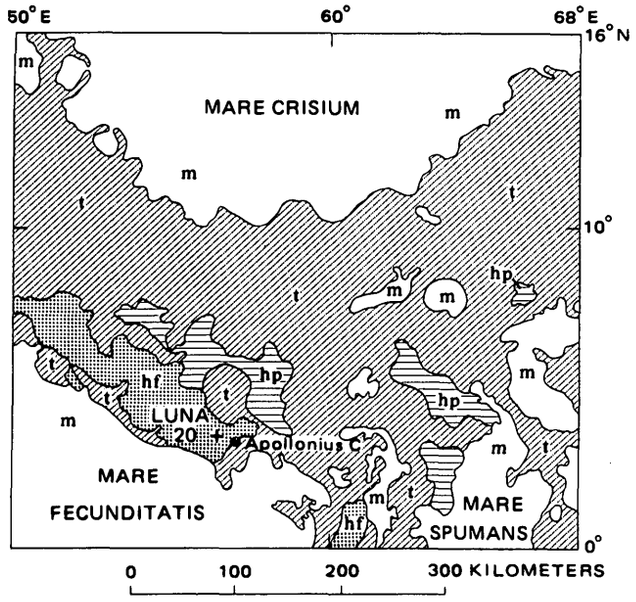

Figure 3.—Geologic province map of the highlands south of Mare Crisium, including the Luna 20 site. Unit hf, hilly and furrowed material; hp, hilly and pitted material; t, other terra and crater material, undivided; m, mare material.

1972; Apollo 16 Preliminary Examination Team, 1973; Warner and others, 1972; Prinz and others, 1973b). While the size fractions represented by samples from the two areas are radically different, the samples can be lithologically compared.

Apollo 16 rocks (Apollo 16 Preliminary Examination Team, 1973; Wilshire and others, 1973) are dominantly breccias composed of light-colored, plagioclase-rich cataclastic material that is generally not annealed and dark, fine-grained material with metamorphic or igneous textures that is chemically similar to the cataclasites. Relict lithic material in these breccias shows that they were derived from a plutonic suite of norite-troctolite-anorthosite with minor grabbro(?), and metamorphic equivalents that have medium-grained, granoblastic-polygonal textures (Wilshire and others, 1973). A smaller proportion of rocks are light-colored metaclastic rocks, mostly with well-developed poikiloblastic texture, and coarse- and fine-grained rocks that may have igneous textures. A very small proportion of documented samples consists mainly of glass, but such fragments form a larger proportion of the rake samples, and a sizable proportion (fig. 4) of coarse fines.

Lithic, glass, and mineral debris from Luna 20 samples in the size range 125–500 μm were classified and counted. About

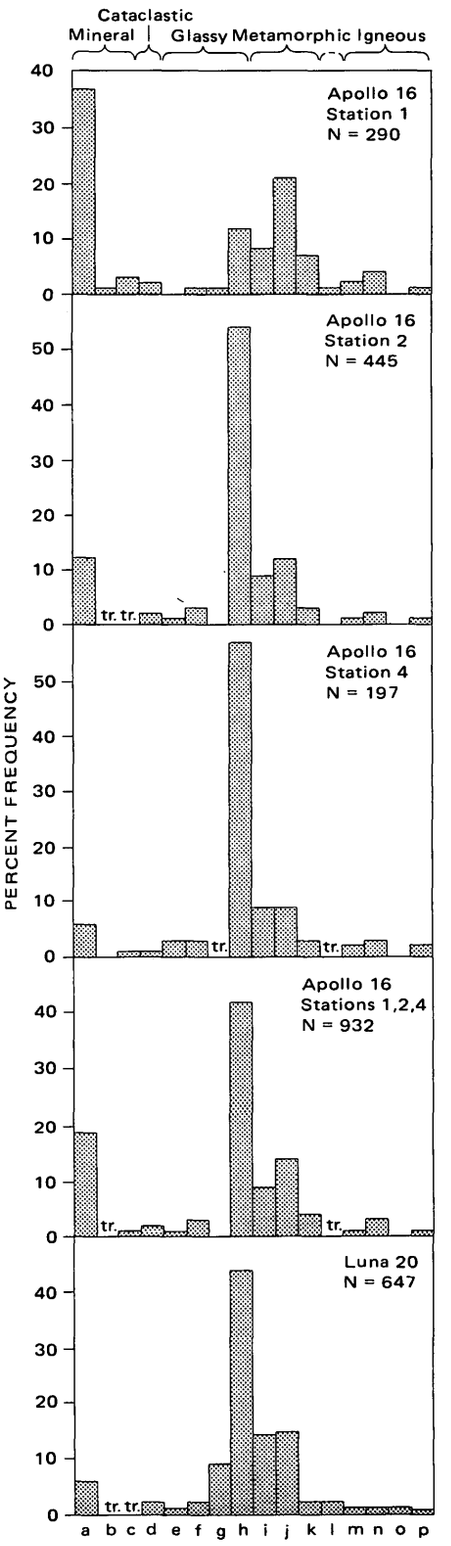

Figure 4—Histograms showing frequency of occurrence of different mineral, glass, and lithic fragments in coarse fines from Apollo 16 (62.5–250 μm range) and Luna 20 (125–500 μm range). N, number of particles counted; tr., trace; a, plagioclase; b, olivine; c, pyroxene; d, cataclasite, plagioclase-rich; e, homogeneous glass; f, devitrified glass, sheaf texture; g, light-gray glassy microbreccia; h, dark brown-gray glassy microbreccia; i, dark-gray metaclastic rock; j, light-gray metaclastic rock; k, granoblastic hornfels, granoblastic-polygonal hornfels; l, pyrometamorphic-poikilitic hornfels; m, intersertal igneous rock; n, ophitic igneous rock; o, Mare basalt; p, unclassified.

650 fragments were counted in 12 grain mounts (fig. 4, bottom). Of the five major categories, glassy materials are clearly dominant (about 55 percent), metamorphic rocks make up 33 percent, and mineral fragments 6 percent. Rocks with igneous texture make up only 3 percent of this size fraction, and the remainder is miscellaneous material.

Homogeneous glass is rare (fig. 4), as it is in finer size fractions (Warner and others, 1972), so that the glass group is composed mainly of glassy microbreccias. These rocks have variable, normally large quantities of mineral and lithic debris. Lithic clasts in the glass are the same as isolated rock fragments, mainly fine-grained metaclastic rocks with small proportions of the other types listed in figure 4. Hence, it appears that the regolith sampled at the Luna 20 site is composed of well-reworked glassy microbreccia with a clast population dominated by fine-grained thermally metamorphosed rocks.

Direct comparison can be made of the Luna 20 soils and Apollo 16 soils in the same size range from stations 1, 2, and 4 (fig. 4). The distributions of particle types at Apollo 16 stations 2 and 4 is virtually identical with that of Luna 20 except that the glassy microbreccias are dominantly dark in the Apollo 16 soils, and the Apollo 16 soils contain a somewhat higher percentage of mineral fragments. These differences are emphasized in the Apollo 16, station 1 soils, but otherwise the soils are strikingly similar and in both areas are dominated by metamorphic lithic debris in glassy matrices.

The close similarity of bulk soil compositions (Apollo 16 Preliminary Examination Team, 1973) from all Apollo 16 stations and their intermediate composition among the analyzed rocks (Prinz and others, 1973b) indicate that the Apollo 16 soils are locally derived from breakdown of rocks like the larger documented samples. The character of the documented rocks is such that further granulation would completely disaggregate the white cataclasites, giving rise to mineral debris, glass, and a small proportion of tough clots of medium-grained granoblastic-polygonal hornfels. The dark- and light-gray fine-grained metaclastic material that forms the matrix of some breccias and the clasts of others (Wilshire and others, 1973) is tough and breaks down to grain size with difficulty; as a consequence, this material provides a source of the metaclastic fragments in the soil. In the Apollo 16 rocks, the dark-gray, fine-grained material that is formed by cataclasis, fusion, and metamorphism of the plutonic rocks commonly has a patchy distribution of fine-grained igneous material where fusion was nearly complete. Although the textures—ophitic, intersertal, and intergranular—of these patches are typically "basaltic," the gradational boundaries with granoblastic breccia matrix and interstitial occurrence in rocks that otherwise have metamorphic textures show that these patches are impact melts and not volcanic; this material has provided the source of small pieces of fine-grained, igneous-textured fragments in the soils.[1] Both the Apollo 16 and Luna 20 sites have a small proportion of exotic mare basalt fragments.

The similarity of fine-grained regolith materials from the Apollo 16 and Luna 20 sites indicates similar source materials. At the Apollo 16 site the source of lithic and mineral debris concentrated in the soils appears to be a suite of norite-troctolite-anorthosite rocks with plutonic rather than volcanic aspect (Wilshire and others, 1973; Prinz and others, 1973a). The likelihood of similar source materials for the Luna 20 samples is considerably enhanced by whole-rock analyses of the fine-grained metaclastic fragments by Prinz and others (1973b), which show that these rocks are chemically like anorthosite, norite, and troctolite. Hence, neither the compositions nor the textures of common rocks at the Apollo 16 and Luna 20 sites are like volcanic rocks but rather appear to be regolith materials developed on ejecta that have been derived from deeper levels of the lunar crust composed of plutonic rocks. This plutonic source, combined with the extensive fusion and thermal metamorphism of the breccias, suggests that the ejecta belong to large multiring basins.

SUMMARY

Photogeologic mapping of the Moon's nearside has shown the widespread occurrence of hilly and furrowed materials and plains-forming (Cayley Formation) units (Wilhelms and McCauley, 1971). Their morphology and lack of apparent age relation to multiring basins led to the supposition that they were volcanic; the hilly and furrowed materials were interpreted as more viscous eruptive products, the Cayley materials as more fluid products of fissure eruptions.

The samples returned by Apollo 16 and Luna 20 do not support the photogeologic interpretation, although the sampling of such widespread units is hardly adequate. Nevertheless, the Cayley Formation samples from the Apollo 16 site show that this formation consists at least locally of basin ejecta. The similarity of the two suites of samples from the two sides suggests the probability that hilly and furrowed units are also basin ejecta. Qualifications to this conclusion are (1) the Descartes materials might not have been sampled at the Apollo 16 site, although we believe they were, (2) the hilly and furrowed terrain directly at the Luna 20 site is not a well-developed example of the unit, and (3) ejecta from the nearby crater Apollonius C (fig. 2) may cover the Luna 20 site and possibly was derived from another unit. Though volcanism has been an attractive explanation of the hilly and furrowed terrains, it is possible to reconcile them with impact origins. For instance, the Luna 20 material may be ejecta from the Crisium basin, partly faulted and grooved by later secondary craters; the Descartes highlands may similarly be related to the Nectaris and (or) Imbrium basins (Hodges, 1972a; Wilhelms,

[1] Igneous-textured rocks 68415, 68416, and 65055 are coarser than any of these patches and conceivably are volcanic.

1972; Head, 1972). It now seems likely that there are few or no hilly volcanic landforms on the lunar highlands. The most critical target to test this possibility further would be the large steep Gruithuisen domes and Hansteen alpha (Wilhelms and McCauley, 1971), which are color anomalies (Whitaker, 1972).

REFERENCES CITED

Apollo Field Geology Investigation Team, 1973, Apollo 16 exploration of Descartes–a geologic summary: Science, v. 179, p. 62–69.

Apollo 16 Preliminary Examination Team, 1973, The Apollo 16 samples–a petrographic and chemical description: Science, v. 179, p. 23–34.

Head, J. W., 1972, Small-scale analogs of the Cayley Formation and Descartes mountains in impact associated deposits, *in* Apollo 16 preliminary science report: Natl. Aeronautics Space Adm. SP-315, p. 29-16 to 29-20.

Hodges, C. A., 1972a, Descartes highlands–possible analogues around the Orientale basin, *in* Apollo 16 preliminary science report: Natl. Aeronautics Space Adm. SP-315, p. 29-20 to 29-23.

____1972b, Geologic map of part of the Descartes region of the Moon–Apollo 16 pre-mission map: U.S. Geol. Survey Misc. Geol. Inv. Map I-748, Sheet 2.

McCauley, J. F., and Wilhelms, D. E., 1971, Geological provinces of the near side of the Moon: Icarus, v. 15, p. 363-367.

Milton, D. J., 1968, Geologic map of the Theophilus quadrangle of the Moon: U.S. Geol. Survey Misc. Geol. Inv. Map I-546.

____1972, Geologic map of the Descartes region of the Moon–Apollo 16 pre-mission map: U.S. Geol. Survey Misc. Geol. Inv. Map I-748, Sheet 1.

Olson, A. B., and Wilhelms, D. E., 1974, Geologic map of the Mare Undarum quadrangle of the Moon: U.S. Geol. Survey Misc. Geol. Inv. Map I-837. (In press.)

Prinz, Martin, Dowty, Eric, and Keil, Klaus, 1973a, Spinel troctolite and anorthosite in Apollo 16 samples: Science, v. 179, p. 74–76.

Prinz, Martin, Dowty, Eric, Keil, Klaus, and Bunch, T. E., 1973b, Mineralogy, petrology, and chemistry of lithic fragments from Luna 20 fines–origin of the cumulate ANT suite and its relationship to high-alumina and mare basalts: Geochim. et Cosmochim Acta, v. 37, p. 979–1006.

Scott, D. H., Lucchitta, B. K., and Carr, M. H., 1972, Geologic maps of the Taurus-Littrow region of the Moon: U.S. Geol. Survey Misc. Geol. Inv. Map I-800.

Scott, D. H., and Pohn, H. A., 1972, Geologic map of the Macrobius quadrangle of the Moon: U.S. Geol. Survey Misc. Geol. Inv. Map I-799.

Trask, N. J., and McCauley, J. F., 1972, Differentiation and volcanism in the lunar highlands–photogeologic evidence and Apollo 16 implications: Earth and Planetary Sci. Letters, v. 14, p. 201–206.

Ulrich, G. E., 1973, A geologic model for North Ray crater, *in* Fourth Lunar Sci. Conf. Abs.: p. 745–747.

Vinogradov, Alexander, 1972, Lunar rock: EOS (Am. Geophys. Union Trans.), v. 53, p. 820–822.

Warner, J., Reid, A. M., Ridley, W. I., and Brown, R. W., 1972, Major element composition of Luna 20 glasses: Earth and Planetary Sci. Letters, v. 17, p. 7–12.

Whitaker, E. A., 1972, Lunar color boundaries and their relationship to topographic features–a preliminary survey: The Moon, v. 4, p. 348–355.

Wilhelms, D. E., 1972, Reinterpretations of northern Nectaris basin, *in* Apollo 16 preliminary science report: Natl. Aeronautics Space Adm. SP-315, p. 29-27 to 29-30.

Wilhelms, D. E., and McCauley, J. F., 1971, Geologic map of the near side of the Moon: U.S. Geol. Survey Misc. Geol. Inv. Map I-703.

Wilshire, H. G., Stuart-Alexander, D. E. and Jackson, E. D., 1973, Apollo 16 rocks–petrology and classification: Jour. Geophys. Research, v. 78, p. 2379–2392.

Jour. Research U.S. Geol. Survey
Vol. 2, No. 1, Jan. - Feb. 1974, p. 7—12

ISOTOPIC COMPOSITION OF CARBON AND HYDROGEN IN SOME APOLLO 14 AND 15 LUNAR SAMPLES

By IRVING FRIEDMAN, KENNETH G. HARDCASTLE,
and JIM D.GLEASON, Denver, Colo.

Abstract.—Isotopic composition of carbon and hydrogen in some Apollo 14 and 15 lunar samples was determined by use of a newly constructed combustion line that yields low blanks for CO_2 and H_2. The results from combustion of fines and breccia from Apollo 14 lunar samples and of fines, breccia, and basalt from Apollo 15 were compared with data obtained by heating samples in vacuo to over 1,350°C. The two techniques gave similar results. Total carbon in the fines ranged from 51 to 110 p/m with a δC^{13} of +12 to -8 per mil (parts per thousand) PDB. The breccias contain 22 to 50 p/m carbon with a δC^{13} of -21 to -25 per mil. The crystalline rock (sample 15555) has a carbon content of about 7 p/m and a δC^{13} of -28 per mil. The total hydrogen in the fines ranges from 66 to 120 p/m with a (D/H) $\times 10^{-6}$ of 39 to 90. The breccias contain 8 to 38 p/m H_2 with a (D/H) $\times 10^{-6}$ of 103 to 144. The crystalline rock contains about 2 p/m H_2 with a (D/H) $\times 10^{-6}$ of about 140. Arguments are presented to show that the contamination by earth materials is not as serious a problem as has been proposed by previous authors.

There has been little agreement among investigators in the results of analysis of the carbon and hydrogen isotopic composition of lunar material. It has always been our belief that much of the apparent disagreement is a result of sample inhomogeneity, as we expressed at the time of the First Lunar Science Conference (Friedman and others, 1970):

> The conclusion seems obvious. The lunar dust is very inhomogeneous and contains varying amounts of CO_2, perhaps CO, elemental carbon, and carbides, all having very different δC^{13}. If any carbonate from carbonaceous chondrites is present, we may expect to find carbon of +58 to +65 per mil, as well as carbon of -3 to -19 per mil. If ordinary chondritic carbon is present, values of -25 per mil can be expected.

CARBON

Kaplan, Smith and Ruth (1970) stated that contamination (probably experimental) has been a contributor to the light δC^{13} found by us and have plotted the δC^{13} as a function of percent carbon to show that the higher the carbon content in samples of the same dust sample, the lower the δC^{13}. Since most terrestrial hydrocarbon and organic carbon materials that might be a source of contamination (including rocket exhaust and excess fuel dumped on the lunar surface) have δC^{13} values from -20 to -35 per mil, their hypothesis seemed reasonable. Epstein and Taylor (1970) also believed that negative values of δC^{13} are due to contamination, and stated that " * * * it is unlikely that carbon sources of different composition and different δ values are mixed together in the lunar soil."

By the time of the Second Lunar Science Conference we had not changed our position. Our additional analysis gave a range of values from -3 to -25 per mil for dust, breccia, and crystalline rocks. Epstein and Taylor (1970) and Kaplan, Smith, and Ruth (1970) had determined a range in carbon values from +20 to -30 per mil.

In order to settle some of the points at issue, we have constructed a new combustion line made of glass and metal, with no organic materials of any kind. The sample is introduced through a copper-gasketed, stainless-steel flange (Varian "Conflat"), and the few valves are of stainless-steel, packless-welded-bellows construction. Stainless-steel to Pyrex seals are used between glass and stainless-steel components, and the valves are connected by Swagelock fittings using aluminum ferrules. Aviator's breathing oxygen containing <7 p/m H_2O is purified by passing it over CuO at ≈ 600°C and by condensing any H_2O or CO_2 in a trap cooled with liquid oxygen. The purified oxygen is introduced into the system at (Denver) atmospheric pressure (≈ 600 mm). The gas is circulated by alternately freezing the oxygen at liquid N_2 temperature and then rapidly warming the condensed liquid O_2.

Before a sample was combusted, it was heated in vacuo in the combustion tube for at least 16 h at a temperature of 125° to 150°C. Blanks were always run before moving the combustion boat from the 125°C section of the Vycor combustion tube into the 950°C section. All these blanks resulted in an amount of gas condensable with liquid N_2 equivalent to less than 1 μg CO_2 and of gas condensable at dry ice temperature equivalent to less than 0.5 μg H_2 as H_2O. These blanks are in contrast to the blanks of 205 μg CO_2 and 88 μg H_2 reported by Epstein and Taylor (1972) in an experiment to determine the blank in a system containing greased stopcocks (the system was never used for the analyses of lunar samples) and ≈ 5 μg C reported by Kaplan and Petrowski (1971). Combustions were carried out for 1 to 1½ h, and the reaction products were

condensed in a trap cooled with liquid oxygen. The excess oxygen was then pumped off and the sample (CO_2, SO_2, H_2O) was transferred to a break-seal tube.

The break-seal tube was opened on the CO_2 mass spectrometer inlet system. CO_2 was taken off at the temperature of freezing ethyl alcohol and analyzed. The SO_2 was pumped off at dry ice temperature, and the remaining H_2O was transferred to a processing line on the H_2 spectrometer where it was converted to H_2 gas by reaction with hot uranium metal (≈750°-800°C) and was pumped with a Hg diffusion pump into the inlet system of the spectrometer.

In order to check reproducibility of the combustion apparatus, small (≈2-mm diam) disks were punched out of filter paper and analyzed. First, several disks equivalent to 500-μg carbon were combusted, then a sample of one-half of a disk, equivalent to 24-μg carbon, was combusted. The large sample gave a δC^{13} of -24.5 per mil, and the small sample, a δC^{13} of -24.6 per mil. Our combustions, except those of the two residues from our pyrolysis, were made with carbon amounts ranging from 8 to 108 μg.

As a further check on our procedures, we exchanged standard samples with the other principal investigators. Prof. I. R. Kaplan furnished us with four standards, each of which was divided, by use of a carefully cleaned microsplitter, into four parts. One aliquot was retained by our laboratory, one was sent to Prof. Samuel Epstein, and two were returned to Prof. Kaplan. Our results on these samples are given in table 1.

From these analyses, we concluded that we could secure δC^{13} analysis by combustion on samples of ≈50 μg with a precision of ±2 per mil and that our error on samples of ≈10μg was probably not greater than ±5 per mil.

In all our previous analyses of lunar material, we found that the nonrare gases that evolved upon heating in vacuo consisted mainly of CO_2, with some CO (or CH_4). We also found more H_2O than H_2, even at temperatures below 600°C.

Epstein and Taylor (1971) found that their samples evolved gas mixtures that were less oxidized—less CO_2 and more CO, less H_2O and more H_2. They took this as proof that our samples were being contaminated with oxygen contained in (or on) the platinum crucible in which we heated our sample. Our procedure had been to heat the platinum crucible to bright redness, allow it to cool in air, outgas it in vacuo at ≈1,400°C, let it cool, expose it to the air while introducing the sample, evacuate and quickly heat the crucible to redness for a moment in vacuo (flash heating), and allow it to cool in vacuo before proceeding with the heating of the sample. Epstein and Taylor loaded their outgassed crucible in a dry box so that it did not "see" the air. However, they did not check the oxygen content of their dry box, nor could they deoxygenate their samples, most of which had "seen" air on return from the moon.

In order to check on the importance of the exposure to air of our outgassed crucible, we built an apparatus that allowed us to completely outgas the equipment and crucible before dropping the outgassed sample into the platinum crucible. The Vycor envelope and crucible were first heated to ≈900°C by use of a tube furnace placed about the apparatus. The furnace was then removed and replaced by an induction heater work coil, and the platinum crucible was then heated to ≈1,400°C. The lunar samples, in the form of ≈0.5-cm cubes and chips, were contained in a sidearm of the apparatus and heated overnight in vacuo at 180°C before being pushed by a magnetically operated pusher into the platinum crucible. The samples were first heated to 760°C by use of the external tube furnace. Temperatures were monitored with a thermocouple and potentiometer and, to 760°C, are accurate to ±10°C. To attain temperatures above 760°C, an induction heater was used, and temperatures were read on an optical pyrometer with ±10°C accuracy. In spite of these precautions, the gases that evolved from the two rocks processed consisted mostly of CO_2 and H_2O. The ratio of total CO_2 to CO (or CH_4) was about 1:5 to 1:10. The H_2O:H_2 ratio ranged from 3 to 40. Most of the oxidized species were found at temperatures of 200° to 600°C, and some were found at higher temperatures; these findings reinforce our previous conclusion that some CO_2 is a primary constituent and not an artifact of our procedures. One sample (14305) appeared to show a lower ratio of CO_2 to CO at the lower temperatures; thus possibly the lower CO_2:CO ratios found by Epstein and Taylor (1971) were evolved at temperatures that are lower than those given by them. It is noteworthy that they used an induction heater for all their heating and that they measured their temperatures with an optical pyrometer. Temperatures below ≈600°C were estimated by them; thus they may have been in error by as much as 100°C.

At temperatures above about 700°C the reduced carbon species present in the sample (C, CO, CH_4) probably react with the iron oxides and silicates to produce a mixture of CO and CO_2. Any free hydrogen will also react to give H_2O. Therefore, we do not think that the proportions of oxidized versus reduced species of carbon and hydrogen that evolved at elevated temperature have any relation to their original ratio in

Table 1.—*δC^{13} and δD analysis of intercomparison samples*

Sample	Description	Carbon μg	Carbon P/m	δC^{13}	$\delta D/H$
3300-11C	Meteorite and sand	73.4	99	-8.9	-89
		171	115	-6.8	-64
3300-12C	do	108	240	-5.5	-80
		157	230	-5.2	-71
3300-13C	Hawaiian basalt	51.8	43	-18.1	-96
3300-14C	Precambrian black chert.	313	99,000	-24.3	...

Table 2.—*Results of heating and combustion of Apollo 14 and 15 lunar samples*

Concentrations = ±20 percent of amount present.
δD=10 per mil, except for samples of <5 μg; values are per mil deviations from SMOW.
δC^{13} = ±1 per mil, except for samples of <10 μg; values are per mil deviations from PDB.
$(D/H)\times10^{-6}$ = ±10 percent; values were calculated from δD SMOW values, using the relation $(D/H)\times10^{-6} = 0.158\,(1000 + \delta D$ per mil).

Sample			Temp (°C)	Vacuum heating								Combustion				Total				
				H_2		H_2O		CO_2		$CO+CH_4$		H		C		H			C	
																	(D/H)			
No.	Type	Wt (g)		P/m	δD	H_2 (p/m)	δD	P/m	δC^{13}	P/m	δC^{13}	P/m	δD	P/m	δC^{13}	P/m	$\times10^{-6}$	δD	P/m	δC^{13}
15271-29	Dust	1.02	950									120	-510	105	-3.9	120	78	-510	105	-4
14422-13	..do..	.93	950									82	-434	11	-8.4	82	90	-434	110	-8
15100-3	Fines	.97	950									90	-554	99	+7.9	90	71	-554	99	+8
15459-30, 15459-37.	Breccia	.34	950									8	-200	22	-25	8	126	-200	22	-25
15459-100	..do..	.30	950									38	-346	50	-22	38	103	-346	50	-22
14305-57	..do..	.74	950									20	-109	50	-21.9	20	141	-109	50	-22
15555-144	Basalt	1.41	950									2.8	-130	7.3	-27.5	2.8	138	-130	7.3	-28
15100-3	Dust	.95	950									66	-617	74	+11.5	66	60	-617	74	+12
15555-144	Basalt	3.49	180- 600	0.22	-62	0.46	-104	1.5	-23.0	0.3	-38									
			600- 1,350	.09	....	.51	-5	4.0	-15.8	.6	-43									
			Combusted									.70	-160	1.3	-28.4	2.0	143	-93	7.7	-24
14305-57	Breccia	2.49	180- 600	.33	-100	13.6	-88	11.3	+22.9	2.3	-24.7									
			600- 760	.04	....	3.1	-79	10.8	-24.6	.5	-27.5									
			760- 1,350	.02	....	.9	-99	17.8	-21.3	.2	....									
			Combusted									1.8	-128	1.9	-27.3	20	144	-90	45	-21
15100-3	Dust	3.0	210- 415	5	-900	18	-598	....	....	....	....									
			415- 585	29	-826	18	-826	1.3	+7.3	....	....									
			585- 760	2.3	-567	10	-756	[1]1.8	[1]+14.3	....	....									
			760->1,350	.1	-370	1.4	-619	43	*8.3	4	+10.3									
			Combusted									1	-284	1	....	85	39	-756	51	+9

[1] Combined $CO+CO_2$.

the unheated sample. In addition, all the samples have been exposed to some atmospheric oxygen, and this contaminant may not be easily removed, especially on dust (soil) samples. Table 2 gives the results of our analyses.

Our experience shows that the two techniques for the determination of carbon content and δC^{13}—stepwise (pyrolysis) and combustion—give virtually identical results (table 3).

Table 3.—*Comparison between pyrolysis and combustion techniques*

Sample			Carbon		Hydrogen	
No.	Wt	Procedure	P/m	δ	P/m	δ
14305-57	2.49	Pyrolysis	45	-21	20	-90
	.74	Combustion	50	-22	20	-109
15100-3	3.0	Pyrolysis	50	+9	85	-760
	.97	Combustion	99	+8	90	-550
	.95	do	74	+11	66	-620
15555-144	3.49	Pyrolysis	7.7	-24	2.0	-90
	1.41	Combustion	7.3	-27	2.8	-130

In figure 1 we have plotted the δC^{13} versus parts per million carbon for all lunar materials that we and other authors (Kaplan and others, 1970, 1971; Epstein and Taylor, 1970, 1971, 1972) have reported. The crystalline rocks range in carbon content from 7 to 78 p/m and in δC^{13} from -17 to -30 per mil. The dust samples range in carbon content from 30 to 188 p/m and in δC^{13} from +20 to -24, with a tendency toward heavier (more positive) δC^{13} values for samples with more carbon. The crystalline rocks were outgassed on melting on the moon and would retain the nonvolatile forms of carbon such as elemental carbon and carbides which have a δC^{13} of about -24 per mil. The dust could contain, in addition to these carbon species, carbon in other forms and from other sources, for example from solar wind and cosmic rays. These later sources of carbon appear to be relatively heavy (≈20 per mil).

HYDROGEN

The total hydrogen, including molecular H_2, H_2O, and CH_4, ranges from 2 p/m and $\approx 143 \times 10^{-6}$ (D/H) for sample 15555 to 120 p/m and 78×10^{-6} (D/H) for sample 15271.

Although terrestrial contamination is always a possibility, as has been discussed by us (Friedman and others, 1970) and by Epstein and Taylor (1971), we believe that the results of our experiments indicate the amount of this contamination. Dust samples that have been combusted at 900°C and then opened to laboratory air and recombusted show a maximum contamination of 5 p/m H_2. Samples that have been melted in vacuum at 1,350°C and then exposed to laboratory air and combusted have given an upper limit of 0.7 to 1.8 p/m H_2 contamination.

H_2 versus $(D/H) \times 10^{-6}$ for all reported analyses is plotted in figure 2. Interestingly, the materials low (below 20 p/m in H_2 tend to give $(D/H) \times 10^{-6}$ values higher than about 130. The interior of a large basalt sample (No. 12051) gave a $(D/H) \times 10^{-6}$ value of 207. In these samples, which are enriched in deuterium compared to earth materials, we have attributed the hydrogen, in part at least, to generation by spallation reactions, an explanation concurred with by Epstein and Taylor.

The samples that are rich in hydrogen (more than 60 p/m H_2) contain hydrogen that is depleted in deuterium (less than 90×10^{-6} (D/H), and this hydrogen is mainly solar wind H_2, although there may be some contribution from hydrogen outgassed from the lunar interior or from lunar rocks melted by

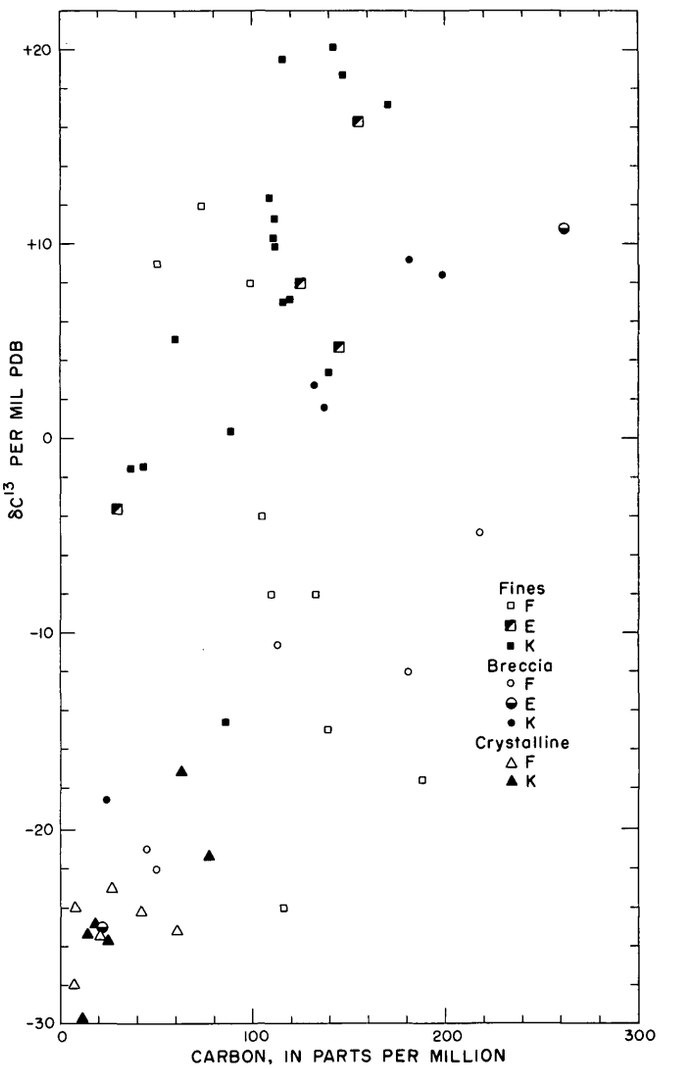

Figure 1.—A plot of the carbon content versus the δC^{13} in lunar samples. The letter symbols refer to published data: F, Friedman, Gleason, and Hardcastle (1970), and Friedman, O'Neil, Gleason, and Hardcastle (1971); E, Epstein and Taylor (1970, 1971, 1972); and K, Kaplan, Smith, and Ruth (1970, and Kaplan and Petrowski (1971).

impact, as well as hydrogen from meteorites. Hydrogen from these later three sources may be adsorbed on, or trapped in, the lunar dust and breccia.

The exact molecular "species" that contains the hydrogen is uncertain and, to some extent, is a semantic problem. Certainly the extraction procedures used by us and by Epstein and Taylor cannot easily differentiate whether the H_2 is present as atomic H in a radiation "hole" or is bound loosely or tightly to oxygen in the silicate or oxide mineral. Hydrogen generated by spallation reactions will probably be more tightly bound than hydrogen "adsorbed" by lunar outgassing, whereas solar wind protons will probably have some intermediate stability in relation to the host lattice. Materials subject to a high degree of shock metamorphism before the introduction of protons may provide a stronger H-O bond than more perfect silicate (or oxide) lattices.

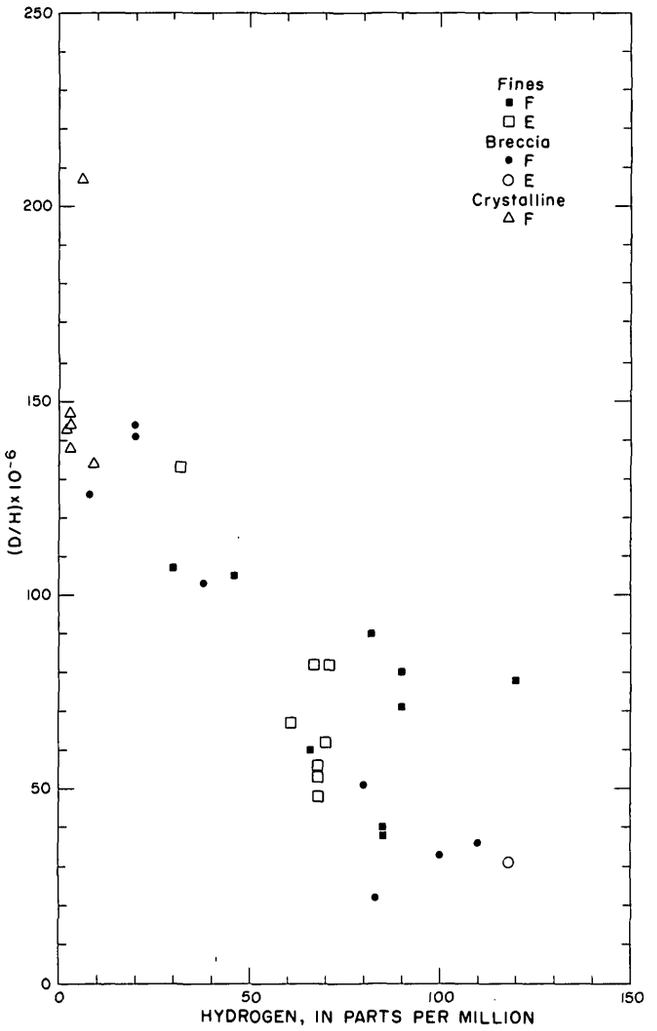

Figure 2.—A plot of the hydrogen content versus the deuterium concentration in lunar samples. The letter symbols refer to published data: F, Friedman, Gleason, and Hardcastle (1970), and Friedman, O'Neil, Gleason, and Hardcastle (1971); E, Epstein and Taylor (1970, 1971, 1972), Kaplan and Petrowski (1971), and Kaplan, Smith, and Ruth (1970).

Epstein and Taylor (1971) attempted to determine the true deuterium concentration of lunar hydrogen by an exchange experiment using deuterium-depleted water. The rationale of their experiment was that inasmuch as the hydrogen and water liberated on heating the lunar soils and breccias tended to interact during extraction, and inasmuch as the water present in the sample was probably a contaminant, then exchanging the easily exchangeable water with light (deuterium-depleted) water should make the hydrogen obtained by heating in vacuo lighter. Their experiments did just that. However, all that they have shown is that:

1. Some of the water is exchangeable with water vapor at 300°C (temperature estimated; it could be as high as 400°C).
2. The hydrogen and water undergo isotopic exchange at the temperatures of extraction.

We do not see that their experiment has any bearing on the true amount and isotopic composition of lunar hydrogen and water.

The deuterium content versus total H_2 (H_2+H_2O) for all lunar samples reported in the literature is plotted in figure 2. Although it is difficult to assess the amount of contamination present in each sample and in spite of the fact that the analyses were made by different techniques by two different analysts, there are certain regularities in the data.

The dust samples cover a wide range in hydrogen and deuterium contents—30 to 120 p/m total H_2 and 37 to 134 p/m D. The breccias cover a similar range, 9 to 118 p/m total H_2 and 22 to 144 p/m D. The crystalline rocks cover a much narrower range—2 to 9 p/m H_2 and 134 to 207 p/m D.

The range in total H_2 in the dust samples leads us to believe that contamination is not as serious a problem as indicated by Epstein and Taylor (1971). From figure 2 data, it would appear that crystalline rocks contain about 2 to 9 p/m H_2 with a deuterium concentration of 134 to 207 p/m. This hydrogen probably consists of spallationagenic hydrogen plus hydrogen remaining after melting and partial outgassing of the rocks.

The dust and breccia contain an additional component of hydrogen that is partially of solar wind origin, partially captured meteoritic hydrogen, and partially captured lunar outgassing hydrogen.

REFERENCES CITED

Epstein, Samuel, and Taylor, H. P., Jr., 1970, The concentration and isotopic composition of hydrogen, carbon and silicon in Apollo 11 lunar rocks and minerals, *in* Apollo 11 Lunar Sci. Conf., Houston, Tex., 1970, Proc.: Geochim. et Cosmochim. Acta, Supp. 1, v. 2, p. 1085–1096.

——1971, O^{18}/O^{16}, Si^{30}/Si^{28}, D/H, and C^{13}/C^{12} ratios in lunar samples, *in* Lunar Sci. Conf., 2d, Houston, Tex., 1971, Proc.: Geochim. et Cosmochim. Acta, Supp. 2, v. 2, p. 1421–1441.

——1972, O^{18}/O^{16}, Si^{30}/Si^{28}, C^{13}/C^{12}, and D/H studies of Apollo 14 and 15 samples, *in* Lunar Sci. Conf., 3d, Houston, Tex., 1972, Proc.: Geochim. et Cosmochim. Acta, Supp. 3, v. 2, p. 1429–1454.

Friedman, Irving, Gleason, J. D., and Hardcastle, K. G., 1970, Water, hydrogen, deuterium, carbon and C^{13} content of selected lunar material, *in* Apollo 11 Lunar Sci. Conf., Houston, Tex., 1970, Proc.: Geochim. et Cosmochim. Acta, Supp. 1, v. 2, p. 1103–1109.

Friedman, Irving, O'Neil, J. R., Gleason, J. D., and Hardcastle, Kenneth, 1971, The carbon and hydrogen content and isotopic composition of some Apollo 12 materials, *in* Lunar Sci. Conf., 2d, Houston, Tex., 1971, Proc.: Geochim. et Cosmochim. Acta, Supp. 2, v. 2, p. 1407–1415.

Kaplan, I. R., and Petrowski, Chari, 1971, Carbon and sulfur isotope studies on Apollo 12 lunar samples, *in* Lunar Sci. Conf., 2d, Houston, Tex., 1971, Proc.: Geochim. et Cosmochim. Acta, Supp. 2, v. 2, p. 1397–1406.

Kaplan, I. R., Smith, J. W., and Ruth, E., 1970, Carbon and sulfur concentration and isotopic composition in Apollo 11 lunar samples, *in* Apollo 11 Lunar Sci. Conf., Houston, Tex., 1970, Proc.: Geochim. et Cosmochim. Acta, Supp. 1, v. 2, p. 1317–1330.

Jour. Research U.S. Geol. Survey
Vol. 2, No. 1, Jan. - Feb. 1974, p. 13–23

STABLE ISOTOPE AND LEAD ISOTOPE STUDY OF THE CORTEZ, NEVADA, GOLD DEPOSIT AND SURROUNDING AREA

By R. O. RYE, B. R. DOE, and J. D. WELLS, Denver, Colo.

Abstract.—Isotope studies of sulfur, carbon, hydrogen, oxygen, and lead were carried out to clarify the age and origin of the Cortez gold deposit and the surrounding mineralized area. The hydrogen isotope data indicate that meteoric water was the dominant component of the ore-forming fluids at Cortez. The hydrogen isotope data support geologic evidence for a Tertiary age for the deposit. The oxidation of the ore probably occurred during the deposition of postore calcite and was caused by waters whose oxygen isotopic composition was distinctly different from that of the ore fluids. The carbon isotope data suggest that the only carbon present in the ore fluids was derived from solution of the host rock. The lead and sulfur data are consistent with a possible sedimentary derivation for the gold in the ore. Lead and sulfur isotope distributions indicate that much of the galena mineralization in the area occurred during the Jurassic.

The Cortez gold mine is located in Lander County, Nev. (fig. 1). It is a low-grade hydrothermal deposit in which the gold is disseminated in the upper part of the Roberts Mountains Formation in lower plate rocks near a Tertiary intrusive. The regional and local geology, mineralogy, geochemistry, and age of the deposit have been described in several papers (Erickson and others, 1966; Wells and others, 1969; Roberts and others, 1971; Wells and others, 1971; Wells and Mullens, 1973). The study by Wells and Mullens (1973) indicated that the host rock Roberts Mountains Formation is a silty, argillaceous, carbonaceous, pyrite-bearing limestone that contains both calcite and dolomite. During mineralization calcite was removed from the finely fractured silty carbonate of the Roberts Mountains Formation, creating micropore space in which pyrite, quartz, and illite were deposited along with gold and arsenic from hydrothermal solutions. The gold occurs mainly in minute specks of arsenian pyrite and in arsenian rims of larger pyrite grains. The gold is invisible at high magnification (X 1,600) in unoxidized ore. Some visible gold occurs in the oxidized zone, indicating that gold was mobilized and concentrated during oxidation. A few small quartz veinlets occur in the deposit, usually with gold and pyrite which has been completely oxidized to goethite-hematite. These rare veinlets are the only megascopic expression of the hydrothermal process. The only other noticeable megascopic features of the deposit are the abundant calcite veinlets which occur as botryoidal masses or acicular crystals in postore fractures.

The study by Wells and Mullens (1973) indicated that the Cortez deposit is probably similar to many Tertiary hydrothermal gold deposits in which the gold, instead of being concentrated into veins, was disseminated in microfractured rocks. However, their study left unsolved the problem of the source of the hydrothermal fluids and the origin of the gold in the deposit. There is also uncertainty about the age of the deposit. Wells, Elliott, and Obradovich (1971) concluded that the deposit was related to either the Oligocene quartz porphyry dikes exposed near the mine or the Miocene rhyolite volcanics that crop out in the Buckhorn area.

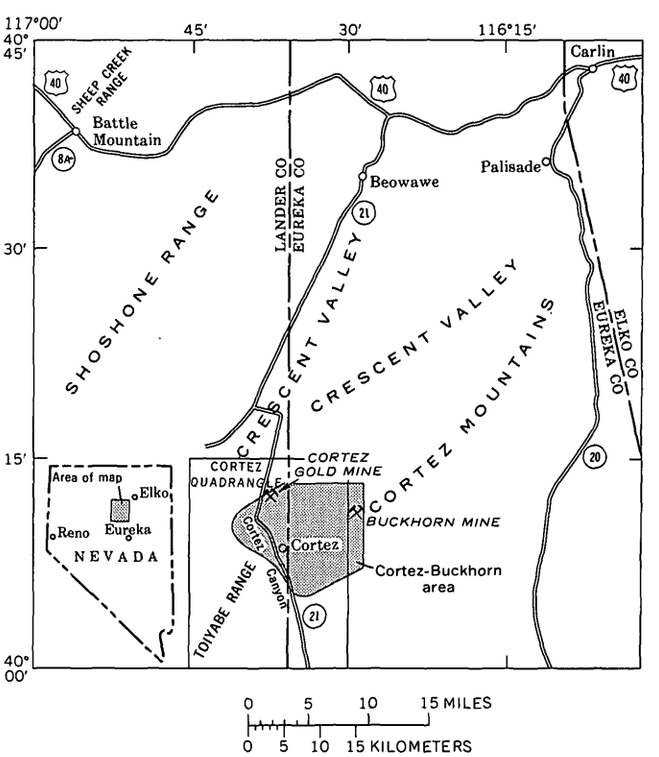

Figure 1.—Index map showing location of the Cortez gold mine in the Cortez-Buckhorn area, Nevada. Base from U.S. Geological Survey, Winnemucca quadrangle, 1:250,000, 1962.

In this study we present all available stable and lead isotope data on the Cortez deposit and on the surrounding area in an attempt to clarify the origin and age of the deposit.

EXPERIMENTAL TECHNIQUES

Stable isotope techniques

The stable isotope analyses for carbon, hydrogen, oxygen, and sulfur were made by widely used standard techniques which have been summarized by Rye and Sawkins (1974). The stable isotope data are presented as δ values which are defined as per mil deviations relative to a given standard. The δ value of hydrogen, for example, is defined as:

$$\delta D = \frac{H/D_{sample} - H/D_{standard}}{H/D_{standard}} \times 1{,}000$$

The δ values for other stable isotopes are defined similarly in terms of sample and standard. The SMOW standard (Craig, 1961) is used for hydrogen and oxygen isotope data. Carbon isotope data are presented relative to PDB (Craig, 1957), and the sulfur isotope data are presented relative to the Cañon Diablo trailite standard. The analytical uncertainty is about ± 0.1 per mil for carbon, oxygen, and sulfur and ± 1.0 per mil for hydrogen.

Lead isotope techniques

Galena samples were dissolved, converted to lead iodide, and run by the PbS-NH_4 NO_3 surface-emission method of solid-source mass spectrometry. Feldspars were decomposed by HF-$HC10_4$ techniques in a clean laboratory, purified by ion exchange and dithizone techniques, and run by the PbS-NH_4NO_3 surface-emission method of solid-source mass spectrometry, except for sample W302 which was run by the H_3PO_4-silica gel emitter technique of solid-source mass spectrometry. Pyrite concentrates were cleaned with HCl and dissolved in 1:1 HNO_3 and analyzed like the feldspar leads. Sediments were split chemically by leaching into an HCl-soluble fraction and an HCl-insoluble fraction (residue). The residue was then treated similarly to the feldspars and the HCl-soluble fraction started at the ion exchange step.

The analytical uncertainties are about 0.27 percent for $^{206}Pb/^{204}Pb$, 0.40 percent for $^{207}Pb/^{204}Pb$, and 0.54 percent for $^{208}Pb/^{204}Pb$ at 2σ, except for sample W302 for which the analytical uncertainties are about 0.15 percent for all ratios.

The stable isotope data are summarized in tables 1–5; the lead isotope data are summarized in table 6 and figure 4; collection localities for all samples are indicated in figures 2 and 3.

RESULTS

Sulfur isotope data

Sulfur isotope geochemistry of ore deposits has undergone a remarkable transformation in recent years. Sulfur isotope fractionations between coexisting sulfides can now often be used to determine temperatures of ore deposition (for example, Czamanske and Rye, 1974). Also the variations of δS^{34} values of specific minerals in ore deposits may now be interpreted in terms of variations in the physical-chemical environment of ore deposition (Ohmoto, 1972).

The isotopic composition of sulfur in sulfides was determined on representative samples from all the mineralized localities in the Cortez-Buckhorn area (figs. 2–3; table 1). These include samples from mineralized rocks at the Mill Canyon, Copper Canyon, Buckhorn, Cortez silver, and Cortez gold deposits. The sample from the Cortez gold deposit consisted of small grains of pyrite in a quartz veinlet which escaped oxidation because of inclusion in the quartz. This pyrite is presumably representative of the microscopic pyrite that was disseminated in the deposit during mineralization. Also analyzed were pyrite from various localities in the Roberts Mountains Formation, sulfur from an active hot spring in Crescent Valley, and barite cement in breccia from Horse Canyon.

The δS^{34} values of all hydrothermal sulfides from the mineralized areas range from 4.5 to 15.3 per mil. In discussing the significance of sulfur isotopic variations it is essential to evaluate how much isotopic variation is due to fractionation among various minerals and to changes in the physical-chemical environment of the hydrothermal fluids as opposed to actual variations in the δS^{34} of the total sulfur content in the ore-forming fluids. Owing to the large fractionations of sulfur isotopes between reduced and oxidized sulfur species in hydrothermal solutions the δS^{34} values of precipitated sulfides can be greatly different from those of the total sulfur in solution. Thus, large variation in the δS^{34} values of specific minerals may reflect variations in the physical-chemical environment of ore deposition and not necessarily the mixing of sulfur from different sources (Ohmoto, 1972).

The absence of sulfates in the sulfide assemblages at all the mineralized areas and the observation that equilibration with the various igneous and limestone host rocks in the area would not result in extreme pH or f_{O_2} conditions in the hydrothermal fluids indicate that H_2S was the dominant sulfur specie in the hydrothermal solutions. Under these conditions the δS^{34} values of pyrite reflect fairly closely the δS^{34} values of the hydrothermal sulfur, and the δS^{34} variations of sulfides in the Cortez-Buckhorn area must reflect variations of the δS^{34} of the total sulfur in the hydrothermal solutions (Ohmoto, 1972). The wide range of δS^{34} values indicates that the hydrothermal sulfur was derived either from a heterogeneous source or from at least two sources of different isotopic composition. The large positive δS^{34} values for the hydrothermal sulfur indicate that all the sulfur in the area was derived from shallow crustal sources as opposed to deep-seated homogenized lower crustal or upper mantle sources from which presumably hydrothermal sulfur with δS^{34} values of 1–2 per mil is derived.

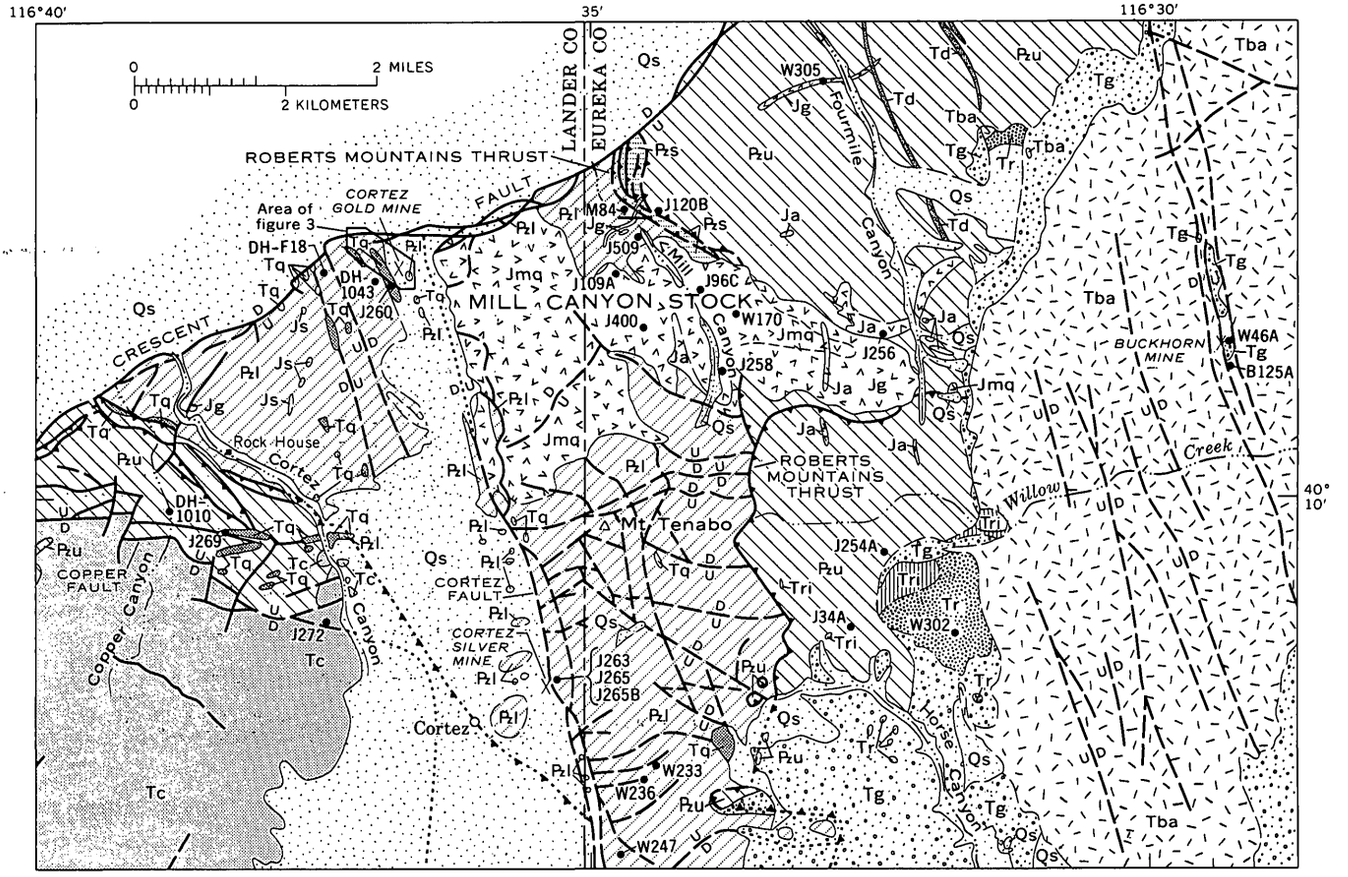

EXPLANATION

Qs — Quaternary surficial deposits

Tri, Tr — Rhyolite
Tri, *plugs*
Tr, *flows*

Tba, Td — Flows and dikes
Tba, *basaltic andesite flows*
Td, *diabase dikes*

Tg — Gravel

Tc, Tq — Volcanic rocks
Tc, *Caetano Tuff*
Tq, *quartz porphyry dikes*

TERTIARY

Jmq, Jmg, Ja, Jg, Js — Jurassic volcanic rocks
Jmq, *quartz monzonite of Mill Canyon stock*
Jmg, *granodiorite of Mill Canyon stock*
Ja, *alaskite*
Jg, *granodiorite*
Js, *augite syenite*

Pzl, Pzu, Pzs — Paleozoic rocks
Pzl, *lower plate eastern carbonate facies; includes Wenban Limestone, Roberts Mountains Formation, Hanson Creek Formation, Eureka Quartzite, and Hamburg Dolomite*
Pzu, *upper plate western siliceous facies; includes Slaven Chert, Fourmile Canyon Formation, Valmy Formation, and Vinini Formation*
Pzs, *sedimentary rocks undifferentiated; in thrust fault zone*

Contact
Dashed where approximately located; short dashed where gradational

U / D — High-angle fault
Dashed where approximately located; dotted where concealed. U, upthrown side; D, downthrown side

Thrust fault
Dashed where approximately located; dotted where concealed. Sawteeth on upper plate

DH-F18 — Sample locality

Figure 2.—Geologic map of the Cortez-Buckhorn area, showing sample localities. Modified from Wells, Elliott, and Obradovich (1971, fig. 2).

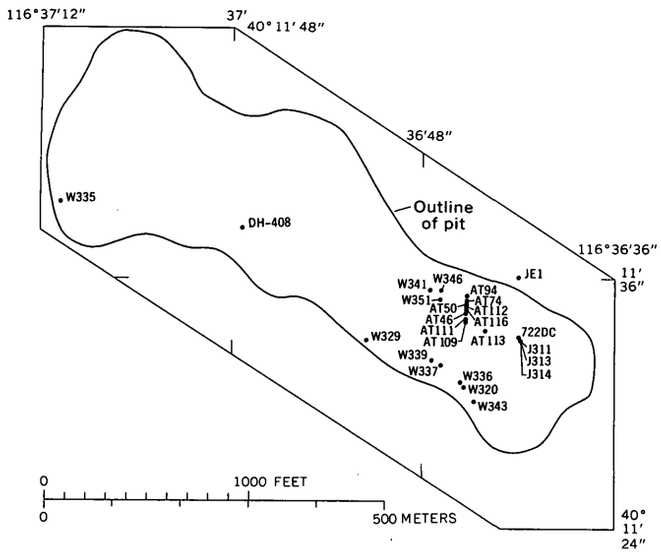

Figure 3.—Sketch map showing localities of samples from the Cortez gold mine. Area of map shown in figure 2.

It is interesting that native sulfur from the thermal springs in Crescent Valley which was formed by the oxidation of H_2S in the springs has a δS^{34} value of 10 per mil. This δS^{34} value indicates that now the hydrothermal sulfur in the area is also predominantly from a shallow crustal source (compare Schoen and Rye, 1970).

The Roberts Mountains Formation contains about 0.5 percent pyrite which is presumably of diagenetic origin. Wells, Stoiser, and Elliott (1969) suggested the pyrite in the Roberts Mountains Formation as a possible source for the gold in the Cortez deposit. In order to evaluate the possibility that the hydrothermal sulfur was derived from the Roberts Mountains Formation we analyzed samples of pyrite from three localities in the Roberts Mountains Formation. Two of these localities are considered to be far removed from possible influence of hydrothermal fluids.

The δS^{34} values for these samples range from 5.0 to 11.9 per mil. If these values are representative of the Roberts Mountains Formation as a whole, all the hydrothermal sulfur could have come from the formation. This observation is also consistent with the lead isotopic data (see later section).

The sulfur isotopic story is somewhat similar to that for Tertiary mineralization in the western Black Hills, S. Dak., where Precambrian sulfides were undoubtedly the source for much of the Tertiary sulfur (Rye and Rye, 1974). This is an important point to keep in mind for the future exploration of such areas because the source of the Tertiary sulfides may be older ore deposits or widely dispersed sulfides in preexisting rocks.

In the vicinity of the Mill Canyon stock δS^{34} values of sulfides tend to show a zonal relationship to the stock. The δS^{34} values or sulfides in the stock are 15.3 to 11.2 per mil, whereas those in the limestones at Mill Canyon and the surrounding mineralization in the area are 8.0 to 4.5 per mil. This distribution of δS^{34} values is similar to that observed for the Zeehan deposits of Tasmania (Both and others, 1969). The data, however, are very limited, and further analyses would be necessary to establish how much of the mineralization in the area has apparent genetic relationship to the Mill Canyon stock. Wells, Elliott, and Obradovich (1971) recognized three periods of igneous activity (Jurassic, Oligocene, Miocene) but could not determine if there were one, two, or three periods of mineralization in the Cortez-Buckhorn area. They noted that some of the mineralization must have occurred during the Miocene. The sulfur and lead isotope data (in later section) suggest that some of the mineralization near the Mill Canyon stock is probably Jurassic, indicating that there were at least two periods of mineralization in the area.

Hydrogen isotope data

Hydrogen isotope data are critical for a discussion of the origin and history of the hydrothermal fluids at Cortez. The hydrogen isotopic composition of the ore-forming fluids was determined directly by the analysis of water in one sample of fluid inclusions from a vuggy quartz veinlet in the oxidized ore zone. Indirect information on the δD of the ore fluids was determined from analyses of the clay alteration in the Oligocene quartz porphyry dike adjacent to the ore deposit. The hydrogen isotopic composition of postore fluids was determined directly from analyses of water in fluid inclusions in milky calcite. Finally, the δD of clay alteration at the Buckhorn mine was determined for comparison with the values at the Cortez gold mine (table 2).

A δD value of -128 per mil was obtained for the water in fluid inclusions in the quartz veinlet and an average value of -143 per mil for the water in inclusions in postore calcite. The δD values of -135 and -167 per mil were obtained for the clay alteration at the Cortez gold mine and the Buckhorn mine, respectively.

Present-day meteoric waters in the area average about -130 per mil. Sheppard, Nielsen, and Taylor (1969) have shown that the δD values of surface waters in most parts of the Western United States have probably not changed significantly since the early Tertiary. Deep-seated waters in hydrothermal fluids normally have δD values of -50 to -70 per mil (Rye and Sawkins, 1974). The large negative δD values prove that the fluids associated with the ore and alteration at the Cortez and the Miocene Buckhorn deposits and with the postore fluids at Cortez were predominantly of meteoric origin. The slight variation of δD values could indicate that some of the ore fluids contained a small percentage of deep-seated water, but there are not enough data to evaluate this possibility. The δD variations could have resulted from normal variations in meteoric waters over a given period of time. The δD data support a Tertiary age for the Cortez gold deposit (compare Wells and others, 1971). The mineralization could have

Table 1.—*The δS^{34} values of Cortez area sulfides, sulfates, and sulfur*
[Sample localities shown in figs. 2 and 3]

Sample	Locality	Sample description	δS^{34} values		
			Pyrite	Sphalerite	Other
M84	Mill Canyon	Oxidized ore in Wenban Limestone from dump.	6.65	....	[1] 4.90
J509	do	Fresh ore from Mays tunnel in Wenban Limestone.	8.05	5.58	[1] 5.89
J400	do	Quartz vein in Jurassic quartz monzonite.	.....	11.20	[1] 11.85
W170	do	Disseminated sulfides in Jurassic quartz monzonite.	15.32	.....	.....
DH-1010	Copper Canyon	Veinlet in drill sample in upper plate cherts and volcanics.	13.07	11.73	.....
W46A	Buckhorn	Pyrite and marcasite in altered breccia of basalt.	6.55	.....	.....
J263	Cortez silver deposit	Oxidized ore in Hamburg Dolomite	.....	.....	[1] 6.49
J265B	do	Unoxidized ore from Arctic tunnel	.....	7.48	.....
W305	Fourmile Canyon	Disseminated sulfides in intermediate dike.	4.69	.....	.....
W351	Cortez gold deposit	Unaltered pyrite preserved in quartz veinlet in oxidized ore.	5.42	.....	.....
DH-F18	0.8 km (0.5 mi) west of Cortez gold deposit.	Pyrite from Roberts Mountains Formation in unmineralized rock near Cortez gold deposit.	5.05	.....	.....
W233	2.6 km (1.6 mi) southeast of Cortez (town).	Pyrite from Roberts Mountains Formation 6.4 km (4 mi) south of Cortez gold deposit.	5.06	.....	.....
115TM	Northwest of Carlin, Nev. (not shown on fig. 2. Lat 40°52.5′ N., long 115°19′W.).	Pyrite from Roberts Mountains Formation in unmineralized area.	11.39	.....	.....
M552-C	Hot Spring in Crescent Valley, 24 km (15 mi) northeast of Cortez gold deposit (not shown on fig. 2. Lat 40°25′00″ N., long 115°30′5″ W.).	Sulfur from active hot springs	.....	.....	[2] 10.00
J34A	Horse Canyon	Barite cement in breccia	.....	.....	[3] 14.58

[1] Galena. [2] Sulfur. [3] Barite.

occurred during either the Oligocene or the Miocene igneous activity in the area. The fact that the Oligocene quartz porphyry dike that is in the Cortez deposit was intensely altered by meteoric waters suggests an Oligocene age as more probable.

Oxygen isotope data

Oxygen isotope data are essential in discussions of the thermal history of hydrothermal fluids and in discussions of the extent of interaction between hydrothermal fluids and wallrock. The δO^{18} values were determined on quartz and hematite in the small veinlets and postore calcites and on the calcite and dolomite components of the Roberts Mountains Formation from localities within and outside the Cortez deposit (tables 3, 4, and 5).

The δO^{18} values of quartz from the Cortez gold mine range from 6.4 to 18.3 per mil. This quartz occurs both as tightly grouped crystals and as chalcedony. The δO^{18} values of the crystalline quartz are considerably larger than those of chalcedonic varieties. Filling temperature of fluid inclusions, determined by Nash (1972, p. C17), indicates a temperature of deposition of about 200°C for the quartz veinlets at Cortez. This is probably near the temperature of ore deposition, assuming that the megascopic and microscopic quartz grains at Cortez are of the same generation.

By using the δO^{18} values for quartz in table 3, the 200° C temperature of deposition, and the experimental quartz-water fractionation curve, the δO^{18} of the hydrothermal fluids can be calculated. (The quartz-water oxygen isotope fractionation curve used in this study is $1{,}000 \ln\alpha = 3.57 \times 10^{-6} T^{-2} - 2.73$, where α is the fractionation factor, $\frac{O^{18}/O^{16}\ \text{quartz}}{O^{18}/O^{16}\ \text{water}}$, and T is the absolute temperature.) These calculations indicated a δO^{18} of about 4.8 per mil for the fluids in equilibrium with

Table 2.—*Hydrogen isotopic data of water in fluid inclusions and clay alteration*

[Sample localities shown in figs. 2 and 3]

Sample	Description	δD
	Cortez gold deposit	
J314 . . .	Fluid inclusions in 2.5-cm (1-in.) quartz veinlet from oxidized ore; well-defined crystals occur in center of the veinlet. Most of quartz is milky, indicating a high density of primary inclusions (see tables 3 and 4 for δO^{18} values and isotopic values of crosscutting calcite)	-128
J260 . . .	Kaolinite alteration in quartz porphyry dike adjacent to the Cortez gold deposit	-135
W336 . .	Fluid inclusions in dense white postore botryoidal calcite (for δO^{18} and δC^{13} values, see table 5)	-145
W346 . .	Fluid inclusions in acicular calcite in postore fracture in oxidized ore	-142
	Buckhorn mine	
B125A .	Kaolinite alteration of andesite volcanics near the Buckhorn mine	-167

Table 3.—*The δO^{18} of quartz and hematite from Cortez gold deposit and other localities*

[Sample localities shown in figs. 2 and 3]

Sample	Locality	Description	δO^{18}
J314 . .	Cortez gold deposit.	2.5-cm (1-in.) quartz veinlet with pyrite oxidized to hematite and crosscutting calcite.	18.23
W320 . .	. . . . do	6-mm (¼ in.) quartz veinlet with later calcite in oxidized ore.	17.59
W339 . .	. . . . do	6-mm (¼ in.) chalcedonic quartz veinlet in oxidized ore.	6.35
W341 . .	. . . . do	6-mm (¼ in.) chalcedonic quartz veinlet with later calcite.	12.48
J400 . .	Mill Canyon	Quartz in sulfide vein from quartz monzonite.	17.36
J265 . .	Cortez silver deposit.	Quartz in sulfide vein from Cambrian dolomite host rock.	17.89
AT113 .	Cortez gold deposit.	Hematite from high-grade gold ore separate.	-9.64
J313 . .	. . . . do	Hematite from quartz veinlet in oxidized ore.	-8.80
DH-408	. . . . do	Hematite from drill hole in oxidized ore.	-9.71

crystalline quartz and -6.8 to -0.7 per mil for the fluids in equilibrium with chalcedonic quartz. The large positive δO^{18} values for the crystalline quartz fluids indicate that the fluids underwent extensive exchange with silicate or limestone wallrocks. The negative δO^{18} values for the chalcedonic quartz fluids indicate that these fluids underwent less extensive exchange with the wallrocks than did the crystalline quartz fluids. This difference of δO^{18} values in the fluids may reflect a variation in the wallrock exchange history of the hydrothermal fluids with time during ore deposition or it may reflect mixing of meteoric waters from two sources in the area of ore deposition such as was observed at the Bluebell mine, British Columbia (Ohmoto and Rye, 1970).

The δO^{18} values of quartz from the other deposits in the area are similar to those observed in the Cortez gold deposit, and suggest deposition from waters having a δO^{18} and temperature that are similar to those of at least part of the mineralization of the Cortez gold deposit.

Calcite was leached from the Roberts Mountains Formation during ore deposition (Wells and Mullens, 1973); only rarely was dolomite leached from the rock. This leaching of calcite from the rock during the period of mineralization is reflected in the decrease of calcite: dolomite mole ratios in the ore versus those in unaltered Roberts Mountains Formation outside the Cortez area (table 4).

The δO^{18} values of calcite in the Roberts Mountains Formation in the ore deposit range from 9.4 to 13.3 per mil. These values are considerably lower than those values observed for the unaltered Roberts Mountains Formation several miles from the ore deposit (17.9 to 21.2 per mil). On the other hand, the δO^{18} values of dolomite in the wallrock in the ore deposit are only slightly lower than those observed in the unaltered parts of the Roberts Mountains. This fact is in accord with the observation that dolomite was generally unaffected by the hydrothermal process. The δO^{18} values of the fluids in equilibrium with the calcite of the Roberts Mountains in the ore deposit can be calculated assuming a temperature of 200°C (see earlier section) and the calcite-water equilibrium of O'Neil, Clayton, and Mayeda (1969). These calculated values range from 0.3 to 4.6 per mil and are compatible with the δO^{18} values calculated from the quartz data.

The postore calcites occur in acicular rhombohedral, botryoidal, and massive varieties whose paragenetic relationships are not known except that the varieties are all considered to be postore. At least one sample (W346) cuts upper Tertiary gravel beds.

The δO^{18} values of the calcites range from 9.3 to 15.5 per mil. The fact that these calcites have the same range of δO^{18} values as the calcite in the altered Roberts Mountains Formation wallrock is considered fortuitous. The temperature of deposition of these calcites is not known, but a reasonable estimate would be 50°C. At 50°C the δO^{18} values of the fluids would range from -15 to -12 per mil. These values are compatible with the negative δD values observed in the water in fluid inclusions in the calcite (Craig, 1961).

The δO^{18} values of the hematite oxidation product of pyrite in the quartz veinlets average about -9.2 per mil. This value is compatible with the δO^{18} value on the postore calcite and indicates that the oxidation of pyrite to hematite occurred at very low temperatures and probably during the precipitation of the calcite.

Table 4.—*The δO^{18} and δC^{13} values of calcite and dolomite in the Roberts Mountains Formation at the Cortez gold deposit and other localities*

[Sample localities shown in figs. 2 and 3]

Sample	Locality	Description	Calcite		Dolomite		Calcite:dolomite
			δO^{18}	δC^{13}	δO^{18}	δC^{13}	
AT46	Cortez gold deposit	Oxidized ore	.....	.....	20.27	-1.99	0
AT50	do	do	.....	.....	20.21	-1.68	0
AT74	do	do	12.38	-3.07	20.64	-1.79	....
AT94	do	Unoxidized host rock near ore.	13.63	-.46	20.92	-.47	1.9
AT109	do	Oxidized ore	.....	.....	20.42	-1.77	0
W320	do	do	.....	.....	16.03	-1.35	0
W335	do	do	12.28	-1.50	18.18	-.70	3.6
DH-1043	do	Unoxidized ore	9.36	-3.27	17.90	-3.67	.8
W233	2.6 km (1.6 mi) southeast of Cortez (town).	Unaltered limestone	17.92	-.88	21.34	-.84	2.3
W236	2.4 km (1.5 mi) southeast of Cortez (town).	do	21.20	-.20	20.93	-1.17	15.4
W247	2.6 km (1.6 mi) southeast of Cortez (town).	do	20.18	-.98	22.04	-1.19	9.5

Table 5.—*The δO^{18} and δC^{13} values of postore calcite at Cortez gold deposit and at Mill and Copper Canyons*

[Sample localities shown in figs. 2 and 3]

Sample	Description	δO^{18}	δC^{13}
	Cortez gold deposit		
AT116	White calcite in oxidized ore zone	10.53	-3.84
AT111	White calcite in brecciated ore	11.68	-2.25
J314	Brown rhombohedral calcite cutting quartz veinlet	11.32	-2.11
J311	White late calcite oxidized ore	10.68	-3.06
W320	Massive white calcite filling interior of quartz veinlet	13.78	-1.47
W329	Brown rhombohedral calcite	10.06	-2.40
W329	White massive calcite cutting brown variety	12.51	-1.50
W335	Clear calcite crystals in small vug	9.34	-2.02
W336	Veinlet of milky rhombohedral calcite crosscutting small quartz-hematite veinlet	12.07	-1.13
W337	Botryoidal calcite in oxidized ore	15.48	-1.43
W341	White botryoidal calcite on chalcedonic quartz	11.71	-2.39
W343	Late botryoidal calcite cementing upper Tertiary gravel	14.69	-1.35
	Mill Canyon		
J509	Rhombohedral calcite from massive ore from Wenban Limestone	4.45	-1.24
	Copper Canyon		
DH-1010	Calcite veinlet from drill sample in upper plate volcanics	10.53	-2.11

Carbon isotope data

Carbon isotope data on calcite can be used to determine the source of carbon in hydrothermal fluids. The carbon in the hydrothermal fluids of many postmagmatic deposits was derived from deep-seated rather than shallow limestone sources (Rye and Sawkins, 1974). In order to determine the δC^{13} of the hydrothermal fluids from δC^{13} data on calcite and limestone, information is needed on the temperature, pH, and f_{O_2} of the fluids (Ohmoto, 1972). There is not enough information available on the Cortez deposit to determine the f_{O_2} and pH of the fluids; however, the lack of evidence in the host rock for extremely low f_{O_2} values in the hydrothermal fluids suggests that most of the carbon in the hydrothermal fluid was present as CO_2 and at 200°C δC^{13} calcite $\approx \delta C^{13}$ $CO_2 \approx \delta C_{\Sigma C}^{13}$ (Bottinga, 1969; Ohmoto, 1972).

The δC^{13} values of the calcite in the Roberts Mountains Formation in the Cortez mine range from -0.5 to -3.3 per mil and are in the range of values observed in the unaltered Roberts Mountains and in the range of unaltered marine limestones in general (Keith and Weber, 1964). The lack of significant δC^{13} changes in the altered limestone host rock indicates that carbon present in the hydrothermal fluids probably had δC^{13} values in the range of those of marine limestones. This similarity is in accord with the observation that calcite was removed from the host rock during ore deposition and was probably the source of most of the hydrothermal carbon. It seems unlikely that a significant amount of deep-seated carbon was present in the hydrothermal fluids.

The δC^{13} values of the postore calcites range from -0.4 to -3.8 per mil. Although not enough is known about the nature of the parent solutions to be conclusive, the δC^{13} values suggest that the postore calcites were derived from the sedimentary marine limestone during thermal spring activity in the area (compare with Friedman, 1970).

Lead isotope data

The isotopic composition of lead in ores, sedimentary rocks, and igneous rocks from northern Nevada is given in table 6 and figure 4. For discussion of lead isotope systematics see Kanasewich (1968).

An unusual opportunity to follow the development of lead isotope ratios in igneous rocks with time is provided by the three periods of igneous activity represented—Jurassic, Oligocene, and Miocene. From figure 4 we see that there is little difference in the lead isotopic composition between the Miocene and Oligocene igneous rocks and that the values of $^{206}Pb/^{204}Pb$ are smaller than for the Jurassic igneous rocks, indicating that the Miocene and Oligocene rocks are somewhat less radiogenic. This relationship is not particularly surprising in that much of the uranium in a rock is easily mobilized and might well be included with its uranogenic lead in the first melting fractions. The value of $^{238}U/^{204}Pb$ must have been considerably reduced, and nonradiogenic lead must have been left behind in the source. The reduction is necessary in order to leave the source at 15–35 m.y. with less radiogenic lead than it had at about 150 m.y., when the approximately 100-m.y. interval for production of additional ^{206}Pb by radioactive decay of uranium is taken into account. Alternatively the Miocene-Oligocene rocks might have had a source different from that of the Jurassic rocks.

The value of $^{206}Pb/^{204}Pb$ in the alaskite dike phase (J256) of the quartz monzonite of the Mill Canyon stock is distinctly greater than for the stock and may be the consequence of natural contamination of the alaskite by country rock lead.

The galena samples are also closely grouped by lead isotope ratios, which are near those of the igneous rocks; this is suggestive of an igneous origin for the lead in the ores as previously concluded by A. P. Pierce and M. E. Delevaux (written commun., 1973). Although the spread in the lead isotope ratios between the Jurassic and Miocene-Oligocene igneous rocks is not great enough to make a good lead isotope "fingerprint" determination possible, four of the six galena samples fall on a mass-fractionation analytical error line of the sample from the Mill Canyon stock (samples H50b and AS96 are the two exceptions). These four galenas are tentatively considered to have resulted from Jurassic hydrothermal mineralization associated with rocks like the Mill Canyon stock or to have been leached from such rocks. Some ores, sample H50b for example, may have resulted from hydrothermal Miocene-Oligocene mineralization such as that which affected the rhyolite of Horse Creek, or they may be leached from such rocks. Values in sample AS96 are of indeterminate

Table 6.—*Lead isotope ratios from samples collected in north-central Nevada*

[Sample localities are shown in figs. 2 and 3 except those indicated by latitude and longitude. M.H. Delevaux, analyst for ores and feldspar W302; B. R. Doe, analyst for rocks. $\mu = {}^{238}U/{}^{204}Pb$, $k = {}^{232}Th/{}^{238}U$]

Sample	Atomic ratios (normalized to absolute) 206:204	207:204	208:204	Description
Ores from Cortez area				
AS96	19.53	15.73	39.09	Galena from upper plate rocks, Silver Prize mine, Lander County (lat 40° 21.5′ N., long 116° 43.6′ W.)
H50b	19.289	15.674	38.959	Galena from granodiorite that intrudes upper plate rocks, 1.6 km (1 mi) NNE. of Granite Mountain, Lander County (lat 40° 24.5′ N., long 116° 44.4′ W.)
J109A	19.47	15.76	38.98	Galena from vein in quartz monzonite (same unit as J96C).
J96C	19.42	15.71	38.79	Boulangerite from vein in quartz monzonite (Mesozoic).
J263	19.34	15.64	38.71	Galena in lower plate, Hamburg Dolomite, Cortez silver mine.
J120B	19.45	15.75	38.94	Galena from vein in lower plate rocks near and probably related to quartz monzonite stock. Vein is in Wenban Limestone.
Igneous rocks from Cortez area				
J269	19.32	15.70	39.12	Potassium feldspar, quartz porphyry at Rock House (upper plate rocks).
J272	19.25	15.67	38.95	Potassium feldspar Caetano Tuff.
J254A	19.38	15.76	39.33	Sanidine, rhyolite plug at Horse Creek (upper plate).
J256	19.74	15.74	39.25	Sanidine (alaskite dike phase of J258) from Fourmile Canyon (upper plate), probably Jurassic.
J258	19.50	15.80	38.87	Microcline, quartz monzonite of Mill Canyon, Jurassic age (lower plate).
W302	19.303	15.708	39.119	Potassium feldspar (Pb, 78.7 p/m; U, 2.36 p/m, Th, 3.42 p/m rhyolite flow on the divide north of Horse Canyon, 3,765 m (12,350 ft) north of Horse Ranch.
Roberts Mountains Formation from Cortez area				
W233	19.63	15.58	38.78	Residue from sample W233. Collected far from known ore, Cortez Mountains; Pb, 7.44 p/m; U, 3.94 p/m; Th, 7.73 p/m (μ 34.7; k, 2.02). Residue was 50.2 percent.

Table 6.—*Lead isotope ratios from samples collected in north-central Nevada*—Continued

Sample	Atomic ratios (normalized to absolute) 206:204	207:204	208:204	Description
Roberts Mountains Formation from Cortez area—Continued				
W233 . .	21.36	15.77	39.04	HCl-soluble fraction from sample W233; Pb, 6.16 p/m; U, 3.06 p/m; Th, 3.25 p/m (μ 33.5; κ 1.10).
W233 . .	20.12	15.69	38.63	Pyrite from sample W233, HNO_3 soluble.
722DC .	[1]19.64 [2]19.58	[1]15.75 [2]15.69	[1]38.81 [2]38.63	Pyrite, HNO_3 soluble. Collected from portal of Cortez gold mine. Only slightly altered.
JE1 . . .	20.30	15.67	39.13	Whole-rock sample of Cortez ore; Pb, 14.92 p/m; U, 4.29 p/m; Th, 5.41 p/m (μ, 19.1; κ, 1.3) 87.6 percent residue.
JE1 . . .	20.25	15.72	39.38	HCl-soluble fraction of Cortez ore. Leach was 35.1 p/m Pb for dissolved fraction or 13.2 p/m in terms of the whole rock; residue was 62.3 percent.
AT112 .	20.31	15.73	39.22	Residue of Cortez ore sample AT112. Pb, 1.21 p/m; U, 3.30 p/m; Th, 5.97 p/m (μ, 181.7; κ, 1.87). Residue was 44.1 percent.
AT112 .	19.64	15.67	38.84	HCl-soluble fraction of Cortez ore sample AT112. Pb, 20.4 p/m; U, 3.23 p/m; Th, 4.33 p/m (μ, 10.4; κ, 1.4).
Ore from Wheeler Peak area				
L-1 . .	19.15	15.68	39.10	Quartz vein outcropping with galena, southern Snake Range, White Pine County (lat 38° 58.5′ N., long 114° 21.5′ W.)
Ores from the Ruby Mountains area				
63W56 .	18.689	15.726	38.607	Galena from a vein in Middle Cambrian limestone about 0.2 km (0.125 mi) from contact with Oligocene pluton, Elko County (lat 40° 17′ N., long 115° 29′ W.).
64W25 .	18.64	15.72	38.30	Galena from a vein in Middle Cambrian limestone about 0.2 km (0.125 mi) from contact with Oligocene pluton, Elko County (lat 40° 21′ N., long 115° 38′ W.).
65W61 .	18.71	15.74	38.17	Galena from a replacement of dolomitized Cambrian limestone at contact with overlying thrust plate of chert and fine-grained quartzite, White Pine County (lat 40° 5′ N., long 115° 38′ W.).

Table 6.—*Lead isotope ratios from samples collected in north-central Nevada*—Continued

Sample	Atomic ratios (normalized to absolute) 206:204	207:204	208:204	Description
Ores from Battle Mountain area				
R-1 . .	19.04	15.45	38.23	Galena from the Nevada mine, Humboldt County (lat 40° 33′ N., long 117° 7.5′ W.).
AEH251	19.260	15.686	39.000	Galena from the White and Shiloh mine, Humboldt County (lat 40° 33′ N., long 117° 8′ W.).
ICPG .	19.24	15.58	38.65	Gold concentrate from Iron Canyon, Humboldt County (may contain some galena) lat 40° 32.5′ N., long 115° 5′ W.).
Ore from the Carlin gold mine				
L-2-10 .	19.77	15.87	39.51	Galena from a veinlet in Carlin gold ore, Eureka County (lat 40° 52.5′ N., long 116° 19′ W.).

[1] Noisy run.
[2] Reinsert at a later time. Quiet run.

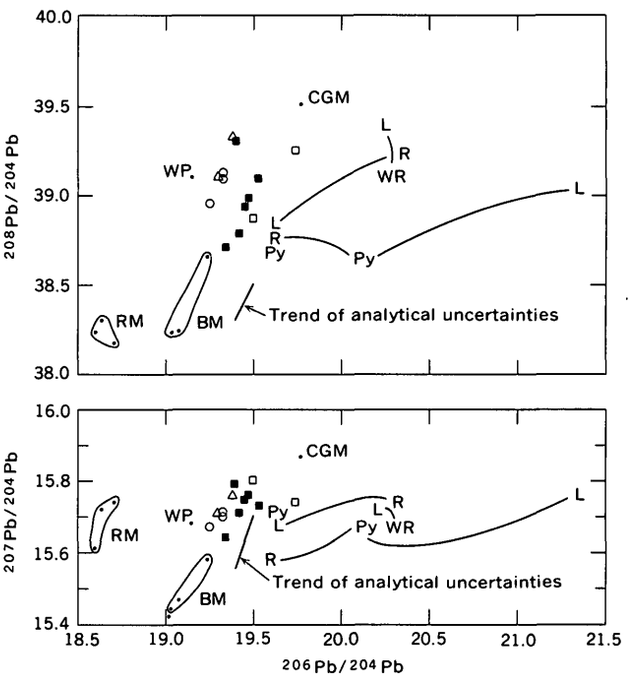

Figure 4.—$^{207}Pb/^{204}Pb$ and $^{208}Pb/^{204}Pb$ versus $^{206}Pb/^{204}Pb$ for ores, sediments, and igneous rocks of northern Nevada. Galenas from the Cortez area (■) and other areas (.): WP, Wheeler Peak; RM, Ruby Mountains; BM, Battle Mountain; CGM, Carlin gold mine. Igneous rocks from Cortez area: □, Jurassic; ○, Oligocene; and △, Miocene. Sedimentary rocks from Roberts Mountains Formation in Cortez area: R, residue; L, HCl leach; WR, whole-rock; Py, pyrite. The different analyzed fractions from an individual sample are connected by the curved lines.

origin, and they well could represent naturally contaminated lead from the Miocene-Oligocene or Jurassic igneous rocks inasmuch as the ore fluid transected country rock and could have acquired additional lead.

The ore-igneous rock fingerprint is more significant when it is compared with analyses of galenas from elsewhere and when data on lead in host sediments of the Cortez gold ore are included (fig. 4), which show that other isotopic compositions are present in the region. In addition, the sulfur isotope data on the ores indicate a zoning pattern around the Mill Canyon stock, which further supports a Jurassic mineralization age for many of the galena ores.

Leads in the Silurian Roberts Mountains Formation, analyzed because the formation is the host of the Cortez gold ore, are generally more radiogenic today than the leads in the igneous rocks. The isotopic ratios in this silty limestone unit are in general similar to those found in Paleozoic limestones elsewhere in Nevada and in Missouri (Doe, 1970). Because the limestones have a significant amount of uranium relative to lead, comparison of present-day lead isotope ratios in the limestone with those of the galenas is not proper unless the galenas formed recently. If we assume that the galena mineralization occurred in the Jurassic and that the value of $^{238}U/^{204}Pb$ for the whole rock has not been altered since then, the unaltered sample of Roberts Mountains (W233) would have had a $^{206}Pb/^{204}Pb$ value 150 m.y. ago, of about 19.7, still greater than the values for galena. The assumption concerning $^{238}U/^{204}Pb$ may not be a bad one for this sample even though other limestones seem to have undergone recent alterations in this ratio (Doe, 1970). The $^{238}U/^{206}Pb$ age for sample W233 is 500 m.y. and was calculated assuming a 500-m.y.-old initial model lead.

The altered, mineralized, and oxidized whole-rock sample (JE1) from the Cortez gold mine would have given a similar $^{206}Pb/^{204}$ Pb value of 19.8 150 m.y. ago, but the other altered, mineralized, and oxidized sample from the Cortez gold mine (AT112) calculated on a whole-rock basis would fall in the ore-igneous rock field (D19.3). Both altered samples would give ages greater than 500 m.y. by the $^{238}U/^{206}Pb$ method, assuming a 500-m.y.-old initial model lead. Because the uranium contents of the altered samples are rather similar to those of the unaltered sample (W233), the old "age" is best accounted for by a net addition of lead to the mineralized samples relative to uranium. Indeed, HCl-leachable lead that is less radiogenic than residue lead is unusual, and it seems likely that ore lead has been added to the HCl-leachable fraction of sample AT112. Lead added to sample JE1 (oxidized ore) appears to have been locally derived limestone lead. The pyrite sample 722DC (slightly altered) also is close to the galena field as if some galena ore lead is contained in it (the uranium and lead contents of the pyrites were not determined, but the uranium contents are usually low; Wampler and Kulp, 1964). The value of $^{206}Pb/^{204}Pb$ for pyrite from the unaltered sample (W-233) is intermediate between the HCl-soluble and residue fractions. There is no evidence of galena lead in this pyrite, and, in addition, the pyrite is almost certainly not diagenetic but must have been formed much after deposition. The unaltered sample may well have been reconstituted in the Jurassic, inasmuch as the leachable lead fraction would have approximated the pyrite lead isotopic composition about 150 m.y. ago, assuming that the observed value of $^{238}U/^{204}Pb$ applies to that period of time. Everything considered, apparently the altered and mineralized Roberts Mountains rock at the Cortez gold mine, rather than being the source of lead for any galena ores, had galena lead added to it, perhaps about 150 m.y. ago but possibly more recently.

No untreated gold was available from the Cortez gold mine; therefore, any conclusions concerning the origin of the gold based on the lead isotope data from altered oxidized rock mineralized are speculative. In one sample of altered host rock for the gold ore there is evidence, which might be taken to support a hydrothermal gold mineralization, of some galena-type lead having been added to the pyrite and to the HCl-soluble phase. In another sample of altered mineralized rock, however, the added lead seems to have been locally derived because the whole-rock lead isotopic composition is similar to that of an unaltered sample, which at least shows that the gold mineralization was not necessarily accompanied by significant introduction of lead. This possibility is in agreement with results of analyses which show very little lead in the ore (Wells and others, 1969). When the lead isotope data of sample JE1 are coupled with the sulfur isotope data, the probabilities slightly favor a local derivation for the gold at the Cortez gold mine.

CONCLUSION

1. The sulfur in the mineralization at Cortez and the surrounding area was derived from either a single heterogeneous source or two independent upper crustal sources. The data are compatible with the possibility that all sulfur was derived from the Roberts Mountains Formation.

2. Meteoric waters were the dominant component in the ore-forming fluids at the Cortez deposit and probably for the Miocene mineralization in the Buckhorn area. Meteoric water, probably in thermal springs, was also responsible for the precipitation of the postore calcite in the Cortez gold deposit. The δD values of the meteoric waters are compatible with the δD values of a Tertiary age for the deposit.

3. The oxidation of the ore was caused by low-temperature ground waters whose δO^{18} values were distinctly different from those of the ore-forming fluids. The oxidation probably occurred during the deposition of the postore calcite.

4. The isotopic data indicate that the δO^{18} of the hydrothermal fluids was highly variable, suggesting either a complex wallrock-exchange history for the meteoric hydrothermal fluids or the mixing of meteoric waters from two different sources in the area of ore deposition.

5. The absence of carbon isotopic alteration of the host rock indicates that little deep-seated carbon was present in the hydrothermal fluids. The precipitation of postore calcite probably resulted from the solution, transport, and redeposition of the host rock in a thermal spring system.

6. Four of the six galenas in the Cortez area have lead isotope ratios similar to those of the Jurassic Mill Canyon stock, suggesting that these ores are genetically related to the stock. The apparent zoning in δS^{34} values in galenas about this stock further supports an origin of the galenas from this stock and a Jurassic age for much of the galena mineralization.

7. When the lead isotope data on mineralized and unaltered Roberts Mountains Formation, the host rock of the gold ore, are coupled with the sulfur isotope data, the probabilities slightly favor a local derivation for the gold at the Cortez gold mine.

ACKNOWLEDGMENTS

We thank the many mine and claim owners for permitting access to their lands and generally facilitating our work. Particular thanks are extended to the Cortez gold mine for access to their property. Samples for the lead isotope study were submitted by C. T. Wrucke, J. E. Elliott, R. J. Roberts, T. G. Theodore, H. A. Tourtelot, C. R. Willden, and D. E. Lee.

REFERENCES CITED

Both, R. A., Rafter, T. A., Solomon, M., and Jensen, M. L., 1969, Sulfur isotopes and zoning of the Zeehan mineral field, Tasmania: Econ. Geology, v. 64, no. 6, p. 618–628.

Bottinga, Y., 1969, Calculated fractionation factors for carbon and hydrogen isotope exchange in the system calcite-carbon dioxide-graphite-methane-hydrogen-water vapor: Geochim. et Cosmochim. Acta, v. 33, no. 1, p. 49–64.

Craig, Harmon, 1957, Isotopic standards for carbon and oxygen and correction factors for mass-spectrometric analysis of carbon dioxide: Geochim. et Cosmochim. Acta, v. 12, nos. 1–2, p. 133–149.

——1961, Standard for reporting concentrations of deuterium and oxygen-18 in natural waters: Science, v. 133, no. 3467, p. 1833–1834.

Czamanske, G. K., and Rye, R. O., 1974, Experimental determination of sphalerite-galena sulfur isotope geothermometer: Econ. Geology. (In press.)

Doe, B. R., 1970, Evaluation of U-Th-Pb whole-rock dating on Phanerozoic sedimentary rocks: Eclogae Geol. Helvetiae, v. 63, no. 1, p. 79–82.

Erickson, R. L., VanSickle, G. H., Nakagawa, H. M., McCarthy, J. H., Jr., and Leong, K. W., 1966, Gold geochemical anomaly in the Cortez district, Nevada: U.S. Geol. Survey Circ. 534, 9 p.

Friedman, Irving, 1970, Some investigations of the deposition of travertine from Hot Springs, Pt. I, The isotopic chemistry of a travertine depositing spring: Geochim. et Cosmochim. Acta, v. 34, no. 12, p. 1303–1315.

Kanasewich, E. R., 1968, The interpretation of lead isotopes and their geological significance, *in* Hamilton, E. I., and Farquhar, R. M., eds., Radiometric dating for geologists: London and New York, Interscience Publishers, p. 147–223.

Keith, M. L., and Weber, J. N., 1964, Carbon and oxygen isotopic composition of selected limestones and fossils: Geochim. et Cosmochim. Acta, v. 28, no. 11, p. 1787–1816.

Nash, J. T., 1972, Fluid-inclusion studies of some gold deposits in Nevada, *in* Geological Survey research 1972: U.S. Geol. Survey Prof. Paper 800-C, p. C15–C19.

Ohmoto, Hiroshi, 1972, Systematics of sulfur and carbon isotopes in hydrothermal ore deposits: Econ. Geology, v. 67, no. 5, p. 551–578.

Ohmoto, Hiroshi, and Rye, R. O., 1970, The Bluebell mine, British Columbia, Canada, Pt. I, Mineralogy, paragenesis, fluid inclusions, and the isotopes of hydrogen, oxygen, and carbon: Econ. Geology, v. 65, no. 4, p. 417–437.

O'Neil, J. R., Clayton, R. N., and Mayeda, T. K., 1969, Oxygen isotope fractionation in divalent metal carbonates: Jour. Chem. Physics, v. 51, no. 12, p. 5547–5558.

Roberts, R. J., Radtke, A. S., and Coats, R. R., 1971, Gold-bearing deposits in north-central Nevada and southwestern Idaho, *with a section on* Periods of plutonism in north-central Nevada, by M. L. Silberman and E. H. McKee: Econ. Geology, v. 66, no. 1, p. 14–33.

Rye, D. M., and Rye, R. O., 1974, Origin of the Homestake gold deposit, South Dakota, in the light of stable isotope studies: Econ. Geology. (In press.)

Rye, R. O., and Sawkins, F. J., 1974, Fluid inclusion and stable isotope studies on the Casapalca Ag-Pb-Zn-Cu deposit, central Andes, Peru: Econ. Geology. (In press.)

Schoen, Robert, and Rye, R. O., 1970, Sulfur isotope distribution in solfataras, Yellowstone National Park: Science, v. 170, no. 3962, p. 1082–1084.

Sheppard, S. M. F., Nielsen, R. L., and Taylor, H. P., Jr., 1969, Oxygen and hydrogen isotope ratios of clay minerals from porphyry copper deposits: Econ. Geology, v. 64, no. 7, p. 755–777.

Wampler, J. M., and Kulp, J. L., 1964, An isotopic study of lead in sedimentary pyrite: Geochim. et Cosmochim. Acta, v. 28, no. 9, p. 1419–1458.

Wells, J. D., Elliott, J. E., and Obradovich, J. D., 1971, Age of the igneous rocks associated with ore deposits, Cortez-Buckhorn area, Nevada, *in* Geological Survey research 1971: U.S. Geol. Survey Prof. Paper 750-C, p. C127–C135.

Wells, J. D., and Mullens, T. E., 1973, Gold-bearing arsenian pyrite determined by microprobe analysis, Cortez and Carlin gold mines, Nevada: Econ. Geology, v. 68, no. 2, p. 187–201.

Wells, J. D., Stoiser, L. R., and Elliott, J. E., 1969, Geology and geochemistry of the Cortez gold deposit, Nevada: Econ. Geology, v. 64, no. 5, p. 526–537.

Jour. Research U.S. Geol. Survey
Vol. 2, No. 1, Jan.-Feb. 1974, p. 25–29

PANTELLERITE FROM THE HART MOUNTAIN AREA, SOUTHEASTERN OREGON—INTERPRETATION OF RADIOMETRIC, CHEMICAL, AND ISOTOPE DATA

By D. C. NOBLE[1], E. H. McKEE, and G. W. WALKER,
Menlo Park, Calif.

Abstract.—Two pantellerites from the Hart Mountain area of southeastern Oregon have been dated at about 25–27 m.y. by potassium-argon methods. Calculated major- and minor-element contents of the groundmass of the phenocryst-rich lavas are very similar to those of high-alumina pantellerite lavas and tuffs from Pantelleria and other localities. An initial Sr^{87}/Sr^{86} ratio of 0.7034±0.0002 determined on phenocrystic anorthoclase from one specimen indicates a subcrustal origin for the parent magmas. The very low initial Sr^{87}/Sr^{86} ratio and the relatively high K:Rb ratios of 450 and 330 strongly suggest that the parent mafic magmas were derived from mantle material that had been markedly depleted in incompatible elements, which are strongly partitioned into a melt phase by a much earlier episode of magma generation. Data on the Hart Mountain rocks support the interpretation that at least some of the early Miocene silicic tuffs and lavas of eastern Oregon and northwestern Nevada are differentiation products of mafic magmas of subcrustal origin.

The first geologic, petrographic, mineralogic, and chemical data on phenocryst-rich pantellerite lavas from the Hart Mountain area, southeastern Oregon (fig. 1) were those of Walker (1961). Although peralkaline silicic tuffs and lavas have since been shown to be common in the northwestern Great Basin (Noble and others, 1968, 1970, 1973; Noble, McKee, and Creasy, 1969; Walker and Swanson, 1968a; Walker, 1969), rocks of the Hart Mountain area remain the most highly peralkaline recognized in the region. Because interpretation of these rocks is important to the understanding of both the origin of peralkaline salic melts and the tectonic significance of middle and late Cenozoic volcanic rocks of the Western United States, we have obtained additional radiometric, chemical, and isotopic data on the two specimens originally studied by Walker.

POTASSIUM-ARGON AGE DETERMINATIONS

The pantellerite lavas of the Hart Mountain area are overlain by mafic and intermediate lavas correlative with part of the Steens Basalt (Walker and Repenning, 1965). In its type section on Steens Mountain, the Steens Basalt has been dated by potassium-argon methods at about 15.3 m.y. (Baksi, York, and Watkins, 1967). South of Hart Mountain, lavas apparently representing a lower part of the Steens Basalt are overlain by the Idaho Canyon Tuff, an areally extensive ash-flow sheet with a potassium-argon age of 15.6 to 16 m.y. (Noble and others, 1970; Walker and Repenning, 1965; D. C. Noble, unpub. data, 1973). Prior to the present work, the pantellerites of the Hart Mountain area were presumed by us to be of middle and late Miocene age, in part because peralkaline silicic volcanic rocks appeared to be restricted to the middle and upper Miocene and Pliocene in other parts of the northwestern Great Basin. Walker and Swanson (1968b), however, recognizing a regional unconformity at the base of the Steens Basalt, suggested the possibility that the unit containing the

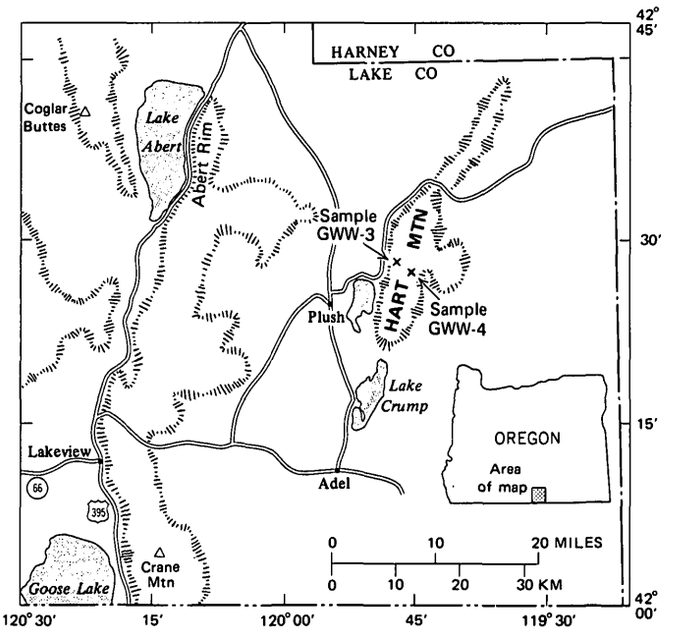

Figure 1.—Sample localities in the Hart Mountain area.

[1] MacKay School of Mines, Univ. Nevada, Reno, Nev. 89507

pantellerites might be as old as Oligocene. Potassium-argon age determinations (table 1) obtained on phenocrystic anorthoclase separated from the two specimens studied by Walker (1961) show that the rocks are of latest Oligocene and (or) earliest Miocene age.

Table 1.—*Potassium-argon age determination on anorthoclase phenocryst separates from two specimens of pantellerite lava*

[Argon determinations by E. H. McKee using standard isotope-dilution methods (Dalrymple and Lanphere, 1969). Potassium analyses by L. B. Schlocker using a flame-photometer procedure with lithium as an internal standard. K^{40} decay constants: $\lambda\epsilon = 0.585\times10^{-10}$ yr^{-1}; $\lambda\beta = 4.72\times10^{-10}$ yr^{-1}. Abundance ratio: $K^{40}/K = 1.19\times10^{-4}$ atom per atom]

Specimen	K^2O (wt percent)	Radiogenic Ar^{40} (mol/g)	Radiogenic Ar (percent)	Age (m.y.)
GWW-3-60	4.89	1.999×10^{-10}	72.66	27.5±0.8
	4.95	1.999×10^{-10}	63.33	27.1±0.8
GWW-4-60	4.87	1.811×10^{-10}	74.52	25.0±0.8

MAJOR- AND MINOR-ELEMENT COMPOSITION

Chemical analyses of two specimens from Hart Mountain and selected pantellerite analyses from the literature are given in table 2. The calculated groundmass composition of specimen GWW-3-60 (table 2) shows how the high phenocryst content (>30 percent, mainly anorthoclase) of the rocks (Walker, 1961) tends to obscure their pantelleritic character. The somewhat low Na_2O content of the Hart Mountain specimens compared with other pantellerites probably reflects the well-known tendency for peralkaline silicic igneous rocks to lose appreciable amounts of Na on crystallization.

Quantitative optical emission spectrographic analyses are supplemented by X-ray fluorescence determinations of Rb and Sr in table 3.

Table 2.—*Major-element analyses, in weight percent, of pantellerites from the Hart Mountain area and other localities*

Specimen	1	2	3	4	5	6
SiO_2	69.4	68.6	71.3	69.7	68.1	69.41
Al_2O_3	13.2	13.5	11.5	10.8	10.2	10.64
Fe_2O_3	3.2	3.1	4.1	1.9	8.56	(1)
FeO	1.8	1.8	2.2	4.2	(2)	6.81
MgO.....	.05	.03	.02	.23	<.1	.26
CaO	.30	.52	.3	.44	.75	.64
Na_2O	5.8	5.8	5.0	6.4	6.30	6.12
K_2O	4.6	4.7	4.5	4.7	4.54	4.46
H_2O	1.0	1.0	.....	.15	.....	.....
TiO_2	.35	.37	.5	.50	.44	1.17
ZrO_2	.08	.08	.12	.18	.13	.....
P_2O_5	.05	.03	.04	.07	<.1	.12
MnO	.18	.17	.2	.30	.18	.36
CO_2	<.05	<.05	.....	.....	.....	.....

[1] Fe_2O_3 not recorded; total iron as FeO.
[2] FeO not recorded; total iron as Fe_2O_3.

Table 2.—*Major-element analyses, in weight percent, of pantellerites from the Hart Mountain area and other localities—Continued*

1. Crystallized pantellerite lava GWW-4-60, Lake County, Oreg. Data from Walker (1961), except ZrO_2 values, from table 3, this paper.
2. Crystallized pantellerite lava GWW-3-60, Lake County, Oreg. Data from Walker (1961), except ZrO_2 values, from table 3, this paper.
3. Approximate groundmass composition (anhydrous) of specimen 2 calculated from modal data and chemical data assuming reasonable Ca contents for the anorthoclase phenocrysts and reasonable compositions for the mafic phases (Carmichael, 1962, tables II, IV, and V).
4. Nonhydrated pantellerite glass of high-alumina type, Pantelleria, Italy. Data from Zies (1960), Carmichael (1962), and Noble and Haffty (1969).
5. Average nonhydrated vitric pantellerite ash-flow tuff, flow unit C, Fantale volcano, Ethiopia. Data from Gibson (1970).
6. Average crystallized pantellerite ash-flow tuff, middle unit, Gran Canaria. Data from Schmincke (1969).

Strontium and barium content

Although the pantellerites from the Hart Mountain area are highly differentiated compared with most silicic igneous rocks, their Sr and Ba contents,[1] sensitive measures of the amount of feldspar fractionation, are higher than those of many comendites and pantellerites (for example, Noble Haffty, and Hedge, 1969; Ewart and others, 1968). The high Ba:Sr ratios (≈25) suggest that the Hart Mountain pantellerites were derived from relatively potassium-poor parent magmas that were unable to crystallize alkali feldspar until relatively late in their differentiation. Crystallization of plagioclase preferentially extracts Sr from igneous melts, whereas Ba is concentrated almost entirely in the residual liquid (Korringa and Noble, 1971). Alkali feldspar, on the other hand, has a strong affinity for both Ba and Sr. Barium would have been less strongly enriched relative to Sr had major early separation of alkali feldspar taken place during the protracted crystal fractionation leading to the generation of the Hart Mountain pantellerites.

Potassium-rubidium ratios

The K:Rb ratios, 450 and 330, of the two Hart Mountain specimens are high for silicic igneous rocks. We feel the value of 450 obtained on specimen GWW-3-60 is more significant, as this rock is denser than GWW-4-60 and less likely to have had Rb added by vapor-phase transport (Hart and others, 1971) or secondary ground-water processes. The anorthoclase phenocryst separate from specimen GWW-3-60 (Korringa and Noble, 1971) has a Rb content of 26 p/m and a K:Rb ratio of 1570.

[1] Part of the Sr in the whole-rock specimens, particularly CWW-4-60, which is relatively porous, may be foreign Sr added through the interaction of strontium-bearing ground water with the fine-grained parts of the rocks. This possibility is based on analytical data on other crystallized silicic volcanic rocks (D. C. Noble, Joseph Haffty, and C. E. Hedge, unpub. data) that suggest that such rocks readily take up Sr from ground water and by the anomalously low distribution coefficient for Sr between melt and phenocryst phases computed using the XRF values for Sr obtained on specimen GWW-3-60 and the anorthoclase specimen from this rock (Korringa and Noble, 1971).

Table 3.—*Quantitative optical emission spectrographic analyses in weight percent, of pantellerites from the Hart Mountain area and other localities*

[Analyses made by methods similar to those described by Bastron and others (1960). Joseph Haffty, analyst. See columnar notes, table 2 for specimen description. N.d. not determined]

Specimen	1	2	4	5
B	0.002	0.004	0.001	N.d.
Ba	.051	.054	.005	0.053
Be	.004	.005	.0005	N.d.
Ce	[1].03	[1].03	N.d.	N.d.
Co	<.0002	<.0002	<.0005	N.d.
Cr	<.0001	<.0001	<.0001	N.d.
Cu	.0004	.0002	.0003	N.d.
Ga	.0035	.0035	.0043	N.d.
La	.012	.008	.023	.010
Mo	.0002	.0003	.0022	N.d.
Nb	.007	.008	.032	.013
Nd	[1].015	[1].015	N.d.	N.d.
Ni	<.0002	<.0002	.0004	N.d.
Pb	.002	.002	.002	N.d.
Rb	[2].0116	[2].0087	N.d.	N.d.
Sc	.0002	.0002	.0006	N.d.
Sn	.0008	.0008	.0014	N.d.
Sr	[2].002	[2].0009	.0003	.003
	.0030	.0019		
V	<.0005	<.0005	<.0005	N.d.
Y	.0077	.0076	.014	.010
Yb	.0008	.0008	.0010	N.d.
Zr	.056	.060	.16	.093

[1] Semiquantitative optical emission spectrographic methods. J. C. Hamilton, analyst.

[2] Quantitative X-ray fluorescence methods. L. F. Espos, analyst.

Simple mass-balance calculations using the modal data given by Walker (1961) show that the Rb content and K:Rb ratio of the groundmass are approximately 106 p/m and 350, respectively. The K:Rb ratio of the groundmass of the rock thus is about 0.22, the same as that of the associated anorthoclase phenocrysts, and in good agreement with the values obtained by Noble and Hedge (1970) for other peralkaline and subalkaline silicic volcanic rocks.

The anorthoclase is low in Sr (32 p/m), and presumably also in Ca, and is not zoned inward to (cored by) sodic plagioclase. This and the very low Sr and Ca contents of the rocks suggest that prolonged fractional crystallization of plagioclase and mafic minerals from more primitive magmas first had to produce a sufficient increase in K and decrease in Ca for anorthoclase to crystallize before significant amounts of anorthoclase could then separate to produce residual liquids of approximately the composition of the whole-rock specimens. A K:Rb ratio greater than 600 for the original liquid prior to separation of 33 wt percent anorthoclase is determined using approximate coefficients for the partition of K and Rb between alkali feldspar and melt phases from the analytical and modal data on specimen GWW-3-60. Although a quantitative inference of the K:Rb ratios of the initial magmas cannot be made, a value of 700, and possibly greater, appears reasonable.

The possibility does exist, although we consider it unlikely, that the elevated K:Rb ratios reflect accumulation of anorthoclase phenocrysts that, prior to eruption, had settled into the Hart Mountain magma from hypothetical overlying magma. Although such a mechanism was suggested by Noble and Hedge (1970) to explain the high K:Rb ratios found in certain highly feldspathic syenites and trachytes within the Black Mountain caldera in southern Nevada, we have no field or other evidence to suggest that it is applicable to the Hart Mountain rocks. Moreover, the rocks from the Hart Mountain area are not the only Cenozoic igneous rocks from the northwestern Great Basin to have high K:Rb ratios. Certain flows of the Steens Basalt in southeastern Oregon have K:Rb ratios of 600 to 900 (Gunn and Watkins, 1970); an early Miocene basalt and an aphyric silicic obsidian of late Miocene age from northwestern Nevada have K:Rb ratios greater than 900 and 600, respectively (Noble and others, 1970; 1973). Clearly, however, K and Rb data on additional specimens are required to bear out or refute the proposed mechanism.

Minor-element and rare-earth content

The somewhat elevated B, Be, Ga, Nb, Sn, Y, Zr, and rare-earth contents of the Hart Mountain specimens are characteristic of peralkaline igneous rocks, but nevertheless are lower than the values observed for many pantellerites (for example, table 3, specimen 4), probably largely because the parent magmas were derived from depleted mantle material, as discussed below. As all the above elements except Ga and perhaps Be are concentrated almost entirely in the residual liquid during fractional crystallization of peralkaline salic melts, the concentration of these elements in the groundmass of the crystal-rich specimens should be about 50 percent greater than in the whole rock.

INITIAL STRONTIUM ISOTOPE COMPOSITION

Because the Hart Mountain rocks are poor in Rb relative to some other peralkaline rocks, anorthoclase phenocryst separates prepared from the specimens have relatively low Rb:Sr ratios (compare Noble and others, 1973), allowing precise determination of the Sr^{87}/Sr^{86} ratio for the time of eruption. The initial Sr^{87}/Sr^{86} ratio of specimen GWW-3-60, 0.7034 (table 4), is lower than the average of values of 0.7033 to

Table 4.—Strontium isotope composition of phenocrystic anorthoclase from specimen GWW-3-60

[Strontium isotope composition was determined in the U.S. Geological Survey laboratories on a 6-in., 60° sector, Neir-type mass spectrometer utilizing a triple rhenium-filament mode of ionization. D. C. Noble, analyst. The mass spectrometer gives a value of 0.7080 for the Eimer and Amend standard $SrCO_3$. All data have been normalized to a value of 0.1194 for Sr^{86}/Sr^{88}. The Rb:Sr ratio was determined by quantitative X-ray fluroescence methods. Subscript i indicates ratio calculated for the time of eruption, o indicates observed ratio]

Rb:Sr	0.800	Sr^{87}/Sr_i^{86}	0.7034
Sr^{87}/Sr_o^{86}	.70428	Deviation (2σ)	.0002

0.7046 obtained on mafic and intermediate lavas of Miocene, Pliocene, and Quaternary age from northwestern Nevada and eastern Oregon (Hedge and others, 1970; Noble and others, 1973). The initial ratio is slightly lower than the average for young basalts from oceanic areas and appreciably lower than the present-day ratio of approximately 0.706 inferred by Peterman and Hedge (1971) for primitive mantle material. Since the amount of radiogenic strontium present in a rock is a time-integrated function of its Rb:Sr ratio, the Rb:Sr ratio of the source material from which the parent magmas of the Hart Mountain rocks were derived probably was lowered relatively early in the Earth's 4.6-b.y. history.

After it was injected to relatively high levels, the parent magma for the Hart Mountain pantellerites underwent intensive low-pressure crystal fractionation. With protracted crystallization and separation of olivine, pyroxene, and plagioclase, Al, Ca, Sr, Mg, and related minor transition-element contents greatly decreased and Si, K, Rb, and Ba contents and Fe:Mg and (Na+K): Al ratios progressively increased. K:Rb ratios decreased very slightly. With continued fractionation, feldspar constituted a progressively larger percentage of the total phenocryst assemblage separating from the melt. Phenocrystic plagioclase became increasingly richer in Na and K and eventually was replaced by Ca anorthoclase and finally by anorthoclase. Separation of anorthoclase caused further decrease in Al, Sr, Ba, and the K:Rb ratio, and increase in Si, Rb, and other minor incompatible elements. Separation of alkali feldspar with (Na+K):Al ratios about 1 from the now peralkaline residual liquids caused the melts to become progressively more peralkaline. Small amounts of Na were probably lost during the separation of an aqueous phase during the latter stages of shallow fractionation and migration toward the surface. Larger amounts of Na were lost, Fe^{+2} partly oxidized, and K, Rb, and Ba possibly locally redistributed during granophyric crystallization (devitrification) of the groundmass material of the lavas.

ORIGIN OF PARENTAL MAGMAS AND THEIR SUBSEQUENT DIFFERENTIATION

The strontium isotopic and K:Rb data together suggest that the pantellerites from the Hart Mountain area were derived from mafic magmas generated from mantle material that much earlier had been partly depleted in Rb, K, and other incompatible elements by one or more episodes of partial melting and magma generation. During the earlier episode or episodes of partial melting, Rb, a very large monovalent cation, was partitioned into the melt phase more strongly than either K or Sr, resulting in an increase in the K:Rb ratio and a decrease in the Rb:Sr ratio of the residual solid material left behind after the magmatic liquid had been drawn off. Magma subsequently produced during the Cenozoic from this depleted source material had an unusually high K:Rb ratio and, because of the low Rb:Sr ratio of the source material, a very low initial Sr^{87}/Sr^{86} ratio. A very similar origin for the type pantellerites from the island of Pantelleria, Italy, has been demonstrated by Korringa and Noble (1972).

REGIONAL IMPLICATIONS

The pantellerites of the Hart Mountain area were erupted at about the same time as the Ashdown Tuff, rhyolite of the Black Rock Range, and associated ash-flow units in northwestern Nevada (Noble and others, 1970; 1973) and silicic ash-flow tuffs of the John Day Formation in northeastern Oregon (Swanson, 1969). Noble (1972) has pointed out that the highly sodic nature of the anorthoclase phenocrysts in the Ashdown Tuff strongly suggests that the magma was produced by protracted large-scale fractional cyrstallization of mafic magma. Both the Ashdown Tuff and related silicic tuffs and lavas in northwestern Nevada and the silicic rocks of the John Day Formation are closely assoicated in space and time with mafic lavas. Consistently low initial Sr^{87}/Sr^{86} ratios of 0.7046 to 0.7059 obtained on early Miocene silicic lavas and tuffs from the northwestern Great Basin (McKee and others, 1972) effectively rule out derivation from or incorporation of appreciable amounts of material of upper crustal origin. The Hart Mountain pantellerites provide additional evidence for a latest Oligocene and early Miocene episode of basalt-derived silicic volcanism in northwestern Nevada and eastern Oregon.

ACKNOWLEDGMENTS

We are indebted to C. E. Hedge for the use of analytical facilities for the determination of strontium isotope composition. Noble was supported by National Science Foundation grant GA-35756 and National Aeronautics and Space Administration grant NGR-22-007-103. The report was improved by the discussions with D. W. Swanson and R. L. Christiansen.

REFERENCES CITED

Baksi, A. K., York, D., and Watkins, N. D., 1967, Age of the Steens Mountain geomagnetic polarity transition: Jour. Geophys. Research, v. 72, no. 24, p. 6299–6308.

Bastron, Harry, Barnett, P. R., and Murata, K. J., 1960, Method for the quantitative spectrochemical analysis of rocks, minerals, ores, and other materials by a powder d-c arc technique: U.S. Geol. Survey Bull. 1084-G, p. 165-182.

Carmichael, I. S. E., 1962, Pantelleritic liquids and their phenocrysts: Mineralog. Mag., v. 33, p. 86–113.

Dalrymple, G. B., and Lanphere, M. A., 1969, Potassium-argon dating–Principles, techniques, and applications to geochronology: San Francisco, W. H. Freeman and Co., 258 p.

Ewart, A., Taylor, S. R., and Capp, A. C., 1968, Geochemistry of pantellerites of Major Island, New Zealand: Contr. Mineralogy and Petrology, v. 17, p. 116–140.

Gibson, I. L., 1970, A pantelleritic welded ash-flow tuff from the Ethiopian Rift Valley: Contr. Mineralogy and Petrology, v. 28 p. 89–111.

Gunn, B. M., and Watkins, N. D., 1970, Geochemistry of the Steens Mountain Basalts, Oregon: Geol. Soc. America Bull., v. 81, no. 5 p. 1497–1516.

Hart, S. R., Gunn, B. M., and Watkins, N. D., 1971, Intralava variation of alkali elements in Icelandic basalt: Am. Jour. Sci., v. 270, no. 4, p. 315–318.

Hedge, C. E., Hildreth, R. A., and Henderson, W. T., 1970, Strontium isotopes in some Cenozoic lavas from Oregon and Washington: Earth and Planetary Sci. Letters, v. 8, p. 434–438.

Korringa, M. K., and Noble, D. C., 1971, Distribution of Sr and Ba between natural feldspar and igneous melt: Earth and Planetary Sci. Letters, v. 11, p. 147–151.

——1972, Genetic significance of chemical, isotopic, and petrographic features of some peralkaline salic rocks from the island of Pantelleria: Earth and Planetary Sci. Letters, v. 17, p. 258–262.

Mckee, E. H., Noble, D. C., Hedge, C. E., and Bonham, H. F., 1972, Strontium isotopic composition of some early Miocene rhyolitic tuffs and lavas from the northwestern part of the Great Basin, *in* Geological Survey research 1972: U.S. Geol. Survey Prof. Paper 800-D, p. D99–D102.

Noble, D. C., 1972, Some observations on the Cenozoic volcano-tectonic evolution of the Great Basin, western United States: Earth and Planetary Sci. Letters, v. 17, p. 142–150.

Noble, D. C., Chipman, D. W., and Giles, D. L., 1968, Peralkaline silica volcanic rocks in northwestern Nevada: Science, v. 160, p. 1337–1338.

Noble, D. C., and Haffty, Joseph, 1969, Minor-element and revised major-element contents of some Mediterranean pantellerites and comendites: Jour. Petrology, v. 10, p. 502–509.

Noble, D. C., Haffty, Joseph, and Hedge, C. E., 1969, Strontium and magnesium contents of some natural peralkaline silicic glasses and their petrogenetic significance: Am. Jour. Sci., v. 267, p. 598–608.

Noble, D. C., and Hedge, C. E., 1970, Distribution of rubidium between sodic sanidine and natural silicic liquid: Contr. Mineralogy and Petrology, v. 29, p. 234–241.

Noble, D. C., Hedge, C. E., McKee, E. H., and Korringa, M. K., 1973, Reconnaissance study of the strontium isotopic composition of Cenozoic volcanic rocks in the northwestern Great Basin: Geol. Soc. America Bull., v. 84, p. 1393–1406.

Noble, D. C., McKee, E. H., and Creasy, J. W., 1969, Late Tertiary peralkaline volcanism in north-central Humboldt County, Nevada [abs.]: Geol. Soc. America Abs. with Programs 1969, pt. 3, p. 48–49.

Noble, D. C., McKee, E. H., Smith, J. G., and Korringa, M. K., 1970, Stratigraphy and geochronology of Miocene volcanic rocks in northwestern Nevada, *in* Geological Survey research 1970: U.S. Geol. Survey Prof. Paper 700-D, p. D23–D32.

Peterman, Z. E., and Hedge, C. E., 1971, Related strontium isotopic and chemical variations in oceanic basalt: Geol. Soc. America Bull., v. 82, p. 493–500.

Schmincke, H. U., 1969, Ignimbrite sequence on Gran Canaria: Bull. Volcanol., v. 33, p. 1199–1219.

Swanson, D. A., 1969, Reconnaissance geologic map of the east half of the Bend quadrangle, Crook, Wheeler, Jefferson, Wasco, and Deschutes Counties, Oregon: U.S. Geol. Survey Misc. Geol. Inv. Map I-568, scale 1:250,000.

Walker, G. W., 1961, Soda rhyolite (pantellerite) from Lake County, Oregon, *in* Short papers in the geologic and hydrologic sciences: U.S. Geol. Survey Prof. Paper 424-C, p. C142–C144.

——1969, Possible fissure vent for a Pliocene ash-flow tuff, Buzzard Creek area, Harney County, Oregon, *in* Geological Survey research 1969: U.S. Geol. Survey Prof. Paper 650-C, p. C9–C17.

Walker, G. W., and Repenning, C. A., 1965, Reconnaissance geologic map of the Adel quadrangle, Lake, Harney, and Malheur Counties, Oregon: U.S. Geol. Survey Misc. Geol. Inv. Map I-446, scale 1:250,000.

Walker, G. W., and Swanson, D. A., 1968a, Laminar flowage in a Pliocene soda rhyolite ash-flow tuff, Lake and Harney Counties, Oregon, *in* Geological Survey research 1968: U.S. Geol. Survey Prof. Paper 600-B, p. B37–B42.

——1968b, Summary report on the geology and mineral resources of the Poker Jim Ridge and Fort Warner areas of the Hart Mountain National Antelope Refuge, Lake County, Oregon: U.S. Geol. Survey Bull. 1260-M, p. M1–M16.

Zies, E. G., 1960, Chemical analyses of two pantellerites: Jour. Petrology, v. 1, p. 304–308.

Jour. Research U.S. Geol. Survey
Vol. 2, No. 1, Jan.-Feb. 1974, p. 31—34

FLUID-INCLUSION STUDIES OF THE PORPHYRY COPPER DEPOSIT AT BAGDAD, ARIZONA

By J. THOMAS NASH and CHARLES G. CUNNINGHAM, JR.,

Menlo Park, Calif.

Abstract.—Quartz in chalcopyrite- and molybdenite-bearing veins at Bagdad contains two predominant types of fluid inclusions: one has moderate salinity (about 8 percent) and filling temperatures in the range from 302° to 373°C; the other has high salinity (30-35 percent) and filling temperatures of 223° to 310°C. Sparse gas-rich inclusions indicate brief periods of boiling. Fluid pressures deduced from fluid-inclusion data are approximately 150 bars; emplacement under about 6,000 ft of cover is suggested. Temperatures and salinities of ore fluids at Bagdad were significantly lower than in other studied porphyry copper deposits, indicating that chemically and physically diverse fluids affect mineralization in these deposits.

Fluid-inclusion data establish limits on the pressure, temperature, and general composition of ore fluids depositing chalcopyrite and molybdenite in veins at Bagdad, Ariz. In addition to characterizing conditions at Bagdad, the data are valuable for the similarities and contrasts they demonstrate in comparison with data from other porphyry-type deposits such as Bingham, Utah (Roedder, 1971). Similarities as well as significant differences in fluid-inclusion filling temperatures and compositions are instructive in understanding the origins of this type deposit and in evaluating exploration targets.

The geology and mineralization at Bagdad are well known (Anderson and others, 1955). Copper mineralization occurs primarily as disseminations and numerous small quartz-sulfide veinlets in a Laramide quartz monzonite intrusion (Anderson and others, 1955). Molybdenum, also economically important, occurs in quartz veinlets that cut quartz-chalcopyrite veinlets. The central part of the stock is altered to a biotite-albite-quartz-orthoclase facies, and quartz-sericite alteration is concentrated along later fracture zones. Quartz-sulfide veinlets that we studied have sericitic alteration envelopes. Breccia pipes occur in the district, and some contain copper minerals. Two of our samples come from the Black Mesa pipe, a mineralized body just outside the Bagdad pit.

Fluid inclusions in vein quartz and wallrocks provide important information about aspects of the origin of the Bagdad copper deposit but raise questions that they alone cannot answer. As in many other complex ore deposits, times of fluid entrapment are obscured by various degrees of deformation and recrystallization and rarity of growth planes. Consequently, the fluid-inclusion data permit reasonable but equivocable interpretations of fluid evolution as well as depth of emplacement and ore deposition.

DESCRIPTION OF INCLUSIONS

Four types of fluid inclusions have been observed in samples from Bagdad. Type 1 inclusions have moderate salinity, contain 15 to 30 percent vapor by volume, and typically have three daughter minerals. The daughter minerals are translucent red hexagonal platelets of hematite; an opaque, nonmagnetic mineral with irregular or pyramidal morphology (possibly chalcopyrite?); and an unknown transparent mineral with low birefringence, moderate relief, and commonly, hexagonal morphology. These daughter minerals do not dissolve when held at the filling temperature for several hours. Moderate salinity is inferred from the absence of cubic salt daughter minerals (equivalent to less than about 26 weight percent NaCl at room temperature). Freezing tests on type 1 inclusions with favorable optics in two samples (Bd-74 and Bd-79, table 1) indicate 5.8 to 9.2 weight percent NaCl equivalent. Type 2 inclusions are gas rich, generally contain approximately 75 percent vapor, and contain hematite in some samples. These inclusions could not be observed in heating tests because of optical limitations but would fill to vapor at an estimated 350°C. They probably represent trapped vapor from a boiling system. Type 3 inclusions are characterized by cubes of halite and typically also by flakes of hematite and an unknown birefringent daughter mineral with nondescript morphology; the vapor bubble amounts to approximately 10 percent by volume. In heating tests on inclusions of this type, the cube of halite dissolves, but other daughter crystals do not. Type 4 inclusions contain liquid CO_2 as a third fluid phase at room temperature; these inclusions are rare in wallrocks and veins and probably represent CO_2-rich vapor.

Ages of inclusions in vein quartz have been difficult to assess because quartz in most samples is massive and intergrown and lacks visible growth planes. Some moderate-salinity inclusions

(type 1) occur on internal fractures through the massive quartz, indicating secondary or pseudosecondary formation. Many moderate-salinity (type 1) and most halite-bearing (type 3) inclusions are isolated, unrelated to visible fractures, and appear to be primary. Inclusion populations and textures are not detectably different in quartz of chalcopyrite- or later molybdenite-bearing veins and provide no evidence regarding the relative ages of types 1 and 3 inclusions. Irregular zones of massive quartz in the chalcopyrite and molybdenite veins contain numerous gas-rich (type 2) inclusions that are rare in other zones. These inclusions are adjacent to type 1 inclusions and probably reflect boiling of moderate-salinity fluids. Somewhat younger quartz-pyrite veins contain only moderate-salinity (type 1) inclusions, suggesting that the later stage fluids were less saline than earlier stages. Evolution from high to moderate salinity is also suggested by euhedral overgrowths on massive quartz in samples Bd-1 and Bd-74 that contain only moderate-salinity inclusions, many of which are primary on growth planes.

In heating tests on the halite-bearing inclusions, the halite cubes dissolved at temperatures in the range from 205° to 270°C, suggesting minimum salinities of 30 to 35 percent from the system NaCl-H_2O (Sourirajan and Kennedy, 1962). Liquid filled these inclusions at temperatures from 223° to 310°C (table 1). Within individual samples rather large scatter in the filling temperatures was observed, which may reflect changes in the inclusions after trapping or trapping at different pressures. In all vein samples studied from the Bagdad pit, filling temperatures of the halite-bearing inclusions were lower than those of adjacent moderate-salinity inclusions. Filling temperatures on the latter type inclusions range from 302° to 373°C.

Two samples (Bd-79 and Bd-5) of quartz encrusted with copper and iron oxides were studied from the the Black Mesa breccia pipe. One sample (Bd-79) contains sparse halite-bearing inclusions; most of the inclusions are type 1 and filled in the range 325° to 339°C. Similar inclusions in sample Bd-5 filled in the range 243° to 260°C. No gas-rich inclusions are present in these samples, which implies that boiling probably did not occur during or after deposition of the quartz and sulfides in the pipe.

Primary and secondary quartz dispersed through the altered wallrocks contain fluid inclusions qualitatively similar to those in the veins. In some samples halite-bearing inclusions constitute approximately half of the population. Gas-rich inclusions (type 2) are present in some wallrock samples and locally constitute as much as 20 percent of the population; they suggest that boiling occurred at some unspecified time and temperature. However, the relatively low abundance of these inclusions suggests that boiling was not as widespread as in many other copper-bearing stocks (Nash, unpub. data). No differences in fluid-inclusion types are noted between samples of unaltered porphyritic quartz monzonite and biotite-albite-quartz-orthoclase facies of altered quartz monzonite (as defined by Anderson and others, 1955), but inclusions are much more abundant in the altered rocks at Bagdad. Disseminated sulfides typically occur in altered quartz monzonite (Anderson and others, 1955); the sulfides could have originally been deposited during crystallization of the very fine matrix of the porphyry, as advocated for Ely by Fournier (1967), and later become remobilized during alteration. Alternatively, the sulfides could have been introduced during alteration. Ambiguous age relations of fluid inclusions preclude an unequivocal estimate of the composition of fluids that affected the alteration and remobilized or introduced base metals.

Table 1.—*Fluid-inclusion data from quartz veins, Bagdad, Ariz.*

[Qc, quartz-chalcopyrite; QM, quartz-molybdenite; QP, quartz-pyrite; 1, moderate salinity; 3, halite-bearing; e, estimated; n.d., not determined]

Sample	Type vein	Type inclusion	Filling temperature range (°C)	Salinity (wt percent NaCl)
Bd-1	QC	1	320–324	N.d.
		3	275e	35e
Bd-62	QC	1	347–373	N.d.
		3	287–298	32
Bd-65a	QC	1	340e	N.d.
		3	250e	30e
Bd-65b	QP	1	302–308	N.d.
Bd-67	QC	1	345–356	N.d.
		3	300e	32e
Bd-69a	QM	1	343–348	N.d.
		3	275–310	35
Bd-69b	QM	1	342–369	
		3	223–266	30
Bd-74	QC	1	340–358	7.4–9.2
		3	255–258	33
Bd-5	Pipe	1	243–260	N.d.
Bd-79	Pipe	1	325–339	5.8–9.0
		3	275e	35e

INTERPRETATION AND DISCUSSION

Geologic evidence in the Bagdad area (Anderson and others, 1955; C. A. Anderson, oral commun., 1972) indicates that the intrusion was not thickly covered during Laramide time. The stock intrudes the Grayback Mountain Rhyolite Tuff of Late Cretaceous or early Tertiary age, which rests unconformably on the Precambrian, as well as dikes and sills of rhyolite. A maximum thickness of 500 ft of these volcanic rocks is exposed in the area, and presumably, the pile must have been considerably thicker. A better approximation of depth and pressure can be made from the fluid-inclusion evidence than from the incomplete geologic record. The depth required must provide enough pressure to prevent sustained boiling at prevailing temperatures but to permit periodic

boiling at times of higher temperature or reduced pressure. A fluid with the composition 10 weight percent NaCl at 350°C, a fair approximation of many type 1 inclusions, would boil if the pressures were less than about 150 bars, equivalent to about 6,000 ft of hydrostatic head (Haas, 1971, extrapolated). Lacking other evidence, we consider this the best estimate of likely cover. If conditions were lithostatic, only about 1,900 ft of cover would be required to generate pressures sufficient to prevent boiling, but we consider it unlikely that lithostatic conditions persisted at these shallow levels.

Physically and chemically diverse fluids were evidently present in various porphyry copper deposits. The prevalence of homogeneous liquids at Bagdad contrasts sharply with fluids at Copper Canyon, Nev. (Nash and Theodore, 1971), and Bingham, Utah (Roedder, 1971; W. J. Moore and Nash, unpub. data), which commonly were boiling. Fluids at Bagdad also were typically less saline than at Copper Canyon and Bingham. However, the fluid regime at Bagdad is not considered unique because similar fluid-inclusion assemblages are noted in the Mineral Park, Ariz., porphyry copper deposit, approximately 90 mi to the northwest, and in several other porphyry-type occurrences (Nash, unpub. data). Drake (1972) and Drake and Ypma (1972) report homogenization temperatures of 450° to 230°C, salinities in the range from 10 to 3 weight percent NaCl, and one period of boiling at Mineral Park. Our observations on nine samples from Mineral Park are consistent with those of Drake and Ypma, and we note sparse halite-bearing inclusions in quartz masses at the core of the intrusive complex and in quartz-molybdenite veins. These inclusions resemble the halite-bearing inclusions from Bagdad in their small vapor fraction; although too small to be tested on the heating stage, we estimate they would fill at about 300°C.

The filling temperatures of halite-bearing inclusions from Bagdad are the lowest known for this type of inclusion in studied porphyry-type deposits. On the basis of probable depths of emplacement, discussed previously, these temperatures probably require a pressure correction of about +15° to 25°C (Lemmlein and Klevtsov, 1961) or certainly no more than +50°C under maximum likely pressures. Temperatures of formation of 300°±50°C may seem unreasonably low for copper-molybdenum-bearing veins within the stock when compared with temperatures of approximately 700°C determined by Roedder (1971) at Bingham. However, typical temperatures of about 400°C or less are likely in the porphyry environment because of the physical setting. Evidence at Bagdad and many other porphyry and stockwork type deposits suggests depths of emplacement of 1,500 to 3,000 m (5,000 to 10,000 ft), where features typical of shallow depth are common, such as pressure quenching, venting, breccia pipes, and pebble dikes. In this environment, temperatures above 400°C are difficult to maintain because of the cooling effects of irreversible adiabatic expansion ("throttling"), boiling, and mixing with ground water (Toulmin and Clark, 1967; Rose, 1970). There is ample evidence in theory and in fluid inclusions that "moderate" temperature (<400°C) hydrothermal fluids can be expected to introduce or remobilize copper or molybdenum within the host intrusion as well as in intruded host rocks as at Copper Canyon (Nash and Theodore, 1971).

The data from Bagdad permit interpretations of fluid evolution; two reasonable models are schematically outlined in figure 1. In model A, halite-bearing inclusions are interpreted to be oldest, whereas in model B some moderate-salinity inclusions are considered to be earliest. Model A is consistent with fluid histories developed for other porphyry copper deposits (Nash and Theodore, 1971; Roedder, 1971) in that highly saline fluids are typically early. However, the postulated thermal regime may be untenable. If moderate salinities are explained by dilution of highly saline fluids by ground water, a reasonable proposition for the porphyry environment, then significant cooling is to be expected (see, for example, Rose,

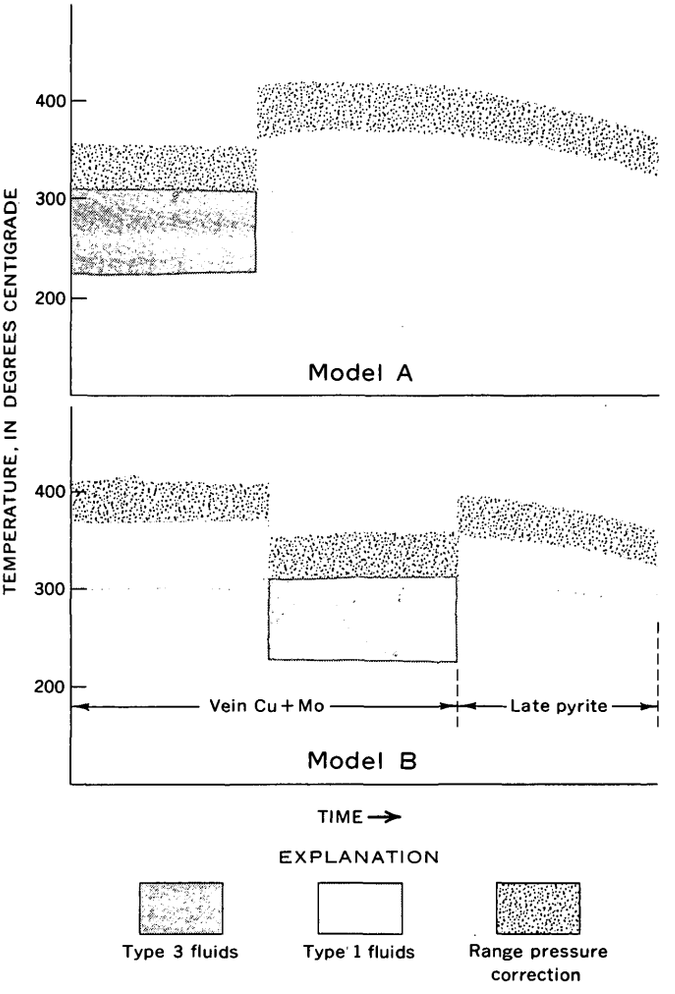

Figure 1.—Two possible time-temperature models from fluid-inclusion data, Bagdad, Ariz. In model A, high-salinity fluids are presumed to be earliest, whereas in model B, moderate-salinity fluids are earliest.

1970); temperatures deduced from fluid inclusions do not show this. Even if the maximum relevant pressure correction ($\approx$+50°C) is applied to filling temperatures of halite-bearing inclusions and none to the temperatures of moderate-salinity inclusions, the inferred temperatures of formation of the halite-bearing type are still lower than those of the more dilute type; hence, model A does not satisfy important thermal considerations.

Model B (fig. 1) is permissible within the uncertainties of inclusion and vein age relationships but is unconventional compared with fluid sequences postulated for other porphyry copper deposits. A sequence of hot, moderately saline fluids followed by cooler, highly saline fluids is reasonable by thermal models. In theory this fluid sequence could be repeated many times in a complex history of intrusion and fracturing. The observed enrichment in salts might be explained by massive boiling above the level of our sampling and descent of the more dense fluid owing to cooling and increased salinity. This model, or variations of it involving several fluctuations in salinity and temperature, is favored by the authors but cannot be substantiated. It should be considered elsewhere.

ACKNOWLEDGMENTS

We thank Rana Medhi, Bagdad Copper Corp., and Ronald Teissere, Duval Corp., for their assistance in collecting samples, and G. K, Czamanske for supplying samples from Bagdad. We thank N. G. Banks and Czamanske, both of U.S. Geological Survey, for helpful discussions.

REFERENCES CITED

Anderson, C. A., Scholz, E. A., and Strobell, J. D., Jr., 1955, Geology and ore deposits of the Bagdad area, Yavapai County, Arizona: U.S. Geol. Survey Prof. Paper 278, 103 p.

Drake, W. E., 1972, A study of ore forming fluids at the Mineral Park porphyry copper deposit, Kingman, Arizona: New York, Columbia Univ., Ph. D. thesis, 245 p.

Drake, W. E., and Ypma, P. J. M., 1972, Fluid inclusion study of the Mineral Park porphyry copper deposit, Kingman, Arizona, *in* Roedder, Edwin, ed., Fluid inclusions research [abs.]: COFFI, Washington, D. C., 1969, p. 15–16.

Fournier, R. O., 1967, The porphyry copper deposit exposed in the Liberty open-pit mine near Ely, Nevada–Pt. 1, Syngenetic formation: Econ. Geology, v. 62, no. 1, p. 57–81.

Haas, J. L., 1971, The effect of salinity on the maximum thermal gradient of a hydrothermal system at hydrostatic pressure and near boiling: Econ. Geology, v. 66, p. 940–946.

Lemmlein, G. G., and Klevtsov, P. V., 1961, Relations among the principal thermodynamic parameters in a part of the system H_2O-NaCl : Geochemistry, no. 2, p. 148–158.

Nash, J. T., and Theodore, T. G., 1971, Ore fluids in the porphyry copper deposit at Copper Canyon, Nevada: Econ. Geology, v. 66, p. 385–399.

Roedder, Edwin, 1971, Fluid inclusion studies on the porphyry-type ore deposits at Bingham, Utah, Butte, Montana, and Climax, Colorado: Econ. Geology, v. 66, p. 98–120.

Rose, A. W., 1970, Zonal relations of wallrock alteration and sulfide distribution at porphyry copper deposits: Econ. Geology, v. 65, p. 920–936.

Sourirajan, S., and Kennedy, G. C., 1962, The system H_2O-NaCl at elevated temperatures and pressures: Am. Jour. Sci., v. 260, p. 115–141.

Toulmin, Priestley, 3d, and Clark, S. P., Jr., 1967, Thermal aspects of ore formation, [Chap.] 10, *in* Barnes, H. L., ed., Geochemistry of hydrothermal ore deposits: New York, Holt, Rinehart and Winston, p. 437–464.

Jour. Research U.S. Geol. Survey
Vol. 2, No. 1, Jan.-Feb. 1974, p. 35—39

COMPOSITION AND RELATION OF ANALCIME TO DIAGENETIC DAWSONITE IN OIL SHALE AND TUFF IN THE GREEN RIVER FORMATION, PICEANCE CREEK BASIN, NORTHWESTERN COLORADO

By DONALD A. BROBST and JERRY D. TUCKER, Denver, Colo.

Abstract.—The variation in composition of analcime was determined in 91 samples of tuff and oil shale collected from exposures of the Parachute Creek Member, Green River Formation (Eocene), in the Piceance Creek basin, Rio Blanco County, Colo. The rocks of the Parachute Creek Member are the products of sedimentation and diagenesis in an alkaline lake. The composition of the analcime, expressed as the quotient of silicon divided by aluminum (Si:Al ratio) was determined by the X-ray method of Saha, published in 1961, in which powdered silicon metal is added to the sample as an internal standard. Analcime in 47 of 56 tuffs without dawsonite has a Si:Al ratio ranging from 2.4 to 2.7; the same limits apply to analcime in 13 of 22 oil shales without dawsonite. The analcime in 8 of 10 samples of dawsonitic oil shale has a Si:Al ratio ranging from 2.7 to 2.9, and therefore is more siliceous than that in rocks lacking dawsonite. The relative abundance of analcime varies inversely with abundance of dawsonite. The relative abundance of quartz is greater in rocks with dawsonite than in those without dawsonite. These data suggest that dawsonite plus quartz were derived during diagenesis from the alteration of analcime in a highly alkaline (pH >9) environment.

Analcime (ideal formula, $NaAlSi_2O_6 \cdot H_2O$) is a common and widespread authigenic zeolite in the lacustrine rocks of the Green River Formation of Eocene age in Colorado, Wyoming, and Utah. The formation includes abundant carbonate rocks (called oil shale where they contain much organic matter), some intercalated layers of altered tuff, and some beds, pods, and scattered crystals of sodium-rich carbonate and bicarbonate minerals that are referred to as saline minerals, according to the definition of Fahey (1962, p. 18). The formation of analcime and other authigenic minerals in these rocks, especially in the tuffs, in the Green River Basin, Wyo., has been discussed recently by Hay (1966, 1970), Iijima and Hay (1968), Bradley and Eugster (1969), Goodwin (1971), and Surdam and Parker (1972).

Analcime occurs abundantly in the tuffs and commonly in the carbonate rocks in the Parachute Creek Member of the Green River Formation in the Piceance Creek Basin which lies mostly in Garfield and Rio Blanco Counties, Colo. (fig. 1). The general geologic features of the basin have been described by Bradley (1930, 1931) and Donnell (1961). Enough is known about the rocks of the Parachute Creek Member to establish that most were deposited in an alkaline lake whose waters were rich in ions of sodium, carbonate, and bicarbonate. In the deeper parts of the basin, the rocks of the Parachute Creek Member contain nahcolite, $NaHCO_3$, dawsonite, $NaAl(OH)_2CO_3$; and halite, NaCl (Smith and Milton, 1966; Hite and Dyni, 1967). In November 1966, we found dawsonite in outcrops of oil shale along lower Piceance Creek. The origin and occurrence of dawsonite is of special interest because of the mineral's potential value as a source of aluminum.

This paper describes an X-ray diffraction study of the composition of analcime and relates the variation in composition to the presence or absence of dawsonite in a suite of 91 samples of tuff and oil shale collected from outcrops along the periphery of the northern half of the Piceance Creek basin. The relative abundance of analcime, dawsonite, and quartz in a suite of 54 samples of dawsonitic oil shale also was examined. The results of the study indicate that dawsonite plus quartz are products of the diagenetic alteration of analcime in a highly alkaline (pH greater than 9) environment.

SAMPLES

A suite of 91 samples of altered tuff and oil shale, some containing dawsonite, was selected for the analcime study from a group of samples collected from stratigraphic sections of the Parachute Creek Member measured along the pipeline right-of-way on the Cathedral Bluffs (sec. 34, T. 2 S., R. 100 W.), along lower Piceance Creek (secs. 11, 14, and 15, T. 1 N., R. 97 W.), and near Rio Blanco along upper Piceance Creek (secs. 5 and 6, T. 4 S., R. 97 W.), in Rio Blanco County (fig. 1).

All the samples containing dawsonite were collected along lower Piceance Creek. Dawsonite, generally invisible to the unaided eye, was detected by X-ray diffraction in oil shale and tuff beds scattered through an exposed stratigraphic interval of

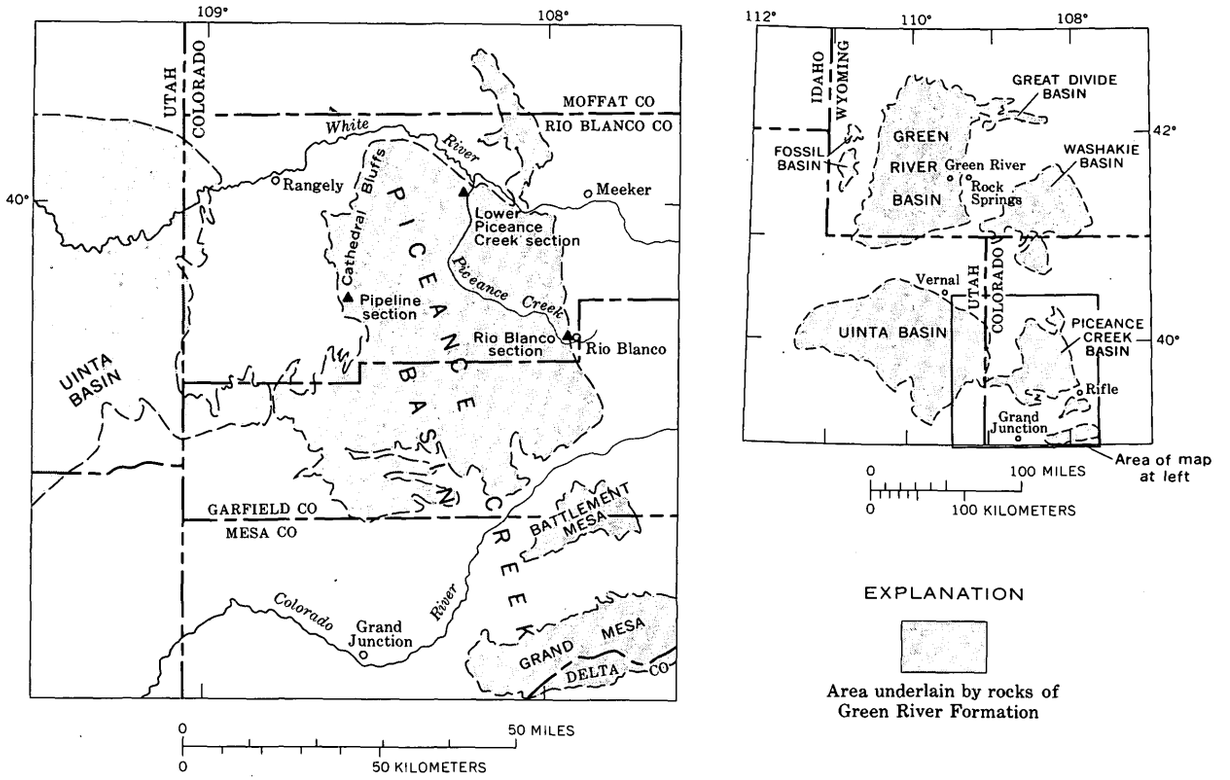

Figure 1.—Index map of the Piceance Creek basin, Colorado, and adjacent areas.

about 111 m (370 ft), from about 60 m (200 ft) above the base of the member to within 21 m (70 ft) of the base of the Mahogany ledge, an extensively distributed sequence of rocks containing the richest oil shale in the member in the Piceance Creek basin. A zone of dawsonitic oil shale, about 15 m (50 ft) thick, is exposed in and around a small cut within about 6 m (20 ft) of the level of the lower Piceance Creek road, 4.3 km (2.7 mi) south of the junction with Colorado Highway 64. The suite of 54 samples that yielded the data plotted in figure 4 was collected from the line of the measured section and in and around the small cut. Of these 54 samples, 17 were included in the group of 91 in which the composition of analcime was determined.

We have prepared a more comprehensive report containing a description of the three measured sections and the details of the mineralogy, including the vertical and lateral variation of the mineral composition, of the rocks in the Parachute Creek Member determined from an X-ray diffraction study of about 650 samples (Brobst and Tucker, 1973).

TUFF BEDS

Most of the tuff beds exposed in the three measured sections are less than 15 cm (6 in.) thick and many are less than 2.5 cm (1 in.) thick. Nearly all the exposed beds are weathered creamy yellow to orange brown, have a sandy texture imparted by the grains of analcime, and commonly form reentrants in the face of outcrops between the enclosing beds of marlstone and oil shale.

The 59 samples of tuff from 51 beds that were examined in this study commonly consist chiefly of different mixtures of analcime, quartz, albite, and potassium feldspar. Less than 25 percent also contain some of the following minerals: muscovite (including illite), biotite, pyrite, dolomite, and calcite. The latter two minerals are abundant in a few beds. Only three samples of dawsonitic tuff were found, all on lower Piceance Creek, with coexisting analcime in sufficient quantity to determine its composition. The other 56 tuff samples studied were collected from the pipeline section (20 samples), the lower Piceance Creek section (23 samples), and the Rio Blanco section (13 samples).

OIL SHALE

The oil shale generally is an extremely fine-grained, laminated, light-yellow-brown to dark-red-brown, carbonate-rich rock that contains different amounts of organic materials. The mineral fraction consists chiefly of different mixtures of dolomite, quartz, analcime, albite, and potassium feldspar, and some calcite, illite, and pyrite. Oil shale containing dawsonite most commonly also contains dolomite, quartz, potassium

feldspar, and illite. Analcime, calcite, pyrite, and albite seem to occur less commonly in dawsonitic rocks.

The composition of analcime was determined in 22 oil shales lacking dawsonite from the pipeline section (3 samples), the lower Piceance Creek section (7 samples), and the Rio Blanco section (12 samples). The composition of analcime was determined only in 10 dawsonitic oil shales from the lower Piceance Creek section because the abundance of analcime was insufficient in other bulk samples to perform the analysis.

COMPOSITION OF ANALCIME

The composition of analcime was determined by the X-ray method of Saha (1961) in which metallic silicon is added to the sample as an internal standard. Saha found that the (639) peak of analcime occurs at higher angles (degrees 2θ, Cu$K\alpha_1$ radiation) for analcime of higher silicon content. The displacement of the (639) peak for analcime was measured against the (331) peak for the silicon internal standard. The variation in the composition of the analcime was expressed by Saha (1961, fig. 2) as the molecular ratio of SiO_2. The composition was recast in relation to the unit-cell contents on the basis of 96 atoms of oxygen by Coombs and Whetten (1967, fig. 1). These workers further recognized that the silicon-to-alumimum ratio of ideally constituted analcime ($NaAlSi_2O_6 \cdot H_2O$) is 2, but that the Si:Al ratio of synthetic analcime ranges from 1.12 to 3. At an Si:Al ratio of 3, the ideal composition of albite ($NaAlSi_3O_8$) is reached.

We homogenized the powdered sample and silicon metal in a mixer mill for 5 min. The mixture was pelletized in a hydraulic press at 22,000 lb/in.^{2}. The pellets were exposed to X-rays in Picker-Nuclear equipment operated at 35 kV, 20 MA, at various scale factors and time constants to obtain maximum resolution in samples which contained different amounts of analcime. The results of scanning the pellet across an arc of $75° - 79°$ 2θ were recorded at a chart speed of 0.25°/min. The Si:Al ratios plotted in figure 2 were calculated from the average value of 10 scans to determine the difference between the position of the two peaks for analcime and silicon.

The composition of analcime in 91 samples from exposures along the periphery of the Piceance Creek basin is shown in figure 2.

About 85 percent (47) of the 56 tuffs lacking dawsonite have analcime with Si:Al ratios ranging from 2.4 to 2.7. Three tuffs containing dawsonite have analcime with a Si:Al ratio greater than 2.63. About 60 percent (13) of the 22 oil shales lacking dawsonite have analcime with Si:Al ratios ranging from 2.4 to 2.7. Eighty percent (8) of the 10 oil shales containing dawsonite have analcime with a Si:Al ratio greater than 2.7. These data indicate that the analcime in rocks containing dawsonite is generally more siliceous than the analcime in rocks lacking dawsonite.

The Si:Al ratio of analcime is compared to the abundance of analcime in tuff and oil shale in figure 3. The Si:Al ratio seems

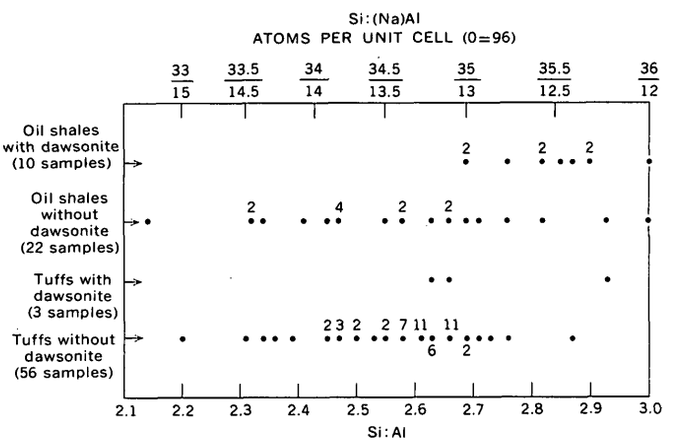

Figure 2.—Composition of analcime in 91 samples of tuff and oil shale from the exposures of the Parachute Creek Member along the periphery of the Piceance Creek basin. Numbers above or below dots refer to number of samples of that composition.

to decrease as the abundance of analcime increases. The dawsonitic oil shale and tuff contain the least analcime, and the oil shale and tuff lacking dawsonite contain the most analcime.

The abundance of minerals described here and in subsequent statements and figures is expressed as X-ray peak height in chart units in parts of 100. The samples were uniformly prepared and exposed to X-rays in Picker-Nuclear equipment operated at 35 kV, 20 MA, scale factor 3K, time constant 1 (Cu$K\alpha_1$ radiation) and recorded at a chart speed of 2°/min. One peak was selected and measured for each mineral: 15.6° 2θ for dawsonite, 15.8° 2θ for analcime, and 20.9° 2θ for quartz. The data in the figures indicate the relative abundance of minerals in different samples and not percentage of the

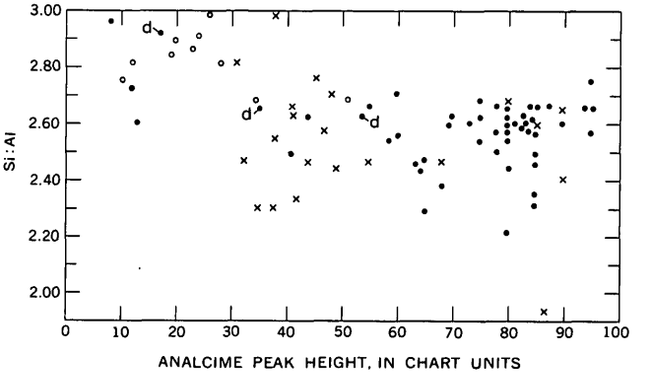

Figure 3.—Comparison of the Si:Al ratio of analcime with abundance of analcime in tuffs and oil shale. Circles are samples of oil shale with dawsonite, X's are samples of oil shale with no dawsonite, dots are samples of tuff with no dawsonite, and d's indicate tuff with dawsonite.

mineral detected in each sample. (See Brobst and Tucker, 1973.)

RELATION OF ANALCIME, DAWSONITE, AND QUARTZ

The relation of analcime, dawsonite, and quartz in 54 samples of dawsonitic oil shale from exposures along lower Piceance Creek is shown in figure 4. The abundance of analcime and quartz is plotted against the abundance of dawsonite. The abundance of analcime decreases as dawsonite increases. The abundance of quartz increases with increasing content of dawsonite.

The relation of the relative abundance of analcime, dawsonite, and quartz to feldspar in the 54 samples also was examined, but no correlation was found.

DISCUSSION

The analcime in the tuff and carbonate beds probably formed at low temperature in moderately alkaline water from clay minerals and zeolite precursors that probably were derived from volcanic glass. The conditions favoring the formation of analcime from other zeolites or the conversion of analcime to feldspar in environments of higher alkalinity (at a pH greater than 9) have been discussed recently by Hay (1966, 1970); Sheppard and Gude (1968, 1969); Iijima and Hay (1968); and Surdam and Parker (1972). The diagenetic alteration of analcime to dawsonite plus quartz perhaps is achieved before analcime is converted to feldspar in a highly alkaline environment. Hite and Dyni (1967, p. 33) reported that abundant dawsonite and quartz at depth in the central part of the basin are associated with small amounts of albite, but that as the content of dawsonite and quartz decreased, the content of albite increased. Analcime is absent in these rocks. It seems possible, therefore, that under different conditions of alkalinity and depth of burial, analcime may be converted to dawsonite and quartz or to feldspar.

The partial pressure of carbon dioxide in the lake water probably played an important role in the formation of dawsonite in the Piceance Creek basin. We agree with Hay (1970, p. 254) who speculated that dawsonite and quartz could have formed from analcime under high partial pressure of CO_2, determined by equilibrium with nahcolite, according to the following equation:

$$NaAlSi_2O_6 \cdot H_2O + CO_2 \longrightarrow NaAl(OH)_2CO_3 + 2SiO_2$$

analcime — organic origin — dawsonite — quartz

The equation perhaps is an oversimplication of a complex chemical system, but the lake waters must have been carbonated principally by the CO_2 provided by the oxidation of some of the organic matter in the system. Under these oxidizing conditions it is perhaps odd that any of the organic matter has been preserved, despite the detection of such preservatives as lauric acid (Bradley, 1970, p. 995). In addition, the organic materials also underwent diagenesis at the same time as the mineral fraction. The organic and inorganic materials are not mutually exclusive aspects in the development of the rocks in the Piceance Creek basin.

A complete sequence of zeolitic alterations may be postulated even though the zeolite precursors of analcime have not been found in the Piceance Creek basin. The absence of zeolite precursors may be explained partly by erosion of the most shoreward deposits around all but the southernmost periphery of the basin, which lies on Battlement and Grand Mesas, south of the Colorado River. Presumably the alkalinity of the water that saturated the beds still preserved north of the Colorado River was sufficiently high to convert all earlier zeolites to analcime. The data on figure 2 show that analcime in 40 of our 56 samples of tuff lacking dawsonite has a composition (34.5 to 35.1 atoms of silicon per unit cell) similar to that of analcime derived from clinoptilolite in tuffs from the Barstow Formation of California described by Sheppard and Gude (1969, p. 29). The close comparison lends weight to the argument that at least some of the analcime was derived from clinoptilolite. Clinoptilolite and mordenite have been reported in the neighboring Washakie and Green River Basins (Roehler, 1972; Goodwin and Surdam, 1967).

The occurrence of dawsonite near the periphery of the basin, in addition to its already known occurrence at depth in the central parts of the basin, indicates that greater amounts of dawsonite are in the Piceance Creek basin than previously recognized.

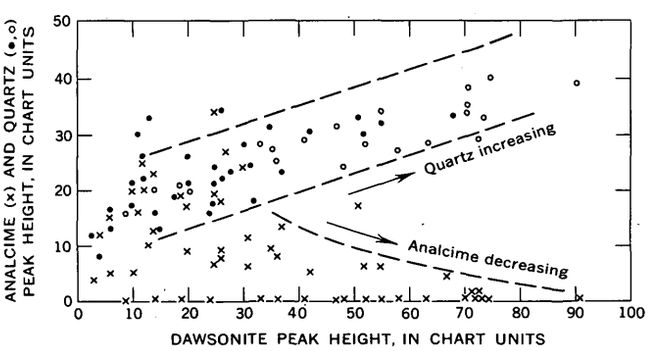

Figure 4.—Abundance of analcime and quartz plotted against abundance of dawsonite in oil shale. Circles indicate samples that contain dawsonite, but no analcime. Dots indicate samples that contain both dawsonite and analcime.

REFERENCES CITED

Bradley, W. H., 1930, The varves and climate of the Green River epoch: U.S. Geol. Survey Prof. Paper 158-E, p. 87–110.

——1931, Origin and microfossils of the oil shale of the Green River Formation of Colorado and Utah: U.S. Geol. Survey Prof. Paper 168, 58 p.

——1970, Green River oil shale—concept of origin expanded—an interdisciplinary problem being attacked from both ends: Geol. Soc. America Bull., v. 81, no. 4, p. 985–1000.

Bradley, W. H., and Eugster, H. P., 1969, Geochemistry and paleolimnology of the trona deposits and associated authigenic minerals of

the Green River Formation of Wyoming: U.S. Geol. Survey Prof. Paper 496-B, 71 p.

Brobst, D. A., and Tucker, J. D., 1973, X-ray mineralogy of the Parachute Creek Member, Green River Formation, in the northern Piceance Creek basin, Colorado: U.S. Geol, Survey Prof. Paper 803, 53 p.

Coombs, D. S., and Whetten, J. T., 1967, Composition of analcime from sedimentary and burial metamorphic rocks: Geol. Soc. America Bull., v. 78, no. 2, p. 269–282.

Donnell, J. R., 1961, Tertiary geology and oil-shale resources of the Piceance Creek basin between the Colorado and White Rivers, northwestern Colorado: U.S. Geol. Survey Bull. 1082-L, p. 835–891.

Fahey, J. J., 1962, Saline minerals of the Green River formation, *with a section on* X-ray powder data for saline minerals of the Green River formation, by M. E. Mrose: U.S. Geol. Survey Prof. Paper 405, 50 p.

Goodwin, J. H., 1971, Authigenesis of silicate minerals in tuffs of the Green River Formation (Eocene), Wyoming: Wyoming Univ. unpub. Ph. D. thesis, 123 p.

Goodwin, J. H., and Surdam, R. C., 1967, Zeolitization of tuffaceous rocks of the Green River Formation, Wyoming: Science, v. 157, no. 3786, p. 307–308.

Hay, R. L., 1966, Zeolites and zeolitic reactions in sedimentary rocks: Geol. Soc. America Spec. Paper 85, 130 p.

——1970,Silicate reactions in three lithofacies of a semi-arid basin, Olduvai Gorge, Tanzania, *in* Mineralogy and petrology of the upper mantle; sulfides; [and] mineralogy and geochemistry of non-marine evaporites–Symposia, 50th, Atlantic City, N.J., 1969: Mineralog. Soc. America Spec. Paper 3, p. 237–255.

Hite, R. J., and Dyni, J. R., 1967, Potential resources of dawsonite and nahcolite in the Piceance Creek basin, northwest Colorado, *in* Symposium on oil shale 4th: Colorado School Mines Quart., v. 62, no. 3, p. 25–38.

Iijima, Azuma, and Hay, R. L., 1968, Analcime composition in tuffs of the Green River Formation of Wyoming: Am. Mineralogist, v. 53, nos. 1–2, p. 184–200.

Roehler, H. W., 1972, Zonal distribution of montmorillonite and zeolites in the Laney Shale Member of the Green River Formation in the Washakie Basin, Wyoming, *in* Geological Survey research 1972: U.S. Geol. Survey Prof. Paper 800-B, p. B121–B124.

Saha, Prasenjit, 1961, The system $NaAlSiO_4$ (nepheline)–$NaAlSi_3O_8$ (albite)–H_2O: Am. Mineralogist, v. 46, nos. 7–8, p. 859–884.

Sheppard, R. A., and Gude, A. J., 3d, 1968, Distribution and genesis of authigenic silicate minerals in tuffs of Pleistocene Lake Tecopa, Inyo County, California: U.S. Geol. Survey Prof. Paper 597, 38 p.

——1969, Diagenesis of tuffs in the Barstow Formation, Mud Hills, San Bernardino County, California: U.S. Geol. Survey Prof. Paper 634, 35 p.

Smith, J. W., and Milton, Charles, 1966, Dawsonite in the Green River Formation of Colorado: Econ. Geology, v. 61, no. 6, p. 1029–1042.

Surdam, R. C., and Parker, R. D., 1972, Authigenic aluminosilicate minerals in the tuffaceous rocks of the Green River Formation, Wyoming: Geol. Soc. America Bull., v. 83, no. 3, p. 689–700.

Jour. Research U.S. Geol. Survey
Vol. 2, No. 1, Jan.-Feb. 1974, p. 41–47

PETROLOGY OF THE NEPHELINE SYENITE OF ST. LAWRENCE ISLAND, ALASKA

By BÉLA CSEJTEY, JR., and WILLIAM W. PATTON, JR.,
Menlo Park, Calif.

Abstract.—Reconnaissance mapping on St. Lawrence Island, Alaska, revealed a 44-km² (17-mi²) area of rubble exposures and float of nepheline syenite of probable mid-Cretaceous age. Petrographic and chemical uniformity suggests a single intrusive body that crystallized under more or less equilibrium conditions. Similar potassium-rich nepheline syenite intrusives of Cretaceous age are associated with oversaturated plutonic rocks in western Alaska and the Chukotsky Peninsula, U.S.S.R. The St. Lawrence nepheline syenite provides further evidence of tectonic continuity between Siberia and Alaska since at least Cretaceous time.

Reconnaissance geologic investigations on St. Lawrence Island, Alaska, by the U.S. Geological Survey during 1971 (Patton and Csejtey, 1972) revealed a small area of poorly exposed nepheline syenite, a rock type not previously known from this part of the Bering Sea region. The present report is a brief description of the petrography, petrology, and regional relations of this nepheline syenite.

St. Lawrence Island, approximately 5,200 km² (2,000 mi²) in area, is in the shelf portion of the Bering Sea between the Seward Peninsula of mainland Alaska, 208 km (130 mi) to the northeast, and the Chukotsky Peninsula of Siberia, U.S.S.R., 64 km (40 mi) to the northwest (fig. 1). More than two-thirds of the island is a wave-cut platform covered by tundra and dotted by numerous small lakes. The remainder of the island consists of isolated groups of barren and rubble-covered mountains, once islands, rising sharply 300 to 600 m (1,000-2,000 ft) above the wave-cut platform.

Previous investigations on the geology of St. Lawrence Island consist of exploratory surveys along the coast at the turn of the century (Dawson, 1894; Emerson, 1904, p. 38–42; Collier, 1906) and an unpublished reconnaissance map compiled by E. H. Muller (Dutro and Payne, 1957). The results of more recent geologic investigations have been published in the following reports: Two short papers on the eastern part of the island (Patton and Dutro, 1969; Patton and Csejtey, 1971a), one report on the western part (Patton and Csejtey, 1971b), a summary of analyses of stream-sediment samples from the entire island (Patton and Csejtey, 1972), and a preliminary report on the granitic rocks of the island (Csejtey and others, 1971).

GEOLOGIC SETTING

Nepheline syenite occurs in the central part of St. Lawrence Island (fig. 2) on the wave-cut platform (fig. 3). Bedrock exposures of frost-riven rubble occur at three localities (fig. 4). Nepheline syenite float of subangular fragments as much as 0.5m (1½ ft) in maximum dimension is sparsely scattered, as part of the extensive surficial deposits, along creek beds and lake shores over an area of approximately 44 km² (17 mi²) (fig. 4). The distribution of the exposures and the float indicates that a significant portion of the 44-km² area is underlain by nepheline syenite. The uniform petrography and chemical composition of the nepheline syenite strongly suggest a single intrusive mass.

Country rocks older than the nepheline syenite are masked by surficial deposits, but they presumably consist of Paleozoic carbonate and Paleozoic to Cretaceous (?) clastic rocks as suggested by the occurrence of these strata in nearby areas (fig. 2; W. W. Patton, Jr., and Béla Csejtey, Jr., unpub. data,

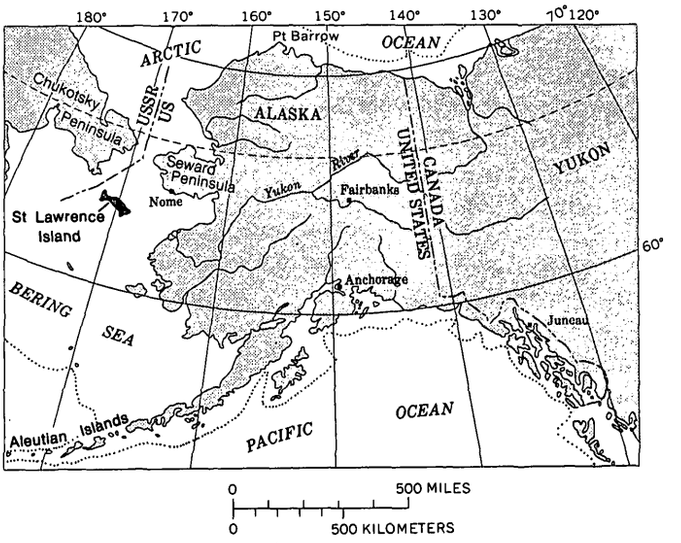

Figure 1.—Index map of Alaska showing location of St. Lawrence Island. Dotted line, 180-m bathymetric contour.

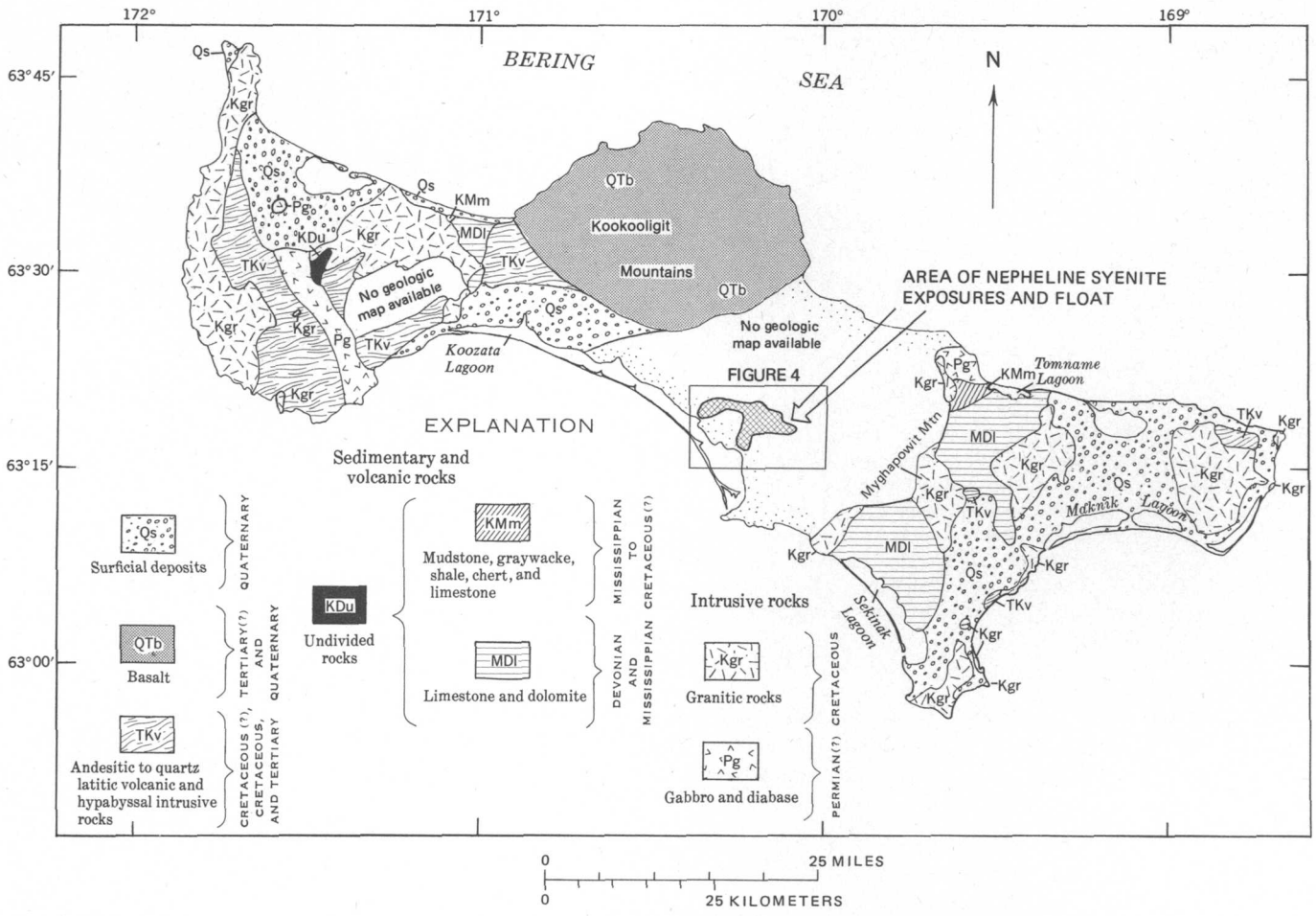

Figure 2.—Generalized geologic map of St. Lawrence Island, Alaska, showing location of nepheline syenite and area of figure 4. Geology from Patton and Csejtey (1971a, b).

Figure 3.— Typical view of lake-dotted wave-cut platform in the central part of St. Lawrence Island. Area of nepheline syenite exposures and float is in far distant center. Looking west from Myghapowit Mountain.

1973). Contacts of the nepheline syenite with the older country rocks are nowhere exposed but are assumed to be sharp and intrusive on the basis of correlation with epizonal nepheline syenite intrusives in adjacent land areas of the Bering Sea region (Miller, 1970a and 1972; Perchuk, 1965). Sharp intrusive contacts are further suggested by the lack of any float of metasomatized country rocks and by the presence of a few boulders of fine-grained probable border-phase nepheline syenite.

The adjacent biotite quartz monzonite and hornblende quartz monzonite plutons (fig. 4) are intrusive into, and therefore younger than, the nepheline syenite, as indicated in rubble exposures by the occurrence of chilled quartz monzonite border phases against coarse-grained nepheline syenite. Other post-nepheline syenite rocks in the unmapped part of central St. Lawrence Island, the blank area on the map (fig. 2), include Tertiary felsic volcanic and volcaniclastic rocks as well as extensive Quaternary surficial deposits (W. W. Patton, Jr., and Béla Csejtey, Jr., unpub. data, 1973).

NEPHELINE SYENITE

Petrography

The nepheline syenite on St. Lawrence Island is remarkably homogeneous. Excluding sparse fine-grained fragments of

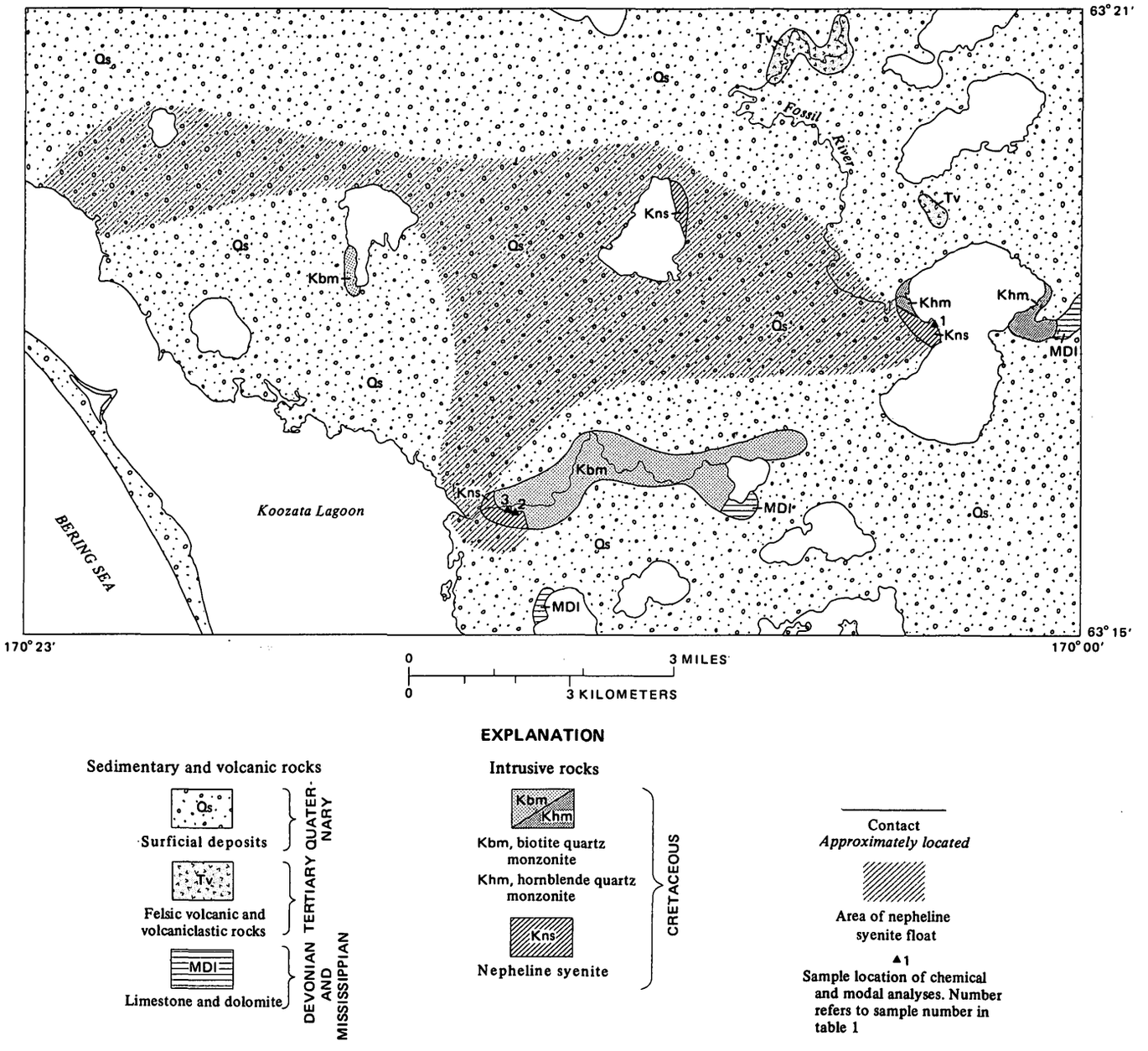

Figure 4.—Generalized geologic map of the nepheline syenite on central St. Lawrence Island, Alaska.

probable chilled border zone, no variants such as hybrid rocks or phases transitional toward more siliceous rocks were found. No late-stage dike rocks or xenoliths were observed.

In hand specimen the nepheline syenite is light to medium gray with a slight blue tint and has a somewhat oily appearance. The texture is coarse to medium grained, granitic to seriate with K-feldspar phenocrysts as much as 4 cm long. The rock is without any obvious linear or planar features.

Thin-section studies reveal the major rock-forming minerals to be K-feldspar, nepheline, biotite, and melanite garnet. The rock contains, in addition, a few small crystals of twinned sodic andesine, as well as sparse anhedral crystals of dark-green to light-greenish-brown hornblende.

The K-feldspar consists of orthoclase in coexistence with lesser microcline. Orthoclase is subhedral to anhedral, twinned, and always perthitic. It is the variation in grain size of the orthoclase that gives the rock its seriate texture. The position and shape of the (201) X-ray diffraction peak (Wright and Stewart, 1968; Wright, 1968) of several K-feldspar samples indicate a molecular composition between 84 and 90 percent orthoclase. In any one sample, the range of albite content is less than 5 percent. Microcline is present chiefly as separate anhedral crystals and commonly shows characteristic grid twinning and uneven extinction. X-ray studies indicate that it

is an intermediate microcline, the difference between 2θ of $(1\bar{3}0)$ and 2θ of (130) with Cu$K\alpha$ radiation being only about 0.3°. A small part of the total microcline occurs as optically continuous overgrowths on, or small irregular patches within, orthoclase crystals (fig. 5*A*). Under crossed nicols. orthoclase crystals containing patches of microcline show a splotchy texture. X-ray diffraction patterns confirm the occurrence of monoclinic orthoclase and triclinic intermediate microcline in the same crystal.

Nepheline in anhedral to subhedral crystals is more or less altered to sericite, zeolites, clay minerals, and minor cancrinite. Some crystals envelop already crystallized microcline and orthoclase (fig. 5*B*). Position of the $(21\bar{3}0)$ and $(20\bar{2}2)$ X-ray diffraction peaks for three samples indicates a composition that ranges from Ne_{71} to Ne_{75} (Hamilton and McKenzie, 1960). The remaining molecular components are estimated, on the basis of Hamilton's data (1961), to range from Ks_{19} to Ks_{25} and Qz_3 to Qz_6.

Biotite in irregular flakes is strongly pleochroic from yellow and light brown to dark green and greenish brown. Inclusions of minute zircon crystals with halos are common.

Melanite garnet, in anhedral to subhedral crystals as much as 1 cm in diameter, is dark to light yellowish brown in plane light; it commonly contains inclusions of sphene, magnetite, small shreds of dark-green biotite, and some feldspar (fig. 5*C*). Semiquantitative spectrographic analysis of a melanite separate indicates a titanium content of 2.0 weight percent. Unit-cell determinations for the same garnet sample, obtained by measuring the position of the (664), (842), and (840) X-ray diffraction peaks, yielded a cell dimension of 1.2038 ± 0.0006 nm (12.038 ± 0.006 A).

Purple fluorite in scattered anhedral crystals as much as 4 mm across is a uniquely characteristic accessory mineral. Sphene, magnetite, zircon, apatite, allanite, and sparse calcite constitute the other accessories.

Chemistry and petrology

Two chemical analyses and three modal counts were obtained on nepheline syenite from St. Lawrence Island (table 1) from two rubbly exposures approximately 8 km (5 mi) apart (fig. 4). The chemical analyses are remarkably similar, and the calculated norms agree well with the modes. The analyses of the St. Lawrence rocks compare quite closely with that of the average juvet-type nepheline syenite of Nockolds (1954).

Although only two samples were analyzed chemically, the good agreement between the analyses, as well as the uniform petrography of the St. Lawrence nepheline syenite, suggests that only one intrusive body is present and that some generalizations about its chemistry and inferred crystallization history may be valid.

The most characteristic chemical feature of the nepheline syenite is its high potassium content and high K_2O : Na_2O

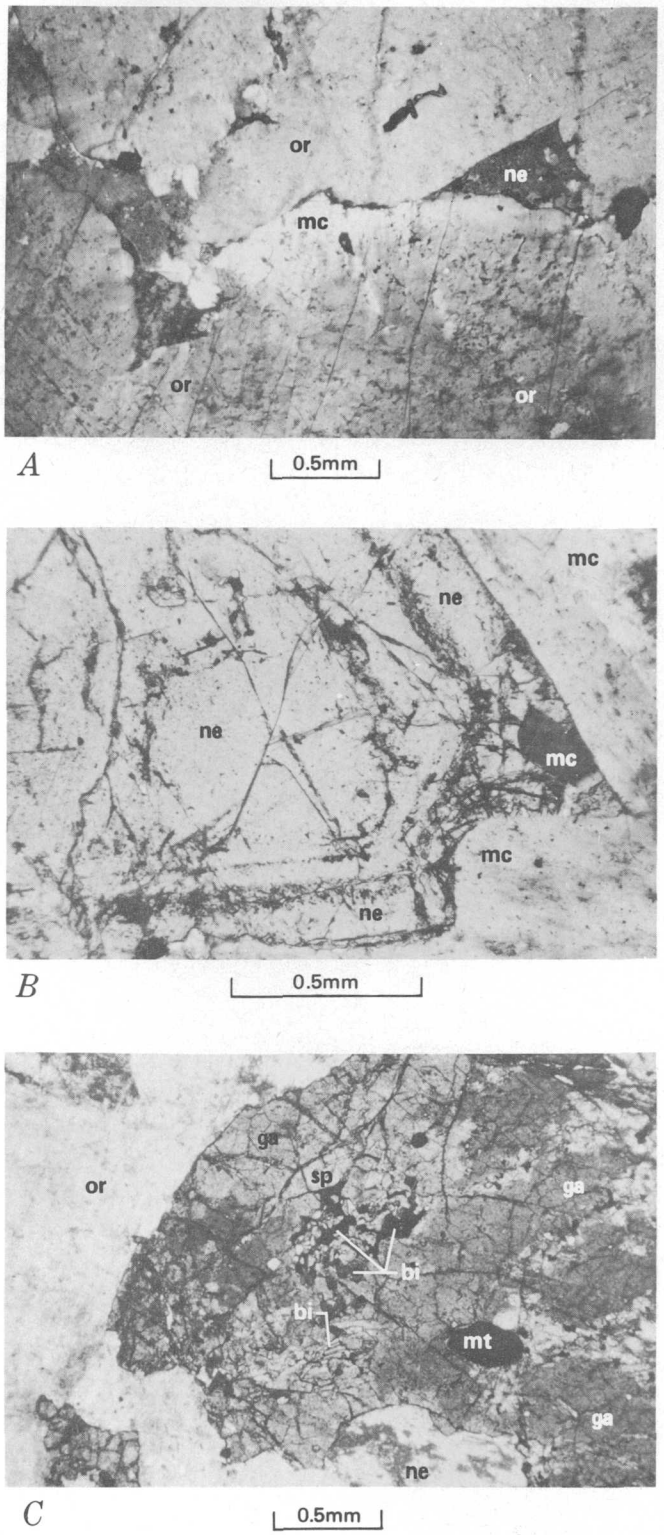

Figure 5.—Photomicrographs of nepheline syenite, St. Lawrence Island, Alaska. *A*, Microcline overgrowth (mc, light) in optic continuity with orthoclase (or, dark); nepheline (ne). *B*, Optically homogeneous nepheline (ne) displaying successive growth lines; late-stage growth is interstitial to and envelops already formed microcline (mc). *C*, Melanite garnet (ga) with minute inclusions of sphene (sp), biotite (bi), and magnetite (mt); orthoclase (or), and nepheline (ne).

Table 1.—*Chemical and modal data of nepheline syenite, St. Lawrence Island, Alaska*

[Rapid rock chemical analyses of samples 1 and 2 by Paul Elmore, Joseph Budinsky, and Leonard Shapiro. Semiquantitative six-step spectrographic analyses by Chris Heropoulos; results are to be identified with geometric brackets whose boundaries are 1.2, 0.83, 0.56, 0.38, 0.26, 0.18, 0.12... but are reported arbitrarily as midpoints of these brackets, 1.0, 0.7, 0.5, 0.3, 0.2, 0.15, 0.1...; the precision of a reported value is approximately plus or minus one bracket at 68-percent confidence or two brackets at 95-percent confidence. Quantitative analyses by W. D. Goss, A. W. Haubert, and Joseph Haffty; method from Haffty and Riley (1968.) D.I., differentiation index (Thornton and Tuttle, 1960). Locations of samples 1–3 are shown in fig. 4]

Chemical analyses

[Results in weight percent]

	1	2	A
SiO_2	54.0	54.4	53.11
Al_2O_3	21.3	23.1	21.39
Fe_2O_3	2.1	1.2	2.54
FeO	.60	.76	1.59
MgO	.25	.09	.72
CaO	4.4	2.2	2.89
Na_2O	4.7	6.6	5.98
K_2O	9.0	9.1	9.23
H_2O+	1.6	1.2	.79
H_2O-	.13	.16	--
TiO_2	.44	.23	.83
P_2O_5	.07	.02	.31
MnO	.15	.11	.12
CO_2	.52	.10	.26
Cl	.073	.11	.07
S	.04	.22	--
F	.42	.09	--
Total	99.793	99.69	99.83

Semiquantitative spectrographic analyses

[Results in parts per million]

	1	2
B	70	10
Ba	700	500
Be	7	3
Cr	2	2
Cu	<0.7	2
La	300	200
Mo	5	10
Nb	20	--
Pb	200	150
Sn	--	--
Sr	2,000	1,500
V	700	30
Y	100	50
Zr	500	150
Ce	500	300
Ga	30	30
Li	700	<200
Yb	7	3
Nd	150	100

Quantitative analyses

[Results in parts per million]

	1	2
Pd	<0.004	<0.004
Pt	< .010	< .010
Rh	< .005	< .005

Mode

[Results in volume percent; X indicates present]

	1	2	3
K-feldspar	65.2	68.8	63.4
Nepheline	28.5	27.3	28.7
Biotite	3.7	1.7	4.2
Garnet	.9	1.7	2.1
Accessory minerals	1.7	.5	1.6
Fluorite	X	X	X

CIPW norms

[Results in weight percent]

	1	2	A
or	53.4	54.2	54.5
ab	10.0	6.8	4.7
an	10.9	6.6	5.0
ne	16.2	26.8	24.1
wo	1.9	1.3	2.4
en	.6	.2	1.8
fs	--	.2	--
mt	1.2	1.8	3.2
hm	1.3	-	.3
il	.8	.4	1.5
ap	.2	.1	.7
fr	.9	.2	--
cc	1.2	.2	.6
salic	90.5	94.4	88.3
femic	8.1	4.4	10.5
D.I.	79.6	87.8	83.3

Table 1.—*Chemical and modal data of nepheline syenite, St. Lawrence Island, Alaska—Continued*

1. 71ACy-285d.
2. 71ACy-276b.
3. 71APa-306ab.

A. Juvet-type nepheline syenite of Nockolds (1954).

ratio. The rock is not peralkaline, however, the ratio $(K_2O+Na_2O):Al_2O_3$ being less than 1. It also has a rather high content of F and Cl. Trace-element concentrations of La, Pb, Sr, and Li are relatively high, whereas those of Ba and Nb are low, according to the data of Turekian and Wedepohl (1961) and Parker and Fleischer (1968). Analyses for platinum-group elements indicate that they are present but in amounts below the limits of determination.

The potassic as well as the undersaturated nature of the St. Lawrence nepheline syenite is also indicated by plotting the normative composition of the analyzed samples in the system nepheline-kalsilite-silica-water at a water-vapor pressure of 1,000 kg/cm^2 (fig. 6; from Hamilton and McKenzie, 1965). The St. Lawrence rocks plot in the leucite field below the albite-orthoclase join outside Hamilton and McKenzie's field of concentration for nepheline syenites.

Plotting the compositions of the coexisting nephelines and alkali feldspars of the analyzed rock samples in figure 6 reveals that the tielines of these mineral pairs lie quite close to the plot of their parent rock samples. The tielines closely parallel tielines of mineral pairs crystallized experimentally under equilibrium conditions by Hamilton (1961) and Fudali (1963). On this basis the St. Lawrence nepheline syenite appears to have crystallized under dominantly equilibrium conditions.

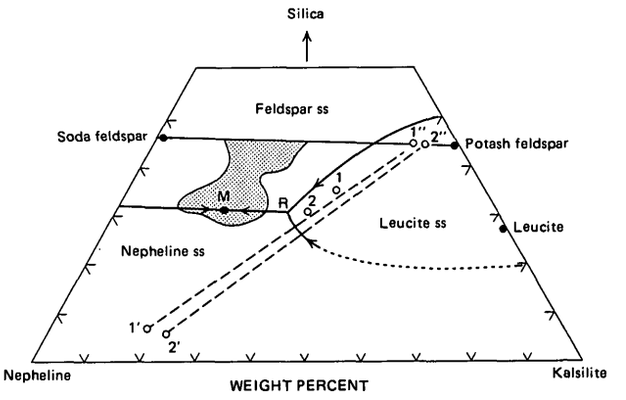

Figure 6.—Normative composition of analyzed samples of nepheline syenite, St. Lawrence Island, Alaska, in the system nepheline-kalsilite-silica-water at P_{H_2O} = 1,000 kg/cm^2 (Hamilton and MacKenzie, 1965). Nos. 1 and 2 refer to samples in table 1. Coexisting alkali feldspars (1'' and 2'') and nephelines (1' and 2') of samples 1 are 2 are connected by tielines. Stippled area is field of concentration for nepheline syenites of Hamilton and MacKenzie. M is a temperature minimum and R is a reaction point.

Crystallization of the nepheline syenite under more or less equilibrium conditions is further suggested by some textural features as compared with Fudali's (1963) experimental work in the system nepheline-kalsilite-silica-water at P_{H_2O} = 1,000 kg/cm^2. According to Fudali's work, under equilibrium crystallization, the final mineral assemblage out of a liquid of the same composition as either of the St. Lawrence samples consists of nepheline and feldspar after the first crystallized leucite disappears at reaction point R (fig. 6). Composition of the last liquid to crystallize lies on the nepheline-feldspar phase boundary not far below R. Such a crystallization history is borne out by several optically homogeneous nepheline crystals displaying growth lines marked by minute inclusions. Earlier growth stages show euhedral outlines, whereas the last stages envelop, or are interstitial to, previously crystallized potash feldspars (fig. 5*B*).

In summary, the nepheline syenite of St. Lawrence Island is interpreted to have crystallized under dominantly equilibrium conditions from the single intrusion of a potassium- and volatile-rich magma. The subsequent intrusion of the granitic rocks indicates that the nepheline syenite magma formed independently of the granites and not by in situ fractionation (Fudali, 1963). The high potassium content of the nepheline syenite may indicate a mantle origin (O'Hara and Yoder, 1967; Carmichael, 1967; Miller, 1972). The low platinum-group element concentrations do not support a mantle origin, but do not necessarily preclude it. Apparent sharp contacts and fine-grained border phases suggest emplacement in the epizone (Buddington, 1959).

Age and correlation

Stratigraphic evidence and regional correlation suggest a mid-Cretaceous age for the St. Lawrence nepheline syenite. No isotope age determinations of the nepheline syenite were made.

A minimum age limit is provided by the transection of the nepheline syenite by biotite quartz monzonite and by hornblende quartz monzonite, the two youngest members of the approximately 100-m.y.-old granitic intrusive series of St. Lawrence Island (Csejtey and others, 1971). Country rocks intruded by the nepheline syenite are nowhere exposed, but the occurrence of Devonian to Cretaceous (?) strata in nearby areas (fig. 2; W. W. Patton, Jr., and Béla Csejtey, Jr., unpub. data, 1973) indicates an oldest possible age of Devonian for the nepheline syenite.

Lack of evidence for pre-mid-Cretaceous (about 100 m.y.) felsic plutonism on St. Lawrence Island and the occurrence of similar mid- and Late Cretaceous feldspathoidal rocks on the Seward Peninsula (Miller, 1970a, 1970b, 1972) and on the Chukotsky Peninsula, U.S.S.R. (Shilo, 1965; Perchuk, 1965; Miller, 1972), suggest that the St. Lawrence nepheline syenite belongs to a plutonic episode roughly 100 m.y. old.

The St. Lawrence nepheline syenite provides additional evidence for the existence of two distinctive suites of Cretaceous epizonal plutons in the northern Bering Sea region—one undersaturated alkaline (Miller, 1972) and one granitic, that is, calcalkaline (Miller, 1970a, 1970b; Csejtey and others, 1971). The alkaline intrusive bodies are about the same age as the considerably more voluminous granitic plutons (approximately 80 to 100 m.y. old) and occur in close spatial association with the granites. Plutons of the two suites form a broad continuous belt that extends from the Seward Peninsula across St. Lawrence Island into the Chukotsky Peninsula, U.S.S.R. The tectonic implication of this plutonic belt is that these land areas and neighboring shelves have belonged to the same tectonic unit—the "North American" plate—since at least mid-Cretaceous time. Thus, the westernmost edge of the "North American" plate, as suggested by Churkin (1972) and by Patton and Tailleur (1972), must be located not in the Bering Sea area but to the west in Siberia.

REFERENCES CITED

Buddington, A. F., 1959, Granite emplacement with special reference to North America: Geol. Soc. America Bull., v. 70, p. 671–747.

Carmichael, Ian S. E., 1967. The mineralogy and petrology of the volcanic rocks from the Leucite Hills, Wyoming: Contr. Mineralogy and Petrology, v. 15, p. 24–66.

Churkin, Michael, Jr., 1972, Western boundary of the North American continental plate in Asia: Geol. Soc. America Bull., v. 83, p. 1027–1036.

Collier, A. J., 1906, Geology and coal resources of the Cape Lisburne region, Alaska: U.S. Geol. Survey Bull. 278, 54 p.

Csejtey, Béla, Jr., Patton, W. W., Jr., and Miller, T. P., 1971, Cretaceous plutonic rocks of St. Lawrence Island, Alaska—A preliminary report *in* Geological Survey research 1971: U.S. Geol. Survey Prof. Paper 750-D, p. D68–D76.

Dawson, G. M., 1894, Geological notes on some of the coasts and islands of the Bering Sea and vicinity: Geol. Soc. America Bull., v. 5, p. 117–146.

Dutro, J. T., Jr., and Payne, T. G., 1957, Geologic map of Alaska: U.S. Geol. Survey, scale 1:2,500,000.

Emerson, B. K., 1904, General geology; notes on the stratigraphy and igneous rocks [of Alaska]: Washington, Smithsonian Inst., Harriman Alaska Series, v. 4: p. 11–56.

Fudali, R. F., 1963, Experimental studies bearing on the origin of pseudoleucite and associated problems of alkalic rock systems: Geol. Soc. America Bull., v. 74, p. 1101–1126.

Haffty, Joseph, and Riley, L. B., 1968, Determination of palladium, platinum, and rhodium in geologic materials by fire-assay and emission spectrography: Talanta, v. 15, p. 111–117.

Hamilton, D. L., 1961, Nephelines as crystallization temperature indicators: Jour. Geology, v. 69, p. 321–329.

Hamilton, D. L., and McKenzie, W. S., 1960, Nepheline solid solution in the system $NaAlSiO_4$-$KAlSiO_4$-SiO_2: Jour. Petrology, v. 1, p. 56–72.

——1965, Phase equilibrium studies in the system $NaAlSiO_4$ (nepheline)-$KAlSiO_4$ (kalsilite)-SiO_2-H_2O: Mineralog. Mag., v. 34, p. 214–231.

Miller, T. P., 1970a, Petrology of the plutonic rocks of west-central Alaska: Palo Alto, Calif., Stanford Univ., Ph. D. thesis, 132 p.

——1970b, Preliminary correlation of Mesozoic plutonic rocks in the Bering Sea region [abs]: Am. Assoc. Petroleum Geologists Bull., v. 54, no. 12, p. 2496.

——1972, Potassium-rich alkaline intrusive rocks of western Alaska: Geol. Soc. America Bull., v. 83, p. 2111–2127.

Nockolds, S. R., 1954, Average chemical compositions of some igneous rocks: Geol. Soc. America Bull., v. 65, p. 1007–1032.

O'Hara, M. J., and Yoder, H. S., Jr. 1967, Formation and fractionation of basic magmas at high pressures: Scottish Jour. Geology, v. 3, pt. 1, p. 67–117.

Parker, R. L., and Fleischer, Michael, 1968, Geochemistry of niobium and tantalum: U.S. Geol. Survey Prof. Paper 612, 43 p.

Patton, W. W., Jr., and Csejtey, Béla, Jr., 1971a, Preliminary geologic investigations of eastern St. Lawrence Island, Alaska: U.S. Geol. Survey open-file rept., 52 p.

_____1971b, Preliminary geologic investigations of western St. Lawrence Island, Alaska: U.S. Geol. Survey Prof. Paper 684-C, p. C1–C15.

_____1972, Analyses of stream-sediment and rock samples from St. Lawrence Island, Alaska, 1966-1971: U.S. Geol. Survey open-file rept., 78 p.

Patton, W. W., Jr., and Dutro, J. T., Jr., 1969, Preliminary report on the Paleozoic and Mesozoic sedimentary sequence on St. Lawrence Island, Alaska, *in* Geological Survey research 1969: U.S. Geol. Survey Prof. Paper 650–D, p. D138–D143.

Patton, W. W., Jr., and Taillcur, I. L., 1972, Evidence in the Bering Strait region for differential movement between North America and Eurasia [abs.]: Geol. Soc. America Abs. with Programs, v. 4, no. 7, p. 623.

Perchuk, L. L., 1965, Magmatic replacement of carbonate bodies involving formation of nepheline syenites and other alkalic rocks, with example of Cape Dezhnev massif: Internat. Geology Rev., v. 7, no. 2, p. 280–296.

Shilo, N. A., ed., 1965, Pozdnemezozoyskiye granitoidy Chukotki [Late Mesozoic granitic rocks of Chukotka]: Akad. Nauk SSSR Sibirsk. Otdeleniye Severo-Vostoch. Kompleks. Nauchno-Issled. Inst. Trudy, vyp. 12, 243 p. [In Russian]

Thornton, C. P., and Tuttle, O. F., 1960, Chemistry of igneous rocks–Pt. 1, differentiation index: Am. Jour. Sci., v. 258, p. 664–684.

Turekian, K. K., and Wedepohl, K. H., 1961, Distribution of the elements in some major units of the Earth's crust: Geol. Soc. America Bull., v. 72, p. 175–192.

Wright, T. L., 1968, X-ray and optical study of alkali feldspar–[Pt.] 2, An X-ray method for determining the composition and structural state from measurement of 2θ values for three reflections: Am. Mineralogist, v. 53, p. 88–104.

Wright, T. L., and Stewart, D. B., 1968, X-ray and optical study of alkali feldspar–[Pt.] 1, Determination of composition and structural state from refined unit-cell parameters and $2V$: Am. Mineralogist, v. 53, p. 38–87.

Jour. Research U.S. Geol. Survey
Vol. 2, No. 1, Jan.-Feb. 1974, p. 49–59

CHAOS CRAGS ERUPTIONS AND ROCKFALL-AVALANCHES, LASSEN VOLCANIC NATIONAL PARK, CALIFORNIA

By DWIGHT R. CRANDELL, DONAL R. MULLINEAUX; ROBERT S. SIGAFOOS, and MEYER RUBIN, Denver, Colo.; Washington, D.C.

Abstract.—The Chaos Crags are a group of dacite domes which lie just north of Lassen Peak in northern California. Extrusion of the domes was preceded by pyroclastic volcanism at the same eruptive center which produced pumiceous tephra and hot pyroclastic flows, some of which traveled as far as 8 km. Radiocarbon dates on charcoal from the pyroclastic-flow deposits range from about 1,000 to 1,200 yr. Four or more domes were then erupted which have an estimated combined volume of about 1 km^3. About 300 yr ago, three or more rockfalls from the domes caused high-velocity, air-cushioned avalanches of rock debris which traveled as far as 4.3 km. Pyroclastic flows are regarded as a potential hazard if future volcanic activity occurs in the Chaos Crags-Lassen Peak area. Large rockfall-avalanches from the steep sides of the Chaos Crags might be triggered by a volcanic explosion, by a severe earthquake, or by the eruption of another dome. Either a pyroclastic flow or a rockfall-avalanche could endanger persons and property in the Manzanita Lake area, which is only 2 km from the base of the Chaos Crags and is the most heavily used part of Lassen Volcanic National Park.

The Chaos Crags eruptive center lies just north of the base of Lassen Peak in north-central California (fig. 1). During an assessment of potential geologic hazards in Lassen Volcanic National Park we concluded that some of the most catastrophic geologic events of the recent past resulted directly or indirectly from volcanism at the site of the Chaos Crags. In brief, the Chaos Crags eruptive episode began with explosive eruptions of dacite pumice, some of which resulted in hot pyroclastic flows; these were followed by the extrusion of dacite domes to form the Chaos Crags. Much later, parts of the domes collapsed and caused avalanches of rock debris which traveled as far as 4.3 km and created the Chaos Jumbles (fig. 1). Both the hot pyroclastic flows and the avalanches covered parts of an area that is now occupied by various facilities at the park's Manzanita Lake visitor center.

Williams (1928, 1932) described the pyroclastic eruptive activity at the site of the Chaos Crags as well as the eruption of the domes and the subsequent rockfall-avalanches. He believed that the volcanism and the avalanches occurred within a short time span about 200 yr ago (Williams, 1932, p. 350, 359). From a subsequent study of the avalanche deposits, however, Heath (1960, 1967) concluded that rockfall-avalanches had occurred at three widely separated times between about 1,500 and 300 yr ago. Macdonald (1963, 1964) mapped the geology of the Manzanita Lake and Prospect Peak quadrangles, in which the Chaos Crags lie, and recognized the presence of pyroclastic-flow deposits.

In the course of our study we found that the Chaos Crags eruptive episode occurred between about 1,000 and 1,200 yr ago and included pyroclastic eruptions separated by intervals of as much as several decades. We also concluded that the Chaos Jumbles were formed by three or more high-speed air-cushioned avalanches, all of which occurred about 300 yr ago. The following discussion describes the evidence on which these conclusions are based, summarizes our view of the sequence of geologic events in the Chaos Crags area, and points out the potential hazards if similar events occur in that area in the future.

The terms "pyroclastic-flow deposit" and "tephra" are defined here because these terms have been used previously in a different sense, or because the events or deposits they describe have had other names applied to them by other workers. We will use the term "pyroclastic-flow deposit" to describe the deposit of a hot dry flow of volcanic rock debris that is propelled chiefly or wholly by gravity and lubricated by air trapped and heated within the debris, or by hot gases emitted by the rock debris, or by both. The deposits described here as tephra originated as fragmental material that was erupted high into the air and then carried laterally either by the force of the eruption or by wind as the material fell back to the land surface.

The 1914–17 volcanic activity at Lassen Peak, which included the eruption of tephra and lava, the formation of lahars, and a hot lateral blast of great force, has been described by Day and Allen (1925), Williams (1932), and others. Although future volcanism of these kinds would surely endanger life and property, the volcanic history and potential hazards of Lassen Peak are not described in this report.

DEPOSITS FORMED DURING THE CHAOS CRAGS ERUPTIVE EPISODE

The Chaos Crags eruptive episode began with eruptions of dacite pumice and nonvesicular rock fragments from vents that are now covered by the Chaos Crags domes. The resulting sequence of tephra deposits in the area adjacent to the south side of the Chaos Crags includes alternating beds of ash, lapilli,

and blocks. The upper part of the sequence may include a few fine-grained pyroclastic-flow deposits, and the sequence is overlain by such a deposit which contains moderately vesicular blocks of dacite as large as 2.5 m across. Most of the tephra deposits consist of white pumiceous rock in which the only abundant Fe-Mg minerals are hornblende and biotite. Orthopyroxene, clinopyroxene, and olivine are sparse in some rock fragments and absent in others.

The tephra deposits are more than 2 m thick in the area between the base of Lassen Peak and the Chaos Crags. To the east they gradually thin to 0.3–0.6 m at a distance of 3–5 km. In the Butte Lake area, about 19 km northeast of the Chaos Crags, the tephra deposits are about 1 cm thick. To the west they thin more abruptly, and are barely recognizable beyond the boundary of Lassen Volcanic National Park 4 km west of the Chaos Crags.

Close to the vents some showers of pumice were hot enough to char vegetation. One such shower which fell to the southwest is represented by a charcoal-bearing pumice deposit as much as 15 cm thick on the west flank of Loomis Peak, 4 km from the Chaos Crags. Charcoal was also found in tephra deposits at several places directly south of the Chaos Crags, and about 3 km southeast of the Chaos Crags in the northwestern part of the Devastated Area.

The eruptions that formed these deposits did not all occur in quick succession. At one place small trees that had taken root in one tephra layer had grown for more than a decade and had reached a height of nearly a meter before they were buried and converted to charcoal by a subsequent fall of hot pumice. Although an exact timespan cannot be assigned to the intervals between pyroclastic eruptions, it may have taken as much as several decades for conifer seedlings to become established on a newly erupted tephra deposit.

Pyroclastic-flow deposits

During the Chaos Crags eruptive episode pyroclastic flows of hot pumice repeatedly moved from the vent areas downslope into the valleys of Manzanita and Lost Creeks. Williams (1928, p. 243) included both the tephra and the pyroclastic-flow deposits in his description of a "thick mantle of tuff, carrying plentiful lapilli and 'bread-crust' bombs of a hornblende dacite, [which] covers the slope which descends from the base of the crags onto the broad plateau west of Manzanita Lake." Macdonald (1963) differentiated the tephra deposits from the "ash flow of Manzanita Creek." He (Macdonald, 1964) also collected charcoal from a possible "glowing avalanche" deposit along Lost Creek, but did not map pyroclastic-flow deposits in the Lost Creek valley.

The pyroclastic-flow deposits are loose unsorted mixtures of breadcrusted blocks and lapilli of dacite pumice in a matrix of sand-sized pumice; angular lapilli of nonvesicular glass are common. The deposits of individual pyroclastic flows are generally 1–4.5 m thick. The multiple nature of the deposits is shown by exposures in the bank of Manzanita Creek 0.7 km east of Manzanita Lake, where four pyroclastic-flow deposits can be seen superposed (measured section 1).

Measured section 1

[Location: NW¼SW¼ sec. 17, T. 31 N., R. 4 E.]

		Meters
9.	Sand and gravel, stratified, consisting of pumice and nonvesicular rock; some beds are white to very pale brown well-sorted medium sand; breadcrusted blocks of pumice on surface of deposit probably were emplaced by a later pyroclastic flow	1.0
8.	Pyroclastic-flow deposit: unstratified and poorly sorted mixture of white ash- and lapilli-sized pumice and nonvesicular rock fragments; upper 0.3 m is light reddish brown	> 1.5
Covered interval		3.3
7.	Sand and gravel, white, contains scattered angular fragments of pumice and nonvesicular rock, horizontally stratified.	> 1.5
6.	Pyroclastic-flow deposit: unstratified and unsorted mixture of pumice and nonvesicular rock fragments as large as 1.5 m in diameter in matrix of white fine to coarse ash, faint pinkish-gray cast in upper 1 m	1.2
5.	Pyroclastic-flow deposit: unstratified and poorly sorted mixture of pumice and nonvesicular rock fragments mostly less than 15 cm in diameter in white ash matrix, contains abundant charcoal (radiocarbon sample W-2137, 1,120±300 yr)	1.0
4.	Silt and fine to medium sand, pinkish-gray; contains scattered fragments of pumice and nonvesicular rock which are mostly less than 2 cm in diameter	0.3–0.5
3.	Pyroclastic-flow deposit(s): medium to coarse white ash mixed with lapilli of nonvesicular rock and breadcrusted blocks of pumice, contains charcoal (radiocarbon sample W-2135: 1,230±300 yr), zone 1.8–2.4 m above base is faintly bedded and may represent a contact between two pyroclastic-flow deposits	3.6
2.	Fine to very fine sand, grayish-brown, horizontally bedded	0.03
1.	Glacial drift: boulders of nonvesicular dacite in matrix of fine to medium sand, oxidized yellowish brown	> 1.0

Charcoal samples from the two lowest pyroclastic-flow deposits along Manzanita Creek had radiocarbon ages of 1,230±300 (W-2135) and 1,120±300 (W-2137) yr. Trees more than 325 yr old grow on top of the youngest pyroclastic-flow deposits at this locality. No evidence was found within the sequence of a time interval between successive pyroclastic flows, and we infer that they all were formed during a single, though intermittent, eruptive episode between about 1,200 and 1,000 yr ago. In a review of volcanism in northern California, Macdonald (1966) reported a radiocarbon date of less than 200 yr (W-812; see Rubin and Alexander, 1960, p. 156) for charcoal from a "glowing avalanche" deposit in the vicinity of Manzanita Lake, and noted that the avalanche "appears to have come from Lassen Peak but may have occurred about the time of the last eruption of the Chaos Crags."

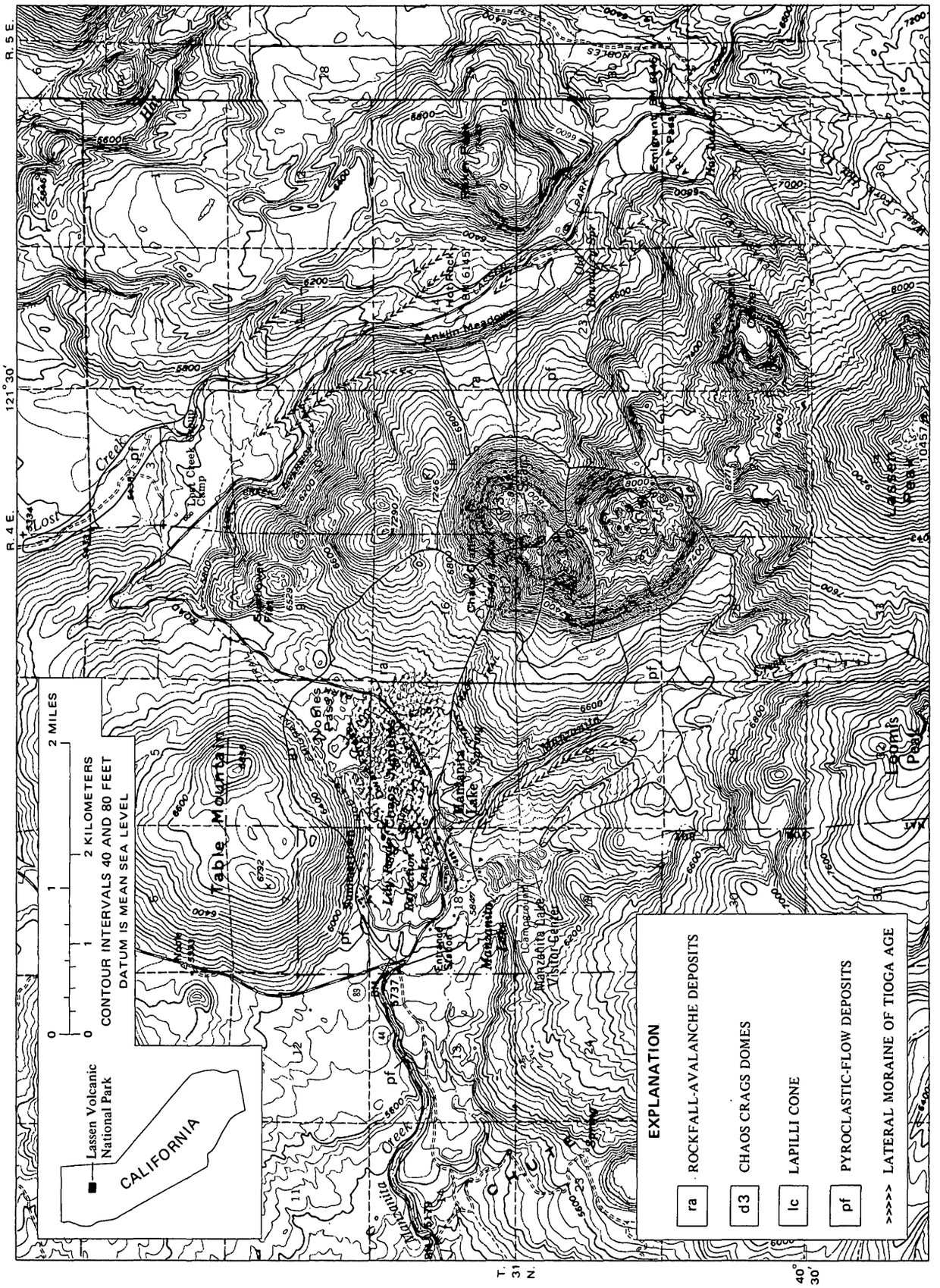

Figure 1.–Map of the northwestern part of Lassen Volcanic National Park, showing distribution of geologic units described in text. Subdivisions of the Chaos Crags domes also are discussed in text.

The significance of the date reported by Macdonald is not known, but our radiocarbon dates and tree-ring data indicate that it does not apply to the pyroclastic-flow deposits discussed here.

The interpretation of units 3, 5, 6, and 8 in measured section 1 as pyroclastic-flow deposits is based on the abundance of pumice in them, poor size-sorting, and on evidence that the deposits were emplaced at a high temperature. This evidence includes the facts that all the wood observed in those units has been converted to charcoal, and that pinkish-gray oxidized zones are present at the tops of some of the deposits. In addition, examination of rock fragments from some of the deposits with a fluxgate magnetometer showed a preferred orientation of remanent magnetism (fig. 2); thus, ferromagnetic minerals in the rock fragments were still above their Curie temperatures (probably at least several hundred degrees C) when the deposits came to rest (Aramaki and Akimoto, 1957; Crandell, 1971, p. 5). Similar deposits at the present ground surface show digitate margins and other features that suggest an origin by flowage.

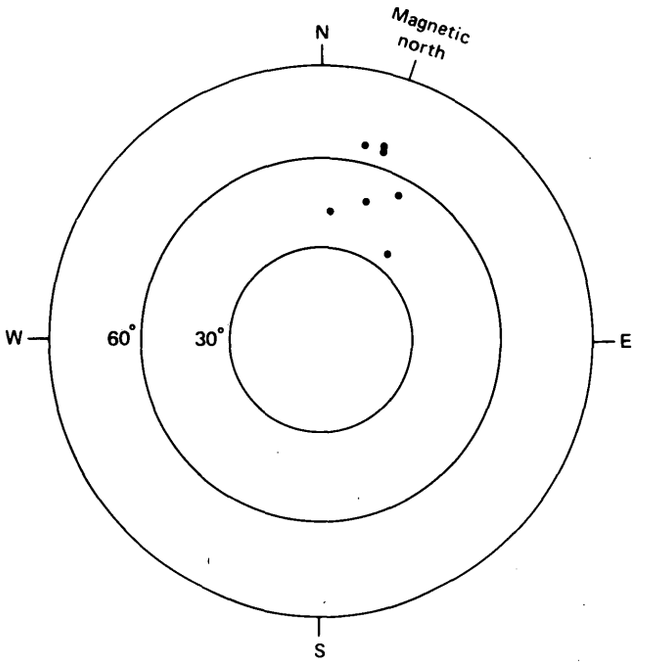

Figure 2.– Point diagram of azimuth and dip of north-seeking poles in pumice fragments from a pyroclastic-flow deposit (unit 3, measured section 1).

Breadcrusted blocks of pumice are so abundant at the surface of some pyroclastic flows that they form a virtual "pavement" (fig. 3). The exposed dimensions of some of these blocks are as much as 2 by 2.5 m, and blocks 0.5 m in diameter are common. Just west of Manzanita Creek, in an area 2.5 km southeast of Manzanita Lake, a pyroclastic-flow deposit that forms the ground surface probably is not more than 2 m thick, but blocks as large as 1.2 by 1.5 by 1.5 m are present at its surface.

The lateral margin of the pyroclastic-flow deposit that forms the ground surface west of Manzanita Creek is digitate; one lobe along the margin is about 15 m long and 5–6 m wide, and another is 8 m long and 2–3 m wide. These lobes stand about 0.5 m higher than the preexisting surface beyond them. Elsewhere the margin of the deposit is somewhat higher than the main body of the deposit and resembles a levee typically formed by a mudflow. Although these marginal features suggest formation by a lahar, remanent magnetism of blocks in one of the lobes indicates that the deposit was emplaced as a hot pyroclastic flow.

The pyroclastic flows that moved westward into the Manzanita Creek drainage seem to have come from at least two vent areas, one at the south end and the other at the north end of the site of the Chaos Crags. The flows originating at the southern vent area followed two principal routes. Some moved northwestward down the Manzanita Creek valley and were channeled by a lateral moraine. At the northern end of the moraine, 0.6 km east of Manzanita Lake, the flows spread out and covered much of the low area east and northeast of the lake. The sequence of deposits in measured section 1 indicates that at least four pyroclastic flows followed this route. Other flows moved directly westward from the southern vent area across the head of Manzanita Creek and extended down a valley parallel to and 0.5 km west of Manzanita Creek, terminating near the southeast edge of the site of Manzanita Lake campground.

The pyroclastic flows originating at the northern vent area moved west along the area now covered by the Chaos Jumbles, and one flow reached nearly 4 km west of the park down the Manzanita Creek valley. The deposit of this pyroclastic flow crops out in roadcuts along State Highway 44, and it is especially well exposed in a roadcut at the junction of Highways 44 and 89 (fig. 4), where it is 1–2 m thick and consists of blocks of breadcrusted pumice in a white ash matrix. It overlies a soil profile developed on a pyroclastic-flow deposit that is more than 32,000 yr old (radiocarbon sample W-2259; Crandell, 1972, p. C182). Abundant charcoal and the preferred orientation of magnetic poles in the pumice blocks indicate that the upper pyroclastic-flow deposit was hot when it came to rest.

Pyroclastic-flow deposits from vents now hidden by the Chaos Crags form a fill terrace in the Lost Creek valley and blanket much of the west valley wall between the base of the Crags and the valley floor upstream from the Lassen Park Road bridge in sec. 14. Four pyroclastic-flow deposits in the valley are well exposed in the west bank of Lost Creek just downstream from the bridge (measured section 2). Pumice blocks from units 4 and 9 of the sequence described here have a preferred magnetic orientation; thus, the deposits were hot

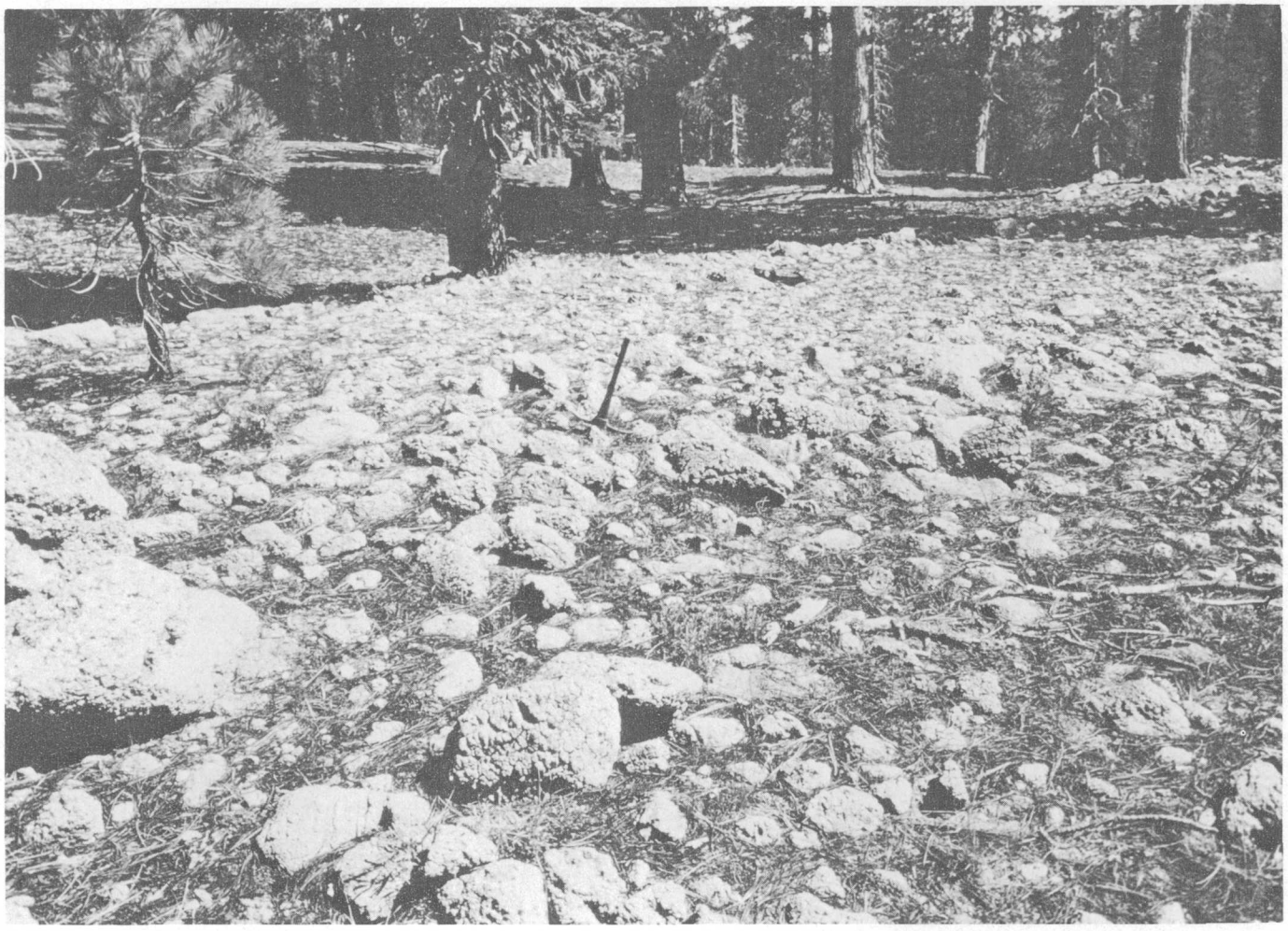

Figure 3.—Ground surface west of the Chaos Crags is made up of a pavement of breadcrusted pumice blocks deposited by hot pyroclastic flows (see text).

when they were emplaced. Macdonald (Rubin and Alexander, 1960, p. 155) collected charcoal from this locality which had a radiocarbon age of 1,320±200 yr (W-758), but the stratigraphic horizon from which the sample was collected is uncertain. A sample of charcoal collected by us for radiocarbon dating from the lowest pyroclastic-flow deposit exposed (unit 4 of measured section 2) had an age of 1,010±250 yr (W-2261). The deposits here are thus about the same age as those in the area west of the Chaos Crags.

Measured section 2

[Location: NE¼NW¼ sec. 14, T. 31 N., R. 4 E.]

		Meters
10.	Tephra: mixture of pumice and nonvesicular rock fragments as large as 5 cm in diameter in a loose ash matrix	0.09
9.	Pyroclastic-flow deposit: pumice blocks as large as 0.3 m and nonvesicular glassy rock fragments 1–6 cm in diameter in a white ash matrix; deposit has a pinkish-gray cast in upper 1.5–1.8 m and contains charcoal; layer of forest duff 5–7 cm thick at top	4.5
8.	Pyroclastic-flow deposit: pumice and nonvesicular rock fragments as large as 7 cm in diameter in a white ash matrix; upper contact is gradational	0.3
7.	Sand and granule gravel, horizontally bedded	0.15
6.	Pyroclastic-flow deposit; pumice blocks in a light-gray to white ash matrix	1.8
5.	Silt and fine sand, pinkish-gray; lower contact is sharp but upper contact is gradational	0.27
4.	Pyroclastic-flow deposit: weakly breadcrusted pumice blocks in a light-gray to white ash matrix, contains charcoal (radiocarbon sample W-2261: 1,010±250 yr)	1.0
3.	Sand and granule to pebble gravel, consists chiefly of white pumice, locally has lenses of white sand at top	1.0
2.	Peat and peaty silt (radiocarbon sample W-2232 from top 0.75 cm: 4,600±600 yr; radiocarbon sample W-2231 from bottom 0.75 cm: 5,400±600 yr)	1.0
1.	Sand and pebble to cobble gravel, consists mostly of gray and reddish-gray dacite.	> 0.7

Figure 4.—Charcoal-bearing pyroclastic-flow deposit overlying an older, weathered pyroclastic-flow deposit in a roadcut near the west edge of Lassen Volcanic National Park (see text).

Pumice deposits on the west valley wall west of the line between secs. 23 and 24 were formed mostly by pyroclastic flows, but those east of that line seem to be wholly tephra. The tephra deposits do not include the breadcrusted pumice blocks that characterize the pyroclastic-flow deposits. Some of the hot pyroclastic flows continued down the Lost Creek valley beyond the north edge of sec. 3.

At least one pyroclastic flow extended up onto the east valley wall of Lost Creek directly east of the highway bridge in sec. 14. The highest flow deposit is about 38 m above the valley floor. If resistance due to friction is not considered, this flow must have been moving at least 100 km/h (60 mi/h) across the valley floor, in order to have reached so high on the valley wall. The pyroclastic flow probably originated at a vent about 2.4 km to the southwest, at an altitude of at least 2,120 m (7,000 ft), and acquired high velocity as it flowed downward through a vertical distance of nearly 330 m to the floor of the Lost Creek valley.

Chaos Crags domes

The dacite domes that form the Chaos Crags cover an area of about 5 km^2 and rise 300–450 m above their base which is at an altitude of about 2,120 m (fig. 5). The Crags include two main "protrusions" (Williams, 1928, p. 245–249). The southern protrusion is a roughly circular dome (labeled d1 on fig. 1) about 1.7 km in maximum diameter. Its southern edge has disrupted a small lapilli cone about 400 m in diameter. The northern protrusion of Williams consists of a cluster of three domes (labeled d2, d3, d4, on fig. 1). Dome 2, on the northwest side of the cluster, was mostly removed by the great rockfalls which formed the Chaos Jumbles. To the east, dome 3 consists of two parts—a high mass on the southwest is separated from a lower northeast mass by an arcuate scarp; this lower mass may actually be another dome.

Areas of hydrothermally altered rock locally stain the Chaos Crags and are especially abundant on domes 2 and 3. The alteration probably occurred mostly during the eruption and cooling of the domes, but large volumes of steam and other gases were reported to be issuing from dome 4 as recently as 1857 (Williams, 1932, p. 347).

The surfaces of all the domes are extremely rough and consist of "a chaotic assemblage of gigantic, loose, angular blocks" (Williams, 1928, p. 246). Williams inferred that the lava which formed the domes moved dominantly upward and that the dacite was too stiff to move far laterally. However, flow banding with a low inward dip indicates some lateral flow near the southern margin of the southern dome (Williams, 1928, p. 245–246), and the westward extension of this dome down across a topographic scarp suggests more than 350 m of lateral movement there.

The volume of the domes seems to be approximately equal to the volume of the tephra and pyroclastic-flow deposits. If it is assumed that the domes have an average thickness of 200 m, their total volume is 1 km^3. The total volume of all the fragmental material probably does not exceed 1 km^3.

There is no direct evidence of the age of the Chaos Crags domes, except that they postdate the pyroclastic-flow deposits which are between about 1,000 and 1,200 yr old. By analogy with similar eruptive sequences which have been observed, Williams (1932, p. 350) suggested that the time interval between the tephra eruptions and the later eruption of a dome from the same vent may not have been more than a few weeks or months. It is not known, however, whether all the domes were erupted at the same time. The charcoal remains of small trees rooted in one tephra layer and buried by another show that perhaps several decades elapsed between tephra eruptions. This, as well as the range of radiocarbon dates, suggests that the various eruptive events which produced tephra, pyroclastic flows, and domes may have been separated by several quiescent intervals.

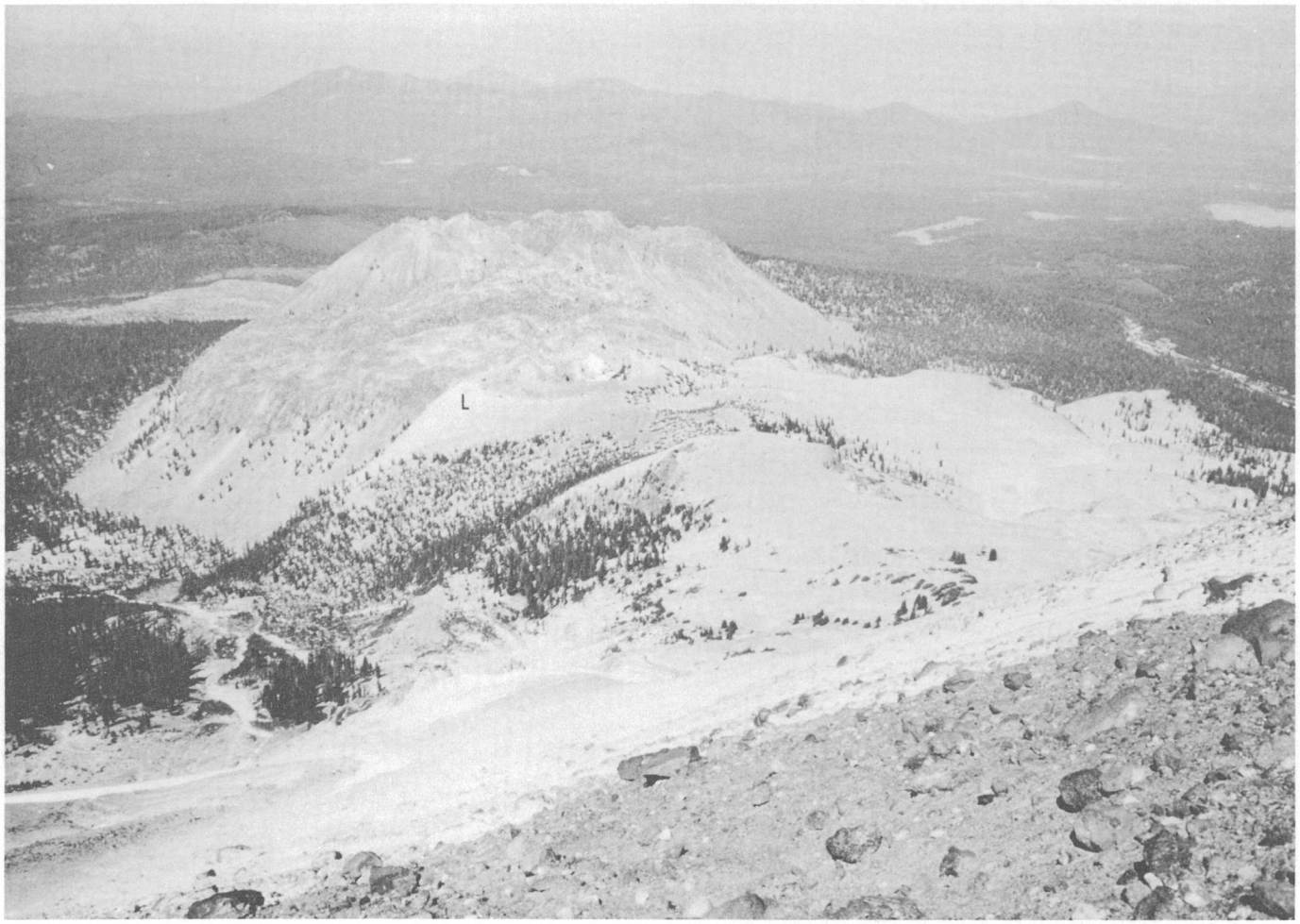

Figure 5.—View from the top of Lassen Peak northward across the Chaos Crags. Light-colored deposits at right center are tephra that probably was mostly erupted from a vent situated at the small lapilli cone (L) at the south margin of the Chaos Crags domes.

CHAOS JUMBLES ROCKFALL-AVALANCHE DEPOSITS

The Chaos Jumbles is a broad band of angular rock debris which extends from the northwest base of the Chaos Crags northwestward and westward for a distance of about 4.3 km and covers an area of nearly 8 km^2 (figs. 1, 6, 7). Individual fragments in the deposit range in diameter from a few millimeters to several meters. The rock debris probably is as much as 40 m thick in its central part. Williams (1928, p. 252) estimated the volume of the debris to be at least 150 million yd^3 (about 115 million m^3), and profiles made from the topographic map suggest that the volume may be as much as 150 million m^3.

Surface features of the Chaos Jumbles include ridges and furrows of rock debris, marginal ridges, steep and abrupt margins, and conical and domelike mounds. Transverse ridges and furrows have wavelengths of about 10 m to 100 m or more; some of these can be traced across at least half the width of a single avalanche deposit. There are, in addition, longitudinal ridges, scarps, and furrows, some of which are more than 1 km long. Where longitudinal and transverse surface features intersect, they typically cross one another without being offset. Reflection Lake and some nearby shallow ponds occupy shallow longitudinal depressions within the avalanche deposits. The surface of the western half of the deposits slopes westward about 60 m/km.

Rock fragments in the Chaos Jumbles are fresh and unaffected by weathering; however, some masses of hydrothermally altered rock form strips a few meters wide and a hundred meters or more long in the deposits between the Lassen Park Road and the base of the Chaos Crags. These strips trend parallel to the long axis of the avalanche deposits and probably resulted from the progressive disaggregation of altered rock masses during transport. Their continuity and restricted distribution suggest an absence of turbulence within the moving avalanche.

The avalanche debris extends up the south slope of Table Mountain to a point that is about 121 m higher than the base

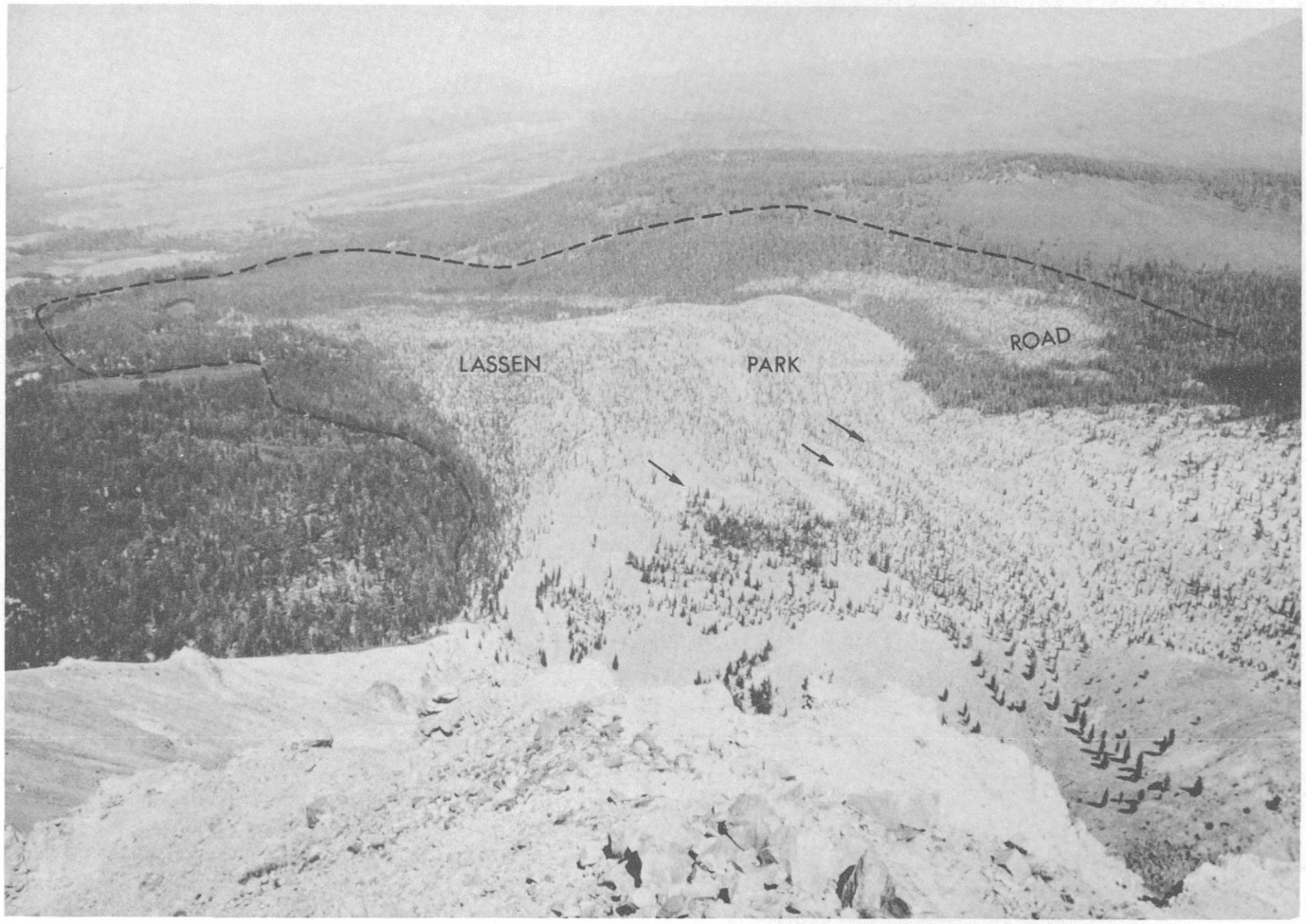

Figure 6.—View from the top of the rockfall scarp on the Chaos Crags westward across the Chaos Jumbles toward Manzanita Lake. Dashed line shows extent of the avalanche deposits. Arrows point to areas of hydrothermally altered rock debris.

of the mountain at Nobles Pass (fig. 1). If it is assumed that as the avalanche reached its highest point its kinetic energy was wholly converted to potential energy, and that no energy had been expended in overcoming frictional resistance, the avalanche must have had a speed at the foot of Table Mountain of no less than 160 km/h (100 mi/h). It seems certain that the actual speed was somewhat greater because frictional resistance would have developed in the avalanche as it moved up the slope of Table Mountain.

Williams (1928, p. 257; 1932, p. 355–356) regarded the Chaos Jumbles as chiefly the deposit of a rapidly moving dry rock stream or avalanche, but in order to explain the great mobility of the moving mass he suggested that its basal part was wet and moved as a mudflow. He suggested that the avalanche was caused by a massive rockfall from the Chaos Crags which had been triggered by a steam explosion soon after formation of the domes.

The general lack of displacement of the transverse and longitudinal ridges and furrows of one by the other over much of the central part of the avalanche deposits, together with the distribution of altered rock, suggests that the avalanche was moving as a nonturbulent sheet of rubble just before it came to rest. Such a sheet, moving above the ground surface on a cushion of compressed air, has been proposed as the origin of other avalanche deposits which show evidence of great velocity and a long distance of movement on low slopes (Shreve, 1968, p. 37–44). Shreve has suggested that the transverse ridges and furrows of such air-cushioned avalanches are formed after the leading edge of the avalanche strikes the ground and as the "zone of impact travels like a wave back up the length of the avalanche." The evident velocity and the surface features of the Chaos Jumbles avalanche deposits indicate that they, too, were formed by avalanches traveling on cushions of compressed air.

Heath (1960) postulated that the Chaos Jumbles were formed by at last three avalanches which were separated by intervals of hundreds of years, and he cited both geological and botanical evidence to support the conclusion. He (1967)

Figure 7.—View southeastward from the Lassen Park Road toward the reentrant formed in the Chaos Crags by rockfalls. The high rock mass on the right is the dome that was reported to be emitting steam and other gases in the mid-1800's. Rock debris of the Chaos Jumbles rockfall-avalanche deposits is in the foreground.

referred to a "300-year-old avalanche," dated by the ages of the oldest trees growing on it, a "750-year-old avalanche," and a "1,500-year-old avalanche," but he pointed out that the latter two ages were subjective estimates.

We have reviewed the evidence for age differences within the avalanche deposits because any assessment of the likelihood of future avalanches would be influenced by the knowledge that avalanches had occurred at several widely separated times in the past, rather than at only one time.

The geologic evidence cited by Heath for widely different ages includes, in the oldest avalanche deposit, the presence of fewer sharp-edged fragments, a higher content of interstitial "soil," and greater rounding and flattening of hummocks; all these features were thought to indicate a greater degree of weathering than is present in the other avalanche deposits. In addition, Heath noted the presence of basalt blocks on the northern margin of the oldest avalanche deposit, which he interpreted to have moved from the slope of Table Mountain down across the avalanche deposit by slow downslope transport. Heath (1960, p. 746) believed that such transport must have required "a long period of time."

To reevaluate this evidence, the surface of the avalanche deposits was examined and shallow pits were dug. No consistent difference was found in edge-rounding or in degree of oxidation between the "oldest" and "youngest" avalanche deposits. There is, however, a higher proportion of fine material in places in the "oldest" deposit. But it seems likely that the fine grain size represents the original texture of the deposit in most places because there is no other evidence of subaerial weathering. Elsewhere, the abundance of fine material seems to be related to the altered nature of the parent rock, which permits it to crumble more rapidly than the unaltered rock debris. This alteration evidently took place in the rocks of the Chaos Crags before the rockfalls occurred. Hummocks are relatively rounded where the overall grain size of the deposit is finer, and their shape probably is related to the grain size. Similar variations in texture and topography are present in deposits of several avalanches that originated on the northeast side of Mount Rainier, Wash., in December 1963 (Crandell and Fahnestock, 1965). These avalanches are known to have occurred within a short period of time, perhaps within minutes of each other, and certainly all within a period of not more than 2 mo.

Basalt fragments derived from the side of Table Mountain are present on the north edge of the "oldest" avalanche deposit, as reported by Heath. But these blocks occur on the tops of hummocks and ridges as well as between them, and cannot have reached positions on top of the hummocks by

slow downslope transport. Instead, they must have been picked up and carried by the avalanche itself, and are now in virtually the same positions as when the avalanche came to rest.

We believe, therefore, that the geologic evidence does not support the hypothesis that the avalanche deposits are of significantly different ages.

Botanical evidence cited by Heath to show age differences between the "oldest," "middle," and "youngest" avalanche deposits included differences in vegetative cover, size of trees, and proportions of species present. Differences in the character of the vegetation are clear from place to place on the deposits. The central part is sparsely dotted by small trees and is bordered on the north by deposits which locally bear a denser growth of larger trees. Still farther north is a narrow band in which trees are very large at the margin of the deposits. Heath postulated that these size differences, as well as differences in distribution of tree species, represented stages of a forest succession that is dependent on time.

The ages of the trees, however, do not indicate a substantial difference in age from one avalanche deposit to the next. Growth-ring counts by Heath and by us show that the oldest trees on the "oldest," "middle," and "youngest" deposits are about the same age, between 260 and 290 yr old. In contrast, trees much older than 300 yr grow on moraines and pyroclastic-flow deposits that are adjacent to the Chaos Jumbles. General agreement exists that trees should begin to grow soon on newly formed surfaces, depending on the availability of seed, the presence of a seedbed of fine-grained material, and a favorable climate (Division of Timber Management Research, 1965; Lutz, 1956; Sigafoos and Hendricks, 1969). These requirements are met on the "oldest" avalanche deposits which are bordered by forest growing on older deposits. Sigafoos and Hendricks (1969) found that under favorable conditions at Mount Rainier, Wash., trees start to grow about 5 yr after a surface becomes stable.

The lack of evidence of one or more generations of trees older than the ones now standing on the "oldest" avalanche deposit also suggests that the deposit is not older than about 300 yr. An important part of evidence for an older generation of trees in a forest is the existence of fallen logs as large or larger than the standing trees. Large logs are not present on the surface of the "oldest" avalanche, yet they are common on the thousand-year-old pyroclastic-flow deposits adjacent to the Chaos Jumbles. Other botanical evidences such as thickness of humus, size of trees, and species frequency of trees on the various parts of the Jumbles were examined by Sigafoos, who concluded that the evidence as a whole does not support a significant difference in age from one part of the avalanche deposits to another.

Consequently, we believe that the ages of the trees on the "oldest" avalanche deposit closely date it, and that the other parts of the Chaos Jumbles are of practically the same age. It seems likely that the trees on the "oldest" avalanche deposit are larger, more abundant, and represent different proportions of species because of microenvironmental differences such as texture of the deposits, light intensity, and available moisture.

As a further check, a brief study was made in 1972 of lichens on the avalanche deposits adjacent to the Lassen Park Road east and southeast of Nobles Pass (fig. 1). Specimens of two lichen species, *Rhizocarpon geographicum* and *Lecidea atrobrunnea*, were examined because studies elsewhere have shown them to have growth rates slow enough to date deposits many hundreds of years old (for example, Beschel, 1961; Benedict, 1967). Representative examples of these lichens, and others, were collected and subsequently identified by Professor William A. Weber, Department of Biology, University of Colorado. Growth rates have not been determined for lichens in this area, although specimens of *R. geographicum* as large as 15 mm in diameter were found in the Devastated Area on blocks of lava which were erupted by Lassen Peak in 1915. Growth-rate curves for *R. geographicum* and *L. atrobrunnea* in other areas show them to have relatively rapid early growth that is followed by slower growth.

The largest diameters of lichens on northward-facing surfaces of rock fragments were measured on each of the three avalanche deposits, with the results tabulated below. *R. geographicum* was not found on the "youngest" avalanche deposit; specimens of the only Rhizocarpons seen there were identified by Professor Weber as *R. ferax* H. Magn.

Maximum diameters, in millimeters, of lichens found on the Chaos Jumbles avalanche deposits

	"Youngest"	*"Middle"*	*"Oldest"*
R. geographicum	...	52	50
L. atrobrunnea	72	83	79

Although the results of this brief study of lichens are not definitive, the absence of appreciable size differences seems to support the view that the three avalanche deposits are of approximately the same age.

In summary, the Chaos Jumbles probably includes the deposits of three or more avalanches, but we believe that both geological and botanical evidence indicates that they all occurred at about the same time. The age of 300 yr, calculated by Heath for the "youngest" deposit, seems to apply to all of the avalanche deposits.

A rockfall-avalanche deposit that is similar to the Chaos Jumbles deposit, but much smaller, underlies an area east of dome 3 of the Chaos Crags (fig. 1). The age of this deposit is not known. There is no large reentrant in the flank of the dome at its head. It is possible that the arcuate scarp of dome 3, mentioned previously, represents a part of a cliff left by a rockfall, and that the lower mass of this dome is actually a younger dome that was erupted after the rockfall occurred.

POSSIBLE CAUSES OF THE ROCKFALLS

Any one of the several events could have triggered the rockfall-avalanches. Williams (1928, p. 251) suggested that the cause was a series of steam explosions at the northwest base of the Chaos Crags domes. If, as we have suggested, the rockfalls followed one another in quick succession, the first might have been started by a steam explosion and the subsequent falls could have resulted from the collapse of steep, unstable cliffs left by the initial rockfall. Another possibility is that the rockfalls were caused by the collapse of steep cliffs during an earthquake.

Still another cause of the rockfalls could have been the intrusion of a dome into the central part of the Chaos Crags, or renewed movement of one of the existing domes. Although we have no direct evidence of either of these events, the fact that dome 4 (fig. 1) was reported to be emitting steam and other gases constantly during the period 1854–57 (Williams, 1932, p. 347) suggests that this dome is younger than the others. It adjoins the domes in which the rockfalls originated. If a new dome had been erupted into the central part of an older group of domes, it could have caused oversteepened slopes by pushing and tilting the surrounding rocks. If these rocks were already highly fractured and unstable, the oversteepening could have resulted in one or more massive rockfalls.

POTENTIAL VOLCANIC HAZARDS

The kinds of volcanic events that are recorded by deposits adjacent to the Chaos Crags include the fall of hot pumice, hot pyroclastic flows, and rapidly moving rockfall-avalanches, although the latter may not be a direct consequence of volcanic activity. If dacitic volcanism should occur again within or close to the Chaos Crags, a sequence of events similar to those of the Chaos Crags eruptive episode probably would recur, namely the eruption of tephra and pyroclastic flows followed by the extrusion of domes. Such a sequence would almost certainly be preceded by a period of activity on a small, relatively harmless scale. Thus, large-scale eruptions would not threaten human life if adjacent areas had been evacuated as a precautionary measure at the start of the eruption.

Areas that would be directly threatened by pyroclastic flows include the zones immediately downslope from the active vent, and especially valley floors for a distance of at least 15 km from the vent. Tephra erupted in the past has mainly been carried eastward by the wind, and the distribution of tephra deposits from future eruptions would likewise be governed by the direction and strength of winds, as well as by the location of the erupting vent.

A potentially more hazardous event than an eruption would be the formation of another rockfall-avalanche at the Chaos Crags or from the flank of a newly erupted dome. Such an avalanche could be caused by a volcanic explosion during the eruption of the dome, or by an earthquake unrelated to volcanism. A rockfall-avalanche might not be preceded by any warning, and the extremely high velocity would surely preclude evacuation in time to prevent loss of life. Because of this, we regard as hazardous the areas within a distance of about 5 km downslope from the Chaos Crags to the east and to the west. There seems to be no way to warn or protect persons in the path of such an avalanche, and we think that future use of the areas which might be affected should be restricted.

REFERENCES CITED

Aramaki, Shigeo, and Akimoto, Syun-iti, 1957, Temperature estimation of pyroclastic deposits by natural remanent magnetism: Am. Jour. Sci., v. 255, p. 619–627.

Beschel, R. E., 1961, Dating rock surfaces by lichen growth and its application to glaciology and physiography (lichenometry), *in* Raasch, G. O., ed., Geology of the Arctic: Univ. Toronto Press, Toronto, v. 2, p. 1044–1062.

Benedict, J. B., 1967, Recent glacial history of an alpine area in the Colorado Front Range, U.S.A., I. Establishing a lichen-growth curve: Jour. Glaciology, v. 6, no. 48, p. 817–832.

Crandell, D. R., 1971, Postglacial lahars from Mount Rainier volcano, Washington: U.S. Geol. Survey Prof. Paper 677, 75 p.

——1972, Glaciation near Lassen Peak, northern California, *in* Geological Survey research 1972: U.S. Geol. Survey Prof. Paper 800-C, p. C179-C188.

Crandell, D. R., and Fahnestock, R. K., 1965, Rockfalls and avalanches from Little Tahoma Peak on Mount Rainier, Washington: U.S. Geol. Survey Bull. 1221-A, p. A1–30.

Day, A. L., and Allen, E. T., 1925, The volcanic activity and hot springs of Lassen Peak: Carnegie Inst. Washington Pub. 360, 190 p.

Division of Timber Management Research, 1965, Silvics of forest trees of the United States: U.S. Dept. Agriculture Forest Service, Agr. Handbook 271, 762 p.

Heath, J. P., 1960, Repeated avalanches at Chaos Jumbles, Lassen Volcanic National Park: Am. Jour. Sci., v. 258, p. 744–751.

——1967, Primary conifer succession, Lassen Volcanic National Park: Ecology, v. 48, p. 270–275.

Lutz, H. J., 1956, Ecological effects of forest fires in the interior of Alaska: U.S. Dept. Agriculture Tech. Bull. 1133, 121 p.

Macdonald, G. A., 1963, Geology of the Manzanita Lake quadrangle, California: U.S. Geol. Survey Geol. Quad. Map GQ-248.

——1964, Geology of the Prospect Peak quadrangle, California: U.S. Geol. Survey Geol. Quad. Map GQ-345.

——1966, Geology of the Cascade Range and Modoc Plateau, *in* Geology of northern California: California Div. Mines and Geology Bull. 190, p. 65–96.

Rubin, Meyer, and Alexander, Corrinne, 1960, U.S. Geological Survey radiocarbon dates, 5: Am. Jour. Sci. Radiocarbon Supp., v. 2, p. 129–185.

Shreve, R. L., 1968, The Blackhawk landslide: Geol. Soc. America Spec. Paper 108, 47 p.

Sigafoos, R. S., and Hendricks, E. L., 1969, The time interval between stabilization of alpine glacial deposits and establishment of tree seedlings, *in* Geological Survey research 1969: U.S. Geol. Survey Prof. Paper 650-B, p. B89–B-93.

Williams, Howel, 1928, A recent volcanic eruption near Lassen Peak, California: California Univ. Dept. Geol. Sci. Bull., v. 17, no. 7, p. 241–263.

——1932, Geology of the Lassen Volcanic National Park, California: California Univ. Dept. Geol. Sci. Bull., v. 21, no. 8, p. 195–385.

Jour. Research U.S. Geol. Survey
Vol. 2, No. 1, Jan.-Feb. 1974, p. 61—71

SPECTROCHEMICAL COMPUTER ANALYSIS—PROGRAM DESCRIPTION

By FRANK G. WALTHALL, Washington, D.C.

Abstract.—The computerized system of spectral analysis performs determinations of 68 elements in geologic materials. The samples are arced under carefully controlled conditions in an argon-oxygen atmosphere and the spectra are exposed on 102- by 508-mm (4- by 20-inch) plates. Transmittance readings taken every 5μm along the spectrum are recorded on magnetic tape, producing more than 90,000 readings in 70 sec. The computer program described examines the data, searches for a maximum of 500 spectral lines, and after treating the results prints concentrations for the elements on a report form. The plates are calibrated every 250 A, transmittances are converted to intensities, backgrounds are subtracted, interferences are recognized, and one final answer is chosen from among several preliminary answers for each element. Concentrations are obtained from analytical curves prepared prior to the sample run. Samples are run under the same carefully controlled conditions that were used to prepare the analytical curves.

A computer program (the final program) has been written to treat transmittance data recorded by the magnetic tape system described by Helz (1973) from plates prepared under the conditions described by Dorrzapf (1973). The program was written in Fortran IV and was designed for execution on a large computer. As the system was to be applied primarily, but not exclusively, to silicate rocks with major emphasis on trace elements, certain procedures were chosen to accommodate the silicates. Additional decisions involved in the design of the total system were influenced by making it no less accurate than the visual semiquantitative spectrographic analysis method in use in Geological Survey laboratories (Myers and others, 1961). The visual method compares previously prepared standard plates with freshly prepared plates of sample spectra. The choice of a 5-μm interval between readings was based on the minimum number of readings required to suitably define a spectral line on our plates while keeping the total number of readings within reasonable bounds. This factor coupled with rapid-scanning capabilities effectively minimizes the recording time and the quantity of data. One reading covering half the length of a spectral line is taken every 5 μm with about 50-percent overlap of successive readings. This number of readings is ample for finding line intensities. A dependable high-speed tape-recording system obviously is necessary to take full advantage of the potential being offered. The instrumentation described by Helz (1973) measures, digitizes, and records over 90,000 three-digit readings in 70 seconds.

The original concept (Helz, 1965) of the computerized emission spectrographic analysis (ESA) system was to have only one computer program which would perform the complete job from two 4- by 10-inch plates covering the desired spectral range. The first program was written in this form and was applied to the low-wavelength half of the spectrum. It started with the taped transmittance data of the split-filter two-step iron spectrum used for plate emulsion calibration curves (PECC), followed by all the standards spectra for the element concentration calibration curves (ECCC) if any, and ended with sample spectra which resulted in a report listing the concentration of elements present in each sample. Analytical lines were found by this program using many fiducial lines which were provided by a minimum of 1 percent iron in the arced sample. The first program was useful to the cyanogen-band region (about 3500 A). To extend its range to 4750 A for additional lines would have required two plates, larger data-storage facilities for the intermediate results, another wavelength table, and a second computer run for the second plate.

A major reexamination of the problem was undertaken and from this came several important improvements. Use of an argon-oxygen arcing atmosphere clears the cyanogen-band region reasonably well, thus making many additional analytical lines available and aids considerably in obtaining a set of constant conditions by helping to control temperature of burning. The adoption of the single plate, 102 by 508 mm (4 by 20 in.), doubles the wavelength range available for a single recording and permits a single computer run for the entire range.

The computer method had been well proven by this time (Helz, and others, 1969) and the reliability of the entire tape-recording system also had been demonstrated. The accuracy of the scanning instrumentation exceeded expectations and was extremely dependable. These factors suggested an entirely new approach to the line-finding procedure. This much more efficient method became a reality at the same time that additional facilities were installed for superimposing the Cd 2748.58 and Cd 4415.70 lines on each spectrum. Means of providing the two-cadmium-line method are discussed by Helz (1973), and its application is described in the section "Line Finding."

The following preliminary preparations are required for the

final program. Once determined, they need only be monitored periodically as long as spectrographic conditions remain unchanged.

1. Wavelengths of iron lines used for plate emulsion calibration need to be selected and their estimated positions determined.
2. Wavelengths of as many as 500 analytical lines need to be selected and their estimated positions determined. The lines are further identified by priority number, atomic number, and element symbol.
3. Coefficients for an analytical curve corresponding to each of the analytical lines are determined, upper and lower concentration limits selected, and a priority number assigned to all the lines of each element. The curve fitting used for all curves is the polynomial regression method consisting of several subroutines from the IBM system/360 scientific subroutine package (version II, H20-0205).
4. The order in which to print answers is selected.

After the preliminary preparations have been completed, a routine run requires only one data card which is described in table 1. Columns 1–14 are ignored when samples from another job request are being run, but columns 15–80 must be completed.

The spectra are prepared in such a way that good reproducibility is realized. The exposure and development conditions described by Dorrzapf (1973) assure the basic requirements of constancy of plate preparation. These constant conditions are necessary and with some care can reasonably be obtained. Future programing will permit large variations in conditions. For example, minimal interference corrections are now being made during routine runs; however, many such corrections ultimately will be available. As they are completed and added, more lines will produce acceptable answers, and an averaging concept will be used to provide the final answer.

Future plans include the application of this computerized system to rocks and minerals in general. The only rock type allowed to influence basic decisions was silicate rock, which can produce a very complex spectrum. Indications are that the system will work equally well with rock types other than silicates; however, these still need extensive investigation.

Table 1.–*Format of data card required for computer analysis*

[The use of fields 1–12 is optional. If left blank, default values (in parentheses under Description) are assumed. If any of the default values are to be changed, all 12 fields must be completed. Type: A, alphanumeric; I, integer; U, undefined. NA, not applicable]

Field	Column	Length	Description	Type	Symbolic name
1	1	1	(Blank)	U	NA
2	2	1	Kind of conditions (type of wavelength table) (2).	I	KOC
3	3	1	Type of plate calibration treatment (0).	I	TPCT
4	4	1	Number of interferences (3).	I	NI
5	5	1	(Blank)	U	NA
6	6–7	2	Number of files read from tape (40).	I	NF
7	8	1	Number of samples, weight <15 mg (0).	I	NFAMBF
8	9	1	Number of first lines (3).	I	NFL
9	10	1	Number of last lines (3).	I	NLL
10	11	1	(Blank)	U	NA
11	12–14	3	Number of records read from each file (200).	I	NRR
12	15–16	2	Symbol preceding sample number (W-).	A	NSS
13	17–22	6	Job number	I	JOBNO
14	23–27	5	Number assigned to job by spectrographic laboratory.	I	GROUP
15	28–36	9	Number of report	A	NOREP
16	37–60	24	Name of person(s) requesting analysis.	A	FOR
17	61–80	20	Name of analyst	A	NANA

SYSTEM REQUIREMENTS AND RESTRICTIONS

Instrumentation.–The absolute integrity of the recording system is important because the position within the spectrum is not recorded but is determined by counting the number of readings. If a few readings were lost, the many-fiducial-line method of line finding would have to be used.

Spectroscopy.–The combination of the use of argon-oxygen atmosphere and the single long plate provides a very good way to take full advantage of the high-speed recording and the computer handling of the accumulated data. Many chemical elements produce potentially useful spectral lines in the cyanogen-band region, and better answers in general will be obtained by studying all lines possible. The many checks made on the instrumentation and the special care taken during sample preparation, exposure, and plate development assure comparable results over a long time. This permits the use of a single set of analytical curves for analyzing sample spectra over an extended period of time.

The set of constant conditions also permits the proper use of the unaltered function of the plate emulsion calibration curve. If proper control of conditions should falter, means are available for shifting those curves affected.

Computer.–The programs are written in Fortran IV (G level) for execution on an IBM system/360, Model 65 computer. The following automatic data processing equipment is being used:

Release 20 MVT (plus HASP) operating system.
450,000-byte core storage.
One 2314 disk unit.
Two 9-track tape drives.
One 7-track tape drive.
CalComp plotter.
Card punch.
Card reader.
High-speed line printer.

Program.–The wavelength table of analytical lines consists of lines which are relatively free from interferences. Three routine interference treatments which greatly affect a few

elements are used, but correcting for interferences in general is not required to accomplish the present aims.

The final program, exclusive of compilation time and the determinations of plate emulsion calibration curves, requires an average of less than 1 minute per analysis for about 400 lines. The routine plate emulsion calibration treatment requires about 1 minute.

The report form tabulates results from a maximum of 10 samples on two pages of computer printout. These are reduced to standard page size and copied for distribution and filing.

PRELIMINARY PREPARATIONS

Before the final program is used, the following must be accomplished: (1) all lines used must be identified, (2) the dispersion must be determined as the number of readings per angstrom to calculate estimated positions for all lines, and (3) the coefficients must be determined for all analytical curves, and upper and lower concentration limits and priority number must be assigned. The variable KOC (kind of conditions) read in from a card (table 1) presently indicates the dispersion used to calculate estimated positions for the wavelength table used. The wavelength table provides information for each line as shown in table 2.

Table 2.—*Format of cards for wavelength table*

[Type: A, alphanumeric; I, integer; R, real; U, undefined. ECCC, element concentration calibration curve; NA, not applicable]

Field	Column	Length	Description	Type	Symbolic name
1	1–3	3	Element atomic number. .	I	EAN
2	4–6	3	Line priority number . . .	I	LP
3	7	1	(Blank)	U	NA
4	8–9	2	Element symbol	A	ELSYM
5	10	1	(Blank)	U	NA
6	11–19	9	Wavelength	R	WL
7	20–27	8	Concentration limit, lower.	R	CONCLL
8	28–36	9	Concentration limit, upper.	R	CONCLU
9	37	1	(Blank)	U	NA
10	38–40	3	Source of ECCC points . .	A	NR
11	41–46	6	Estimated position	I	EP
12	47	1	(Blank)	U	NA
13	48–58	11	ECCC coefficient for constant term.	R	CQCEL
14	59–69	11	ECCC coefficient for first-degree term.	R	CQ1EL
15	70–80	11	ECCC coefficient for second-degree term.	R	CQ2EL

Five programs perform much of the preliminary work required.

1. The RPA (readings per angstrom) program finds 23 dispersion lines in each step of the split-filter iron spectrum, calculates 22 dispersions as number of readings per angstrom, averages the wavelengths used, and fits these points as a straight-line dispersion curve. Although the dispersion curve is not truly linear, a straight-line fit permits estimation of 50-A distances with acceptable accuracy. Averaging several of these curves produces a curve which can be used as long as conditions remain the same.

2. The VFL (virtual fiducial lines) program finds 219 iron lines (same ones used for plate emulsion calibration curves) and by using the dispersion curve from the RPA program calculates the estimated positions of imaginary lines from wavelengths increasing every 50.0 A, commencing with 2250.0 A. Averaging results from several plates gives positions of the virtual fiducial lines.

3. The CEP (calculate estimated positions) program calculates the estimated positions of all wavelengths read in by using the positions of the virtual fiducial lines, calculated by VFL, with the dispersion curve from RPA.

4. The EPL (estimated position of lines) program performs line finding for all wavelengths read in for analytical lines from recordings of standards spectra. These results are carefully studied because they will considerably influence any decision to adjust the estimated positions or to use them as calculated. Also, these results provide the points which are fitted as element concentration calibration curves.

5. The PS (point selecting) program fits points from the EPL program as second-degree analytical curves, suggests concentration limits, and rates the curves on a 0–10 basis as an aid in assigning priorities. Our first wavelength table consisted of lines which had been used in other spectrographic methods. We are now using about 400 lines which we consider the most useful of the more than 10,000 lines which have been investigated. This PS program is discussed in more detail in the section "Element Concentration Calibration Curves."

The dispersion curve and the positions of the virtual fiducial lines are calculated from five plates and averaged before being used to calculate estimated positions of desired element lines. After the estimated positions have been calculated, they are used by the EPL program to find lines in spectra from standards. The positions where lines are actually found are given considerable weight as a basis for adjusting the calculated estimated positions. These EPL program results from standards provide information for selecting the permanent estimated positions for the wavelength table which will be used for sample spectra. The manual selection of the data from the EPL runs to be fitted by the PS program for element concentration calibration curves provides ample opportunity for a thorough examination of each point which will be fitted. This becomes useful information when finally deciding upon a curve. All the analytical curves to be used for a sample run are selected prior to the sample run. The PS program prepares a tape for use by the CalComp plotter. Both the points and the smoothed curve are plotted (see fig. 4). This visual aspect is most helpful in making many decisions about a curve—for example, setting the concentration limits and assigning priorities.

FINAL PROGRAM

During a routine analysis by the final program the following occurs:

1. The plate emulsion is calibrated 10 times, once each 250 A between 2250 and 4750 A, thus determining 10 plate emulsion calibration curves.
2. Line finding is performed and followed by an evaluation of the results.
3. Preliminary answers are calculated where possible by using the appropriate coefficients of an element concentration calibration curve and, if not possible, a code is assigned.
4. Temporary answers are selected.
5. By using priorities and concentration limits a final answer is selected for each element.
6. The final answers are saved until the 10th sample, or the last sample of a group, or the last spectrum is recorded, at which time a report form is printed (fig.1).

Each spectrum on the plate is recorded as a file on tape. A 2,400-foot reel of tape (7 track) recorded at a density of 800 bits per inch with records of 1,500 digits (binary coded decimal) in length is ample for recording an entire plate having a maximum of 40 spectra. The first record in each file is 12 digits long and is used for identification purposes. Each succeeding record is a set of 500 three-digit numbers (10 times percent transmittance) with all digits being significant when re-recording the same spectrum.

Large variations in the spectrographic analysis of a sample can always be expected. These variations are minimized by rigidly controlling both the methods of sample preparation and the exposure conditions, including an argon-oxygen atmosphere, and by careful plate development.

Correlating the line position in the spectrum with the transmittance reading in the recording is accomplished by starting the recording at a known position and by counting the readings thereafter. This assumes a reasonably constant dispersion of the spectral lines on the plate, and assumes no missed readings during the digitizing-recording step. The possibility of an occasional missed reading caused by input-ouput errors is ever present. However, the programed error-handling procedure has effectively taken care of all input-output errors encountered thus far.

Each digit of the first record, 12 digits long, in each file is entered manually by using a thumb-wheel switch. The first field within the fixed data (table 3) is designated by the symbolic name ICODE and identifies the type of spectrum from which the transmittances following it have been recorded. There is, in addition, a fixed order in which the spectra are recorded on the tape. The unfiltered step of the split-filter iron calibration spectrum is recorded first and is followed by the filtered step. The variable TPCT (type of plate calibration treatment), which is read in from a card (table 1) and becomes the first digit of the program number, provides a means for bypassing routine plate emulsion calbration curve treatment by reading in coefficients.

Standards may be run as samples, the difference being they will not appear on the report form. An ICODE of "61" is entered for the last sample of a grouping, and a report form will be printed including that file but not the next file; it means that a card is to be read which contains information for the next report form. After the last full spectrum is recorded one additional short file is recorded consisting of a set of fixed data, the first digit of which must be an "8" followed by at least one full record of transmittance data. This "8" signals the end of the recording. However, the variable NF (number of files to read) read in on a card provides the option of not reading the entire recording. Similarly NRR (number of records to read from each file) makes possible the reading of a tape having no end-of-file marks.

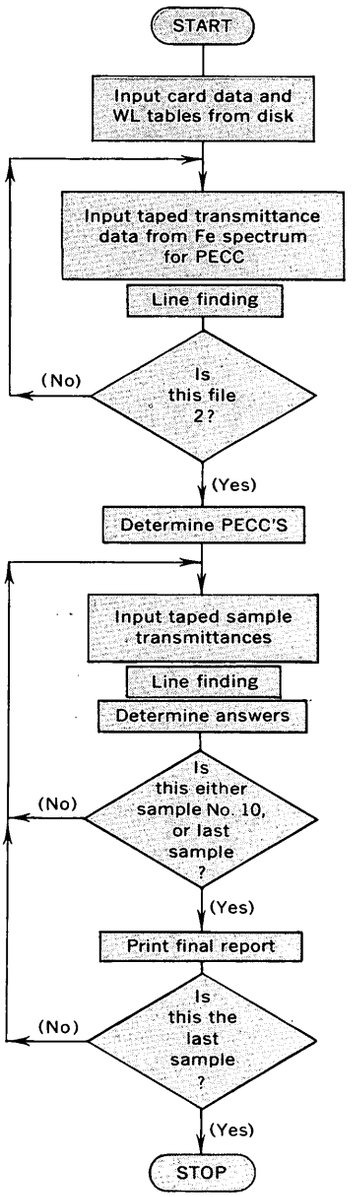

Figure 1.–Flow chart of major functions of the final emission spectrographic analysis computer program. WL, wavelength; PECC, plate emulsion calibration curves.

Table 3.—*Types of fixed data*

Field	Number of digits	Description	Symbolic name
		Iron spectrum (unfiltered) ICODE 1	
1	1	Identification code	ICODE
2	3	Plate number	PLANO
3	2	Month recorded	IMO
4	2	Day recorded	IDA
5	2	Year recorded	IYR
6	2	Spectrum number on plate	NOSPEC
		Iron spectrum (filtered) ICODE 2	
1	1	Identification code	ICODE
2	4	Page number in recording book	PGNO
3	4	Transmittance of less-filtered part of split filter.	IPCTU
4	3	Transmittance of more-filtered part of split filter.	IPCTF
		Standards ICODE 31	
1	2	Identification code and internal standard treatment.	ICODE
2	6	Concentration (percentage element $\times 10^6$).	ICONC
3	2	Number of file being recorded	FINO
4	2	Spectrum number on plate	NOSPEC
		Unknowns [1] ICODE 41	
1	2	Identification code and internal standard treatment.	ICODE
2	6	Sample number	NOSAMP
3	2	File number being recorded	FINO
4	2	Spectrum number on plate	NOSPEC

[1] ICODE 41 is used if a report form is intended, ICODE 51 if not.

FEATURES

Line finding

The line-finding procedure as presently programed for routine use is an efficient but not restrictively rigid method. Estimated positions (EP's) are read in for all lines as part of the wavelength table. A line is recognized by first searching for a minimum transmittance among 11 readings, 5 on each side of the EP. A peak is defined as the transmittance which is at least 0.2 percent less than that of the readings on each side. If more than one reading differs by less than 0.2 percent the peak is considered to have a flat top. A peak is too flat if it is more than five readings wide. The position of the peak is the position of the minimum transmittance unless it has a flat top; if so, it is the midpoint (rounding toward the EP). If two legitimate peaks are found within the search area, the darker of the two is chosen. To be considered as a possible answer, the peak position must be located within two readings of the EP. Also, it must fit the program definition of a line—that is, the transmittance difference between peak and background must be at least 1 percent.

A well-established starting point must be known before commencing the line-finding procedure. The method used to find lines in the iron spectra differs from that used in other spectra by the method of determining both the spread correction and the zero position. Both methods, however, have all the transmittances recorded for the spectrum in core storage at one time throughout the line-finding procedure.

The first minimum transmittance that is less than 80 percent and is within the first 30 readings of the iron spectra must be the peak of a known line. It may be either the Fe 2327.394, Fe 2331.307, or Fe 2332.797 line (or the Cd 2288 line). The variable NFL (number of first lines), which may equal 1 through 4, is read in on a card and identifies which of these four lines to expect—beginning with Cd 2288 if NFL=4, or on to Fe 2332 if NFL=1, and similarly with NLL (number of last lines). Whatever the choice, the position from which all the remaining lines are measured is the position of the peak of the Fe 2332 line, which by definition is zero in all spectra. For determining the stretch correction, the average of the positions of all the first lines used is taken as the lower boundary. By measuring from the position of the 2332 line, the estimated positions of the several last lines are used to find the Fe 4665.594, Fe 4662.609, and Fe 4654.785 lines. After the lines are found, their actual positions are averaged, thus providing the upper boundary for the stretch determination. The number of readings between the upper and lower boundaries is calculated and any spread correction is determined by comparison with the spread assumed when estimated positions were calculated. Any difference is corrected if its absolute value is less than 10—if more than 10 the spectrum is skipped.

For spectra other than those for plate calibration, the first line to search for is the Cd 2748 line. Two sections of the spectra are masked to permit the centering of cadmium lines 2748 and 4415, and these two lines serve for making any spread correction and for line finding. The recording of these spectra commences at approximately the same position as the iron calibration spectra. The Cd 2748 line is located by finding the first peak darker than 80 percent between readings 16,080 and 16,480, if recorded from our plates. Once the Cd 2748 line has been located, the Cd 4415 line is the first peak found between reading 64,920 (from the Cd 2748) and the next 100 readings. The number of readings between cadmium lines 2748 and 4415 is determined and compared with the expected difference. This comparison becomes the basis for making any spread correction that may be needed. The position zero for these spectra is taken as 16,105 readings below the Cd 2748 position.

The basic estimated position which is read in for each line is never permanently changed by the program but may be altered temporarily for a single spectrum when the need for it is indicated by the measurement of the length of the spectrum. A spread correction is made on estimated positions for any deviation of 10 or less from the expected distance as follows: The spectrum is divided into the number of sections which equals one more than the absolute value of the correction itself. The length of each section in readings is determined by dividing the number of sections into 90,000. The correction made in the first section is zero, and the correction for each

succeeding section advances by one until the correction in the last section is the full value of the spread correction, which is applied through reading 100,000. Each basic estimated position is temporarily adjusted at the time of line finding to produce the estimated position appropriate for the spectrum being analyzed.

Background and interferences

The background is determined by calculating from a straight line the value directly under the EP (estimated position). The straight line is formed by connecting two points, one on each side of the EP. The points are the maximum transmittances within 100 readings (2.5 A) of the EP. In the event of equal maximum transmittances, the one nearest the EP is used. The program adequately corrects for background. Other interferences such as interelement effects are being investigated, and the program will be modified to correct for these.

For routine use of the program the fewest possible interference treatments are being used. At present only three very simple ones are in the program, and these are applied only after temporary answers have been chosen. Many gross interferences are effectively handled by means of the priority number concept when selecting temporary and final answers. The entire basis of answer selection lies in the proper application of the priority concept. The priority-one line is the most sensitive line which is relatively interference free. The priority-two line is a little less so on both counts, and similarly down the unbroken priority sequence. After the continuity is broken by skipping priority number, priorities may be assigned indiscriminately through 99 for any purpose desired. Answers are selected only from the unbroken sequence of priorities beginning with priority one. By definition, as priorities increase, the assigned concentration limits never decrease while in the unbroken sequence. Those beyond the skipped priority are unaffected by these restrictions. The process of selecting answers starts with the priority-one line and ends with the last line in the priority chain. Any line having a peak transmittance less than 2.0 percent is too dark for evaluation and is skipped, as is any line producing an answer greater than the upper concentration limit of its analytical curve. The procedure for selection of answers is described further in the section "Final Answers and Report Form."

The investigation of interferences presently has top priority to upgrade many lines, thus making many more potential answers available. The three interference treatments being used now generally perform as follows:

1. If the final answer for iron is above 13 percent, an answer from the K 4047 line is unacceptable.
2. If either magnesium, iron, or chromium is above a certain concentration (a different concentration for each), a sodium answer is accepted from only its priority-one or priority-two lines.
3. If neither platinum nor palladium is present, osmium, iridium, ruthenium, and rhodium are reported as less than their lower limits.

The variable NI (number of interferences) which is read in from a card and which is the last digit of the program number, simply indicates the number of interference subroutines in the program.

Plate emulsion calibration curve

The plate emulsion calibration curve (PECC) relates percentage transmittance to intensity. The method chosen for this work utilizes the change in transmittance of a line as measured from each step of a single iron burn exposed through a two-step (split) filter. A total of 219 iron lines is found in each step, and by pairing the transmittance of a line from the most filtered step of the two-step iron exposure (T_F) with its transmittance from the least filtered step (T_U) a point is defined for the preliminary calibration curve, a second-degree curve, (fig. 2). A different curve is determined for use over a 250-A range by using data from 26 lines which permits a few overlapping lines for each. By including an additional two points, one on each end weighted 26 times, the curve is well controlled without actually being forced. The weighted points are (1.0, 1.5) and (99.0, 100.0), thus providing 78 points to be fitted with the abscissa, ln T_U, being the independent variable and the ordinate, ln T_F, the dependent variable. The generic equation is $y=ax^2+bx+c$ with a always negative and y greater

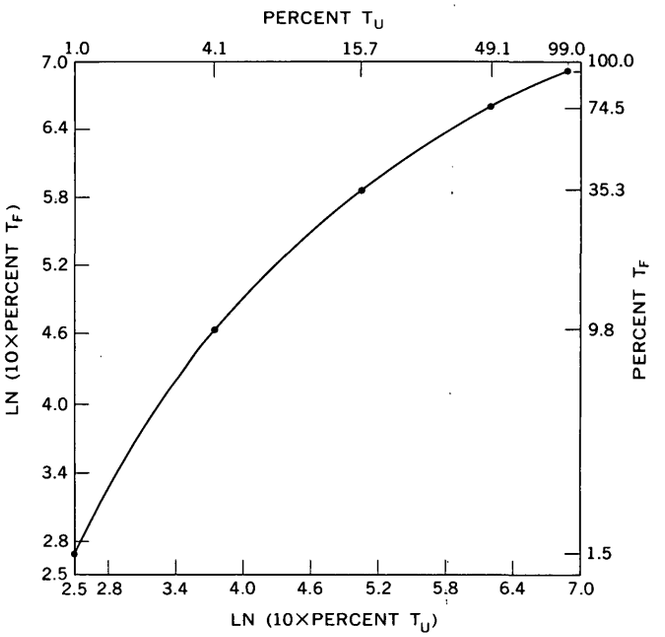

Figure 2.–Preliminary plate emulsion calibration curve relating transmittance from the unfiltered step, T_U, to the filtered step, T_F.

than x. This fitted curve provides the ordinate component, the natural logarithm of the percentage transmittance, of the points for the final PECC. The natural logarithm of the filter factor provides the abscissa component of the points (equally spaced along the x-axis). The filter factor (about 2) is the ratio of the percentage transmittances of the unfiltered half of the filter and the filtered half of the filter. A few selected points are identified in figure 2.

Points for the final plate emulsion calibration curve (PECC) (fig. 3) are obtained as follows: The first point obtained from the preliminary PECC is called the inflection point (IP) of the final PECC. It is defined as that point near the 45° slope point on the preliminary PECC which will produce the first calculated point above it at the same distance away as the first calculated point below it. To select points above the IP, the y component of the IP is substituted into the preliminary PECC equation as x and a new y is calculated. This y is substituted into the equation as x, and this continues until a new y exceeds 6.86 (ln 10×95.4 percent transmittance). At this point, y is increased regularly at the rate of 0.01 (about 1 percent transmittance) per point until it exceeds ln 10×100 percent, this point being set equal to ln 10×100 percent. To select points below the IP, the x component is substituted into the equation as y and a new x is calculated. This continues until a new x is calculated which is less than 1 percent transmittance. This is the lowest point calculated.

The inflection point is placed on an imaginary line having a slope of 315° and passing through the point ln 10 percent transmittance and ln 100,000 intensity. The final PECC is built from the inflection point in both directions. The preliminary PECC provides a most accurate and convenient measure of the relative change in transmittance. This nicely smoothed and averaged measure of transmittance change provides an excellent source of points to be used with the natural logarithm of the ratio of the split-filter transmittances. The points of the final PECC produce a curve generally S-shaped but one which cannot be adequately represented by a cubic equation. An algorithm is used in the program utilizing the preliminary PECC quadratic with the natural logarithm of the filter factor producing an "exact fit" final PECC. This permits all the averaging and fitting to remain in the preliminary PECC which utilizes the newly measured quantites. All the points initially obtained from a preliminary PECC for the final PECC are shown in figure 3.

Element concentration calibration curves

To prepare the element concentration calibration curve (ECCC), separate programs are used which perform the entire job for many curves and most of the work required in the

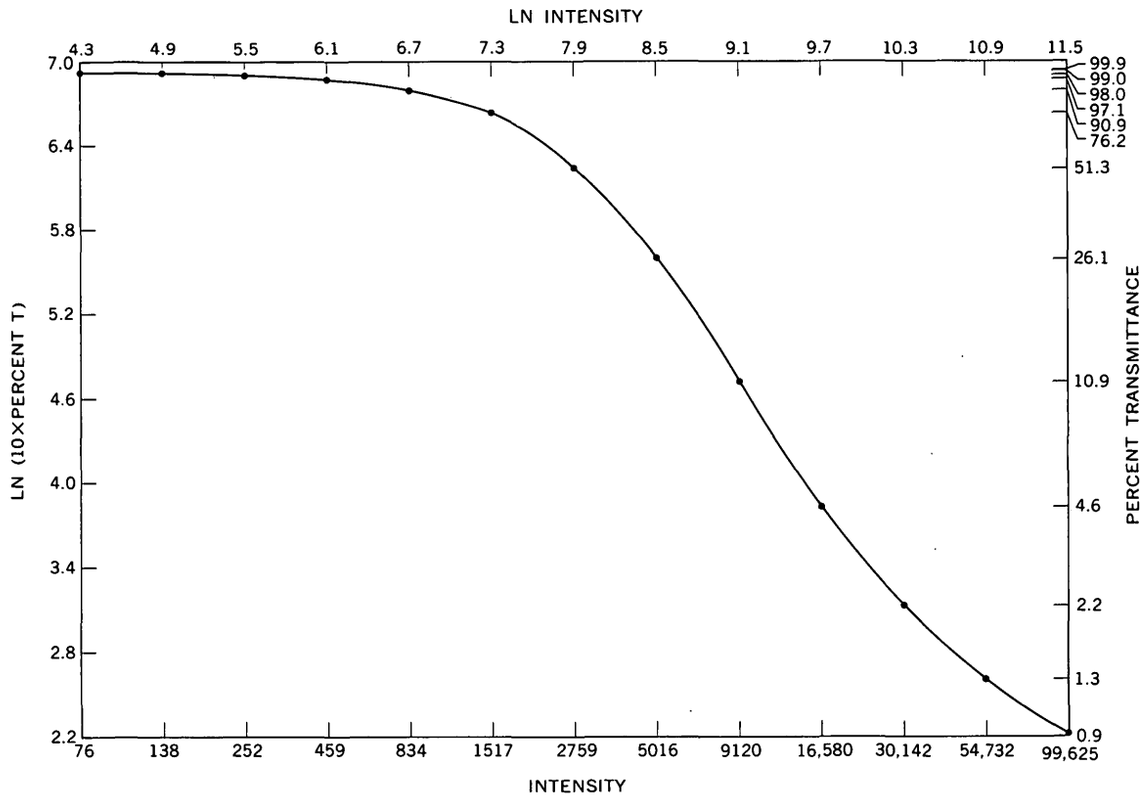

Figure 3.—Final plate emulsion calibration curve relating intensity to transmittance.

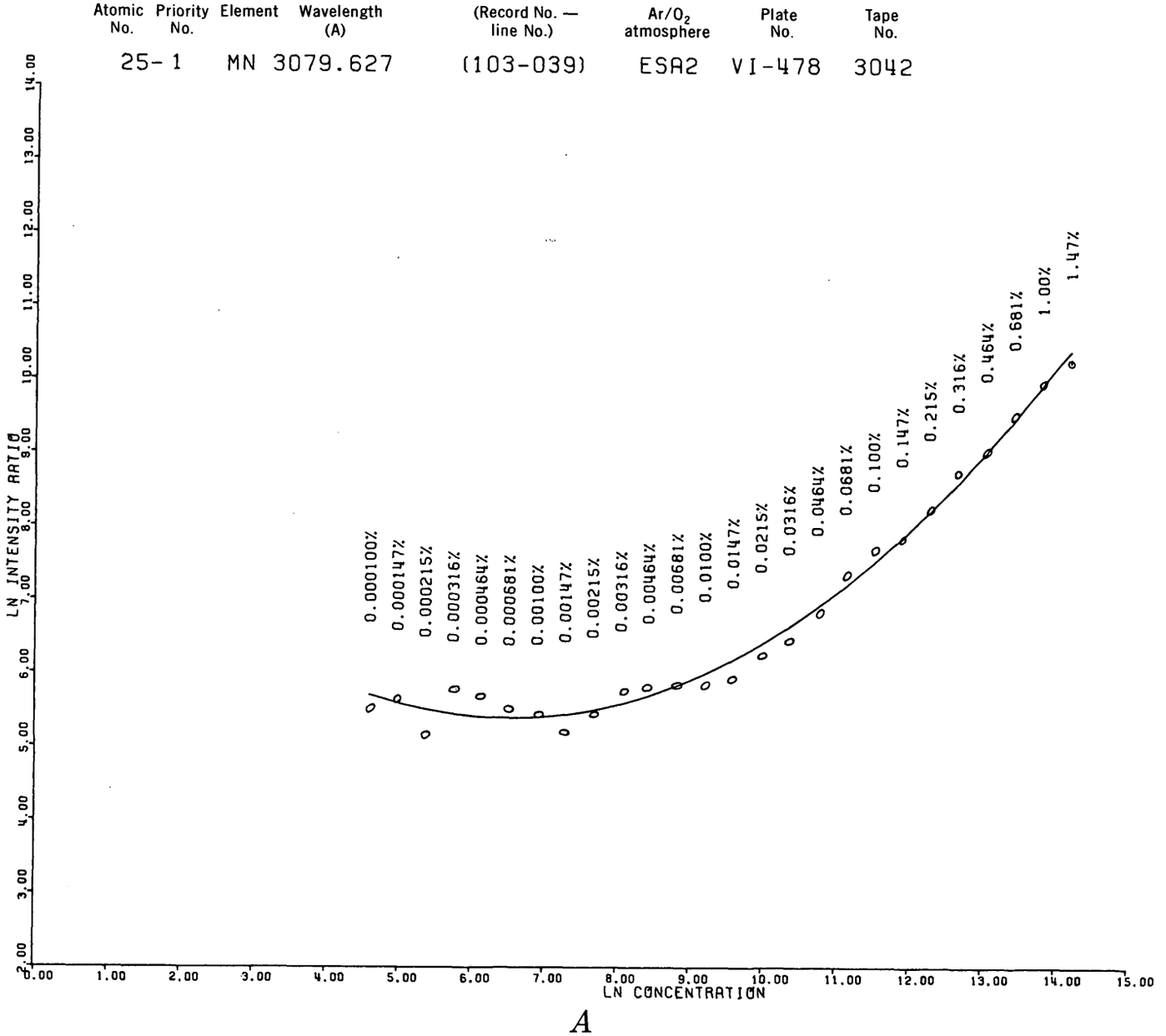

A

Figure 4.–Element concentration calibration curves using a Mn 3079.627 line plot as an example. *A*, first fitting (without limits); *B*, second fitting (with limits).

preparation of the others. Standards are prepared to give six evenly divided points between orders of magnitude of concentration (Myers, and others, 1961). Transmittances from these standard spectra are recorded on magnetic tape in order of descending concentration. A search for analytical lines from the wavelength table is made in each file of transmittances, and selected data from all standard spectra are printed. After this is completed, all the data accumulated for each line are evaluated and the resulting points are fitted by the PS (point selecting) program. A second-degree curve is the highest degree fitted, and two of these fittings are accomplished for each line–one without limits and one with limits (fig. 4). The first fitting, without limits, omits points taken from a record having an input-output error (that is, the entire record is skipped), any with a peak-background difference of less than 1 percent transmittance, those with a peak transmittance of less than 2 percent (too dark), and data from any blank or matrix spectrum (that is, concentration equals zero). A limited statistical study and an analysis of variance are made for each fitting, and a table of raw points and smooth points with residuals is also prepared for the highest degree fitted. The second fitting, with limits, fits only those points remaining by examining points starting with the highest concentration and using all with regularly decreasing intensities.

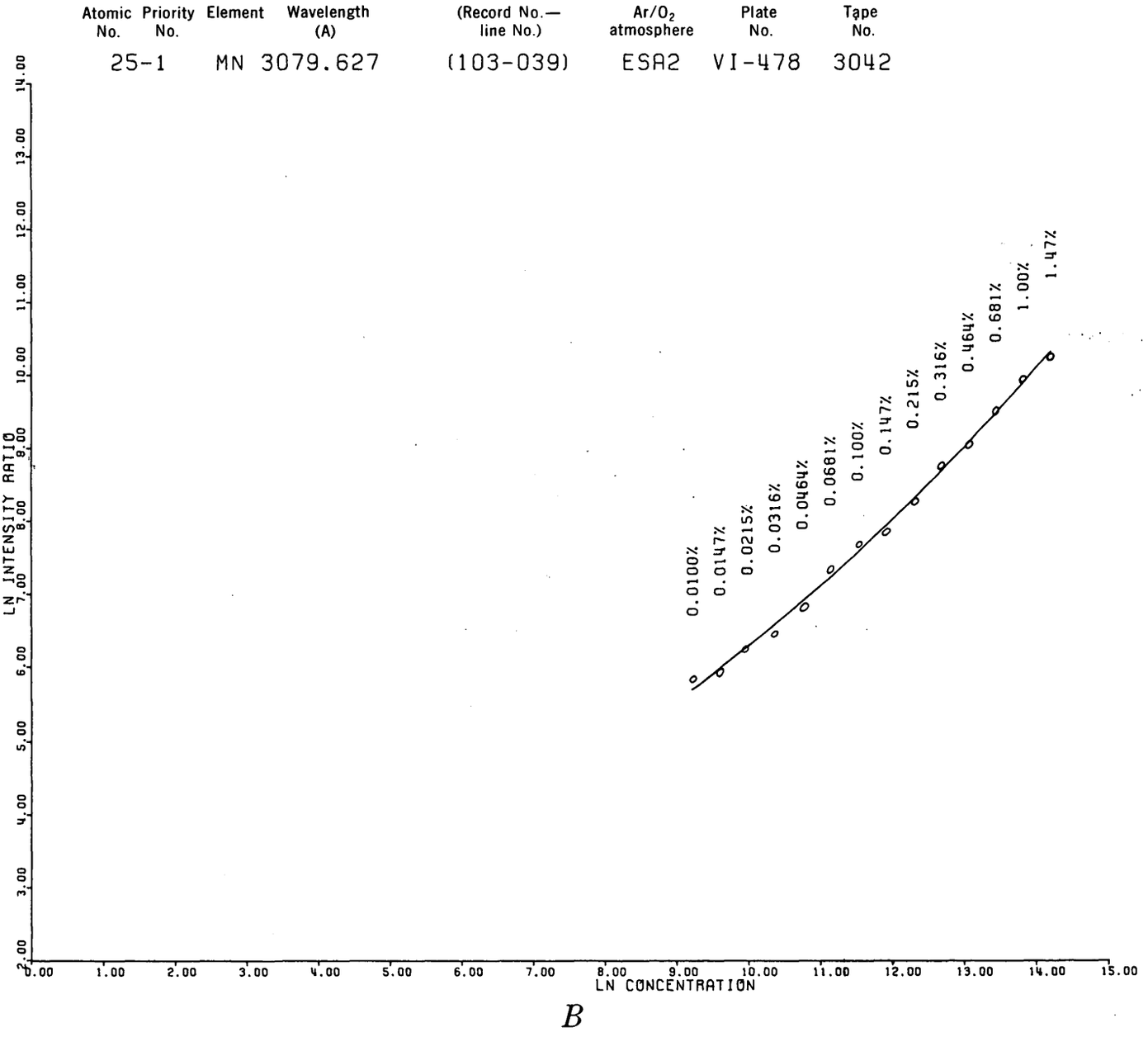

B

Figure 4.

Statements are included which provide for the preparation of a tape for use by the CalComp plotter. Both curves, without and with limits, are plotted, each producing a plot 7 by 10 inches. These dimensions may be altered by changing only one program card. Provision is made for printing full identification of the curve on the plot.

If the second-degree fit is better than the straight-line fit, both sets of coefficients are available. The first-degree fitting is not classified. However, the evaluation for the second-degree fitting proceeds as follows:

Class 0, if <3 points are supplied for fitting,
1, for 3 points, and
2, for 4 points if the standard deviation (sd) is greater than 0.5.

Beyond this, the value of the class may range up to a maximum of 10 as shown in the following calculation:

Class = (points factor + sigma factor + residual factor)/3, where

Points factor = 4 if there are 4 points to fit, or
= 10 for 5 or more points, and

Sigma factor = 6 if there are 4 points to fit, or
= 1 if sd >0.9, or
= 10 - 10.0 X sd, and

Residual factor = 10 X (fraction of points having a residual ≤0.1).

EMISSION SPECTROGRAPHIC ANALYSIS PAGE 1-A

REPORT 72-WSH-00 PROGRAM NO. 203 FOR: GEORGE G. GEOLOGIST A. B. CHEMIST (ANALYST)
JOB NO. 11223344 PLATE NO. VI-6789 DATE: 12/21/72
GROUP NO. 123456 RECORDING NO. 987 P. S. LEADER (PROJECT LEADER)

FIELD NO. SAMPLE SPECTRUM		W-999990 2	W-999991 3	W-999992 4	W-999993 5	W-999994 6	W-999995 8	W-999996 9	W-999997 10	W-999998 11	W-999999 12
SI	%	17.8	17.9	19.8	18.5	21.7	19.5	17.9	21.8	19.6	18.9
AL	%	6.10	6.23	6.73	7.25	7.87	6.56	6.33	8.03	7.65	7.87
FE	%	10.4	8.33	9.30	7.50	8.93	9.53	9.81	8.82	9.86	9.23
MG	%	6.50	6.74	6.92	6.73	7.64	6.40	5.68	6.23	6.62	6.41
CA	%	4.85	4.98	5.63	5.99	7.12	6.14	5.59	5.65	5.94	5.99
NA	%	> 0.316	> 0.316	> 0.316	> 0.316	> 0.316	> 0.316	> 0.316	> 0.316	> 0.316	> 0.316
K	%	0.695	< 0.0681	0.230	0.383	0.355	0.463	0.545	0.539	< 0.0681	0.248
TI	%	1.34	0.573	0.446	0.466	0.603	0.781	0.870	0.968	0.434	0.933
P	%	0.703	0.101	< 0.0464	0.140	< 0.0464	0.293	0.425	0.369	< 0.0464	0.172
MN	%	0.201	0.156	0.167	0.153	0.177	0.171	0.182	0.164	0.176	0.186
AG	PPM	< 0.10	< 0.10	< 0.10	< 0.10	< 0.10	< 0.10	< 0.10	< 0.10	< 0.10	< 0.10
AS	PPM	< 100	< 100	< 100	< 100	< 100	< 100	< 100	< 100	< 100	< 100
AU	PPM	< 6.81	< 6.81	< 6.81	< 6.81	< 6.81	< 6.81	< 6.81	< 6.81	< 6.81	< 6.81
B	PPM	< 10.0	< 10.0	< 10.0	< 10.0	< 10.0	< 10.0	< 10.0	< 10.0	< 10.0	< 10.0
BA	PPM	403	109	141	181	180	223	300	396	133	170
BE	PPM	1.35	< 1.00	< 1.00	< 1.00	< 1.00	< 1.00	< 1.00	< 1.00	< 1.00	< 1.00
BI	PPM	< 1.00	< 1.00	< 1.00	< 1.00	< 1.00	< 1.00	< 1.00	< 1.00	< 1.00	< 1.00
CD	PPM	< 14.7	< 14.7	< 14.7	< 14.7	< 14.7	< 14.7	< 14.7	< 14.7	< 14.7	< 14.7
CE	PPM	166	< 20.0	< 20.0	< 20.0	< 20.0	< 20.0	101	115	< 20.0	< 20.0
CO	PPM	45.1	44.9	51.7	40.8	52.8	47.0	42.8	42.2	58.8	57.5
CR	PPM	137	212	488	255	469	240	157	206	288	115
CS	PPM	< 3160	< 3160	< 3160	< 3160	< 3160	< 3160	< 3160	< 3160	< 3160	< 3160
CU	PPM	51.5	19.1	46.4	24.2	47.4	45.4	46.5	56.5	56.0	66.7
DY	PPM	9.77	< 3.16	< 3.16	< 3.16	< 3.16	< 3.16	< 3.16	9.14	< 3.16	< 3.16
ER	PPM	< 2.15	< 2.15	< 2.15	< 2.15	< 2.15	< 2.15	< 2.15	< 2.15	< 2.15	< 2.15
EU	PPM	3.07	< 1.00	< 1.00	1.08	< 1.00	1.80	2.53	2.52	< 1.00	2.00
GA	PPM	14.9	6.45	7.16	7.41	9.17	12.7	14.5	15.5	8.16	13.5
GD	PPM	12.1	5.04	6.31	5.32	4.82	4.62	5.55	4.46	5.06	7.28
GE	PPM	< 1.00	< 1.00	< 1.00	< 1.00	< 1.00	< 1.00	< 1.00	< 1.00	< 1.00	< 1.00
HF	PPM	< 10.0	< 10.0	< 10.0	< 10.0	< 10.0	< 10.0	< 10.0	< 10.0	< 10.0	< 10.0
HG	PPM	< 147	< 147	< 147	< 147	< 147	< 147	< 147	< 147	< 147	< 147
HO	PPM	< 1.00	< 1.00	< 1.00	< 1.00	< 1.00	< 1.00	< 1.00	< 1.00	< 1.00	< 1.00
IN	PPM	< 4.64	< 4.64	< 4.64	< 4.64	< 4.64	< 4.64	< 4.64	< 4.64	< 4.64	< 4.64
IR	PPM	< 6.81	< 6.81	< 6.81	< 6.81	< 6.81	< 6.81	< 6.81	< 6.81	< 6.81	< 6.81
LA	PPM	40.9	< 14.7	< 14.7	< 14.7	< 14.7	< 14.7	26.8	35.2	< 14.7	< 14.7
LI	PPM	< 31.6	< 31.6	< 31.6	< 31.6	< 31.6	< 31.6	< 31.6	< 31.6	< 31.6	< 31.6
LU	PPM	< 3.16	< 3.16	< 3.16	< 3.16	< 3.16	< 3.16	< 3.16	< 3.16	< 3.16	< 3.16
MN	PPM	2010	1560	1670	1530	1770	1710	1820	1640	1760	1860
MO	PPM	4.77	3.89	7.87	3.96	10.2	3.67	3.98	6.01	7.39	6.05
NB	PPM	30.1	2.42	4.98	5.10	8.36	7.54	11.6	20.6	4.78	11.8
ND	PPM	H	< 14.7	< 14.7	17.2	H	< 14.7	34.9	< 14.7	< 14.7	< 14.7
NI	PPM	57.8	91.0	147	91.0	208	93.8	60.2	72.8	122	111
CS	PPM	< 21.5	< 21.5	< 21.5	< 21.5	< 21.5	< 21.5	< 21.5	< 21.5	< 21.5	< 21.5
PB	PPM	7.29	1.11	2.63	3.85	2.91	5.28	4.85	5.72	3.14	4.60
PD	PPM	< 0.22	< 0.22	< 0.22	< 0.22	< 0.22	< 0.22	< 0.22	< 0.22	< 0.22	< 0.22
PR	PPM	H	< 2.15	H	6.46	H	7.63	10.1	10.5	H	H
PT	PPM	< 2.15	< 6.81	< 2.15	< 2.15	< 2.15	< 6.81	< 2.15	< 2.15	< 2.15	< 2.15
RB	PPM	< 14700	< 14700	< 14700	< 14700	< 14700	< 14700	< 14700	< 14700	< 14700	< 14700
RE	PPM	< 10.0	< 10.0	< 10.0	< 10.0	< 10.0	< 10.0	< 10.0	< 10.0	< 10.0	< 10.0
RH	PPM	< 0.10	< 0.10	< 0.10	< 0.10	< 0.10	< 0.10	< 0.10	< 0.10		< 0.10
RU	PPM	< 0.46	< 0.46	< 0.46	< 0.46	< 0.46	< 0.46	< 0.46	< 0.46	< 0.46	< 0.46
SB	PPM	< 68.1	< 68.1	< 68.1	< 68.1	< 68.1	< 68.1	< 68.1	< 68.1	< 68.1	< 68.1
SC	PPM	26.9	29.5	40.4	34.8	> 46.4	31.4	27.8	35.7	42.0	41.8
SM	PPM	5.91	< 4.64	< 4.64	< 4.64	< 4.64	< 4.64	< 4.64	< 4.64	< 4.64	< 4.64
SN	PPM	< 3.16	< 3.16	< 3.16	< 3.16	< 3.16	< 3.16	< 3.16	< 3.16	< 3.16	< 3.16
SR	PPM	324	179	196	242	233	286	358	376	187	269
TA	PPM	< 147	< 147	< 147	< 147	< 147	< 147	< 147	< 147	< 147	< 147
TB	PPM	< 6.81	< 6.81	< 6.81	< 6.81	< 6.81	< 6.81	< 6.81	< 6.81	< 6.81	< 6.81
TE	PPM	< 316	< 316	< 316	< 316	< 316	< 316	< 316	< 316	< 316	< 316
TH	PPM	< 21.5	< 21.5	< 21.5	< 21.5	< 21.5	< 21.5	< 21.5	< 21.5	< 21.5	< 21.5
TL	PPM	< 3.16	< 3.16	< 3.16	< 3.16	< 3.16	< 3.16	< 3.16	< 3.16	< 3.16	< 3.16
TM	PPM	< 2.15	< 2.15	< 2.15	< 2.15	< 2.15	< 2.15	< 2.15	< 2.15	< 2.15	< 2.15
U	PPM	< 215	< 215	< 215	< 215	< 215	< 215	< 215	< 215	< 215	< 215
V	PPM	345	281	317	308	336	337	290	306	333	343
W	PPM	< 10.0	< 10.0	< 10.0	< 10.0	< 10.0	< 10.0	< 10.0	< 10.0	< 10.0	< 10.0
Y	PPM	53.5	14.7	18.8	16.4	19.9	25.2	34.8	36.5	17.8	29.3
YB	PPM	6.48	2.29	2.63	2.64	3.21	3.93	4.62	4.16	2.96	4.59
ZN	PPM	193	108	124	110	119	152	173	145	115	130
ZR	PPM	629	86.9	120	112	184	156	256	293	94.0	217

MAJORS RECALCULATED AS OXIDES

SIO2	%	38.1	38.2	42.3	39.6	46.4	41.6	38.3	46.6	41.9	40.5
AL2O3	%	11.5	11.8	12.7	13.7	14.9	12.4	12.0	15.2	14.5	14.9
FE2O3	%	14.8	11.9	13.3	10.7	12.8	13.6	14.0	12.6	14.1	13.2
MGO	%	10.8	11.2	11.5	11.2	12.7	10.6	9.42	10.3	11.0	10.6
CAO	%	6.78	6.97	7.88	8.38	9.97	8.59	7.82	7.90	8.31	8.38
NA2O	%	> 0.426	> 0.426	> 0.426	> 0.426	> 0.426	> 0.426	> 0.426	> 0.426	> 0.426	> 0.426
K2O	%	0.837	< 0.0820	0.278	0.462	0.428	0.558	0.656	0.650	< 0.0820	0.299
TIO2	%	2.23	0.955	0.744	0.774	1.01	1.30	1.45	1.61	0.725	1.56
P2O5	%	1.61	0.231	< 0.106	0.321	< 0.106	0.671	0.973	0.844	< 0.106	0.393
MNO	%	0.259	0.202	0.215	0.198	0.229	0.221	0.235	0.212	0.227	0.240

Figure 5.–Example of an emission spectrographic analysis report printout.

Also calculated are the points on the curve where the slope is 50° and where it is 30°. This information defines the best section of the curve. All these calculations are most useful when assigning priorities.

The program suggests upper and lower concentration limits for those second-degree curves fitted with limits. The upper limit is the highest concentration with a peak transmittance ≥2 percent, and a tangent slope ≥0.3 (16.7°). The lower limit is the lowest concentration with a tangent slope ≥0.3 (16.7°) but with an intensity no less than that of any lower concentration.

A knowledge of possible interferences is necessary when making the initial selection of lines for fitting. After the points are fitted and the plots are visually examined, the fitting statistics are considered and the coefficients are put into the wavelength table. The lines and curves are further evaluated on the basis of the results from different samples and standards before being assigned a priority in the chain. Considered in selection of lines are general reliability for producing right answers, the existence of an effective interference correction if the need for one is indicated, and the possibility of making the line useful, if by changing concentration limits, some interference corrections can be bypassed.

FINAL ANSWERS AND REPORT FORM

After the line finding has been completed by the final program, the transmittances are converted to intensities and the background is subtracted from the peak. This intensity difference is substituted into the appropriate element concentration calibration curve, and the equation is solved. Three types of answers obtained by this program are preliminary, temporary, and final. A preliminary answer of some kind is assigned each line. Some of the lines at this time may have several preliminary answers assigned because of certain recognized error conditions. Preliminary answers possible are:

- -1 = input-output error,
- -2 = no coefficients,
- -3 = no peak but EP<2 percent transmittance,
- -4 = no peak but EP≥2 percent transmittance,
- -5 = peak too flat,
- -6 = peak too far away from EP,
- -7 = peak minus background <1 percent transmittance,
- -8 = peak too dark,
- -9 = equation unsolvable (below vertex),
- -10 = equation unsolvable (above vertex).

The temporary answer for the line is selected from among the several preliminary answers for the line.

The answer selected as the temporary answer is the first one found in the order -1 to -10. All final answers are selected from these temporary answers by examining them in the order of the preassigned priority numbers which were read in as part of the wavelength table. The final answer accepted is the first answer less than the assigned lower limit or the first answer falling between the limits. Any answer examined greater than its upper limit permits the examination of the line next in the priority chain. Temporary negative answers treated as less than the lower limit answers are -4, -6, -7, and -9. Those treated as greater than the upper limit answers are -8, and -10. The -1, -2, -3, and -5 answers are skipped during examination of the answers.

Final answers may be altered at this point only if less than a 15-mg sample was used or if an interference treatment is applicable. The value of the variable NFAMBF (table 1) is the number of samples less than 15 mg weight.

All the final answers determined for a spectrum are stored until the report is printed. A report (fig. 5) is printed at the first occurrence of 10 samples saved for printing, end of job, or last file on tape. All necessary identification data are printed on the report except the field number which is assigned by the geologist for his own convenience; a space is provided for the geologist to insert this.

Ten elements are defined as majors and are reported first as percentage element. The remaining 58 elements are reported as trace elements in parts per million. Manganese is reported as both a major and a trace for the convenience of geologists. The majors repeated at the bottom of the report have been recalculated as oxides for the convenience of those using data as oxides. The present format for the analytical report incorporates many suggestions received from many sources.

Additionally, a tape is prepared by writing each report form as a file on the tape. This provides for short-term storage for additional copies or for other purposes such as correction of erroneous input data.

REFERENCES CITED

Dorrzapf, A. F., Jr., 1973, Spectrochemical computer analysis—argon-oxygen d-c arc method for silicate rocks: U.S. Geol. Survey Jour. Research, v. 1, no. 5, p. 559–562.

Helz, A. W., 1965, The problem of automatic plate reading and computer interpretation for spectrochemical analysis, *in* Geological Survey Research 1965: U.S. Geol. Survey Prof. Paper 525-B, p. B160–B164.

—— 1973, Spectrochemical computer analysis—instrumentation: U.S. Geol. Survey Jour. Research, v. 1, no. 4, p. 475–482.

Helz, A. W., Walthall, F. G., and Berman, Sol, 1969, Computer analysis of photographed optical emission spectra: Appl. Spectroscopy, v. 23, no. 5, p. 508–518.

Myers, A. T., Havens, R. G., and Dunton, P. J., 1961, A spectrochemical method for the semiquantitative analysis of rocks, minerals, and ores: U.S. Geol. Survey Bull. 1084-I, p. 207–229.

Jour. Research U.S. Geol. Survey
Vol. 2, No. 1, Jan.-Feb. 1974, p. 73–79

IMPROVED TECHNIQUES FOR SELECTIVE STAINING OF FELDSPAR AND OTHER MINERALS USING AMARANTH

By MEADE B. NORMAN II, Menlo Park, Calif.

Abstract.—An improved method of etching feldspars with hydrofluoric acid, selectively staining potassium feldspar with sodium cobaltinitrite, and after a barium chloride dip, staining plagioclase, including albite, with amaranth (F.D. & C. Red No. 2) is described in detail. The most variable factor in the staining process seems to be the etching in hydrofluoric acid, which is affected by the freshness and concentration of the acid and by the etching time. Data are also given on the results of applying this process to apatite and to a wide variety of silicates and carbonates containing alkaline earths or lead.

This paper provides a detailed description of improved staining procedures for feldspars and other minerals using a combination of amaranth (F.D. & C. Red No. 2 or Acid Red 27, C.I. 16185)[1] and sodium cobaltinitrite, as first introduced by Laniz, Stevens, and Norman (1964). Amaranth stains the etch residue on plagioclase red, and cobaltinitrite stains the etch residue on potassium feldspar yellow, thus providing a marked color contrast on slabs and in thin sections that greatly facilitates modal analyses and rock identification. This staining process reveals textural relations and the presence of plagioclase crystals with significant differences in An content; it also accentuates features in feldspar that result from zonation, albitization, and sericitization. Stained slabs provide colorful examples for laboratory or classroom instruction, demonstrations, and exhibits.

The staining of potassium feldspar with sodium cobaltinitrite, which leaves the plagioclase etched white, was a technique first introduced by Gabriel and Cox (1929) and then changed or improved by Keith (1939), Chayes (1952), Jackson and Ross (1956), Rosenblum (1956), and Hayes and Klugman (1959). The latter suggested using a 0.5 percent solution of eosin B to color the etch residue pink on plagioclase sand grains, but the first attempts to preferentially stain plagioclase were made by Graham (1955), using malachite oxalate, and by Reeder and McAllister (1957), using hematein. Bailey and Stevens (1960) showed that the staining of plagioclase could be accomplished by replacing Ca ions in the etched feldspar with Ba ions, which react with potassium rhodizonate to produce a red insoluble barium rhodizonate precipitate. Subsequent methods have been based upon this idea of ionic substitution, which in this paper has been reported in some Pb, Sr, and Mg minerals as well. The potassium rhodizonate has been discontinued in favor of the less expensive and more stable amaranth.

Referring to the cobaltinitrite staining procedure, Van der Plas (1966) wrote that "the fact that so many authors found it necessary to comment on the details of the procedure proves that, in practice, there are some difficulties to overcome." Chayes and Zies (1961) attempted to explain the relative insensitivity of many sanidines and anorthoclases to the cobaltinitrite stain. A possible explanation was presented by Sclar and Fahey (1972). Ford and Boudette (1968) discovered anorthoclase could be stained with amaranth using a modification of the feldspar staining method described by Laniz, Stevens, and Norman (1964). Laduron (1966) applied a variation of this same method to metamorphic, igneous, and sedimentary rocks. An extensive compilation of staining tests for a wide variety of minerals was prepared by Reid (1969). Friedman (1971) compiled and edited a chapter on effective staining techniques for minerals in sedimentary rocks, including some feldspar staining procedures as well as methods of preparing stained peels. Lyons (1971) combined the processes of dipping the rock slab in hydrofluoric acid, as proposed by Laniz, Stevens, and Norman (1964), and of fuming it over hydrofluoric acid for 3 min, as mentioned by Bailey and Stevens (1960), with a heat-drying step in between. Lyons also suggested etching unsealed, badly weathered rocks for as long as 45 s, but he admitted the long etch had a destructive effect on the dark minerals.

Staining, as used in this paper, implies the actual deposition of a precipitate. Examples of adsorption are so designated, or if doubtful, the term "stained" in quotation marks is used.

STANDARD FELDSPAR-STAINING PROCEDURE FOR ROCK SLABS

1. Cut the slab with a rock saw using water-soluble cutting oil to eliminate the need for special cleaning afterwards.

[1] The F.D. & C. dyes mentioned in this report are products of the Wm. J. Stange Co., P.O. Box 3687, Hayward, CA 94544. Use of these terms in this paper is for descriptive purposes only and does not constitute an endorsement of the product by the U.S. Geological Survey.

Rough grind the slabs on a lap with No. 60–90 grit, seal with Lakeside 70C if necessary, and then grind smooth with Nos. 100 and (or) 240 grit.

Discussion.—Weathered or poorly indurated rocks should be sealed with Lakeside, or a similar thermoplastic, before coarse-grinding off the saw marks. If the rock is fractured or too friable to survive drying with compressed air, it should be warmed under a heat lamp until it will very easily melt the Lakeside, which should be applied to the surface and edges. Next, cool the slab, face down in water, and again grind smooth with No. 100 grit. Finish grinding with No. 240 grit for coarse-grained rock and No. 400 grit for fine-grained rock. To distinguish Lakeside from quartz more easily, the slab may be warmed under a heat lamp until the frosted Lakeside surfaces become glossy, but overheating will cause the Lakeside to bubble.

Procedures for staining sand grains have been described by Hayes and Klugman (1959), Van der Plas (1966, p. 50–51), and by Laniz, Stevens, and Norman (1964). After the grains are mounted in Lakeside, the standard procedure for slabs can be followed.

2. Immerse the face of the dry slab in concentrated HF (52 percent, at room temperature for 5 to 15 s. High-calcium feldspars generally require only 5 to 8 s.

Discussion.—Pour HF into a polyethylene petri dish large enough to accommodate the slab. Caution! Use HF only under a well-ventilated hood, and wear glasses and acid-proof gloves. Note: Etching time will vary depending on the temperature and freshness and concentration of the HF, as well as on the composition of the rock. Sometimes, as a result of overetching, the etch residue on feldspar will flake off when the slab is dried by compressed air, or after staining by amaranth, the plagioclase may have a mottled appearance or be pink instead of dark red. Low-An plagioclase will invariably stain pink.

Rocks that contain calcite or dolomite in addition to feldspar, such as some dike rocks, should be first etched in HCl, then rinsed in water, and dried. For calcite, etch in 10 percent HCl for about 45 s; for dolomite, etch in 50 percent HCl for 1 or 2 min. This treatment reduces the relief of the carbonate minerals so that after staining they can be distinguished easily from other minerals.

3. Rinse the entire slab sufficiently in tap water to remove the excess HF. If desired, dry with compressed air to facilitate observation of the etch residue to see if the slab is properly etched.

Discussion.—Van der Plas (1966) suggests heating the slab after vapor-etching in an electric furnace at 400°C for about 5 min to fix the etch residue. After rinsing, Lyons (1971) suggests drying the slab in an oven at 80°C. Drying with compressed air followed by ovendrying at this stage is optional; good results can be obtained without it, especially on fresh or sealed rocks. Some rocks, particularly those that are unsealed or weathered, may need to be ovendried at 85° to 90°C for 15 min or longer to eliminate all HF. This removal of acid also prevents contamination of the cobaltinitrite solution.

If the plagioclase is albitic, follow the procedure given in the section on "Staining Albite."

4. Immerse the face of the slab in a tray containing a saturated solution of sodium cobaltinitrite for 15 s.

Discussion.—The etch residue of hieratite, cubic K_2SiF_6 (Sclar and Fahey, 1972), produced on the potassium feldspar in step 2 now reacts with the cobaltinitrite solution to form a yellow precipitate reported by Feigl (1958) to be $K_2Na[Co(NO_2)_6]$.

The sodium cobaltinitrite solution must be saturated, and undissolved excess should be frequently stirred up during use so that it retains its yellow color. When not in use, keep the tray tightly covered so that the solution will not dry up.

5. Rinse the slab thoroughly in running tap water to remove excess cobaltinitrite, dry with compressed air, and then dry in an oven for 15 to 20 min at 85° to 90°C.

Discussion.—Heating should be sufficient to remove the remaining HF from pores in the rock. If the evaporation of excess HF leaves an orangish discoloration on the yellow-stained potassium feldspar, this residue can be rinsed off with water. Do not overheat slabs sealed with Lakeside as the sealant may bubble up over the stained surface.

At this point the potassium feldspar is stained bright yellow, and the white to yellowish-white color of the etched plagioclase usually provides a suitable contrast for modal analysis. Sanidine may stain with only a trellis-work pattern of cobaltinitrite; this diagnostic feature can be used to identify sanidine. To form a light but usable stain on sanidine, Chayes and Zies (1961) suggest repeated 15-s etches by HF acid fumes, each followed by 5-min immersions in cobaltinitrite. Heat-drying after fuming may help, or follow steps 1 through 6 of the procedure outlined for albite. The very pale yellow cobaltinitrite stain on sanidine and anorthoclase, according to Sclar and Fahey (1972), possibly results from the presence of nonreactive malladrite, rhombohedral Na_2SiF_6, intimately mixed with hieratite in the etch residue.

6. Remove the slab from the oven, and while it is still as warm as can be handled comfortably, dip the face of the slab in a saturated solution of barium chloride ($BaCl_2$) for 5 to 10 s. Next, dip the face of the slab twice in tap water to remove excess $BaCl_2$, and then dry the face and sides of the slab quickly with compressed air.

Discussion.—The Ca ions in the etch residue produced on plagioclase in step 2 are now replaced with Ba ions

that react with amaranth in step 7 to produce the red precipitate.

The $BaCl_2$ solution will become cloudy with precipitate after repeated use but is still effective. Shake the solution well before using, and keep it in a closed flask. When testing for the presence of a barium feldspar, such as celsian, or another barium silicate or carbonate, omit step 6. A potassium feldspar, such as hyalophane, may also be tested for barium by omitting the dip in sodium cobaltinitrite.

7. Dip the face of the warm slab in saturated solution of amaranth for 1 or 2 s.

   Discussion.—Keep the amaranth solution in a closed flask when not in use, and shake well before using. A small amount will last a long time as it can be used over and over again. Occasionally, it may be necessary to add water to replenish that lost by evaporation, but the solution should be kept saturated. Of the available food dyes that give a good contrast with the yellow potassium cobaltinitrite, amaranth is the least expensive. Other more expensive dyes, such as F.D. & C. Green No. 3 (Food Green 3, C.I. 42053) and F.D. & C. Blue No. 1 (Acid Blue 9, C.I. 42090) will stain the plagioclase equally well but tend to discolor the yellow cobaltinitrite.

8. Dip the face of the slab two or more times in a bowl of water to remove most of the excess amaranth.

   Discussion.—Dip-rinse the face of the slab enough so that the potassium feldspar shows up well. Be careful not to rinse the slab too much because the red precipitate is slowly soluble in water. If blackish-red blotches appear where the $BaCl_2$ solution was not adequately rinsed off, the excess amaranth can be gently rubbed off with a finger while the slab is still wet.

9. While holding the slab with stained side down in a tilted position, use compressed air to quickly sweep away any remaining excess amaranth from the face and sides of the slab; then dry the slab, face side up.

   Discussion.—If the slab has not been sealed sufficiently, it may be necessary to heat-dry it again at this point or even to reseal and restain it. The plagioclase should now be stained a purple-red in sharp contrast to the yellow-stained potassium feldspar and the unstained quartz. The plagioclase may be stained only some shade of pink either because it is albite or oligoclase or because the slab was over-etched or the HF was not fresh enough. If the plagioclase is albitic, refer to the section on "Staining Albite." Overetching is indicated by windows in the plagioclase etch residue where it has flaked off. These areas can be distinguished from the unstained quartz by their lower relief.

Additional results and variations

As a result of this staining procedure, biotite commonly is light to medium green after step 5 or a mottled reddish black to golden brown after step 9 and in many samples can be distinguished from hornblende, which is unstained if not etched too long. Muscovite and garnet are generally unstained, but some muscovite may be faintly pink. Sphene is stained a light pink to red. Apatite is stained dark red to pink.

If desired, after etching, rinsing, and heat-drying, omit the cobaltinitrite stain, and stain the plagioclase red using the $BaCl_2$-amaranth treatment. Potassium feldspar will be "stained" a light pink and will be texturally different from the unstained quartz. Hornblende remains unstained, but biotite will stain a lavender to dark purple. Since apatite will be stained a dark red, the staining and rinsing processes can be regulated to render plagioclase a lighter pink color that will contrast with small grains of red-stained apatite when viewed through the microscope. However, if the plagioclase is albitic and only stains a faint pink, it may be difficult to distinguish from potassium feldspar.

Clay minerals, some limestones, porous sandstones, fibrous minerals, and chalky minerals may adsorb amaranth rather than be stained by a chemical reaction. Therefore, specimens of such materials should be sealed with lakeside and ground smooth. Then test the rock for adsorption by processing it without etching according to steps 6 through 9 of the standard procedure, but leave it in amaranth for 15 s. After rinsing well and drying, if the minerals are "stained" red, they have adsorbed the amaranth. As a check, process another slab of the rock through the entire standard procedure and compare it with the unetched rock. A more intense depth of color in the etched rock than in the unetched rock indicates that the minerals have been chemically stained. Preferential adsorption of amaranth by unetched minerals can provide color contrasts that in some samples are useful in distinguishing minerals.

STAINING THIN SECTIONS

To stain thin sections for potassium feldspar and plagioclase, use the following procedure, which is modified after Keith (1939), Rosenblum (1956), Bailey and Stevens (1960), and Laniz, Stevens, and Norman (1964):

1. Use shallow etching vessels with an opening on top slightly smaller than the glass slide. Fill with concentrated 52 percent HF to about 5 mm from the top. Place the uncovered sections face down across the tops of the vessels so as to cover the openings completely, and etch for 15 to 30 s with HF acid vapor. Do not rinse. Rest the section on end, and dry it over the hot-air vent on the oven. Do not overheat.
2. Immerse the section face up in saturated sodium cobaltinitrite solution for 15 to 30 s.
3. Rinse the section in tap water to remove excess cobaltinitrite, and dry gently with compressed air. Potassium feldspar is stained yellow.
4. Warm the section again over the hot-air vent on the oven, and immerse it for 15 s in a saturated solution of barium chloride.

5. Dip the section once or twice in water, and dry gently with compressed air.
6. Immerse the section for 5 s in saturated solution of amaranth.
7. Dip the section once or twice in water to remove excess dye, and dry gently with compressed air. Plagioclase, except low-An albite, is stained pink.

Note: If deeper colored stains on the feldspars are desired, the polished surface of the blank to be mounted for a thin section is first stained and then mounted with the stained surface down on the glass slide. The section is then ground to the proper thickness and again etched and stained as just described.

Boone and Wheeler (1968) have described a variation of this procedure involving a 7-s re-etching before dipping in $BaCl_2$ solution in order to achieve a better amaranth stain.

STAINING ALBITE

When pure albite (An_0), which does not contain any Ca, is etched with HF, it yields a Ca-free residue of malladrite that is nonreactive with $BaCl_2$ and therefore remains unstained by amaranth. If the albite is An_2 to An_3, its etch residue contains some Ca ions for the Ba ions to replace and will then stain a very faint pink; plagioclases with a progressively higher An content will stain a progressively darker pink to red color. The pink to light red color prevails to about An_{15}. Plagioclase very high in Ca stains a very dark purple-red. The shade of red also depends on the concentrations of solutions used, the duration of etching in HF, and the amount of rinsing.

If desired, all the feldspar including the albite can be stained yellow if the cobaltinitrite dip is first preceded by a 15-s dip in a 20 percent solution of potassium chloride and then rinsed, as suggested by Bailey and Stevens (1960). This process is also effective on a variety of other minerals such as anorthoclase, nephrite jade, and possibly sanidine.

If albite or anorthoclase and potassium feldspar occur together in the rock and if a darker amaranth stain is desired on the albite (or anorthoclase), then special preliminary steps are necessary. To obtain a more uniform and darker amaranth stain on low-Ca plagioclase, the following procedure is suggested:

1. Seal the slab with Lakeside if necessary, and then coarse grind with No. 60–90 or No. 100 grit.
2. Immerse the face of the dry slab in concentrated HF for approximately 10 s.
3. Note: Do not rinse. Instead, rest the slab on its edge so that it can drip dry under a well-ventilated hood for about 15 to 20 min.
4. Finish drying in oven at 85° to 90°C for about 20 min to remove all HF from the rock. Do not overheat if sealed with Lakeside.
5. Immerse the face of the warm slab in a saturated solution of sodium cobaltinitrite for about 15 s.
6. Rinse the slab thoroughly in tap water, and dry with compressed air.
7. Heat dry in oven again until the slab is as warm as can be handled comfortably. The time will vary with the size of the rock.
8. Continue with steps 6 through 9 of the standard procedure.

Using the above procedure, albite An_4 stained about the same shade of red as that obtained on oligoclase An_{25} using the standard procedure. Muscovite was "stained" pink, and some of the mafic minerals were partly covered with an orange-colored crust that could be readily flaked off. Potassium feldspar was stained yellow, and quartz remained unstained. Using this method, albite as low as An_1 or An_2 has been stained a dull red, and two normally unaffected minerals, white prehnite and white datolite, were stained pink and light red, respectively. This procedure is possibly effective on other minerals that are not affected by the standard procedure. Anorthoclase, for example, was first stained a very pale but uniform yellow by cobaltinitrite and subsequently stained a dull orange-red after the $BaCl_2$-amaranth treatment. If the cobaltinitrite dip is omitted, then anorthoclase is stained a darker purplish red.

AMARANTH STAINING OF OTHER MINERALS

As mentioned by Laniz, Stevens, and Norman (1964), various silicate and carbonate minerals containing alkaline earth metals or lead can be etched with HF, rinsed, dried, dipped in $BaCl_2$ solution, and stained with amaranth. However, not all these react significantly because sometimes little etch residue remains to retain the stain. Generally, test for adsorption first; then use the standard procedure as outlined earlier. However, some minerals or rock types will require a longer period of immersion in HF, and some may require the special procedure outlined for staining albite. Grain orientation will sometimes cause adjacent grains of the same mineral to be stained different shades of red. Other F.D. & C. colors mentioned in the standard procedure can be used if desired.

The rest of this report, including tables 1 and 2, lists the reaction of some minerals to amaranth stain, and it is quite probable that there are other minerals that can be stained with amaranth. Beryl does not stain, but there may be some Be minerals that do.

Calcium and magnesium silicates

Scapolite.—Scapolite (meionite content 40) in a carbonate granofels from the Wallace Formation, near Fernwood, Idaho, stained red. Some scapolite porphyroblasts had recrystallized partly to calcite, which stained light pink, and partly to quartz, which remained unstained.

Melilite.—Melilite may take the amaranth stain, although it has not been tested. Shand (1939) has shown that it and feldspathoids can be stained using phosphoric acid and methylene blue.

Table 1.—*Effect of amaranth stain on barium silicates and carbonates, lead and strontium carbonates, and calcium and magnesium carbonates and phosphates*

Mineral	Remarks
Barium silicates and carbonates	
Ba-feldspars, barytocalcite, benitoite, celsian, harmotome, hyalophane, sanbornite, and witherite.	These minerals, and feldspars containing Ba, can be tested for Ba by eliminating the $BaCl_2$ dip (step 6) before dipping in amaranth. A red stain will indicate the presence of Ba. Both hyalophane, a potassium-barium feldspar, and harmotome, a barium-potassium zeolite, should stain red, provided that the sodium cobaltinitrite dip and the $BaCl_2$ dip are omitted.
Lead and strontium carbonates	
Cerussite and strontianite	Cerussite will take a definite pink stain, whereas anglesite is relatively unaffected. Strontianite in a Lakeside-sealed limestone from Bloomington, Ind., stained red, and the limestone was rendered a pink color.
Calcium and magnesium carbonates and phosphates	
Ankerite, apatite, aragonite, calcite, dolomite, magnesite, and rhodochrosite.	Many kinds of dolomite are stained red, which contrasts with the faint pink color on associated calcite. Aragonite is stained pink, and some ankerite also takes the amaranth stain. However, not all calcite, dolomite, and aragonite will react the same way, possibly owing to differences in Ca:Mg content and minor constituents. Some dolomite yields only a pink stain. The fluorescent calcite from Franklin, N.J., which contains Pb, Mg, and Mn, stained a definite pink color. A dense magnesite nodule from Anderson Reservoir, Santa Clara County, Calif., did not stain, but softer, chalky types will absorb the dye. Rhodochrosite from Silverton, Colo., did not stain. A calcite specimen from the Thaynes Formation, Beaverhead County, Mont., stained pink, and the apatized microfossils in it stained red.

Table 2.—*Effect of amaranth stain on calcium and magnesium silicates, grouped according to Strunz's (1957) classification.*

Mineral	Effect of amaranth	Remarks; contrasts with other minerals
Framework structures (tectosilicates)		
Scapolite	Stained red*	
Melilite	(*)	
Zeolites	(*)	
Double structures (sorosilicates)		
Prehnite, white	Normally unstained	Will stain pink using procedure for albite. From California.
Ring structures (cyclosilicates)		
Cordierite	(*)	
Sheet structures (phyllosilicates)		
Serpentine	(*)	
Chain structures (inosilicates)		
Amphiboles	(*)	
Pyroxenes	Generally unstained	Seal with Lakeside; polish before etching.
Diopside	In some rocks, it "stained" faint pink.	Color may be due to staining of incorporated impurities.
Augite	Unstained	Black, vitreous crystal. From Alaska.
Rhodonite	(*)	
Bustamite	Stained red	Associated rhodochrosite unstained. From Colorado.
Wollastonite	Stained dark red.	
Pectolite	Stained red	
Isolated structures (nesosilicates)		
Olivine group	(*)	
Monticellite	Stained dark red.	Associated vesuvianite unstained. From California.
Datolite, white	Normally unstained	Will stain pink if etched longer or if procedure for albite is used. From California.
Sphene	Stained light pink to red	

*See text for description.

Zeolites.—Stewart (1970) mentions that laumontite in a graywacke was stained pink with amaranth to distinguish it from associated albite. Some other calcium zeolites might be similarly affected.

Cordierite.—By varying the etching time, it was found that cordierite would stain a lighter to a darker red than the associated plagioclase, depending upon the amount of etch residue on each. Usually, etch residue on cordierite was less abundant and appeared grayer than etch residue on plagioclase, and the cordierite stained a lighter red. Boone and Wheeler (1968) obtained a lighter amaranth stain on the cordierite than on the plagioclase in thin section. They have also shown that cordierite can be stained with trypan blue without staining the plagioclase unless the specimen is immersed in the solution for a longer time.

Serpentine.—Massive serpentine stains various shades of purplish red. Weathered specimens partly adsorbed the amaranth and thus enhanced the color of the stain. Whereas chrysotile, fibrous brucite, and other asbestos minerals will all adsorb the amaranth, the fiberized or ground-up chrysotile and brucite can be differentiated from these other asbestos minerals by their unique adsorption of a 1 percent solution of iodine in glycerine, which renders them brown, as shown by Morton and Baker (1941). Fibrous brucite adsorbs amaranth to a greater extent than the massive variety and consequently is "stained" a darker red. A specimen of massive brucite from Mineral County, Nev., after being sealed with Lakeside, was etched for 1 min in HF, rinsed, heat-dried, and given the $BaCl_2$-amaranth

treatment. Probably owing to some adsorption, the brucite was rendered a light pink, but the associated small grains of dolomite were all stained a dark red.

Amphiboles.—A Cape San Martin, Calif., specimen of dark-green nephrite jade—the compact, matted, fibrous form of amphibole chemically similar to actinolite or tremolite—stained a purple-red color. However, associated green crystals, which may be a broad prismatic form of tremolite or actinolite with a lower content of Ca ions, were "stained" only a faint purplish pink. A purple-red stain was achieved on amphibole veinlets in a polished specimen of massive talc from Jade Cove, Calif., suggesting that the veinlets may be nephrite jade. Specimens of bladed tremolite "stained" a light pink. Further tests on fresh amphiboles and pyroxenes are necessary to determine if any others take a genuine stain.

Rhodonite.—In this manganese silicate, some calcium generally replaces the manganese and therefore can be stained. For pink rhodonite a different F. D. & C. color than Red No. 2 should be used.

Wollastonite.—Narrow bands of wollastonite in a skarn stained dark red. These alternated with bands that stained light pink and were composed of an intimate mixture of fine-grained wollastonite, diopside, and unstained leucoxene.

Olivine group.—The 1- to 2-min etching in concentrated HF of polished slabs of peridotites, feldspathic pyroxenites, and pyroxene gabbros aids in distinguishing the different minerals present, according to Jackson and Ross (1956). If desired, their procedure can be augmented with the $BaCl_2$ dip and amaranth stain. In an unpolished peridotite nodule containing abundant forsteritic olivine, from the Marshall quadrangle of southwestern Alaska, the olivine acquired a red stain that differentiated it from unstained enstatite, chrome diopside, and chrome spinel. In an unpolished specimen of pyroxenite from south of Lake Chabot, Hayward quadrangle, California, diopsidic pyroxene was rendered various shades of purplish pink, depending on the orientation of the crystals, and the grains of an olivine-serpentine mixture stained a darker red. However, the pyroxene in a polished specimen of the same rock remained unstained.

Minerals not affected by amaranth

Minerals not previously mentioned that remained unstained by the standard procedure include epidote, scheelite, staurolite, lawsonite, zoisite, smithsonite, willemite, hemimorphite, jadeite, axinite, hematite, magnetite, ilmenite, rutile, chromite, fluorite, and pyrite. Probably all sulfides, oxides, and halides would remain unstained by amaranth. Buddingtonite, an ammonium feldspar with zeolitic water, was also tested. A semiquantitative spectrographic analysis of the specimen used showed approximately 0.03 percent Ca, 0.15 percent Na, 2.0 percent K, and 0.15 percent Ba. These trace elements are finely disseminated in the buddingtonite, and attempts to show them by staining with cobaltinitrite and amaranth yielded inconclusive results. Even though sealed with Lakeside, the high porosity of the sample further hampered the test. Pale-yellow and pink casts on the specimen were probably the result of adsorption of the stains.

ACKNOWLEDGMENTS

I am especially indebted to E. H. Bailey and D. C. Ross for critical reviews of this manuscript and helpful suggestions and to Julius Schlocker, J. M. Hoare, E. H. Pampeyan, and A. B. Ford for providing samples and suggestions.

REFERENCES CITED

Bailey, E. H., and Stevens, R. E., 1960, Selective staining of K-feldspar and plagioclase on rock slabs and thin sections: Am. Mineralogist, v. 45, p. 1020–1025.

Boone, G. M., and Wheeler, E. P., 1968, Staining for cordierite and feldspars in thin section: Am. Mineralogist, v. 53, p. 327–331.

Chayes, Felix, 1952, Notes on the staining of potash feldspar with sodium cobaltinitrite in thin sections: Am. Mineralogist, v. 37, p. 337–340.

Chayes, Felix, and Zies, E. G., 1961, Staining of alkali feldspars from volcanic rocks: Carnegie Inst. Washington Year Book 60, p. 172–173.

Feigl, Fritz, 1958, Spot tests in inorganic analysis [5th ed.]: New York, Van Nostrand, p. 230.

Ford, A. B., and Boudette, E. L., 1968, On the staining of anorthoclase: Am. Mineralogist, v. 53, p. 331–334.

Friedman, G. M., 1971, Staining, *in* Carver, R. E., ed., Procedures in sedimentary petrology: New York, Wiley-Interscience, p. 511–528.

Gabriel, Alton, and Cox, E. P., 1929, A staining method for the quantitative determination of certain rock minerals: Am. Mineralogist, v. 14, p. 290–292.

Graham, E. R., 1955, Rapid determination of quartz, potash minerals, and plagioclase feldspars: Chemist-Analyst, v. 44, no. 2, p. 37–38.

Hayes, J. R., and Klugman, M. A., 1959, Feldspar staining methods: Jour. Sed. Petrology, v. 29, p. 227–232.

Jackson, E. D., and Ross, D. C., 1956, A technique for modal analysis of medium- and coarse-grained (3–10 mm) rocks: Am. Mineralogist, v. 41, p. 648–651.

Keith, M. L., 1939, Selective staining to facilitate Rosiwal analysis: Am. Mineralogist, v. 24, p. 561-565.

Laduron, D., 1966, Sur les procédés de coloration sélective des feldspaths en lame mince: Soc. Géol. Belgique Annales 89, p. 281–294.

Laniz, R. V., Stevens, R. E., and Norman, M. B., 1964, Staining of plagioclase feldspar and other minerals with F.D. and C. Red No. 2: U.S. Geol. Survey Prof. Paper 501-B, p. B152–B153.

Lyons, P. C., 1971, Staining of feldspars on rock-slab surfaces for modal analysis: Mineralog. Mag., v. 38, p. 518–519.

Morton, Maurice, and Baker, W. G., 1941, Identification stain for chrysotile asbestos: Canadian Inst. Mining and Metallurgy Trans., v. 44, p. 515–523.

Reeder, S. W., and McAllister, A. L., 1957, A staining method for the quantitative determination of feldspars in rocks and sands from soils: Canadian Jour. Soil Sci., v. 37, p. 57–59.

Reid, W. P., 1969, Mineral staining tests: Colorado School Mines Mineral Industries Bull., v. 12, no. 3, p. 1–20.

Rosenblum, Samuel, 1956, Improved techniques for staining potash feldspars: Am. Mineralogist, v. 41, p. 662–664.

Sclar, C. B., and Fahey, J. J., 1972, The staining mechanism of potassium feldspar and the origin of hieratite: Am. Mineralogist, v. 57, p. 287–291.

Shand, S. J., 1939, On the staining of feldspathoids and on zonal structure in nepheline: Am. Mineralogist, v. 24, p. 508–513.

Stewart, R. J., 1970, Petrology, metamorphism and structural relations of graywackes in the western Olympic Peninsula, Washington: Palo Alto, Calif., Stanford Univ. Ph. D. thesis, 107 p.

Strunz, Hugo, 1957, Mineralogische Tabellen: Leipzig, Geest and Portig, Akad. Verlagsgesellschaft, 448 p.

Van der Plas, Leendert, 1966, The identification of detrital feldspars: Amsterdam, Elsevier Publishing Co., 305 p.

Jour. Research U.S. Geol. Survey
Vol. 2, No. 1, Jan.-Feb. 1974, p. 81–88

SOME AMMONOIDS FROM THE RIPLEY FORMATION OF MISSISSIPPI, ALABAMA, AND GEORGIA

By W. A. COBBAN, Denver, Colo.

Abstract.—Heteromorph ammonoids occur in the Coon Creek Tongue of the Ripley Formation of Late Cretaceous (Maestrichtian) age in northeastern Mississippi and in the age-equivalent part of the Ripley Formation along the Chattahoochie River separating Alabama and Georgia. Ammonoids treated in this report are *Nostoceras alternatum* (Tuomey), *Exiteloceras* sp., *Axonoceras?* sp., and the new species *Solenoceras nitidum* and *Axonoceras sohli*. None of these species is known outside the eastern part of the Mississippi embayment area.

Ammonoids representing the genera *Baculites, Hoploscaphites?, Solenoceras, Axonoceras, Exiteloceras,* and *Nostoceras* are present in the U.S. Geological Survey's collections of fossils from the lower part (Coon Creek Tongue) of the Ripley Formation of northeastern Mississippi and the time-equivalent part of the Ripley Formation along the boundary between Alabama and Georgia. *Baculites* and *Hoploscaphites?*, represented by a very few fragmentary specimens, are not included in the present report. The ammonoids represent a single zone herein referred to as the zone of *Nostoceras alternatum* (Tuomey).

The Ripley Formation in northeastern Mississippi attains a thickness of nearly 350 ft and is divisible into five units as follows, from oldest to youngest: transitional clay, Coon Creek Tongue, McNairy Sand Member, sand of the upper part of the Ripley, and Chiwapa Member (Sohl, 1960, p. 10–20; 1964, fig. 12). Ammonoids representing the zone of *Nostoceras alternatum* occur in the Coon Creek Tongue in Tippah and Union Counties. Southward from Union County the Ripley Formation thins rapidly, and the five lithologic units lose their identity (Sohl, 1960, pl. 1). Farther southward in Mississippi the thinned Ripley becomes calcareous and grades into impure sandy chalk. Far to the southeast, along the Chattahoochie River forming part of the boundary between Alabama and Georgia, the Ripley consists of about 135 ft of dark-gray micaceous clayey sand (Eargle, 1955, p. 57–59).

The ammonoids from Tippah and Union Counties and from the exposures along the Chattahoochie River are very well preserved and usually retain their nacreous shell material. The figured specimens are at the National Museum of Natural History, Washington, D.C., and plaster casts of some are at the U.S. Geological Survey, Federal Center, Denver, Colo. Robert E. Burkholder, of the Geological Survey, photographed the specimens.

AMMONOID RECORDS FROM THE RIPLEY FORMATION

References to ammonoid species are scarce in the literature concerning the Ripley Formation of Mississippi, Alabama, and Georgia. The earliest record seems to be that of Tuomey (1854, p. 168), who briefly described the new species *Turrilites alternatus* from Noxubie County, Miss. Six years later Conrad (1860, p. 284) described as a new species *Turrilites spinifera* from Eufaula, Ala., and Tippah County, Miss. Although neither Tuomey nor Conrad illustrated his specimens, the descriptions suggest the same species which is best assigned to *Nostoceras.*

The Ripley Formation was named by Hilgard (1860, p. 93, 95), who reported the presence of Conrad's *Turrilites spinifera* [*Nostoceras alternatum*] in it from Tippah County as well as *Solenoceras annulifer* (Morton), a species known previously only from older strata in Delaware. The *Solenoceras* from Tippah County is probably the new species *S. nitidum.*

Nostoceras alternatum was recorded as *Turrilites alternatus* from the Ripley Formation of northeastern Mississippi by Crider (1906, p. 21) and Stephenson (1914, table 2) and from the Ripley along the Chattahoochie River in Alabama and Georgia by Stephenson (1911, p. 178, 211, 213; 1914, table 8). Stephenson and Monroe (1940, chart opposite p. 182) recorded *Nostoceras* sp. from the Ripley Formation of Union County, Miss., and Cooke (1943, p. 30) reported *N. stantoni* Hyatt? from the Ripley of Georgia. These specimens are probably all *N. alternatum.*

LOCALITIES OF COLLECTIONS

Localities that contain heteromorph ammonoids in the Coon Creek Tongue of the Ripley Formation and in the age-equivalent part of the Ripley of Alabama and Georgia are listed in the following descriptions from the northwest to the southeast. The location of the collection site is followed by the name of the collector, the year of collection, and the stratigraphic assignment. Collections that contain only baculites or scaphites are not included. The largest and best

collections of heteromorphs are from localities described by Stephenson and Monroe (1940, p. 182–192) and Sohl (1960, p. 28–31). These authors presented stratigraphic sections for some of the collecting localities. Most of the northeastern Mississippi fossil localities are shown on a map by Sohl (1960, pl. 2). For the Chattahoochie River area, the reader is referred to the sketch map by Stephenson (1911, fig. 6).

USGS Mesozoic localities 542, 708. Bullock's old overshot mill, 2 mi south of Dumas, in sec. 36, T. 5 S., R. 4 E., Tippah County, Miss. L. C. Johnson, 1888; T. W. Stanton, 1889. This locality, in the Coon Creek Tongue of the Ripley Formation, was described by Stephenson and Monroe (1940, p. 188) and Sohl (1960, p. 28).
Baculites cf. *B. undatus* Stephenson
Solenoceras nitidum Cobban
Exiteloceras? sp.
Axonoceras sohli Cobban
Nostoceras alternatum (Tuomey)

USGS Mesozoic locality 709. W. O. Kelly farm 2.3 mi south of Dumas in the NE¼ sec. 35, T. 5 S., R. 4 E., Tippah County, Miss. T.W. Stanton, 1909. Coon Creek Tongue of Ripley Formation (Sohl, 1960, p. 28).
Solenoceras nitidum Cobban
Nostoceras alternatum (Tuomey)
Hoploscaphites? sp.

USGS Mesozoic locality 25407. Roadcut on northeast-facing slope of Hall Creek 2.9 mi southwest of Dumas, in the center of the S½NW¼ sec. 34, T. 5 S., R. 4 E., Tippah County, Miss. N. F. Sohl, 1950–52. Coon Creek Tongue of Ripley Formation (Sohl, 1960, p. 28).
Nostoceras alternatum (Tuomey)

USGS Mesozoic localities 18078, 18629, and 25411. Scraped area north of dam of Union County Lake, 1.1 mi northeast of Pleasant Ridge, in the NW¼NE¼NE¼ sec. 11, T. 6 S., R. 4 E., Union County, Miss. L. C. Conant and Andrew Brown, 1939; L. W. Stephenson and W. H. Monroe, 1940; N. F. Sohl, 1950–52, 1955; G. R. Scott, 1961. This highly fossiliferous locality near the base of the Coon Creek Tongue of the Ripley Formation has been mentioned in several reports (Stephenson and Monroe, 1940, p. 182, 192; Conant, 1942, p. 22–25, fig. 3; Harbison, 1945, p. 75; Sohl, 1960, p. 31).
Baculites sp.
Solenoceras nitidum Cobban
Exiteloceras sp.
Axonoceras sohli Cobban
Nostoceras alternatum (Tuomey)

USGS Mesozoic localities 6873, 25408. Lee's old millsite, roadcut on northeast-facing slope of Tallahatchie River valley, 2 mi north-northeast of Keownville, in the NW¼NE¼ sec. 17, T. 6 S., R. 4 E., Union County, Miss. L. W. Stephenson, 1910; N. F. Sohl, 1950–52. Upper part of Coon Creek Tongue of Ripley Formation (Sohl, 1960, p. 30–31). See Stephenson and Monroe (1940, p. 191) for a photograph of this locality.
Axonoceras sohli Cobban
Exiteloceras sp.
Nostoceras alternatum (Tuomey)

USGS Mesozoic locality 712. Bluff on North Branch of Wilhite Creek, 3 mi south of Molino and 0.8 mi south of Mount Olivet School, in the NW¼ sec. 21, T. 6 S., R. 4 E., Union County, Miss. T. W. Stanton, 1889. Coon Creek Tongue of Ripley Formation (Sohl, 1960, p. 30). *Nostoceras* sp. was identified from this locality by Stephenson (Stephenson and Monroe, 1940, chart opposite p. 182).
Solenoceras nitidum Cobban
Nostoceras alternatum (Tuomey)

USGS Mesozoic locality 857. Chattahoochie River, 2 mi below the landing at Eufaula, Ala. T. W. Stanton, 1891. Ripley Formation (Stephenson, 1911, p. 178).
Nostoceras alternatum (Tuomey)

USGS Mesozoic locality 27883. Falls on Lumberyard Creek near center of sec. 4, T. 10 N., R. 29 E., Barbour County, Ala. N. F. Sohl and A. Karl, 1961. Ripley Formation.
Nostoceras alternatum (Tuomey)

USGS Mesozoic locality 28434. Left bank of Barbour Creek downstream from bridge of U.S. Highway 431, in the SE¼NE¼SE¼ sec. 7, T. 10 N., R. 29 E., Barbour County, Ala. N. F. Sohl and R. L. Rieke, 1961. Ripley Formation.
Baculites sp.
Nostoceras alternatum (Tuomey)

USGS Mesozoic locality 27923. Bluff on right bank of Barbour Creek at first bend above bridge of U.S. Highway 431, in the NW¼SE¼ sec. 7, T. 10 N., R. 29 E., Barbour County, Ala. N. F. Sohl and A. Karl, 1961. Ripley Formation.
Nostoceras alternatum (Tuomey)

USGS Mesozoic locality 28437. Right side of Chattahoochie River 0.5–0.7 mi below Tabannee Creek and 1.8 mi below the landing at Eufaula, in the SW¼NE¼ sec. 9, T. 10 N., R. 29 E., Quitman County, Ga. N. F. Sohl and R. L. Rieke, 1961.
Solenoceras sp.
Nostoceras alternatum (Tuomey)

USGS Mesozoic localities 27542, 28431. Left bank of Chattahoochie River about 2 mi below crossing of Central of Georgia Railroad, Quitman County, Ga. N. F. Sohl and S. C. Crosby, 1959; Sohl and R. L. Rieke, 1961. Ripley Formation.
Baculites cf. *B. undatus* Stephenson
Solenoceras nitidum Cobban
Nostoceras alternatum (Tuomey)

USGS Mesozoic locality 28438. Left bank of Chattahoochie River in Quitman County, Ga., 2.6–2.7 mi below the landing at Eufaula, Ala. N. F. Sohl and R. L. Rieke, 1961. Ripley Formation.
Nostoceras alternatum (Tuomey)

USGS Mesozoic locality 26014. Bluff on left bank of Chattahoochie River 2.8 mi below Eufaula landing, Quitman County, Ga. N. F. Sohl and H. I. Saunders, 1955. Ripley Formation.
Nostoceras alternatum (Tuomey)

USGS Mesozoic locality 25991. Bluff on left side of Chattahoochie River about 0.25 mi above the mouth of Barbour Creek, 4 mi south of Eufaula in Quitman County, Ga. N. F. Sohl and H. I. Saunders, 1955. Ripley Formation.
Nostoceras alternatum (Tuomey)

SYSTEMATIC DESCRIPTIONS

Phylum MOLLUSCA
Class CEPHALOPODA
Order AMMONOIDEA
Family NOSTOCERATIDAE Hyatt, 1894

Genus *SOLENOCERAS* Conrad, 1860

Type (by original designation).—Hamites annulifer Morton, 1842.

Conrad's (1860, p. 284) definition of *Solenoceras* was brief: "Differs from PTYCHOCERAS, *D'Orbigny*, in the smaller tube lying in a furrow, of the larger one, which is straight only for a short distance from the junction, and then suddenly recurved." He cited *Hamites annulifer* Morton (1841, p. 109; 1842, p. 213, pl. 11, fig. 4) as the type and recorded its presence in Tuomey's collection from Eufaula, Ala. The

holotype was said to have come from "the Ferruginous sand at the Deep-cut of the Chesapeake and Delaware canal" (Morton, 1842, p. 213). The deep cut is chiefly in the early Campanian Merchantville Formation (Pickett, 1970). Additional specimens of *S. annulifer* have not been reported from the deep cut since Conrad's original record. This species, however, does occur in the younger Mount Laurel Sand farther east along the canal. At the well-known Biggs farm fossil locality (Groot and others, 1954, p. 37; Richards and Shapiro, 1963; Owens and others, 1970, fig. 6, p. 16, 44) several examples of *S. annulifer* were found by Mrs. Eldon Homsey and Dr. W. A. Sheppard of Wilmington, Del. Other ammonoids in the Homsey-Sheppard collections from this locality include *Didymoceras cheyennense* (Meek and Hayden) and *Anaklinoceras reflexum* Stephenson which suggest that *S. annulifer* lies somewhere in the zone of *D. cheyennense* or in the zone of *Baculites compressus* Say in terms of the ammonoid sequence of the western interior region (Izett and others, 1971, table 1, p. A15). *Solenoceras annulifer* is much younger than the early Campanian age (Merchantville and Woodbury Formations) usually assigned to it (Richards, 1962, p. 227), and the record of the holotype from the deep cut of the Chesapeake and Delaware Canal is questionable.

Gabb (1861, p. 89–90) noted that the holotype of *S. annulifer* was not "suddenly recurved" at its larger end as indicated in Conrad's definition of the genus. Morton's (1841, p. 109) original description of the specimen was brief, but Whitfield (1892, p. 273, pl. 45, figs. 6–8) and Reeside (1962, p. 121, pl. 70, figs. 8–10) later described the specimen in detail. In summary the type consists of a complete body chamber 21 mm long that is nearly straight for most of its length and is sharply recurved into an elbow at its older end. Its dorsum has a pronounced concave impressed area where it grew over the venter of the more or less straight septate limb. Ribbing is dense and slightly rursiradiate. Each rib bears a very small bullate tubercle on each side of the venter; these tubercles are conspicuous on the elbow but become almost indiscernible on the shaft. A constriction is present on the middle of the straight limb and on the middle of the elbow. The impressed area on the dorsum reveals that at least two constrictions were present on the septate limb. Two high ribs bounding a constriction lie near the aperture.

Solenoceras nitidum Cobban, n. sp.

Figures 1*a–k*, 2

This species is about the size of the genotype from which it differs mainly by having a smaller impressed area or none at all on the body chamber and by lacking tubercles. The type lot consists of three complete or nearly complete body chambers (fig. 1*a–f*, *i–k*) and almost a dozen smaller fragments of body chambers and septate limbs from USGS Mesozoic locality 18078 near Pleasant Ridge, Union County, Miss.

The holotype (fig. 1*a–c*) is largely an internal mold of a body chamber that has part of the septate limb attached. Some shell material is preserved on the venter and flanks near the aperture. The specimen is 21 mm long, and the subcircular intercostal section at the larger end is 4.5 mm high and 4.8 mm wide. The internal mold of the septate limb does not touch the body chamber, but the original shelled limbs probably were in contact. A distinct impressed dorsal area is lacking on the body chamber (fig. 1*f*, *i*). Ribs, which are rounded and are narrower than the interspaces, are prorsiradiate on the septate limb and rectiradiate to slightly rursiradiate on the body chamber. The ribs are arched forward a little on the dorsum (fig. 1*f*) and very slightly so on the venter of some specimens (fig. 1*d*). The rib spacing index (whorl height ÷ distance between crests of two adjacent ribs) is 4 on the septate limb and 6 on the body chamber. The aperture is not preserved, but a nearly complete body chamber is indicated by the occurrence near the adoral end of a constriction followed by two high ribs separated by a very thin rib.

Two paratypes reveal the details of the apertural end. One has a high rib followed by two very weak ribs and then the slightly flared aperture (fig. 1*d*). The other has two high ribs bounding a constriction and then three weak ribs followed by the slightly flared aperture (fig. 1*k*).

The figured paratypes differ very little from the holotype, and the fragments of other specimens in the type lot suggest that *S. nitidum* does not vary much in the size of adults and in the nature of the ribbing. One specimen, however, shows a considerable gap between the limbs at the elbow (fig. 1*h*).

The suture is very simple (fig. 2). The lateral and umbilical lobes are symmetrically bifid and a little narrower than the siphonal lobe. The saddles are symmetrically bifid and about twice as wide as the lateral and umbilical lobes.

Solenoceras nitidum is easily separated from other species by its lack of tubercles. The nearest species is probably *S. minimus* (Basse, 1931, p. 17, pl. 1, figs. 20–22) from Madagascar which, however, has minute tubercles.

Types.—Holotype USNM 187711; paratypes USNM 187712–187714.

Genus *EXITELOCERAS* Hyatt, 1894

Type species.—*Ancyloceras jenneyi* Whitfield, 1877.

Exiteloceras includes heteromorph ammonoids loosely coiled in a plane. The early whorls may consist of straight limbs connected by semicircular elbows. The venter is flattened and is narrower than the dorsum. Ribs are narrow and numerous and usually terminate in a ventrolateral tubercle, but on some forms nontuberculated ribs may separate tuberculated ones. Opposite tubercles on the venter are connected by one or two low ribs.

Exiteloceras sp.

Figure 1*s–v*, 3

Two fragments of heteromorphs from Tippah County, Miss. (loc. 25411), may represent some species of *Exiteloceras*. One

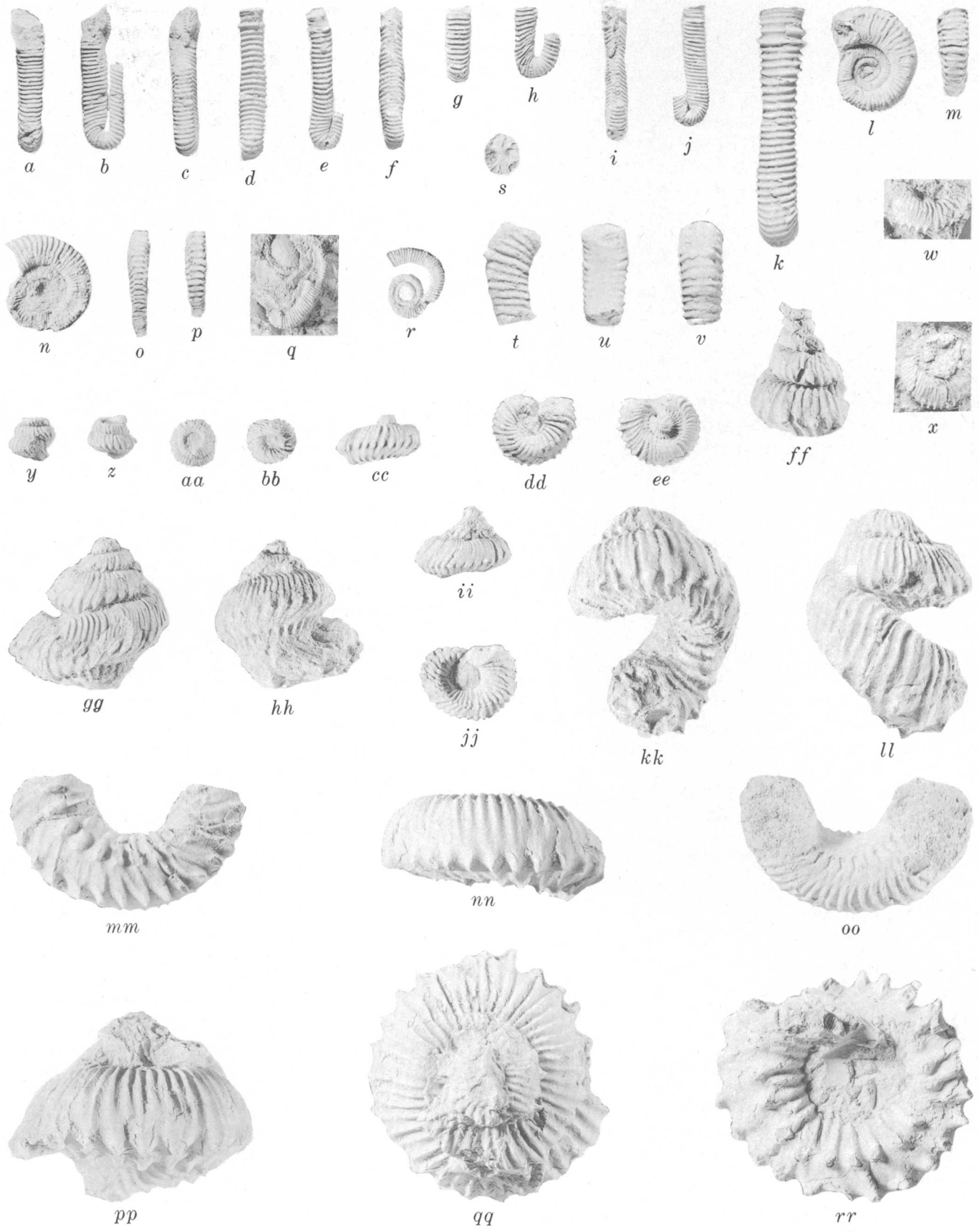
a
b
c
d
e
f
g
h
s
i
j
k
l
m
n
o
p
q
r
t
u
v
w
x
y
z
aa
bb
cc
dd
ee
ff
gg
hh
ii
jj
kk
ll
mm
nn
oo
pp
qq
rr

fragment consists of only the side of a curved limb. The other and better preserved fragment, 19 mm long, is part of a curved limb retaining some shell material. Its cross section is a little higher than wide; the dorsum is broader than the venter which is slightly flattened, and the flanks are broadly rounded. Ribs are narrowly rounded, prorsiradiate, weakest on the dorsum, and strongest on the upper part of the flank where their spacing index is 5. Every other rib terminates in a tubercle that is flat topped on the internal mold, but where some shell material is preserved, a sharp spine is present. Tubercles on opposite sides of the venter are connected by two low ribs. The suture (fig. 3) resembles that of the type of the genus, *Exiteloceras jenneyi* (Whitfield, 1880, pl. 16, fig. 9).

Type.—Figured specimen USNM 187715.

Genus *AXONOCERAS* Stephenson, 1941

Type species.—*Axonoceras compressum* Stephenson, 1941.

Stephenson (1941, p. 422) proposed this genus for "long slender shells coiled in one plane, with numerous closely spaced ribs and two rows of ventral nodes. * * * The shells may be closely coiled, though not involute, but most of them are more or less loosely and irregularly coiled." The genus seems to be also characterized by its small size and by the presence of constrictions. *Axonoceras* has been recorded previously only from Texas (Stephenson, 1941, p. 422–425), Colorado (Izett and others, 1971, p. A7), and Angola (Haas, 1943, p. 7–10; Antunes and Sornay, 1969, p. 88)

Axonoceras sohli Cobban, n. sp.

Figures 1*l*–*p*, 4

This species is characterized by its flattened flanks and venter and by the presence of tubercles on every rib on the body chamber as well as on each rib of at least the last septate whorl. The innermost whorls have not been observed. Whorl sections are higher than wide and decidedly rectangular. Ribs are numerous, rectiradiate to rursiradiate, and, on the body chamber, slightly flexuous. They are spaced along the venter of the body chamber at 5 to 6 for the whorl height.

The holotype (fig. 1*l*, *m*) is a somewhat distorted adult 19.6 mm in diameter that has parts of the shell material preserved. The last quarter whorl consists of body chamber and possibly represents half of it. Two and a half septate whorls are preserved, and although they are crushed and distorted, they appear to have been slightly helical. Ribs on these whorls are rounded, a little narrower than the interspaces, and number four for the whorl height. Five constrictions are present on the last half septate whorl, and most constrictions are bounded on their adapical side by a high rib. Ribbing is slightly denser on the portion of body chamber preserved, and two constrictions are visible. Ventrolateral tubercles are small and pointed.

A complete suture was not observed. Much of the suture is visible on the holotype where it consists of a moderately incised pattern characterized by squarish lobes and rectangular saddles (fig. 4). The lateral and umbilical lobes are about equal in size and a little narrower than the siphonal lobe. The first two saddles are wider than the external lobe and are symmetrically bifid.

Axonoceras sohli is an uncommon species; only six specimens can be assigned to it with certainty. This species readily differs from the genotype *A. compressum* (Stephenson, 1941,

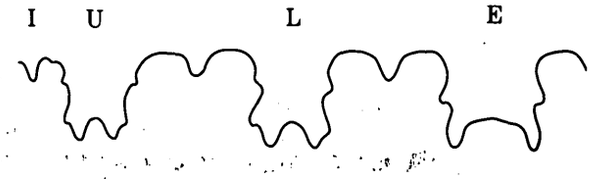

Figure 2.—Suture, X 12, of the holotype of *Solenoceras nitidum* n. sp., USNM 187711. Lobes are external (E), lateral (L), umbilical (U), and internal (I).

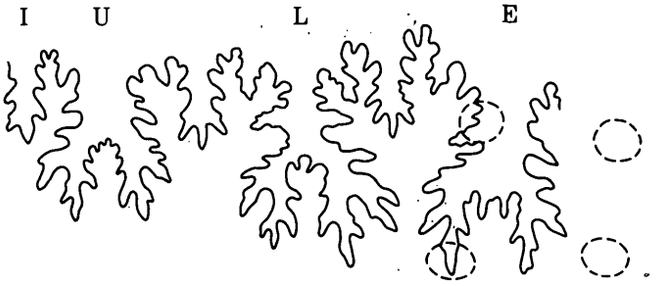

Figure 3.—Suture, X 6, of *Exiteloceras* sp. Figured specimen USNM 187715. Lobes are external (E), lateral (L), umbilical (U), and internal (I).

Figure 1.—Ammonites from the Ripley Formation, all natural size except figure 1*k*.

a–*k*. *Solenoceras nitidum* Cobban, n. sp., from locality 18078. *a*–*c*, holotype USNM 187711; *d*–*f*, paratype USNM 187712; *g*, *h*, paratype USNM 187713; *i*–*k*, paratype USNM 187714 (*k* is enlarged X 2 to show details of ribbing near aperture).

l–*p*. *Axonoceras sohli* Cobban, n. sp., *l*, *m*, holotype USNM 187716 from locality 18078; *n*–*p*, paratype USNM 187717 from locality 708.

q–*r*. *Axonoceras* sp. *q*, figured specimen USNM 187718 from locality 708; *r*, figured specimen USNM 187719 from locality 18078.

s–*v*. *Exiteloceras* sp. from locality 25411, figured specimen USNM 187715.

w–*rr*. *Nostoceras alternatum* (Tuomey). *w*, hypotype USNM 187729 from locality 27542; *x*, hypotype USNM 187730 from locality 26014; *y*–*bb*, hypotype USNM 187720 from locality 18078; *cc*–*ee*, hypotype USNM 187725 from locality 25411; *ff*, hypotype USNM 187721 from locality 18078; *gg*, *hh*, hypotype USNM 187722 from locality 18078; *ii*, *jj*, hypotype USNM 187723 from locality 18078; *kk*, *ll*, hypotype USNM 187728 from locality 708; *mm*–*oo*, hypotype USNM 187727 from locality 18629; *pp*–*rr*, hypotype USNM 187724 from locality 25411.

p. 422, pl. 89, figs. 1–5) by having flatter flanks and venter and by having tubercles on every rib. *A. angolanum* (Haas, 1943, p. 8, text figs. 3, 10–13) from Angola also has more inflated flanks and rounded venter as well as a more incised suture with narrower lobes and saddles.

The species is named for Norman F. Sohl in recognition of his important contributions to the paleontology and stratigraphy of the Ripley Formation.

Types.—Holotype USNM 187716, paratype USNM 187717.

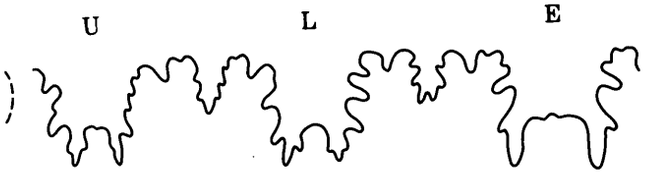

Figure 4.—Most of the suture, × 15, of the holotype of *Axonoceras sohli* n. sp., USNM 187716. Visible lobes are external (E), lateral (L), and umbilical (U).

Axonoceras? sp.

Figure 1*q*, *r*

Two small heteromorphs from Tippah County, Miss. (locs. 708, 18078), are loosely and irregularly coiled in a plane. Inasmuch as some individuals of *Axonoceras* are irregularly coiled (Haas, 1943, figs. 10a, b, 11a), the Ripley specimens could be interpreted as aberrant forms of the genus.

The more complete of the two specimens consists of two whorls in contact followed by half of an arcuate whorl considerably removed from the other whorls (fig. 1*r*). The half whorl, part of a body chamber, has a cross section higher than wide with somewhat flattened flanks and rounded venter. Its rib index along the venter is 5. A few inconspicous constrictions are present, and one is bounded on its adapical side by a high thickened rib. Tubercles are absent which, combined with the irregular coiling, suggest that the specimen represents a different species than *A. sohli*. The other specimen, part of an asymmetrically curved limb, also lacks tubercles (fig. 1*q*). The irregular planospiral coiling of these specimens recalls that of *Exicrioceras diabloense* Anderson (1958, p. 208, pl. 72, figs. 1–3) from the upper Campanian or Maestrichtian of California.

Types.—Figured specimens USNM 187718, 187719.

Genus *NOSTOCERAS* Hyatt, 1894

Type species.—*Nostoceras stantoni* Hyatt, 1894.

Ammonoids assigned to this genus have a tight spire of several septate whorls and a body chamber that bends away from the spire or, in some species, bends downward away from the spire and then curves back toward it forming a U-shape. Ribbing is usually dense, and constrictions are present on the spire. Two rows of tubercles are ordinarily present.

Nostoceras alternatum (Tuomey)

Figures 1*w*–*rr*, 5

1854. *Turrulites alternatns* [sic] Tuomey, Acad. Nat. Sci. Philadelphia Proc., v. 7, no. 5, p. 168.
1860. *Turrilites spinifera* Conrad, Acad. Nat. Sci. Philadephia Jour., 2d ser., v. 4, p. 284.
1861. *Turrilites alternatus* Tuomey. Gabb, Am. Philos. Soc. Proc., v. 8, p. 91.
1861. *Turrilites spinifera* Tuomey. Gabb, Am. Philos. Soc. Proc., v. 8, p. 92.

Tuomey (1854, p. 168) described this species as *Turrulites* [*Turrilites*] *alternatns* [*alternatus*]. His description was brief: "Shell turreted, spire dextral; whorls angulated, lower side ornamented by two tuberculated carinae, transversely plaited; plaits double the number of tubercles, alternately terminating in a tubercle." The specimen, which was not illustrated, was said to have come from Noxubee County, Miss. The whereabouts of the holotype is unknown; it was not listed among the types at the Academy of Natural Sciences of Philadelphia (Johnson, 1905).

Six years after the publication of Tuomey's paper, Conrad (1860, p. 284) described as a new species, *Turrilites spinifera*, an ammonoid that was apparently the same species as that of Tuomey. Conrad's description was also brief: "Sinistral, conical; ribs numerous, rounded, alternately ending in a sharp spine; on the angle of the body whirl the spines are erect, those on the spire projecting very obliquely over the contiguous whirl; umbilicus wide, profound, longitudinally ribbed within. Length 1¾ inches. Diameter the same nearly." Conrad gave Eufaula, Ala., and Tippah County, Miss., as localities without stating which produced the holotype. The type specimen was never illustrated, and it may be lost.

Ammonoids like those described by Tuomey and Conrad are present in many of the U.S. Geological Survey's collections from the Ripley Formation. The largest collection, from near Pleasant Ridge, Tippah County, Miss. (locs. 18078, 18629, 25411), contains 34 specimens and fragments of which 21 are sinistral and 13 are dextral. These specimens reveal the general characteristics of the species—a tight spire of about four whorls followed by a slight uncoiling of the younger part of the body chamber; numerous ribs; and the two rows of tubercles occupying a basal position on the whorls (fig. 5).

The earliest whorls are not preserved in any of the collections. The smallest whorl observed (fig. 1*ff*) is rather loosely wound and lacks an impressed area suggesting that the earliest whorls may have formed a loose helicoid spire. The four whorls following the loosely coiled one are tightly wound, and a conspicuous impressed area is present on each. Spire angles of *N. alternatum* range from 45° to 90°. An unusually long body chamber is present occupying 1¼ to almost 1½ whorls of which the first complete whorl is part of the tightly wound spire. The younger part of the body chamber pulls away from the spire at angles ranging from 15°

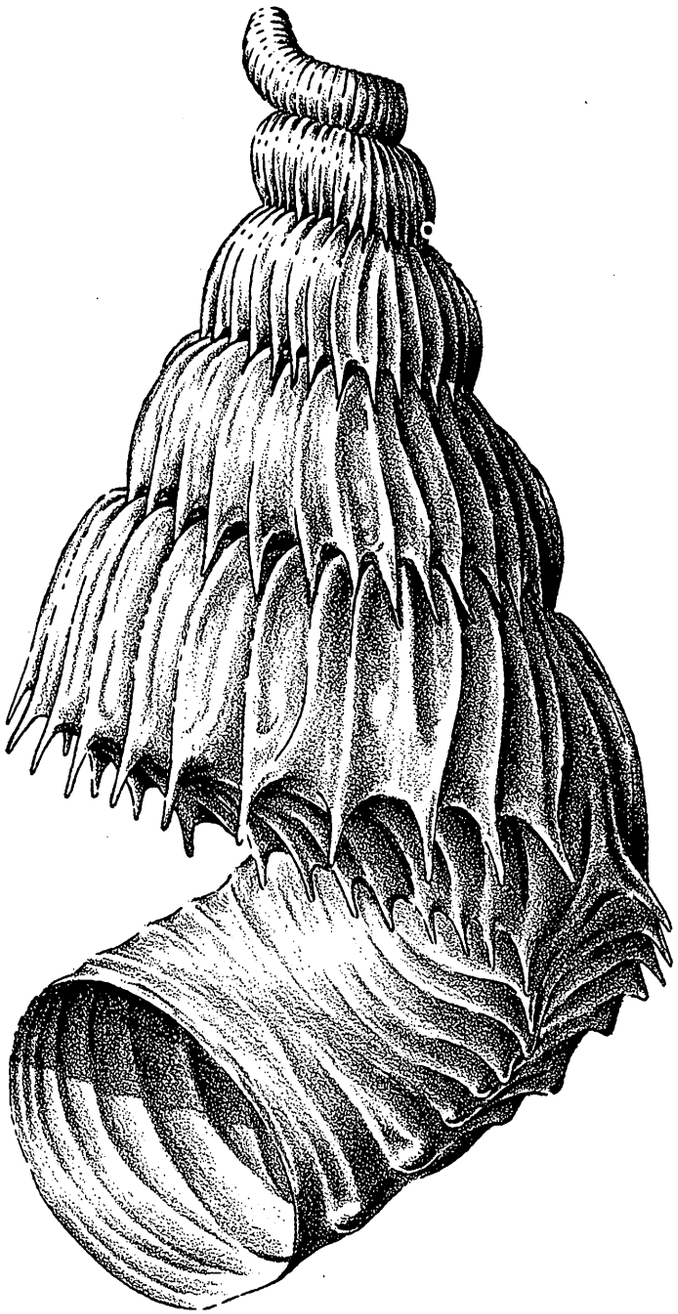

Figure 5.—Restoration of *Nostoceras alternatum*, × 4, based on the specimens shown in figure 1*w–rr*. Drawing by John R. Stacy, of the U.S. Geological Survey.

(fig. 1*gg*) to 30° (fig. 1*ll*). A complete mouth border is not preserved on any of the specimens.

Ribs are conspicuous, narrowly rounded, and not as broad as the interspaces. They are strongest at the top of the whorl where they number 40 to 50 per whorl. Each pair of ribs usually terminates in a sharp tubercle at the base of the whorl (fig. 1*nn*). From each tubercle a low rib may obliquely cross the base of the whorl and terminate in a sharp umbilical tubercle (fig. 1*rr*) or two ribs may extend from an outer tubercle and connect to two adjacent umbilical tubercles in a zigzag manner (fig. 1*mm*). One or two ribs extend from each umbilical tubercle into the umbilicus. Well-preserved specimens reveal that both rows of tubercles supported spines (fig. 1*w*, *x*, *hh*).

Adult specimens show a considerable range in size. The smallest adult (fig. 1*gg*) is about one-half as large as the largest specimen (fig. 1*pp*).

The suture (fig. 6) is not as incised as those of other species of *Nostoceras* such as the one illustrated from Angola by Haas (1943, fig. 1) and Howarth (1965, figs. 16, 17) and the one from New Jersey figured by Whitfield (1892, pl. 45, fig. 5). As in other species of helical ammonoids, the external lobe is considerably offset from the position of the siphuncle.

Figure 6.—Part of the suture, × 5, of *Nostoceras alternatum* (Tuomey) from locality 25411. Hypotype USNM 187726. Visible lobes are external (E), lateral (L), and umbilical (U).

Nostoceras alternatum is easily distinguished from most species of the genus by the low position of its tubercles. A closely related form is the species described by Favre (1869, p. 30, pl. 7, figs. 5a–c) from France as *Helicoceras schloenbachi*. Many different heteromorphs have been referred to the French species, but certain specimens resemble *N. alternatum*. Among these is a whorl from Poland figured as *Heteroceras polyplocum* Roemer var. *schloenbachi* Favre by Nowak (1914, p. 386, pl. 41, fig. 14) which has the tubercles low on the flank and a distinct angularity developed at the position of the upper row. Except by having fewer ribs, the Polish specimen resembles some whorls from the Ripley Formation such as those shown in figure 1*cc*. Several specimens from Madagascar illustrated by Basse (1931, p. 19, pl. 2, figs. 11–15) as *Turrilites* (*Bostrychoceras*) *schloenbachi* (Favre) resemble *N. alternatum* by their dense ribbing and presence of constrictions, but their tubercles are higher on the flank.

Another closely related species is *Nostoceras obtusum* Howarth (1965, p. 384, pl. 10, fig. 2, text fig. 17) from Angola which has the tubercles on the base of the whorls. The African species differs from *N. alternatum* chiefly by its very low spire and wide umbilicus.

Types.—Hypotypes USNM 187720–187730.

REFERENCES CITED

Anderson, F. M., 1958, Upper Cretaceous of the Pacific coast: Geol. Soc. America Mem. 71, 378 p., 75 pls.

Antunes, Telles, and Sornay, Jacques, 1969, Contributions à la connaissance du Crétacé supérieur de Barra do Dande, Angola: Lisboa Univ. Fac. Ciênc. Rev., 2d ser. C, v. 16, pt. 1, p. 65–104, 10 pls.

Basse, Éliane, 1931, Monographie paléontologique du Crétacé de la Province de Maintirano, Madagascar: Service Mines, Govt. Gén. Madagascar et Dépendances, 86 p., 13 pls.

Conant, L. C., 1942, Union County mineral resources; Geology by Louis Cowels Conant, Tests by Thomas Edwin McCutcheon: Mississippi Geol. Survey Bull. 45, 158 p., illus.

Conrad, T. A., 1860, Descriptions of new species of Cretaceous and Eocene fossils of Mississippi and Alabama: Acad. Nat. Sci. Philadelphia Jour., 2d ser., v. 4, p. 275–298, pls. 46, 47.

Cooke, C. W., 1943, Geology of the Coastal Plain of Georgia: U.S. Geol. Survey Bull. 941, 121 p., illus. [1944].

Crider, A. F., 1906, Geology and mineral resources of Mississippi: U.S. Geol. Survey Bull. 283, 99 p., illus.

Eargle, D. H., 1955, Stratigraphy of the outcropping Cretaceous rocks of Georgia: U.S. Geol. Survey Bull. 1014, 101 p., illus.

Favre, Ernest, 1869, Description des mollusques fossiles de la craie des environs de Lemberg en Galicie: Paris, Genève et Bale, 187 p., 13 pls.

Gabb, W. M., 1861, Synopsis of the Mollusca of the Cretaceous formation, including the geographical and stratigraphical range and synonymy: Am. Philos. Soc. Proc., v. 8, p. 57–257.

Groot, J. J., Organist, D. M., and Richards, H. G., 1954, Marine Upper Cretaceous formations of the Chesapeake and Delaware Canal: Delaware Geol. Survey Bull. 3, 62 p., 7 pls.

Haas, Otto, 1943, Some abnormally coiled ammonities from the Upper Cretaceous of Angola: Am. Mus. Novitates 1222, 17 p., 1 pl.

Harbison, Anne, 1945, Upper Cretaceous mollusks of the lower Ripley formation near Dumas, Mississippi: Acad. Nat. Sci. Philadelphia Proc., v. 97, p. 75–92, 6 pls.

Hilgard, E. W., 1860, Report on the geology and agriculture of the State of Mississippi: Jackson, Miss., E. Barksdale, 391 p., illus.

Howarth, M. K., 1965, Cretaceous ammonites and nautiloids from Angola: British Mus. (Nat. History) Bull., Geology, v. 10, no. 10, p. 335–412, 13 pls.

Izett, G. A., Cobban, W. A., and Gill, J. R., 1971, The Pierre Shale near Kremmling, Colorado, and its correlation to the east and west: U.S. Geol. Survey Prof. Paper 684-A, 19 p., illus.

Johnson, C. W., 1905, Annotated list of the types of invertebrate Cretaceous fossils in the collection of the Academy of Natural Sciences, Philadelphia: Acad. Nat. Sci. Philadelphia Proc., v. 57, p. 4–28.

Morton, S. G., 1841, Description of several new species of fossil shells from the Cretaceous deposits of the United States: Acad. Nat. Sci. Philadelphia Proc., v. 1, p. 106–110.

——1842, Description of some new species of organic remains of the Cretaceous group of the United States, with a tabular view of the fossils hitherto discovered in this formation: Acad. Nat. Sci. Philadelphia Jour., v. 8, p. 207–227, pls. 10, 11.

Nowak, Jan, 1914, Untersuchungen über die Cephalopoden der oberen Kreide in Polen, Pt. 3: Acad. Sci. Cracovie Bull. Internat., 1913, ser. B, p. 335–413, pls. 40–44.

Owens, J. P., Minard, J. P., Sohl, N. F., and Mello, J. F., 1970, Stratigraphy of the outcropping post-Magothy Upper Cretaceous formations in southern New Jersey and northern Delmarva Peninsula, Delaware and Maryland: U.S. Geol. Survey Prof. Paper 674, 60 p., illus.

Pickett, T. E., 1970, Geology of the Chesapeake and Delaware Canal area, Delaware: Delaware Geol. Survey Geologic Map Ser. 1.

Reeside, J. B., Jr., 1962, Cretaceous ammonites of New Jersey, *in* The Cretaceous fossils of New Jersey, Pt. 2: New Jersey Bur. Geology and Topography Bull. 61 [pt. 2], p. 113–137, pls. 68–75.

Richards, H. G., 1962, Table showing distribution by formations of Cretaceous invertebrate fossils of New Jersey, App. D *in* The Cretaceous fossils of New Jersey, Pt. 2: New Jersey Bur. Geology and Topography Bull. 61 [pt. 2], p. 209–229.

Richards, H. G., and Shapiro, Earl, 1963, An invertebrate macrofauna from the Upper Cretaceous of Delaware: Delaware Geol. Survey Rept. Inv. 7, 37 p., 4 pls.

Sohl, N. F., 1960, Archeogastropoda, Mesogastropoda, and stratigraphy of the Ripley, Owl Creek, and Prairie Bluff formations: U.S. Geol. Survey Prof. Paper 331-A, 151 p., pls. 1–18.

——1964, Neogastropoda, Opisthobranchia, and Basommatophora from the Ripley, Owl Creek, and Prairie Bluff Formations—Late Cretaceous gastropods in Tennessee and Mississippi: U.S. Geol. Survey Prof. Paper 331-B, p. 153–344, pls. 19–52.

Stephenson, L. W., 1911, Cretaceous, *in* Veatch, Otto, and Stephenson, L. W., Preliminary report on the geology of the coastal plain of Georgia: Georgia Geol. Survey Bull. 26, p. 66–215, illus.

——1914, Cretaceous deposits of the eastern Gulf region and species of *Exogyra* from the eastern Gulf region and the Carolinas: U.S. Geol. Survey Prof. Paper 81, 77 p., 21 pls.

——1941, The larger invertebrate fossils of the Navarro group of Texas: Texas Univ. Bull. 4101, 641 p., 95 pls.

Stephenson, L. W., and Monroe, W. H., 1940, The Upper Cretaceous deposits [Mississippi]: Mississippi Geol. Survey Bull. 40, 296 p., illus.

Tuomey, Michael, 1854, Description of some new fossils from the Cretaceous rocks of the Southern States: Acad. Nat. Sci. Philadelphia Proc., v. 7, no. 5, p. 167–172.

Whitfield, R. P., 1880, Paleontology of the Black Hills of Dakota, *in* Newton, Henry, and Jenney, W. P., Report on the geology and resources of the Black Hills of Dakota: U.S. Geog. and Geol. Survey Rocky Mtn. Region (Powell), p. 325–468, 16 pls.

——1892, Gasteropoda and Cephalopoda of the Raritan clays and greensand marls of New Jersey: U.S. Geol. Survey Mon. 18, 402 p., 50 pls.

Jour. Research U.S. Geol. Survey
Vol. 2, No. 1, Jan.-Feb. 1974, p. 89–95

STRATIGRAPHIC SECTION OF THE WOOD RIVER FORMATION, BLAINE COUNTY, IDAHO

By W. E. HALL, JOHN BATCHELDER; AND R. C. DOUGLASS,
Menlo Park, Calif.; Washington, D.C.

Abstract.—The Wood River Formation is subdivided into seven units that have a total stratigraphic thickness of approximately 2,987 m (9,800 ft). The formation is restricted to a basal conglomerate and overlying thick sequence of calcareous sandstones and quartzites. An overlying sequence of noncalcareous siltstones, shales, and siltites originally included in the formation is separated as a new formation, and the top of the Wood River Formation is thus delimited for the first time. Units 1, 2, and 3 of the Wood River Formation are Middle Pennsylvanian (Des Moinesian) in age; units 4, 5, and the lower part of 6 are of late Pennsylvanian (Virgilian) age; the upper part of unit 6 and all of unit 7 are Early Permian (Wolfcampian) in age.

The Wood River Formation was named by Lindgren (1900, p. 89) for a series of argillites, sandstones, limestones, and conglomerates of late Paleozoic age in the vicinity of Big Wood River in the vicinity of Ketchum and Hailey, south-central Idaho. The formation was subsequently restricted to rocks in the upper part of the sequence that are of Pennsylvanian and Permian age; the lower part of the sequence, comprising argillites and thin micritic limestone beds, was named the Milligen Formation (Umpleby and others, 1930; Bostwick, 1955, p. 941; Ross, 1960, p. B232).

The Wood River Formation crops out across the northern part of the Bellevue quadrangle and underlies large areas of the Hailey 30-minute quadrangle between Hailey and the North Fork of the Big Lost River (Umpleby and others, 1930, pl. 1). During the mapping of the Bellevue 15-minute and Baugh Creek SW 7½ minute quadrangles (fig. 1), we subdivided the Wood River Formation into seven stratigraphic units, described herein, and defined the top of the formation.

The mapping, measuring of sections, and collecting of samples were done by Hall and Batchelder. The age determinations and fossil identifications, where not otherwise credited, were made by Douglass.

Early measured sections of the Wood River Formation indicate a thickness of 2,350–3,650 m (7,700–12,000 ft). This large range results in part from the lack of any one section of the formation being complete and the fact that all measurements are summations of partial sections. Umpleby, Westgate, and Ross (1930, p. 29) pieced together several partial sections

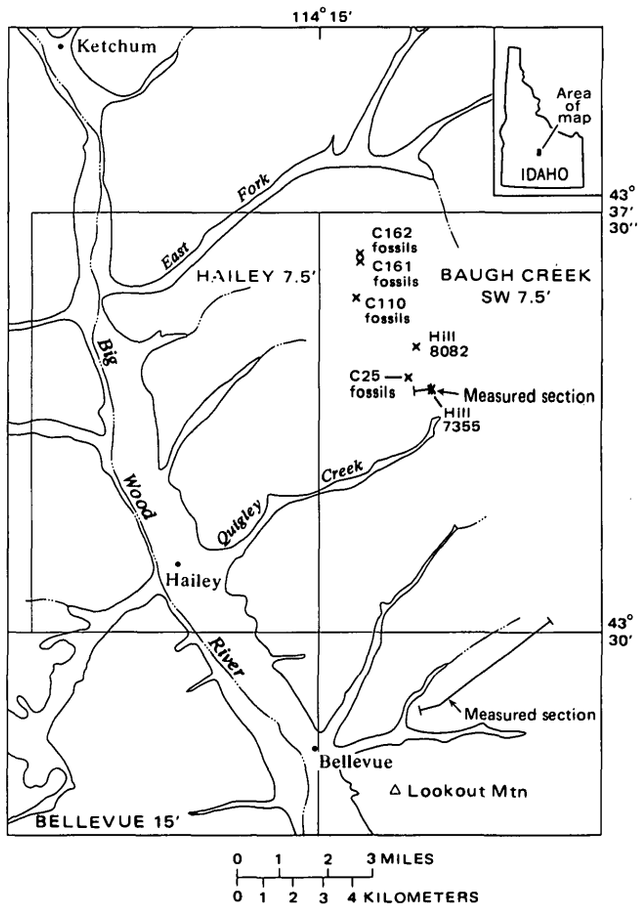

Figure 1.—Location of measured sections in Big Wood River area, south-central Idaho.

of the Wood River Formation that gave a minimum thickness of 2,350 m. Bostwick (1955) measured a section 3,650 m thick along the ridge 4.3 km (2.7 mi) east of Bellevue on the north side of the Bellevue-Muldoon road. Neither of these papers describes the lithology of the Wood River Formation in detail. Thomasson (1959b, p. 52) reported the minimum thickness of the Wood River Formation in the Trail Creek area

east of Ketchum to be 2,636 m (8,647 ft) and subdivided the formation into four members.

THICKNESS AND STRATIGRAPHIC RELATIONS

We measured a partial section of Wood River Formation east of Bellevue in the same general area as Umpleby (1917) and Bostwick (1955) and a partial section of the upper part of the formation in the Quigley Creek drainage for a combined thickness of 2,983 m (9,788 ft). This thickness is considerably less than measured by Bostwick because we corrected for a faulted anticline that repeats part of the section. The upper part of the section east of Bellevue is very poorly exposed; consequently, the upper 762 m (2,500 ft) of unit 6 is our best approximation of its thickness, although unexposed structural complications could make this figure considerably in error. Unit 7 was measured in the Quigley Creek drainage.

At most places the contact between the Wood River and underlying Milligen Formation is a regional thrust fault. The thrust fault is poorly exposed but is delineated by fracture cleavage in competent layers above the thrust, by discontinuities in structure on opposite sides of the thrust, by boudins of sheared chert conglomerate, by drag folds in cherty and siliceous argillite beds below the thrust, and by seepages and springs in the thrust zone.

The upper contact of the Wood River Formation is defined in this paper as the top of unit 7, which is overlain conformably by a thick sequence of noncalcareous siltstones, siltites, and mudstones of unknown age. This contact is best exposed in the measured section of unit 7 at an altitude of 2,225 m (7,300 ft) in the southwest quarter of sec. 16, T. 3 N., R. 19 E., in the Baugh Creek SW quadrangle. The overlying noncalcareous siltstone sequence is exposed southeast of this contact on hill 7355 and on hill 8082. This siltstone sequence was included in the Wood River Formation by Umpleby, Westgate, and Ross (1930, pl. I). We herein restrict the Wood River Formation to the sequence of calcareous siltstones, limestones, and limy quartzites of Pennsylvanian and Early Permian age. The sequence of noncalcareous siltstones, siltites, and mudstones is so lithologically distinctive from the Wood River Formation that we consider it a separate formation, which we shall name in a later paper.

LITHOLOGY

The Wood River Formation is composed predominantly of fine-grained calcareous sandstones and quartzites but includes conglomerate, limestone, shaly limestone, siltite, and argillite. The formation is divided into seven units that have been recognized over the extent of the Wood River valley. Six of the units are exposed in the area east of Bellevue. Unit 7, the uppermost unit, is exposed in the western part of the Baugh Creek SW quadrangle (fig. 1).

Hailey Conglomerate Member (unit 1)

The basal unit of the Wood River Formation was named the Hailey Conglomerate Member by Thomasson (1959b, p. 52; 1959a) for its type section, a sequence of chert pebble conglomerates exposed at the west end of the bridge over the Big Wood River at Hailey. The basal conglomerate forms a distinctive horizon marker that generally stands in bold relief from the underlying and overlying less competent rocks. It is well exposed at the type section at Hailey, on the hills east of Bellevue, and on the east side of the Big Wood River valley between Hailey and Bellevue. The conglomerate consists of interbedded conglomerate, quartzite, and brown silty and sandy limestone. The conglomerate and quartzite are thick bedded or massive; the limestone is thin bedded and commonly displays penecontemporaneous deformation.

The Hailey Conglomerate Member is about 122 m (400 ft) thick in the measured section on the ridge 4.3 km (2.7 mi) east of Bellevue at an altitude of 1,948 m (6,390 ft). Thomasson (1959b, p. 53) measured a thickness of 300 m (986 ft) at the type locality. The conglomerate in many places has a lenticular distribution or locally may be separated into two or more parts as a result of its being the sole of a major thrust fault along which the conglomerate was strongly sheared, disrupted, and dragged out.

The following section of the Hailey Conglomerate Member was measured along the ridge 4.3 km (2.7 mi) N. 75°E. of Bellevue at an altitude of 1,948 m (6,390 ft):

Unit 2. Conformable contact.	*Feet*
Hailey Conglomerate Member (unit 1):	
Chert pebble conglomerate, light-gray, siliceous cement	5
Limestone, brown, fine-grained, algal; and chert pebble conglomerate beds 1–2 ft thick	41
Chert pebble conglomerate, siliceous cement	1
Limestone, brown, fine-grained, algal, with 10 percent fine-grained quartzite beds ½–1 in. thick	53
Chert pebble conglomerate, light-gray and brownish-gray, siliceous cement. Subrounded clasts. Near top several percent rounded brown limestone clasts as much as 8 in. long and 2 in. wide. Few light to medium-gray quartzite clasts	210
Limestone, micritic, brown, silty, in part silicified	2
Chert pebble conglomerate, light-gray, chalcedonic matrix	12
Limestone, brown, fine-grained, sandy	5
Chert pebble conglomerate, siliceous matrix, chert and quartzite clasts; and quartzite, light-green, fine-grained, thick-bedded	55
Limestone, sandy, brown	1
Chert pebble conglomerate, light-gray, thick-bedded, siliceous cement, a few well-rounded light-brown limestone and white quartzite clasts. Chert pebbles 3/8 to 1 in. long, ratio minor to major axis about 1:2. Clasts subrounded. Color of clasts, light and dark gray	10
	395
	(120m)

Disconformable contact.

Milligen Formation.

Age.—The Hailey Conglomerate Member is Middle Pennsylvanian (Des Moinesian) in age (table 1). On the age of the Hailey Conglomerate Member, Betty Skipp (written commun., 1971) reports:

> Limestone interbedded in the upper part of the Hailey Conglomerate Member contains abundant phylloid (leaf-like) green algae. All of the fragments are recrystallized and the genera are indeterminate, but most are codiacean and a few are dasycladacean algae. Red algae are either absent or very rare. Phylloid algal limestone is a distinctive Permo-Pennsylvanian facies in the United States (Wray, 1968). The fact that the forms are mostly green algae, rather than red, and that the principal genera of phylloid green algae first occur in rocks of Atokan age and are common in rocks of Des Moinesian age (Wray, 1968) suggests that the Hailey Conglomerate is no older than Middle Pennsylvanian (Des Moinesian or possibly Atokan).

The Hailey Conglomerate Member is overlain by limestone of Des Moinesian age and is therefore no younger than Des Moinesian.

Bostwich (1955, p. 944–945) reported *Wedekindellina euthysepta* (Henbest) and *Fusulina* sp. (now known as *Beedeina)* from the brown limestone near the top of the unit, which he stated indicates an early Des Moinesian age.

Unit 2

Unit 2 consists of medium- to thick-bedded bluish-gray and white fine-grained limestone that locally contains abundant crinoidal debris, bryozoa, and brachiopod fragments. The limestone contains 5–10 percent detrital quartz grains 0.02–0.08 mm in diameter and a small amount of sericite and tremolite. This unit overlying the Hailey Conglomerate Member forms the best horizon marker in the Wood River Formation. Unit 2 is 15 m (49 ft) thick in the measured section 4.3 km (2.7 mi) east of Bellevue. Hewett (in Umpleby and others, 1930, p. 211) measured 14.3 m (47 ft) of limestone above the basal conglomerate.

Age.—Unit 2 is Middle Pennsylvanian (Des Moinesian) in age (table 1). W. J. Sando, J. T. Dutro, Jr., and Douglass (written commun., 1971) report:

> The megafossils in all collections from unit 2 are forms that have a possible age-range of Pennsylvanian to Permian. A single fusulinid found in USGS 24323-PC has an important bearing on the age of the unit because it occurs only 10 feet above the base. Douglass reports that this specimen is a *Beedeina* of Des Moines (Middle Pennsylvanian) age. (table 1.)

> In an effort to confirm a Middle Pennsylvanian age for the unit 2 limestone, Dutro and Sando examined the fossils identified by Girty and listed in USGS Bull. 814 (p. 33–34). In this report, the fossils listed by Girty as Group 3 were said to be from a sandy limestone unit immediately above the basal conglomerate of the Wood River Formation. Presumably Girty's Group 4 fossils are from the same level, a surmise supported by notes in our files pertaining to these collections. Among these old collections, USGS numbers 2992-PC, 3002-PC, 3003-PC, 3004-PC contain large suites of brachiopods that proved critical for age determination. Dutro identified *Mesolobus, Chonetina, Linoproductus, Antiguatonia, Anthracospirifer, Neospirifer, Hustedia, Reticulariina,* and *Schizophoria* in these collections and concluded that they represent a Middle Pennsylvanian assemblage.
>
> The weight of evidence definitely favors a Middle Pennsylvanian (probably Des Moines) age for unit 2.

Betty Skipp (written commun., 1970) reports on a collection from the limestone from 3 m (10 ft) above the basal conglomerate in the measured section:

> Small calcareous Foraminifera exclusive of the fusulines:
> *Endothyra* sp., neoarchaediscid
> *Tetrataxis* sp.
> Algae: *Komia?*
> *Lithostroma*
> Age: Des Moinesian. May be early Des Moinesian.

Unit 3

Unit 3 consists of thin-bedded pink and gray shaly limestone and thick-bedded bluish-gray limestone. This unit is generally poorly exposed and is distinguished by abundant pink shaly limestone float. The following section was measured along the ridge 4.8 km (3 mi) N. 73° E. of Bellevue at an altitude of 1,989 m (6,525 ft):

Unit 4.

Conformable contact.

Unit 3:	Feet
Limestone, purple, brownish-gray, silty	137
No exposure	22
Limestone float, pink, purplish-gray, brownish-gray, silty and shaly.	130
Limestone, pink, gray, brownish-gray, silty, some worm tracks.	91
Limestone, pink, gray, brownish-gray, shaly	180
Limestone, pink, shaly.	64
Limestone, bluish-gray, thick-bedded	16
Float limestone, pink, bluish-gray, light-brown, shaly	71
	711
	(217m)

Base not exposed.

Age.—Unit 3 consists predominantly of sandy and silty calcilutite and calcirudite. The calcilutite is nearly barren of microfossils or macrofossils. Thin beds of coarse-grained sandy calcirudite interbedded 61 m (200 ft) below the top of the unit contain abundant crinoidal, algal, and foraminiferal material in a recrystallized lime-mud matrix and in lithic fragments. The fusulinid *Beedeina* is present, indicating a Middle Pennsylvanian (Des Moinesian) age (table 1). Betty Skipp (written commun., 1972) recognized *Tetrataxis* sp. of the group *T. conica*, *Endothyra* sp., *Globivalulina* sp., a paleotextularid, and green algae.

The lower three units of the Wood River Formation are therefore of Middle Pennsylvanian (Des Moinesian) age (table 1).

Table 1.—*Distribution of fusulinids, Wood River Formation*

System	Pennsylvanian														Permian					
Series	Middle			Upper											Lower					
Provincial series	Des Moinesian			Virgilian											Wolfcampian		Leonardian (?)			
Formation	Wood River																			
Unit	Hailey Cgl. Mbr.	2	3	4		5	6								7					
Collection sample	Bostwick	A235A	A706-12-4	A239	A240	A997	A706-17	A706-22	A706-26	A706-27	A706-28	A706-29	A439A	A583	A566	A741	C161	C162	C25	C110
Wedekindeilina euthysepca (Henbest).	X	...	...	...	...	...	...	...	...	...	...	...	...	...	...	...	...	...	...	...
Beedeina sp.	X	X	X	...	...	...	...	...	...	...	...	...	...	...	...	...	...	...	...	...
Pseudofusulinella sp.	.....	...	...	...	X	...	X	...	...	...	...	...	...	...	...	...	...	...	...	...
Triticites sp.	.....	...	...	X	...	X	...	...	...	...	...	...	...	...	...	...	...	...	...	...
T. sp. aff. *T. cullomensis* Dunbar and Condra.	.....	...	...	...	X	...	...	...	...	...	...	...	...	...	...	...	...	...	...	...
T. spp. undet.	.....	...	...	...	...	...	X	X	X	X	X	X	...	X	X	...	...	...	...	...
T. ex. gr. *T. ventricosus*	.....	...	...	...	...	...	...	...	...	...	...	...	X	...	X	...	...	...	...	...
Staffella sp.	.....	...	...	...	...	...	X	...	...	...	...	...	...	...	?	...	...	...	...	...
Schubertella sp.	.....	...	...	...	...	...	...	...	...	...	...	...	...	X	...	...	...	...	...	...
Schwagerina sp.	.....	...	...	...	...	...	...	...	...	...	...	...	...	...	?	?	X	?	X	X
Pseudofusulina sp.	.....	...	...	...	...	...	...	...	...	...	...	...	...	...	X	X	...	...	...	...
Parafusulina sp.	.....	...	...	...	...	...	...	...	...	...	...	...	...	...	...	...	...	...	?	?

Unit 4

Unit 4 consists of interbedded light-gray, brown-weathering, fine-grained calcareous sandstone, gray limestone, and sandy limestone. The unit crops out on the ridge 4.8 km (3 mi) N. 75° E. of Bellevue and in a belt extending northwest through the Baugh Creek SW into the Hailey 7½-minute quadrangle. Beds are mostly 5–61 cm (2 in.–2 ft) thick. The calcareous sandstone consists of rounded grains of quartz, potassium feldspar, plagioclase, and zircon in a calcareous matrix. The feldspars constitute about 5 percent of the sand grains. Much of the potassium feldspar has grid twinning. The plagioclase is An_{25-35}. The quartz contains abundant primary and secondary fluid inclusions that are two phase and contain a bubble that averages about 25 percent by volume of the inclusion.

The following section of unit 4 was measured on the ridge 5.1 km (3.2 mi) N. 75° E. of Bellevue at an altitude of 2,042 m (6,700 ft):

Unit 5.

Conformable contact.

	Feet
Unit 4:	
Sandstone, calcareous, gray, fine-grained, brown-weathering	236
Quartzite, brown, fine-grained, shattered	5
Sandstone, calcareous, gray, fine-grained, brown-weathering. Beds 1–2 ft thick	218
Shattered zone. Displacement interpreted to be small	11
Limestone, gray, sandy; and gray calcareous sandstone, fine-grained, brown-weathering. Beds 4 in.–2 ft thick	35
Sandstone, calcareous, fine-grained, gray, brown-weathering; and gray limestone. Beds 2–12 in. thick. Some fine crossbedding with tops east. Fossil collection A239 at 0 and A240 at 120 ft	189
	694
	(212m)

Conformable contact.

Unit 3.

Age.—Unit 4 is of Late Pennsylvanian (Virgilian) age (table 1). A collection (A239) from the base of the unit contains crushed specimens of a small *Triticites;* a collection (A240) from 37 m (120 ft) above the base has better preserved material: *Pseudofusulinella* sp. and *Triticites* sp. aff. *T. cullomensis* Dunbar and Condra.

Unit 5

Unit 5 consists predominantly of thick-bedded and massive, fine-grained quartzite and limy quartzite with some interbedded calcareous sandstone and sandy limestone. The unit is well exposed in the measured section along the ridge 5.4 km

(3.4 mi) N. 75° E. of Bellevue at an altitude of 2,134 m(7,000 ft), and it underlies much of the southwestern quarter of the Baugh Creek SW quadrangle in Slaughterhouse Gulch and in the vicinity of Quigley Creek (fig. 1). The unit is resistant to weathering and stands out as prominent ledges that contrast with the adjacent calcareous sandstones. The quartzite is a brittle unit; in outcrop it generally consists of highly shattered rocks with blocks several inches on a side (fig. 2).

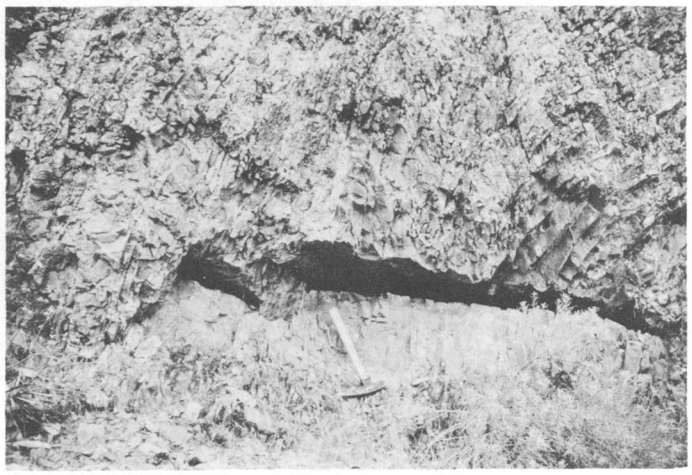

Figure 2.—Shattered brown fine-grained quartzite of unit 5 displaying strong fracture cleavage. This shattering is characteristic of the quartzite in unit 5.

A section of unit 5 was measured along the ridge 5.4 km (3.4 mi) N. 75° E. of Bellevue between 2,073 and 2,164 m (6,800–7,100 ft). This section is disrupted by a reverse fault that repeats 6.7 m (22 ft) of the top of unit 4 and most of unit 5. The section on the east side of the fault is as follows:

Unit 6.

Conformable contact. *Feet*

Unit 5:

Quartzite, brown, fine-grained, shattered	72
Quartzite, brown, fine-grained; and limestone, gray, sandy, fine-grained	40
Quartzite, brown, fine-grained, shattered	13
Quartzite, brown, fine-grained with limestone beds, sandy, gray, 2 to 6 in. thick	22
Quartzite, brown, fine-grained, thick-bedded	78
Quartzite float, light-brownish-gray, fine-grained	77
Fault, strike N. 60° E., dip 62° N. Displacement apparently small.	
Quartzite, brown, fine-grained, thick-bedded, shattered	243
	545
	(166m)

Conformable contact.

Unit 4:

Limestone, gray, sandy, fine-grained, fine crossbedding (22 ft). Fault contact east side up (repeats 22 ft of unit 4 and 400 ft of unit 5).

The predominant rock type is light-brown, fine-grained quartzite. Most of the quartzite, 90 to 95 percent, consists of a mosaic of quartz grains 0.08 to 0.15 mm in diameter. The remaining 5 to 10 percent is made up of clasts of potassium feldspar, plagioclase, zircon, and opaque minerals in a small amount of calcite, sericite, and limonitic matrix. The mineralogy and grain size are the same as in the calcareous sandstones.

Age.—Unit 5 is Late Pennsylvanian (Virgilian) in age. It is nearly devoid of fossils, and none were found in the measured section. However, fusulinids were collected from the basal part of unit 5 from a thin sandy limestone bed interbedded in light-brown fine-grained thick-bedded quartzite on the north side of Quigley Creek in the north-central part of sec. 31, T. 3 N., R. 19 E. at an altitude of 1,817 m (5,960 ft). The bed is a sandy crinoidal-foraminiferal packstone that contains some bryozoan and brachiopod fragments and algae. The grain size is less than 1 mm except for the large fusulinids. Collection A997 contains fragments of fusulinids, some of which are recognizable as *Triticites* sp. of Late Pennsylvanian (Virgilian) age (table 1).

Unit 6

Unit 6 is characterized by a thick sequence of gray and light-brown, fine-grained calcareous sandstone that weathers dark brown and dark reddish brown. Interbedded in the calcareous sandstone are fine-grained sandy limestone, fine to medium-grained bioclastic limestone, and brown thick-bedded quartzite. Float from this unit is resistant to weathering, and much talus of dark-brown slabby calcareous sandstone masks slopes for hundreds of feet below its outcrops. The Milligen Formation, for example, commonly is completely masked by talus from this unit.

Unit 6 is well exposed in the measured section on the ridge 5.6 km (3.5 mi) N. 75° E. of Bellevue at an altitude of 2,164 m (7,100 ft) and along the ridge to the northeast for 3.4 km (2.1 mi). The unit is widespread in the Baugh Creek SW quadrangle. The section northeast of Bellevue is as follows:

Unit 7.

Conformable contact. *Feet*

Unit 6.

Quartzite, brown and reddish-brown, fine-grained; limestone, sandy, gray, contains fusulinids at 0 and 600 ft; and gray limestone granule conglomerate	600
Limestone, sandy, gray; and calcareous sandstone, gray, fine-grained, weathers dark brown and reddish brown, float. Fossil collection A583 at 600 ft	650
Quartzite, fine-grained, red, brown, and reddish gray; and calcareous sandstone, fine-grained, gray, weathers dark brown, float	750
Quartzite, gray and reddish-brown; and calcareous sandstone, gray, weathers dark brown, fine-grained	500
Sandstone, brown, fine-grained, calcareous; and quartzite, brown, fine-grained	560
Sandstone, gray and light-brown, fine-grained, calcareous, weathers dark brown	87

Limestone, coarse-grained, with abundant fusulinids Collection A439A	41
Limestone, gray, sandy, float	41
Sandstone, gray and light-brown, fine-grained, calcareous, weathers dark brown; limestone, gray, sandy; and quartzite, brown. Fusulinids at 190 (colln. A706-26), 270 (colln. A706-27), 360 (colln. A706-28), and 560 ft (colln. A706-29)	600
Fault breccia. Displacement unknown.	
Sandstone, gray and light-brown, fine-grained, calcareous, weathers dark reddish brown	85
Fault. Displacement apparently small.	
Sandstone, light-brown, fine-grained, calcareous, weathers dark brown and dark reddish brown; and limestone, gray, sandy	359
Quartzite, light-brown, thick-bedded, weathers dark brown; and calcareous sandstone, fine-grained, brown. Shattered	19
Sandstone, gray and light-brown, fine-grained, calcareous, weathers dark brown; and limestone, gray, sandy. Beds 2–4 in. thick	229
Laminated sandstone, dark-gray and brown, fine-grained; and limestone, gray, sandy. Beds 2–4 in. thick. Contains fusulinids at 150 (colln. A706-21) and 200 ft (colln. A706-22)	225
Sandstone, gray and light-brown, fine-grained; weathers dark brown. Beds 2–4 in. thick. Fracture cleavage at 50–62 ft	96
Quartzite, light-brown, fine-grained, thick-bedded	15
Sandstone, light-brown and gray, fine-grained, calcareous, weathers dark brown. Contains fusulinids at 26 ft. (colln. A706-17)	175
Limestone, gray, sandy, fine-grained. Contains fusulinids	1
Sandstone, gray, fine-grained, calcareous, weathers dark brown, thick-bedded. Conspicuous fracture cleavage	117
Limestone, gray, sandy, fine-grained	18
Sandstone, gray, calcareous, fine-grained; some gray limestone interbeds. Weathers brick red, reddish brown, and dark brown	172
Limestone, gray, fine-grained; sandstone, gray, calcareous, weathers dark brown; and quartzite, gray, fine-grained	80
Sandstone, gray, calcareous, fine-grained, weathers dark brown; and limestone, gray sandy. Conspicuous fracture cleavage. Beds 6 in.–2 ft thick	56
Sandstone, gray, brown-weathering, calcareous, fine-grained, locally crossbedded; and thin beds of gray sandy limestone. Contains fusulinids of Virgilian age. Beds 1–2 ft thick	218
	5,694
	(1,736m)

Conformable contact.

Unit 5.

Calcareous sandstone, which makes up the bulk of unit 6, is mineralogically similar to sandstone in unit 4. Subrounded quartz grains 0.05 to 0.4 mm in diameter are the predominant clasts; potassium feldspar, plagioclase, zircon, and opaque minerals constitute as much as 15 percent of the clasts. Some potassium feldspar grains have grid twinning. Plagioclase grains have a composition of about An_{30}. The matrix is calcite and a little sericite and cryptocrystalline quartz. This mineralogy suggests that the craton was the source.

Age.—Unit 6 includes rocks of Late Pennsylvanian and Early Permian age (table 1). Fragments of fusulinids are found at several horizons within this unit. The lowest collection with fusulinids (A706-17) includes fragments of *Triticites* sp., *Pseudofusulinella* sp., and *Staffela* sp. The other collections through A706-29 contain fragments of *Triticites* spp., none of which appear to represent forms younger than Late Pennsylvanian (Virgilian) age. Collection A439A from 37 m (120 ft) higher than A706-29 contains the first fragments of a form suggesting *Triticites ventricosus* (Meek and Hayden) of Early Permian age, and collection A583 near the top of unit 6 contains *Triticites* sp. and *Schubertella* sp. of probably Early Permian age.

Unit 7

Unit 7 is characterized by banded dark-gray chert and gray sandy limestone in beds 1.7–5 cm (½–2 in.) thick. At most places the unit is poorly exposed, but abundant dark-gray chert float makes this unit readily recognizable. The unit crops out extensively in the Baugh Creek SW quadrangle on the east side of the Wood River Formation, dipping unconformably under the Challis Volcanics or conformably under an unnamed sequence of noncalcareous siltstones and siltites of unknown age.

A stratigraphic section of unit 7 was measured in the Quigley Creek drainage in sec. 21, T. 3 N., R. 19 E. The stratigraphic section was started 701 m (2,300 ft) north of the SW corner of section 21 and measured toward the east up the ridge from an altitude of 2,024–2,225 m (6,640–7,300 ft) (fig. 1). The section in the Quigley Creek drainage is as follows:

Siltstone, unnamed formation.

Conformable contact.

Unit 7:	*Feet*
Limestone, gray, sandy with 1-in.-thick black chert beds	320
Limestone, gray, sandy, laminated; and chert, black and dark-gray. Beds 6 in.–6 ft thick	660
Calcarenite, coarse-grained, crinoidal	25
Limestone, sandy, crinoidal, gray, and quartzite, fine-grained, gray and grayish-brown	65
Chert, dark-gray; and calcarenite, gray, crinoidal. Beds ¼–1½ in. thick. Fossil locality A741 at top.	650
Shattered banded gray limestone and dark-gray chert	10
	1,730
	(527m)

Fault contact.

Unit 6.

Age.—Unit 7 is of Early Permian age (table 1). Collection A566 at the base of the formation contains many fragments of fusulinids including species of *Triticites*, a possible *Staffella* sp., a possible *Schwagerina* sp., and *Pseudofusulina* sp., suggesting an Early Permian (Wolfcampian) age.

A collection of crinoidal calcarenite (A741) 201 m (660 ft) above the base of the unit in the measured section contains fragments of a possible *Schwagerina* sp. and *Pseudofusulina* sp., also of Wolfcampian age. Collections C25 and C110 contain *Schwagerina* sp. and possible *Parafusulina* sp. and are of possible Leonardian age.

SUMMARY

Two partial sections of the Wood River Formation were measured that total approximately 2,987 m (9,800 ft). They represent the total Wood River Formation as redefined in this paper. The formation is restricted to a basal chert pebble conglomerate and a thick sequence of calcareous sandstones and quartzites. The uppermost noncalcareous siltstones, shales, and siltites included in the Wood River Formation by Umpleby, Westgate, and Ross (1930) are herein considered part of an overlying unnamed formation.

REFERENCES CITED

Bostwick, D. A., 1955, Stratigraphy of the Wood River Formation, south-central Idaho: Jour. Paleontology, v. 29, p. 941-951.

Lindgren, Waldemar, 1900, The gold and silver veins of Silver City, DeLamar, and other mining districts in Idaho: U.S. Geol. Survey 20th Ann. Rept., pt. 3, p. 65–256.

Ross, C. P., 1960, Diverse interfingering carboniferous strata in the Mackay quadrangle, Idaho *in* Short papers in the geological sciences: U.S. Geol. Survey Prof. Paper 400-B, Art. 104, p. B232–B233.

Thomasson, M. R., 1959a, Late Paleozoic stratigraphy and paleotectionics of central and eastern Idaho: Dissert. Abs., v. 20, no. 3, p. 999.

——1959b, Late Paleozoic stratigraphy and paleotectionics of central and eastern Idaho: Wisconsin Univ., Madison, Ph. D. thesis, 244 p.

Umpleby, J. B., 1917, Geology and ore deposits of the Mackey region, Idaho: U.S. Geol. Survey Prof. Paper 97, 127 p.

Umpleby, J. B., Westgate, L. G., and Ross, C. P., 1930, Geology and ore deposits of the Wood River region, Idaho: U.S. Geol. Survey Bull. 814, 250 p.

Wray, J. L., 1968, Late Paleozoic phylloid algal limestones in the United States, *in* Genesis and classification of sedimentary rocks: Internat. Geol. Cong., 23d, Prague 1968, Proc., sec. 8, p. 113–119.

Jour. Research U.S. Geol. Survey
Vol. 2, No. 1, Jan. - Feb. 1974, p. 97—104

STRATIGRAPHY AND MICROFAUNA OF THE OQUIRRH GROUP IN THE WESTERN TRAVERSE MOUNTAINS AND NORTHERN LAKE MOUNTAINS, UTAH

By R. C. DOUGLASS[1], W. J. MOORE[2], and J. W. HUDDLE[1],
Washington, D.C.[1]; Menlo Park, Calif.[2]

Abstract.—Sedimentary rocks of Pennsylvanian age in the western Traverse Mountains and northern Lake Mountains, Utah, are assigned to the Oquirrh Group and divided into three formations that are correlated with those recognized in the Bingham mining district. The West Canyon Limestone of Early Pennsylvanian age, the Butterfield Peaks Formation of Middle Pennsylvanian age, and the Bingham Mine Formation of Late Pennsylvanian age are recognized on the basis of lithologic and faunal criteria. Conodonts, but no fusulinids, are listed from the West Canyon Limestone. Fusulinids are listed and typical forms illustrated from the Butterfield Peaks and Bingham Mine Formations.

Sedimentary rocks of Pennsylvanian age in the western Traverse Mountains and northern Lake Mountains, Utah, are divided into three major stratigraphic units that are correlated with formations in the type section of the Oquirrh Group as designated by Tooker and Roberts (1970). These are the West Canyon Limestone of Early Pennslyvanian (Morrowan) age, the Butterfield Peaks Formation of Middle Pennsylvanian (Atokan? and Des Moinesian) age, and the Bingham Mine Formation of Late Pennsylvanian (Missourian and Virgilian) age.

Lithologic characteristics of the Oquirrh Group in the area of study (fig. 1) are comparable to those in its type section. The West Canyon Limestone is an arenaceous bioclastic limestone sequence containing several thin calcareous quartzite beds. The overlying Butterfield Peaks Formation is a cyclically repeated sequence of cherty limestone, platy arenaceous limestone, calcareous sandstone, and calcareous quartzite; the formation has a distinctive banded aspect resulting from differences in color and resistance to erosion of beds within cyclical intervals. The overlying Bingham Mine Formation is composed chiefly of interbedded orthoquartzite and quartzose sandstone; thin arenaceous limestone and calcareous sandstone beds occur near the base and in the upper part of the formation.

Megafossils in rocks of the Oquirrh Group from the western Traverse Mountains are neither as abundant nor as well preserved as in units from its type section. In addition, certain marker beds recognized in the type section are missing in the Traverse Mountains. Microfossils therefore had to be used to demonstrate age equivalence of provisionally correlative formational units. A total of 33 microfossil collections have been studied by Douglass (fusulinids) and Huddle (conodonts). Douglass also searched the lower parts of the section and made fusulinid collections from the Butterfield Peaks Formation in 1971. Field localities for the collections are indicated on figure 1. More accurate locations are shown on the map (Moore, 1973) from which figure 1 was adapted.

GEOLOGIC SETTING

The Traverse Mountains form an east-trending extension of the central Oquirrh Mountains, but structural relations between the two are obscured by an intervening sequence of Tertiary volcanic breccias and flows (fig. 1). Paleozoic sedimentary rocks in the Traverse Mountains and Lake Mountains several miles to the south belong largely to the Oquirrh Group. Sedimentary rocks that underlie the Oquirrh Group are not considered in this report.

Observations pertaining to the overall distribution of volcanic rocks and to structural and stratigraphic relations in sedimentary rocks west of Tickville Gulch generally agree with those of earlier field studies (Gilluly, 1932; Bullock, 1951; Bissell and Rigby, 1959). The relatively broad open folds in this area are a continuation of the northwest-trending fold belt in the central and southern Oquirrh Mountains. The trend, asymmetry, and local overturning exhibited by these folds have resulted from compressive deformation during northeastward movement of the upper plate of the Midas thrust fault (Tooker, 1971).

In the Traverse Mountains east of Tickville Gulch fold amplitudes decrease, and steepened or overturned beds of the West Canyon Limestone and lower Butterfield Peaks Formation are separated from a normal section of the Oquirrh Group by a small thrust fault. The pattern of deformation, characterized by an en echelon series of minor folds, resembles that developed near the lead edge of the Midas thrust fault in the

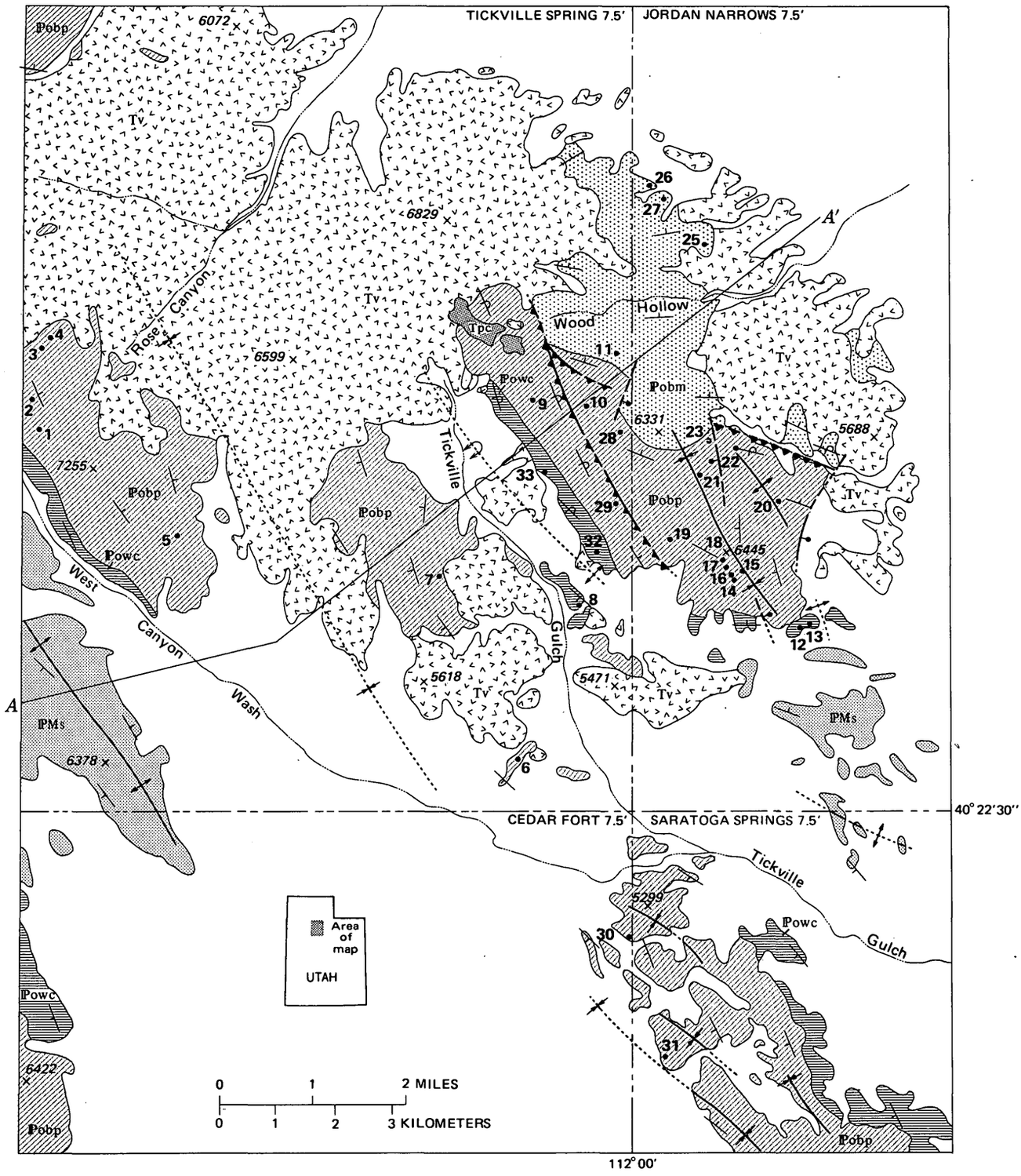

Figure 1.—Generalized geologic map of western Traverse Mountains and northern Lake Mountains, Utah. Adapted from Moore (1973).

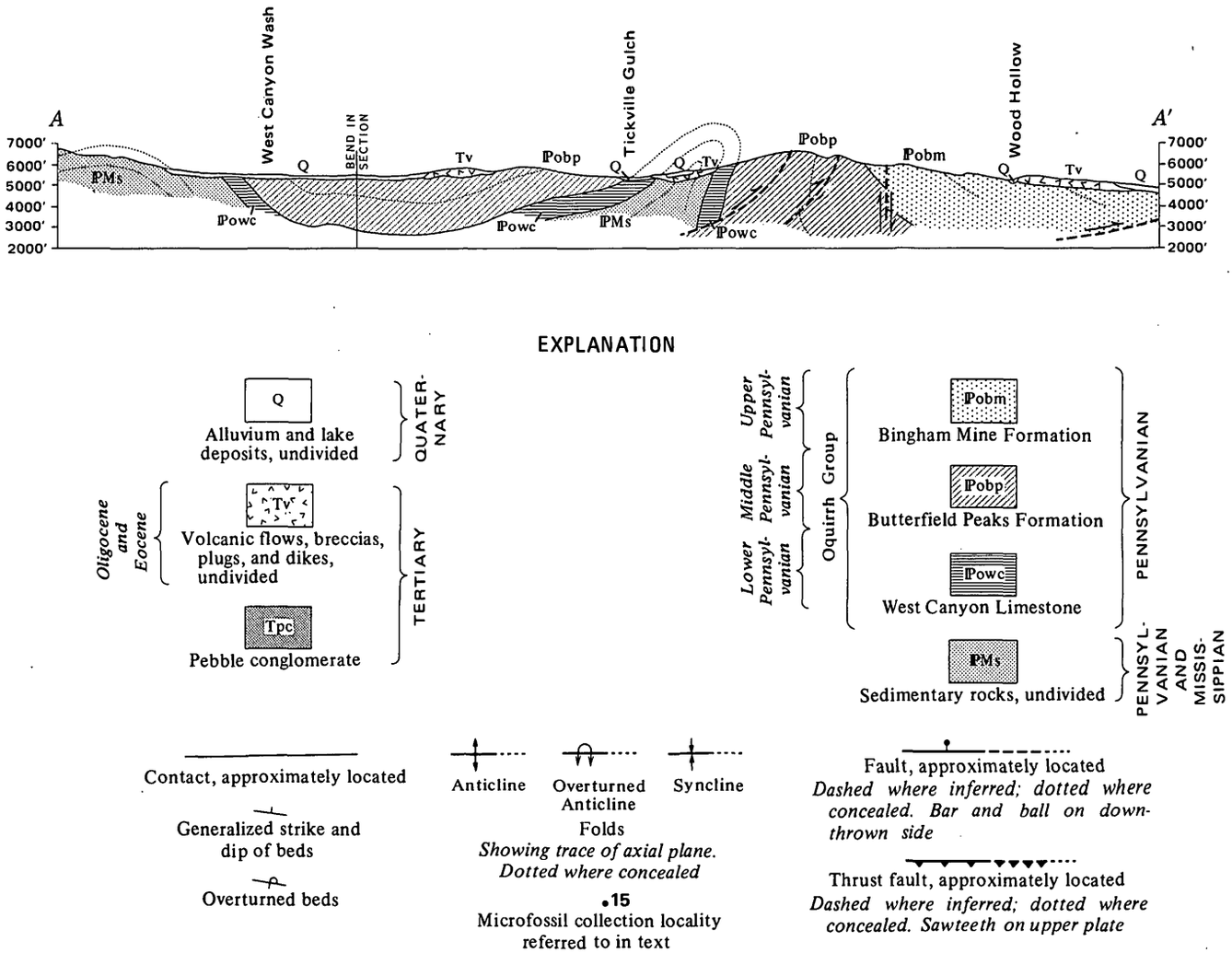

Figure 1.—Continued.

Bingham mining district (James and others, 1961; Tooker and Roberts, 1970, fig. 2) and suggests that a comparable fault may be concealed by alluvium and lake bed deposits east of the map area.

CONODONTS FROM THE WEST CANYON LIMESTONE

Conodonts were found in five samples from the West Canyon Limestone at localities listed below and indicated in figure 1. They all suggest an Early Pennsylvanian (Morrowan) age, although some of the forms present have more extended ranges.

Locality 8, USGS 24769-PC
- *Streptognathodus anteeccentricus* Dunn
- *Adetognathus gigantus* (Gunnell)
- *A. lautus* (Gunnell)
- *Hindeodella* sp.

Locality 12, USGS 24771-PC
- *Idiognathoides sinuatus* Harris and Hollingsworth
- *Adetognathus gigantus* (Gunnell)
- *A. lautus* (Gunnell)

Locality 13, USGS 24770-PC
- *Spathognathodus muricatus* (Dunn)
- *Adetognathus gigantus* (Gunnell)
- *A. lautus* (Gunnell)

Locality 32, USGS 25030-PC
- *Adetognathus lautus* (Gunnell)
- *Hindeodella* sp.
- *Neognathodus bassleri symmetricus* (Lane)
- *Ozarkodina* sp.
- *Rhachistognathus muricatus* (Dunn)

Locality 33, USGS 25031-PC
- *Adetognathus lautus* (Gunnell)
- *Hindeodella* sp.

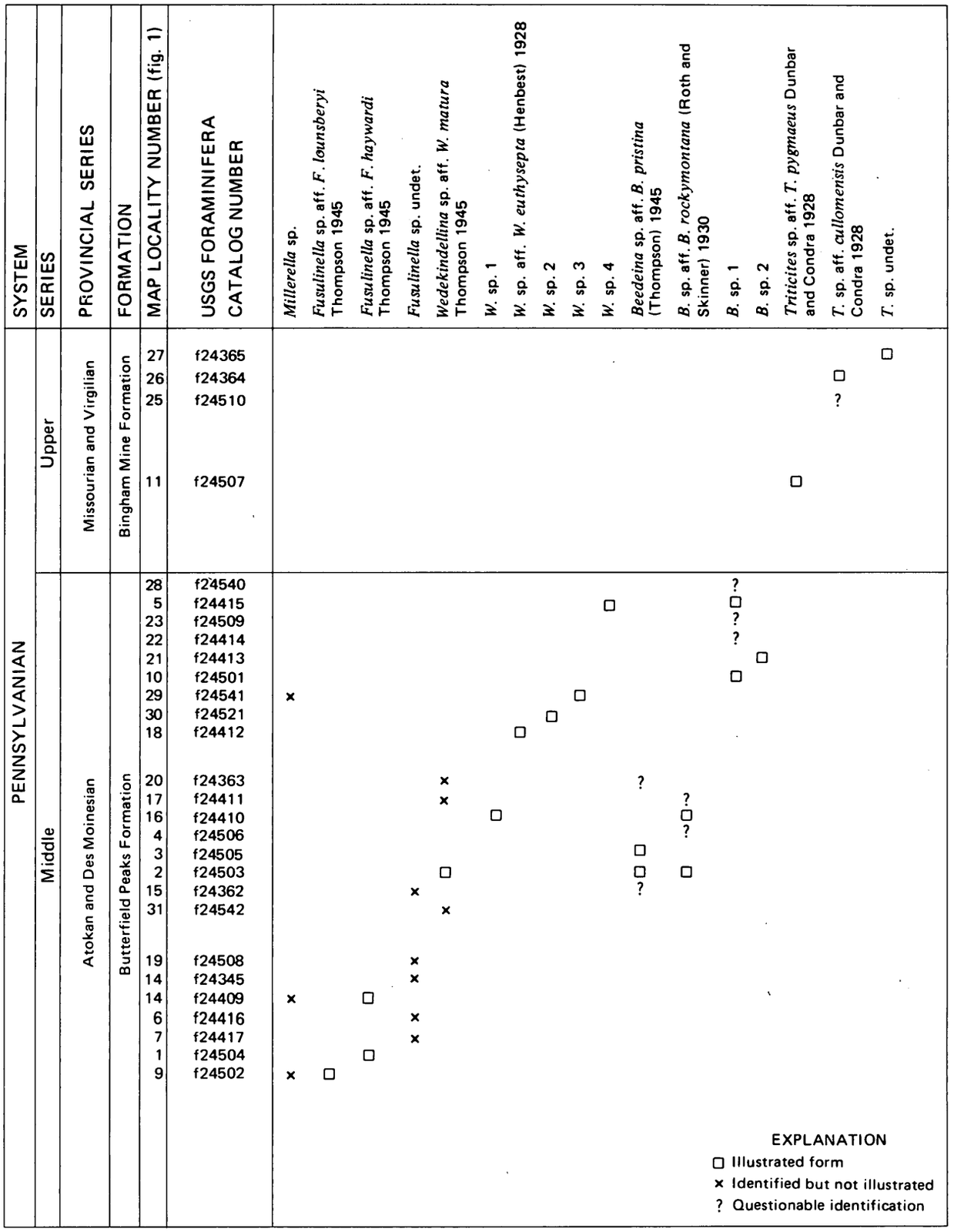

Figure 2.—Distribution of fusulinids in the Oquirrh Group.

FUSULINID FAUNAS

Fusulinids were found in rocks of Middle and Late Pennsylvanian age (fig. 2). Welsh and James (1961, p. 11) reported *Profusulinella* in their Maple Formation, and Bissell (1959, p. 106) reported *Profusulinella* from his Meadow Canyon Member of the Oquirrh Formation. Tooker and Roberts (1970, p. A7 and fig. 5) correlated these units with the West Canyon Limestone and the lower part of the Butterfield Peaks Formation. No fusulinids were found in rocks considered to be time equivalents of the West Canyon Limestone. The oldest fusulinids found in this study are from Butterfield Peaks Formation equivalents and include *Millerella* sp. and *Fusulinella* spp. resembling forms described by Thompson (1945) from his Hells Canyon Formation of the Uinta Mountains. Their age is not fully documented, but they appear to be latest Atokan to early Des Moinesian. Seven samples representative of this age were studied. The samples are listed in figure 2, and several typical forms are illustrated in figure 3 from samples f24409, f24502 and f24504 in this group.

A second group of samples representing slightly younger age contains specimens of *Fusulinella* sp., *Wedekindellina* spp., and *Beedeina* spp. resembling forms described by Thompson (1945) from his Youghall Formation of the Uinta Mountains. This fauna seems comparable with that listed by Welsh and James (1961, p. 11) from their "White Pine" Formation (assigned to the Butterfield Peaks Formation by Tooker and Roberts in 1970). Eight samples representing this group were studied (fig. 2). Typical specimens are illustrated in figure 3 from samples f24410, f24503, and f24505. A middle Des Moinesian age assignment for this group seems most reasonable on the basis of the stage of development of the species of *Beedeina* represented.

A third group of samples of late Des Moinesian age is from the upper part of the Butterfield Peaks Formation (fig. 2). It contains *Millerella* sp., *Wedekindellina* spp., and *Beedeina* spp. The fauna is probably similar to that listed by Welsh and James (1961, p. 11) from their Butterfield Formation and is similar to the fauna reported by Tooker and Roberts (1970, p. A67, A68) from the upper part of the Butterfield Peaks Formation. Typical specimens from samples f24412, f24413, f24415, f24501, f24521, and f24541 are illustrated in figure 4. The *Beedeina* species are as advanced morphologically as any from this part of Utah, but they are not the highly

Figure 3.—Fusulinids from the Butterfield Peaks Formation.

a–c. USGS f24410. *Wedekindellina* sp. 1 (× 20). Associated with *Climacammina* sp. in this sample. *a*, *b*, axial sections; *c*, equatorial section.

d–f. USGS f24410. *Beedeina* sp. aff. *B. rockymontana* (Roth and Skinner) 1930 (× 10). Associated with *Climacammina* sp. in this sample. *d*, *e*, equatorial sections; *f*, axial section.

g–m. USGS 24505. *Beedeina* sp. aff. *B. pristina* (Thompson) 1945 (× 10). Associated with *Bradyina* sp. and *Climacammina* sp. in this sample. *g–j*, axial sections; *k–m*, equatorial sections.

n. USGS f24503. Axial section of *Beedeina* sp. aff. *B. rockymontana* (Roth and Skinner) 1930 (× 10). Associated with *Globivalvulina* sp. in this sample.

o–r. USGS f 24503. *Beedeina* sp. aff. *B. pristina* (Thompson) 1945 (× 10). Associated with *Globivalvulina* sp. in this sample. *o*, axial section; *p–r*, equatorial sections.

s–w. USGS f24503. *Wedekindellina* sp. aff. *W. matura* Thompson 1945 (× 20). Associated with *Globivalvulina* sp. in this sample. *s*, *t*, equatorial sections; *u–w*, axial sections.

x–aa. USGS f24409. *Fusulinella* sp. aff. *F. haywardi* Thompson (1945) (× 20). Associated with *Millerella* sp., *Globivalvulina* sp., and algae in this sample. *x*, *y*, axial sections; *z*, *aa*, equatorial sections.

bb–dd. USGS f24504. *Fusulinella* sp. aff. *F. haywardi* Thompson (1945) (× 20). Associated with an endothyrid, algae, and *Globivalvulina* sp. in this sample. *bb*, axial section; *cc*, *dd*, equatorial sections.

ee–hh. USGS f 24502. Small *Fusulinella* sp. resembling *F. lounsberyi* Thompson (1945) (× 20). Associated with *Millerella* sp., *Tetrataxis* sp., *Climacammina* sp., and algae in this sample. *ee*, *ff*, axial sections; *gg*, *hh*, equatorial sections.

Figure 4.—Fusulinids from the Bingham Mine and Butterfield Peaks Formations.

a–e. USGS f24365, Bingham Mine Formation. *Triticites* sp. (× 10). This is the most advanced form of *Triticites* found in the Oquirrh Group in the western Traverse Mountains, *a–c*, axial sections; *d*,*e*, equatorial sections.

f, *g.* USGS f24364, Bingham Mine Formation. *Triticites* sp. aff. *T. cullomensis* Dunbar and Condra 1928 (× 10). *f*, axial section; *g*, equatorial section.

h, *i.* USGS f24507, Bingham Mine Formation. *Triticites* sp. aff. *T. pygmaeus* Dunbar and Condra 1928 (× 10). *h*, axial section; *i*, equatorial section.

j, *k.* USGS f24415, Butterfield Peaks Formation. *Wedekindellina* sp. 4 (× 10). *j*, axial section; *k*, equatorial section.

l. USGS f24415, Butterfield Peaks Formation. Axial section of *Beedeina* sp. 1 (× 10).

m, *n.* USGS f24501, Butterfield Peaks Formation. *Beedeina* sp. 1 (× 10). This sample also contains fragments of gastropods and brachiopods, crinoid columnals, an endothyrid, and *Climacammina*? sp. *m*, equatorial section; *n*, axial section.

o–q. USGS f24413, Butterfield Peaks Formation. Small, thin-walled *Beedeina* sp. 2 (× 10). Associated with *Globivalvulina* sp. *o*, axial section; *p*, *q*, equatorial sections.

r, *s.* USGS f24541, Butterfield Peaks Formation. *Wedekindellina* sp. 3 (× 20). Associated with *Millerella* sp. and *Bradyina* sp. *r*, axial section; *s*, equatorial section.

t–v. USGS f24521, Butterfield Peaks Formation. *Wedekindellina* sp. 2 (× 20). *t*, axial section; *u*,*v*, equatorial sections.

w, *x.* USGS f24412, Butterfield Peaks Formation. *Wedekindellina* sp. aff. *W. euthysepta* (Henbest) 1928 (× 20). Associated with *Climacammina* sp. in this sample. *w*, axial section; *x*, equatorial section.

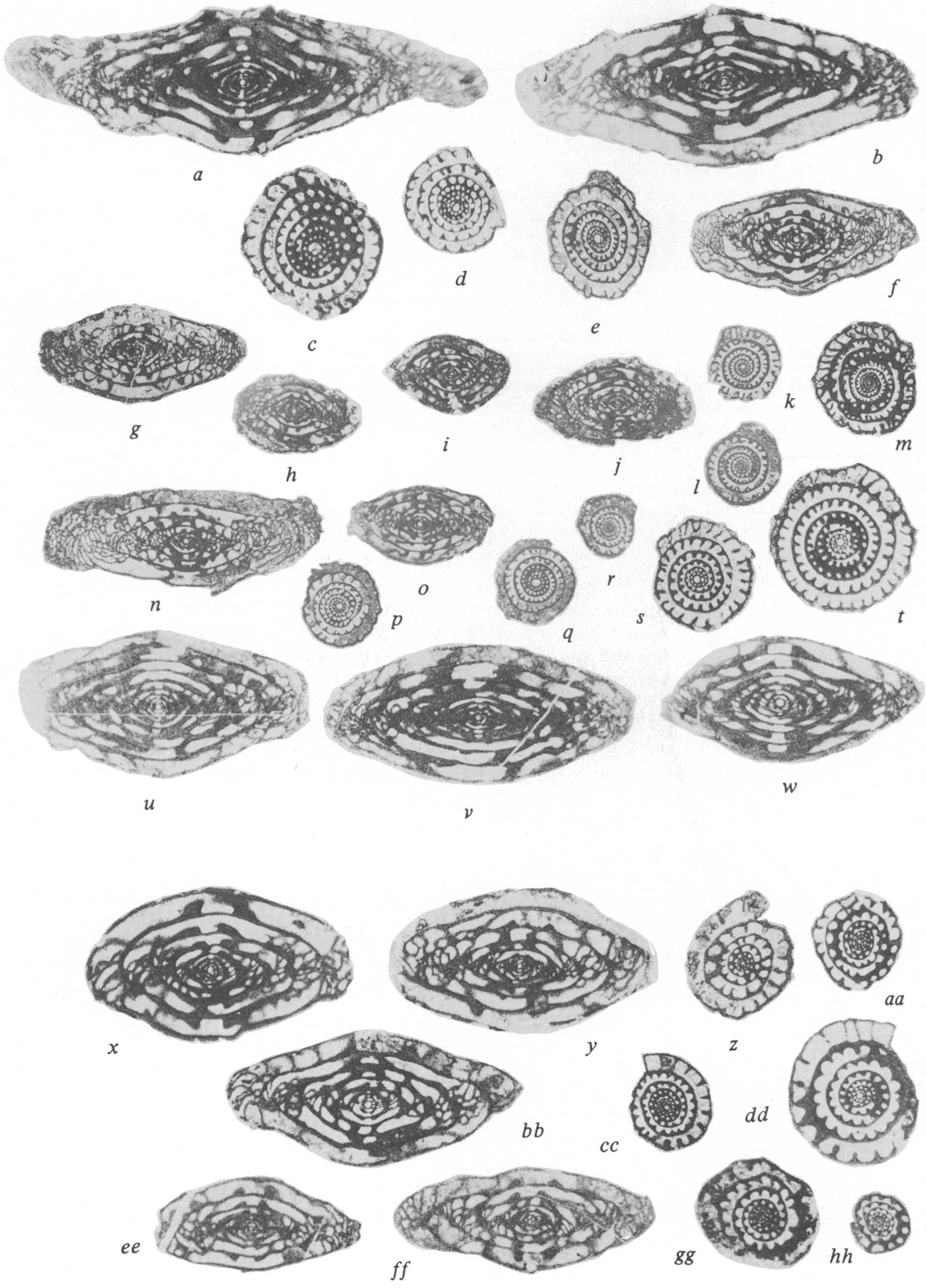

Figure 3.

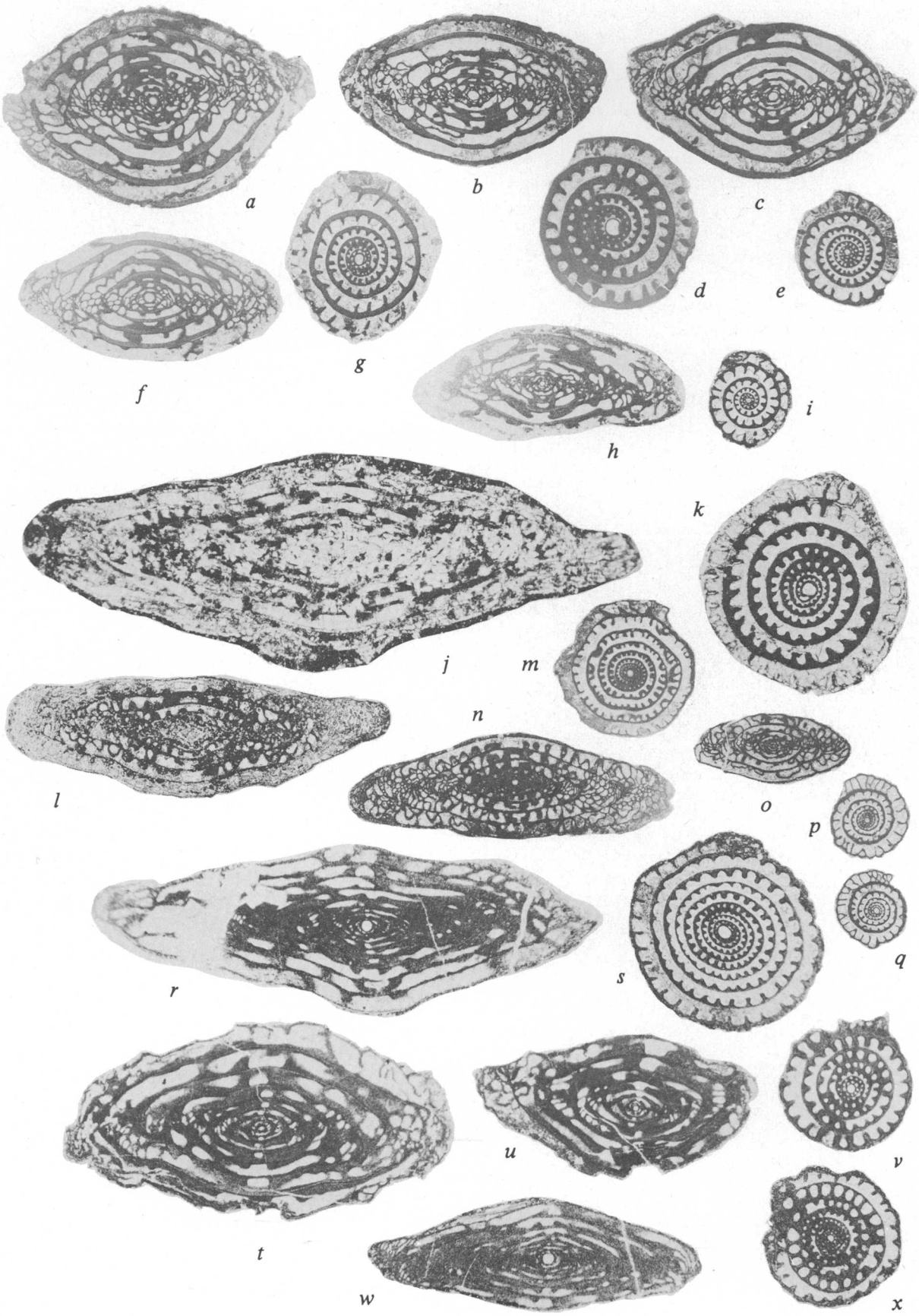

Figure 4.

specialized forms reported from Nevada by Verville, Thompson, and Lokke (1956) or from Illinois by Dunbar and Henbest (1942).

The fusulinid fauna of the Bingham Mine Formation in the Traverse Mountains is more restricted than that in the Bingham mining district. The lowest *Triticites*, collected near the base of the formation, is similar to forms found more than 365 m (about 1,200 ft) above the base of the Clipper Ridge Member in its type section. This *Triticites* sp. resembles *T. pygmaeus* Dunbar and Condra 1928 and suggests a Missourian age for this part of the formation. None of the elongate *Triticites* supp. illustrated by Thompson, Verville, and Bissell (1950) from the Missourian part of the Oquirrh Formation in the Wasatch Mountains were found.

The youngest collections from the Bingham Mine Formation contain species of *Triticites* of Virgilian age (fig. 2). Reports of Wolfcampian fusulinids by Bissell (1959, p. 126) from the area southwest of the Traverse Mountains suggest that younger Oquirrh Group may be present there, but none was found in the area studied. Typical specimens from samples f24364, f24365, and f24507 are illustrated in figure 4.

REFERENCES CITED

Bissell, H. J., 1959, Pennsylvanian System, *in* Bissell, H. J., ed., Geology of the southern Oquirrh Mountains and Fivemile Pass-northern Boulter Mountain area, Tooele and Utah Counties, Utah: Utah Geol. Soc. Guidebook to the geology of Utah, no. 14, 262 p.

Bissell, H. J., and Rigby, J. K., 1959, Geologic map of the southern Oquirrh Mountains, Tooele and Utah Counties, Utah, *in* Bissell, H. J., ed., Geology of the southern Oquirrh Mountains and Fivemile Pass-northern Boulter Mountain area, Tooele and Utah Counties, Utah: Utah Geol. Soc. Guidebook to the geology of Utah, no. 14, pl. I.

Bullock, K. C., 1951, Geology of Lake Mountain, Utah: Utah Geol. and Mineralog. Survey Bull. 41, 46 p.

Dunbar, C. O., and Condra, G. E., 1928, The Fusulinidae of the Pennsylvanian system in Nebraska: Nebraska Geol. Survey Bull. 2, 2d ser., 135 p,

Dunbar, C. O., and Henbest, L. G., 1942, Pennsylvanian Fusulinidae of Illinois: Illinois Geol. Survey Bull. 67, 218 p.

Gilluly, James, 1932, Geology and ore deposits of the Stockton and Fairfield quadrangles, Utah: U.S. Geol. Survey Prof. Paper 173, 171 p.

Henbest, L. G., 1928, Fusulinellas from the Stonefort limestone member of the Tradewater formation: Jour. Paleontology, v. 2, p. 70–85.

James, A. H., Smith, W. H., and Welsh, J. E., 1961, General geology and structure of the Bingham district, Utah, *in* Cook, D. R., ed., Geology of the Bingham mining district and northern Oquirrh Mountains: Utah Geol. Soc. Guidebook to the geology of Utah, no. 16, p. 49–69.

Moore, W. J., 1973, Preliminary geologic map of western Traverse Mountains and northern Lake Mountains, Salt Lake and Utah Counties, Utah: U.S. Geol. Survey Misc. Field Studies Map MF-490.

Roth, Robert, and Skinner, J. W., 1930, The fauna of the McCoy Formation, Pennsylvanian, of Colorado: Jour. Paleontology, v. 4, p. 332–352.

Thompson, M. L., 1945, Pennsylvanian rocks and fusulinids of east Utah and northwest Colorado correlated with Kansas section: Kansas Geol. Survey Bull. 60, 1945 Reports of Studies, pt. 2, p. 17–84,

Thompson, M. L., Verville, G. J., and Bissell, H. J., 1950, Pennsylvanian fusulinids of the south-central Wasatch Mountains, Utah: Jour. Paleontology, v. 24, no. 4, p. 430–465,

Tooker, E. W., 1971, Regional structural controls of ore deposits, Bingham mining district, Utah, U.S.A.: Japan Soc. Geol., Spec. Issue 3, p. 76–81.

Tooker, E. W., and Roberts, R. J., 1970, Upper Paleozoic rocks in the Oquirrh Mountains and Bingham mining district, Utah: U.S. Geol. Survey Prof. Paper 629-A, 76 p.

Verville, G. J., Thompson, M. L., and Lokke, D. H., 1956, Pennsylvanian fusulinids of eastern Nevada: Jour. Paleontology, v. 30, no. 6, p. 1277–1287,

Welsh, J. E., and James, A. H., 1961, Pennsylvanian and Permian stratigraphy of the central Oquirrh Mountains, Utah *in* Cook, D. R., ed., Geology of the Bingham mining district and northern Oquirrh Mountains: Utah Geol. Soc. Guidebook to the geology of Utah, no. 16, p. 1–16,

Jour. Research U.S. Geol. Survey
Vol. 2, No. 1, Jan.- Feb. 1974, p. 105—118

TERTIARY HISTORY OF LITTLE FISH LAKE VALLEY, NYE COUNTY, NEVADA, AND IMPLICATIONS AS TO THE ORIGIN OF THE GREAT BASIN

By E. B. EKREN, G. D. BATH, G. L. DIXON, D. L. HEALEY,
and W. D. QUINLIVAN, Denver, Colo.

Work done in cooperation with the U.S. Atomic Energy Commission

Abstract.—Little Fish Lake Valley is a north-trending nearly symmetrical graben in the central Great Basin. It lies along a regional axis of anticlinal symmetry; to the east most ranges in the Great Basin dip eastward, and to the west most dip westward. Little Fish Lake Valley and Monitor Valley to its west are the two highest major valleys in the Great Basin and lie within a zone where the crust is thicker than normal for the Great Basin. North-trending Little Fish Lake Valley is superimposed on several east-trending aeromagnetic discontinuities: one of these, referred to herein as the Tulle Creek-Pritchards Station lineament, can be traced eastward for 64 km (40 mi) from Tulle Creek in the Monitor Range through the Pritchards Station quadrangle. The exact nature of the lineament is in doubt, but in central Nevada it serves as a volcanic province boundary between an area to the north that is underlain by thick intermediate lavas and an area to the south where these lavas are virtually absent. During part of its history the lineament has been a left-lateral strike-slip fault, and in the Hot Creek Range, between Little Fish Lake Valley and Pritchards Station, the strike-slip fault is interpreted as passing into a low-angle thrust. The strike-slip faulting and associated thrusting and the development of the Little Fish Lake Valley graben all postdate the youngest tuff in the region, the Bates Mountain Tuff, dated at 23 m.y., but predate tuffaceous sediments that yield vertebrate fossils of late Miocene or early Pliocene age.

In late 1966, the U.S. Geological Survey began geological and geophysical investigations in central Nevada in an attempt to find an underground nuclear testing area for the U.S. Atomic Energy Commission supplemental to the Nevada Test Site. Geographic remoteness and at least 1,800 m (6,000 ft) of alluvium and (or) volcanic rocks were required. Testing at the Nevada Test Site had shown previously that these lithologies provide ideal media for underground nuclear testing. Little Fish Lake Valley (fig. 1) met the geographic requirement admirably, but could not satisfy the geologic requirement.

This report presents the three-dimensional data derived principally from the 1966–67 investigations and discusses the structural setting and age of Little Fish Lake Valley, the nature of east-trending magnetic lineaments that transect the valley and adjacent ranges, and the bearing the structure and history of the valley have on the origin of the Great Basin.

STRATIGRAPHY

The oldest rocks exposed in the Little Fish Lake Valley area are Paleozoic (fig. 2). These were mapped principally by Kleinhampl and Ziony (1967) as part of the northern Nye County mapping and by H. W. Dodge, Jr. (unpub. data), as part of the Morey Peak quadrangle mapping; these maps have been generalized and modified for this report. The Paleozoic rocks of northern Nye County were described briefly by Kleinhampl and Ziony (1967), and the assemblages in central

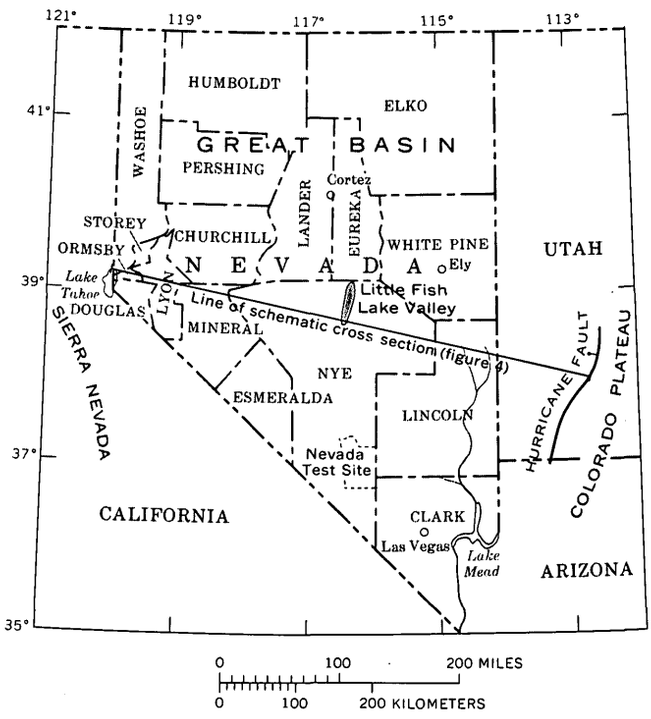

Figure 1.—Index map of Nevada, showing location of Little Fish Lake Valley and line of schematic cross section.

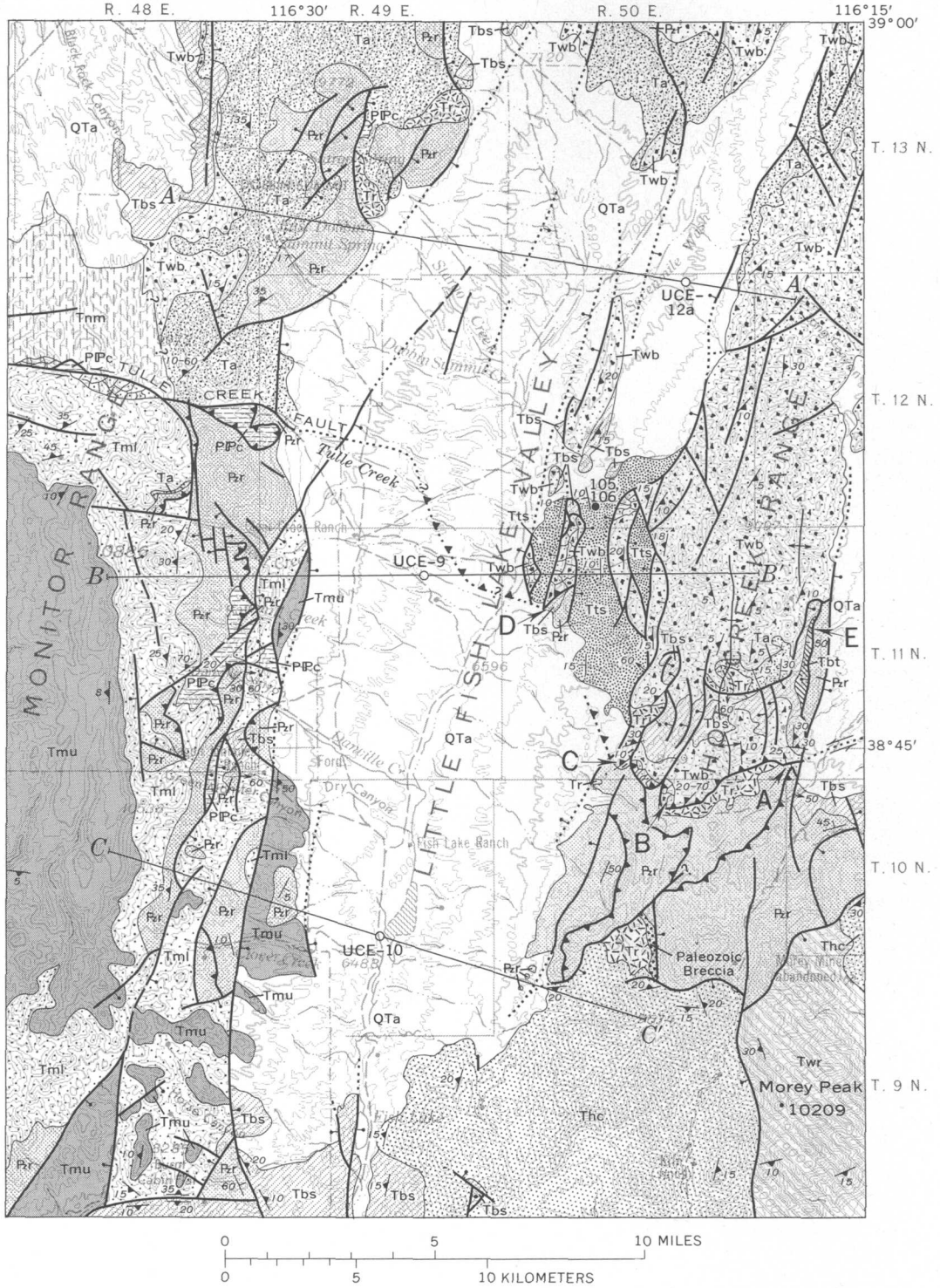

Figure 2.—Reconnaissance geologic map and stratigraphic sections of Little Fish Lake Valley area, Nye County, Nevada. Base from U.S. Geological Survey, Tonopah 1:250,000 quadrangle, 1956–62.

Nevada have been described elsewhere in a multitude of reports: Merriam (1963), Lowell (1965), Nolan, Merriam, and Williams (1956), Winterer and Murphy (1960), and Quinlivan and Rogers (1974). The rocks in the area are chiefly miogeosynclinal carbonates of early and middle Paleozoic age, but include dark cherts and carbonaceous shale of late

CORRELATION OF MAP UNITS

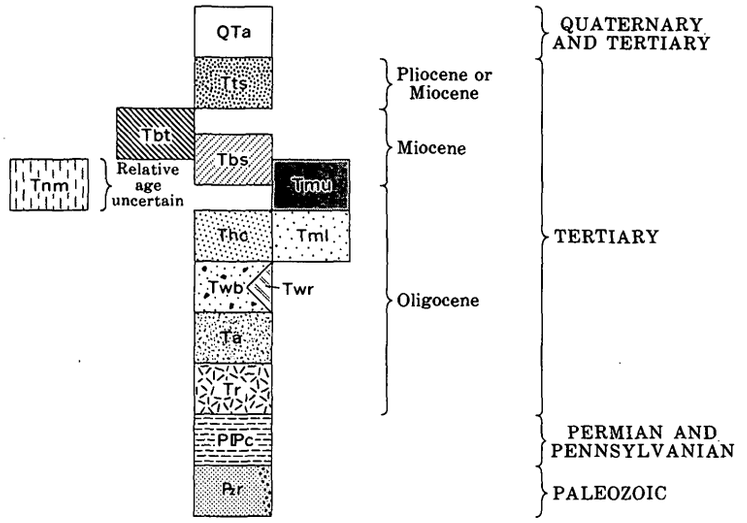

DESCRIPTION OF MAP UNITS

QTa	Alluvium (Quaternary and Tertiary)
Tts	Tuffaceous sedimentary rocks (Pliocene or Miocene)
Tbt	Stratified breccia and reworked tuff (Miocene)
Tbs	Principally Bates Mountain Tuff and Shingle Pass Tuff (Miocene) — Also includes tuffs of Lunar Cuesta, Kiln Canyon, Orange Lichen Creek, Pott Hole Valley, and Crested Wheat Ridge
Tnm	Tuff of the northern Monitor Range (Tertiary — Age relative to other Tertiary rocks uncertain)
	Tuff of the Monitor Range (Miocene and Oligocene)
Tmu	Upper unit
Tml	Lower unit
Thc	Tuff of Hot Creek Canyon (Oligocene)
Twb	Windous Butte Formation (Oligocene)
Twr	Tuff of Williams Ridge and Morey Peak (Oligocene)
Ta	Intermediate lavas (Oligocene)
Tr	Rhyolite lavas (Oligocene)
PIPc	Dark-gray to black chert and shale (Permian and Pennsylvanian)
Pzr	Paleozoic rocks — Stippled where brecciated

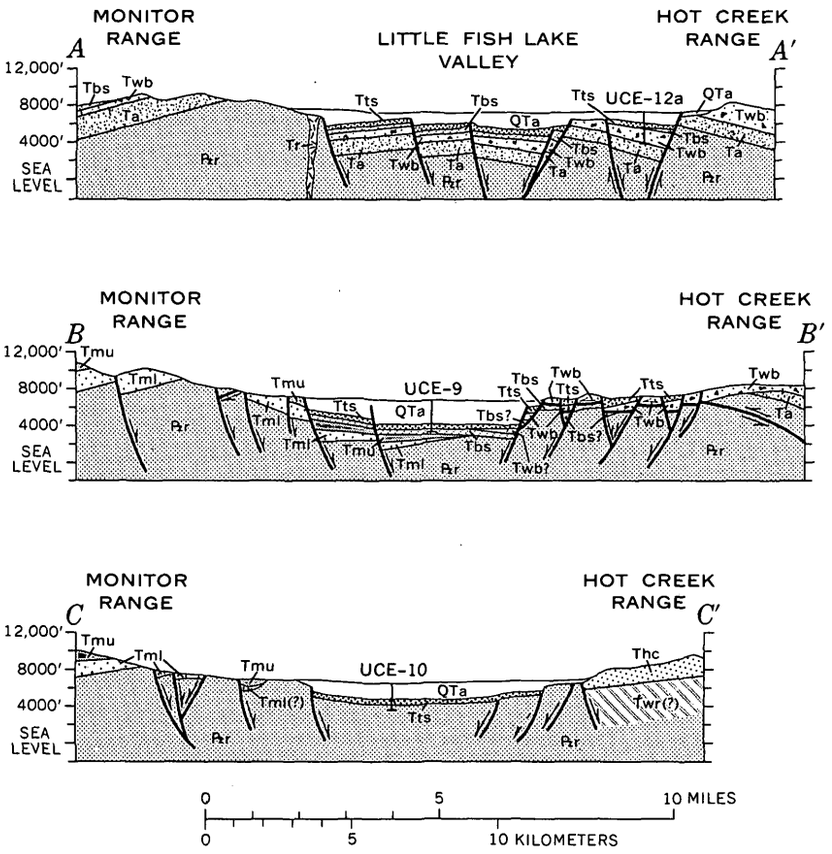

35 Contact — showing dip

60 Fault — Showing dip. Dashed where approximately located or inferred; dotted where concealed. Bar and ball on downthrown side; arrows show direction of inferred relative movement

Low-angle fault of compressional or gravity-slide origin — Approximately located; dotted where concealed. Sawteeth on upper plate

Cracked and broken rock — Showing random dips

Trace of axial plane of anticline — Approximately located

22 Strike and dip of beds

25 Strike and dip of eutaxitic structure in welded tuff

105, 106 Fossil locality

UCE-12a Exploratory drill hole

Figure 2.—Continued.

Paleozoic age in the Monitor Range south of Tulle Creek which are mapped as allochthonous.

The oldest Tertiary rocks are rhyolite lavas that constitute discontinuous piles in the Hot Creek Range and in the Monitor Range north of Tulle Creek. Most of the rhyolite is crystal poor, nearly aphyric, but some flows at the top of the pile in

the Hot Creek Range are crystal rich and grade in composition toward quartz latite. East of the Hot Creek Range, in the Moores Station quadrangle (Ekren and others, 1973), the rhyolite lavas were dated by R. F. Marvin (written commun., 1970) at 37.2±1.0 m.y.

The rhyolites are overlain locally by intermediate lavas that range in composition from andesite to quartz latite. The intermediate lavas underlie the north half of the valley and are widespread to the north and east, nearly blanketing the Pritchards Station quadrangle and the next 15-minute quadrangle to the east. Near Ninemile Peak, about 16 km (10 mi) north of Little Fish Lake Valley, the intermediate lavas have been dated at 35.2±1.1 m.y. (F. J. Kleinhampl and R. F. Marvin, written commun., 1971). Phenocryst compositions of the principal volcanic rocks discussed are shown by histograms in figure 3.

Along the northeast and northwest flanks of the valley the intermediate lavas are overlain by the Windous Butte Formation (Cook, 1965). The Windous Butte consists of a hundred meters or more of rhyolitic welded tuff that grades upward to a thick quartz latitic caprock (fig. 3). The unit is as much as 480 m (1,600 ft) thick in the Hot Creek Range, 390 m (1,300 ft) thick in drill hole UCE-12a in northeastern Little Fish Lake Valley, and about 60 m (200 ft) thick in the Monitor Range north of Tulle Creek. It is not present in the Monitor Range south of Tulle Creek. The age, paleomagnetic properties, and areal distribution of the Windous Butte are discussed by Grommé, McKee, and Blake (1972), who concluded that the unit is 30.7 m.y. old and that it has a reversed magnetic polarity.

At Morey Peak in the southeastern part of the mapped area a thick prism of welded tuff, the tuff of Williams Ridge and Morey Peak, occurs which is at least 910 m (3,000 ft) thick. W. J. Carr (written commun., 1972) concluded that this tuff lies within a resurged part of a large caldera. The tuff is lithologically similar to the upper quartz latitic part of the Windous Butte Formation, and potassium-argon analyses indicate that the two units are virtually the same age. The Windous Butte is inferred to have been extruded from either the Morey Peak area or another part of the central Nevada caldera complex that lies east of Morey Peak (U.S. Geological Survey, 1970, p. A39–A40).

Welded tuffs younger than the tuff of Williams Ridge and Morey Peak crop out on the west flank of Morey Peak; the principal one of these tuffs is the tuff of Hot Creek Canyon, which consists of several ash-flow tuff cooling units (H. W. Dodge, Jr., unpub. data). These cooling units are compositionally zoned from rhyolitic bases to quartz latitic tops (no "representative" histograms are shown in fig. 3). Potassium-argon analyses indicate that they are between 28 and 30 m.y. old. The tuff of Hot Creek Canyon is overlain by the Shingle Pass Tuff (fig. 2) and also by local units in the vicinity of Morey Peak (H. W. Dodge, Jr., unpub. data).

In the Monitor Range, south of Tulle Creek, the ash-flow

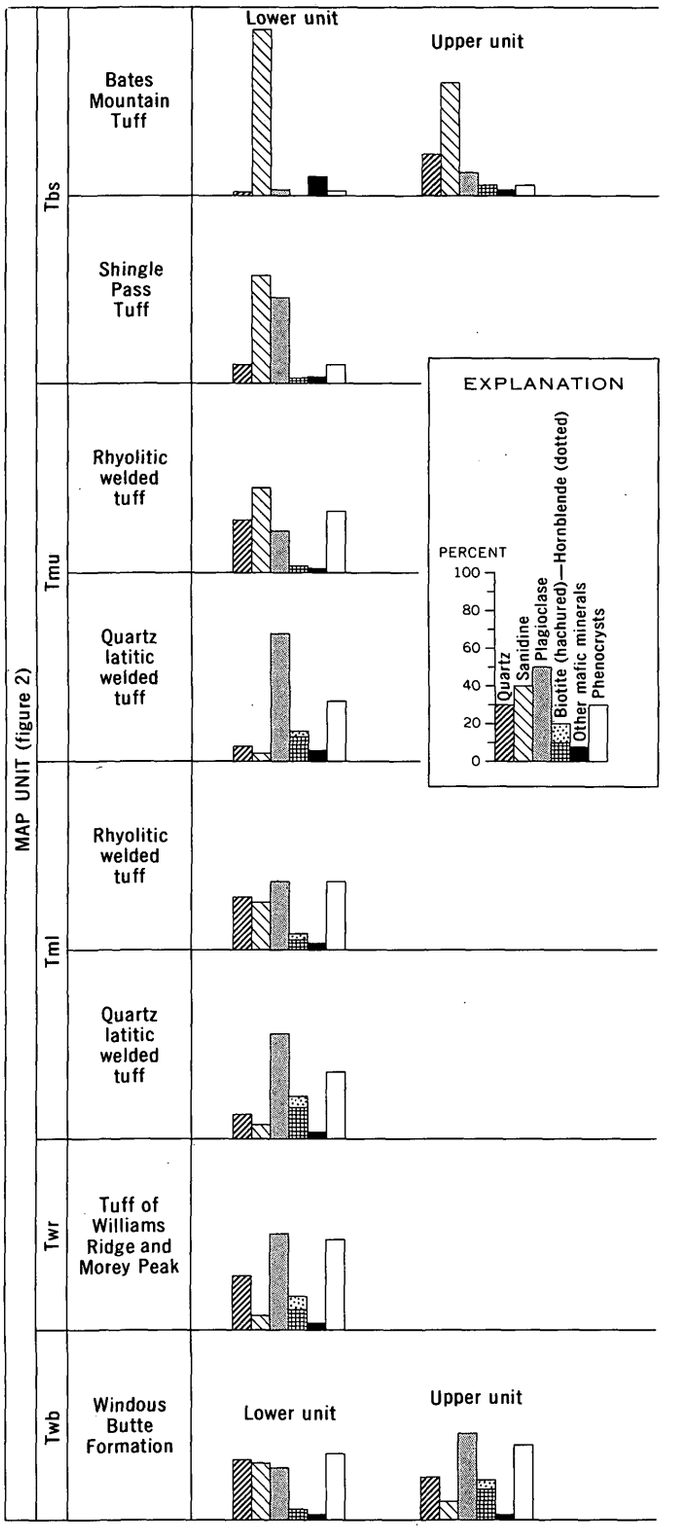

Figure 3.—Histograms showing volume of phenocrysts and abundance of six crystal components of principal volcanic rocks of Little Fish Lake Valley area.

tuffs are divided into two units. The lower unit of the Monitor Range (fig. 2) is rhyolite and quartz latite tuffs, highly altered in most exposures and superficially resembling the tuff of Hot Creek Canyon. The upper unit of the Monitor Range includes three ash-flow tuff cooling units. The lowest two are quartz latitic mafic-rich tuffs which have been dated at 26.5±0.7 m.y. (R. F. Marvin, written commun., 1972). The upper most cooling unit is rhyolitic and relatively poor in mafic minerals.

North of Tulle Creek, within the mapped area, the tuffs of the Monitor Range, which are thick and widespread south of the creek, are absent and several local tuffs of the northern Monitor Range are present. In the vicinity of a fault wedge of Pennsylvanian-Permian black chert and shale the exposed tuff is nonwelded to partially welded, highly altered, and unlike either the lower unit or the upper unit of the Monitor Range exposed south of the creek. This altered tuff is overlain by a distinctive quartz-rich mafic-poor tuff that has not been recognized south of Tulle Creek. Both the altered partially welded tuff and the quartz-rich tuff are inferred to be younger than the Windous Butte which rests depositionally on the intermediate lavas.

The Shingle Pass Tuff is present at the south end of Little Fish Lake Valley, on dip slopes of the Hot Creek Range, and in drill holes UCE-9 and -12a. Except for a landslide mass north of Tulle Creek it is not present in the Monitor Range north of the south boundary of the map (fig. 2). The Bates Mountain Tuff (Stewart and McKee, 1968; Sargent and McKee, 1969) is present in both ranges and in drill hole UCE-9. It has been dated at 23.1±0.6 m.y. (Grommé and others, 1972), and the Shingle Pass has been dated at 25.1±1.0 m.y. (Sargent and McKee, 1969).

Those tuffs in the mapped area exclusive of the Shingle Pass and Bates Mountain are typically calc-alkaline, and certain nearly identical lithologies occur in many different cooling units. In contrast, the Bates Mountain and Shingle Pass Tuffs are phenocryst poor, rich in alkali feldspar, and provide very distinctive marker horizons.

Overlying the Shingle Pass and Bates Mountain Tuffs along the east flank of Little Fish Lake Valley are tuffaceous sedimentary rocks that include weakly lithified conglomeratic mudstone, reworked bedded tuff, zones of thin-bedded Paleozoic debris, and very thin bedded yellow-weathering argillaceous limestone. One fossil locality in this sedimentary unit found by E. N. Hinrichs (105, fig. 2) yielded 64 vertebrate fragments. These were examined by G. E. Lewis (written commun., 1967), who reported that six fragments are referable to a small equid characteristic of the upper part of the Miocene. Another locality (106) yielded 42 fragments, 4 of them referable to a camelid, genus and species indeterminate, of medium size comparable to that of the genus *Procamelus* (whose age range is late Miocene to early Pliocene). These strata are very similar to, and probably the same age as, tuffaceous sediments that overlie the Shingle Pass Tuff in the northwestern part of the Moores Station quadrangle (Ekren and others, 1973). Rocks of similar lithology were found at the base of the valley fill in the three drill holes in Little Fish Lake Valley. We infer, therefore, that these rocks constitute the oldest graben-filling sediments and that locally they have been relatively uplifted, tilted, and exposed to erosion. The dissection and exposure of the older alluvium in Little Fish Lake Valley is due in part to the effective lowering of the base level in the valley following the breaching of the valley at its south end by the headwaters of Hot Creek.

Along the east flank of the Hot Creek Range (loc. E, fig. 2), adjacent to a north-trending fault, is a sequence of stratified breccia derived principally from the Windous Butte tuff. The breccia is interbedded with ash-fall tuff. The stratified breccia is as much as 60 m (200 ft) thick and reflects rapid accumulation of debris and landslipped blocks presumably shed from the adjacent footwall block lying to the east that has been completely denuded of volcanic strata. The possibility that this deposit accumulated during a period of strike-slip movement in the area is discussed in the following section on structure.

The valley-filling alluvium, as indicated by cuttings and a few cores from the three drill holes, consists mostly of gravel and sand and interbeds of silt and mud. The coarsest material was in drill hole UCE-12a (the hole nearest to bedrock source terrane), and the finest in UCE-10 where the strata are mainly of lacustrine origin. The abundance of lacustrine strata in drill hole UCE-10, which is adjacent to a present-day temporal lake, suggests that lakes have existed in the south-central part of the valley from the beginning of graben development.

STRUCTURE

Little Fish Lake Valley (fig. 1) is a nearly symmetrical graben (Stewart, 1971) that lies in the central Great Basin, equidistant between Lake Tahoe in the Sierra Nevada and the Hurricane fault at the edge of the Colorado Plateau. Along the latitude of Little Fish Lake Valley, the ranges of the Great Basin display a well-defined symmetry (fig. 4). East of Little Fish Lake Valley nearly all the ranges, as defined by Tertiary strata, dip to the east; west of the valley most dip to the west. This anticlinal symmetry does not persist throughout the Great Basin (Stewart, 1971), although, in general, most of the ranges in the east half of the Great Basin dip to the east and most in the west half dip to the west.

Little Fish Lake Valley and Monitor Valley to its west are the two highest valleys in the Great Basin and lie within a regional gravity low (fig. 5). If isostatic balance is assumed (Pakiser, 1963; Mabey, 1960), the crust in the area of Little Fish Lake and Monitor Valleys is thicker than is normal for the Great Basin. Seismic data support the inference that the crust is thicker in this central zone (Eaton, 1963; Hill and Pakiser, 1966; Warren, 1968; and Prodehl, 1970). The central area of high average altitude in the central Great Basin and its general relation to gravity is shown by Gilluly (1970, fig. 1,

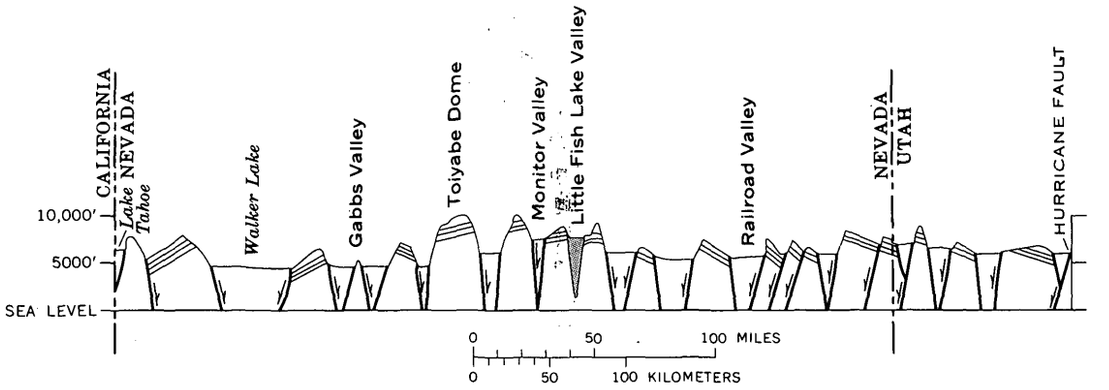

Figure 4.—Schematic cross section between Lake Tahoe, Nevada-California, and the Hurricane fault, Utah, showing medial location of Little Fish Lake Valley and its relationship with east-dipping and west-dipping fault blocks. Vertical exaggeration approximately X20. Dips not exaggerated, but generalized. Attitudes of blocks west of Monitor Valley from Kleinhampl and Ziony (1967), Calkins and Thayer (1945), Reid (1911), and Smith (1904). Attitudes in Utah from Mackin (1960). All others are based on our own observations.

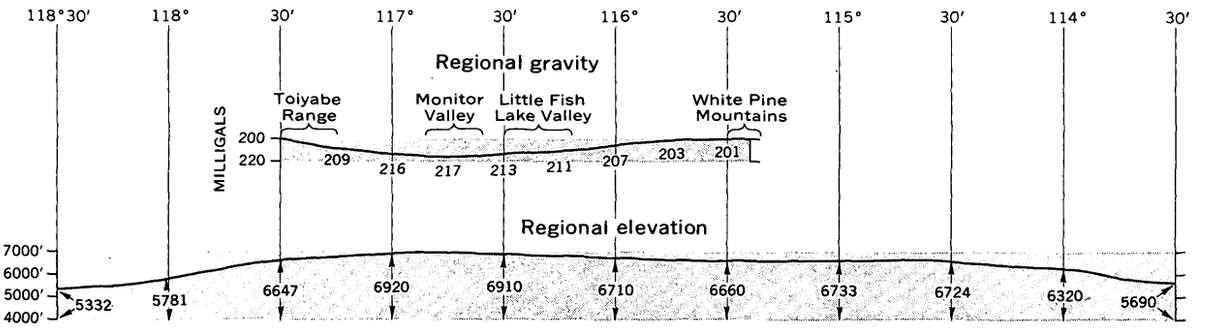

Figure 5.—Profiles comparing surface elevations averaged over an 80-km (49-mi) radius and regional gravity along latitude 39° N. Data from Diment, Stewart, and Roller (1961), Mabey (1960), and our own surveys.

p. 48). The north-trending valley is superimposed on several east-trending aeromagnetic discontinuties: one of these can be traced for a distance of 64 km (40 mi) eastward from Tulle Creek in the Monitor Range (figs. 2, 6) through the Pritchards Station quadrangle. On the following pages this discontinuity will be referred to as the Tulle Creek-Pritchards Station lineament. The exact nature of the lineament is in doubt, but during part of its history, it has been a strike-slip fault.

Tulle Creek-Pritchards Station lineament and other east-trending magnetic features

The Tulle Creek-Pritchards Station lineament on the aeromagnetic map (fig. 6) separates a northern area underlain by thick normally polarized intermediate lavas, which are associated with strong magnetic highs, from a southern area underlain by reversely polarized welded tuffs and local rhyolite-quartz latite lavas that give rise to magnetic lows. This magnetic discontinuity can be traced across Little Fish Lake Valley beneath the valley-fill alluvium and also beneath the Windous Butte Formation in the Hot Creek Range. There is no surface expression of the lineament in either the valley or the Hot Creek Range. At Tulle Creek in the Monitor Range, however, the lineament coincides with a major east-west fault, and in the Pritchards Station quadrangle it coincides with an east-trending zone interpreted by Dixon, Hedlund, and Ekren (1973) as a left-lateral transcurrent fault.

The major fault at Tulle Creek juxtaposes different Oligocene volcanic strata and places a block of Paleozoic strata on the south, which contains a thick sequence of Pennsylvanian-Permian black chert and shale, against a block to the north that contains little chert and shale. F. J. Kleinhampl and J. I. Ziony (written commun., 1972) consider the black chert and shale sequence to be part of an upper plate that presumably was thrust from west to east. Although the authors are well aware of the fact that numerous explanations can account for the virtual absence of the chert sequence north of the Tulle Creek fault, that absence is consistent with an interpretation

of left-lateral strike-slip faulting—movement of the northern block westward with respect to the southern block. A wedge of black chert caught between two branches of the Tulle Creek fault (fig. 2) seemingly is best accounted for as having been dragged to this position by left-lateral movement along the fault. The stratigraphic relationships of the Tertiary volcanic rocks likewise support a left-lateral strike-slip fault interpretation. For example, north of the Tulle Creek fault the Paleozoic rocks are overlain directly by at least 450 m (1,500 ft) of intermediate lavas (principally andesite and quartz latite). The lavas are absent south of Tulle Creek except for a small slide mass that is intercalated in the lower unit of the tuff of Monitor Range and a thin andesitic flow(?) less than 15 m (50 ft) thick that rests on Paleozoic strata in a fault block north of Danville Canyon (not shown on fig. 2). The andesite at Danville Canyon, however, is nearly aphyric and does not have a counterpart north of Tulle Creek; it could be a thin sill or dike. The virtual absence of the andesite lavas south of the Tulle Creek fault and the juxtaposition along the fault of Windous Butte Formation and thick piles of ash-flow tuff (lower tuffs of the Monitor Range, fig. 2), which are unknown in exposures to the east, are most easily explained by left-lateral strike-slip movements along the Tulle Creek fault.

East of the mapped area in the Pritchards Station quadrangle (Dixon and others, 1973), the relations are very similar to those at Tulle Creek in the Monitor Range. The aeromagnetic lineament (fig. 6) coincides with an east-trending fault zone that separates contrasting Tertiary volcanic sequences. North of the fault zone the Windous Butte Formation is as much as 485 m (1,600 ft) thick, and the underlying intermediate lavas, together with an older welded tuff, the Stone Cabin Formation (Cook, 1965), are 300–600 m (1,000–2,000 ft) thick. South of the fault zone between lat 38°45′ and 38°40′ the Windous Butte is present only as parts of large completely brecciated allochthonous masses that include intermediate lavas and the Stone Cabin. Autochthonous intermediate lavas and the underlying Stone Cabin are present for about 1.6 km (1 mi) south of the fault zone. Apparent offsets of the contact between Stone Cabin Formation and intermediate lavas suggest from 3 to 10 km (2–6 mi) of left-lateral offset across the fault zone. The allochthonous masses south of the fault zone are not easily accounted for as simple gravity-slide blocks, because they occur at virtually the same elevations as their in situ counterparts north of the fault zone. The masses appear to be best explained as remnants of a thrust plate associated with strike-slip movement along the east-trending fault zone.

In the Hot Creek Range (figs. 2, 6), we infer that the Tulle Creek-Pritchards Station strike-slip fault passes into a low-angle thrust which shoulders or shoals along the belt of Paleozoic rocks exposed north of Morey Peak. The low-angle fault dips northward, and the upper plate is inferred to progressively thicken northward. At some location beneath the range the fault probably approaches a vertical attitude. This location does not necessarily coincide precisely with the aeromagnetic lineament (fig. 6). The thrusting is somewhat analogous to that described by Sharp (1967, p. 710, 711, fig. 3, pl. 1) along the right-lateral strike-slip San Jacinto and Coyote Creek faults in the Peninsular Ranges of southern California. Our interpretation of thrusting in the Hot Creek Range is based on (1) the direct observation of a low-angle fault that dips 20°–30° N. at locality A (fig. 2), (2) intense local brecciation where the Windous Butte Formation abuts older volcanic rocks or Paleozoic rocks along the south edge of the plate (fig. 2), (3) the occurrence of an anticlinal fold that affects only upper-plate rocks south of the Tulle Creek-Pritchards Station lineament, and (4) the occurrence of several normal faults that affect only the upper-plate rocks. At locality A (fig. 2), the upper plate consists of the uppermost part of the Windous Butte Formation. The tuff is brecciated, and attitudes are chaotic. Between localities A and B the upper plate rests on or abuts the old rhyolite, and very little brecciation occurs there. In this area abundant north-trending normal faults (only two of which are shown in fig. 2) consistently drop the strata down to the west. These faults appear to be entirely confined to the upper plate and have displacements ranging from 3.0 m (10 ft) or less to as much as 46 m (150 ft). Their cumulative effect is to greatly thin and extend the upper plate. At locality B, the rhyolite lava is cut out and the upper plate is again badly broken where it rests directly on Paleozoic strata. Between localities B and C, two normal faults in the upper plate cannot be traced into the underlying Paleozoic rocks. They appear to merge with the sole of the thrust. At locality C the rhyolite is not brecciated where the fault is inferred to pass between the rhyolite and Paleozoic rocks, but the Paleozoic rocks are badly fractured and, adjacent to the rhyolite, strike parallel to the fault contact. At locality D the upper plate, consisting of the Windous Butte (and including the Bates Mountain Tuff at the north end of the ridge) is locally crackled throughout. It rests directly on Paleozoic rocks along the southeast flank of the ridge and on the Bates Mountain Tuff at the southwest end of the ridge. The Bates Mountain Tuff in this locality includes the tuff of Pott Hole Valley, which is about 25 m.y. old, based on K-Ar dates of underlying and overlying strata. The tuff of Pott Hole Valley appears to be in depositional contact with the Paleozoic rocks. The structural inversion of the Windous Butte over a much younger tuff and the fact that the Bates Mountain Tuff is involved in the thrusting place a definite lower limit of 23 m.y. on the age of thrusting and associated strike-slip faulting. In this area tuffaceous sediments containing equid and camelid fossils of late Miocene and (or) early Pliocene age are faulted down against the plate (fig. 2). This places an upper limit on the age of sliding and probably also dates the onset of valley formation. (See discussion on valley configuration.)

At locality E, a north-trending fault drops the upper plate down to the west exposing the lower plate, which consists of brecciated strata ranging in age from Ordovician to Permian.

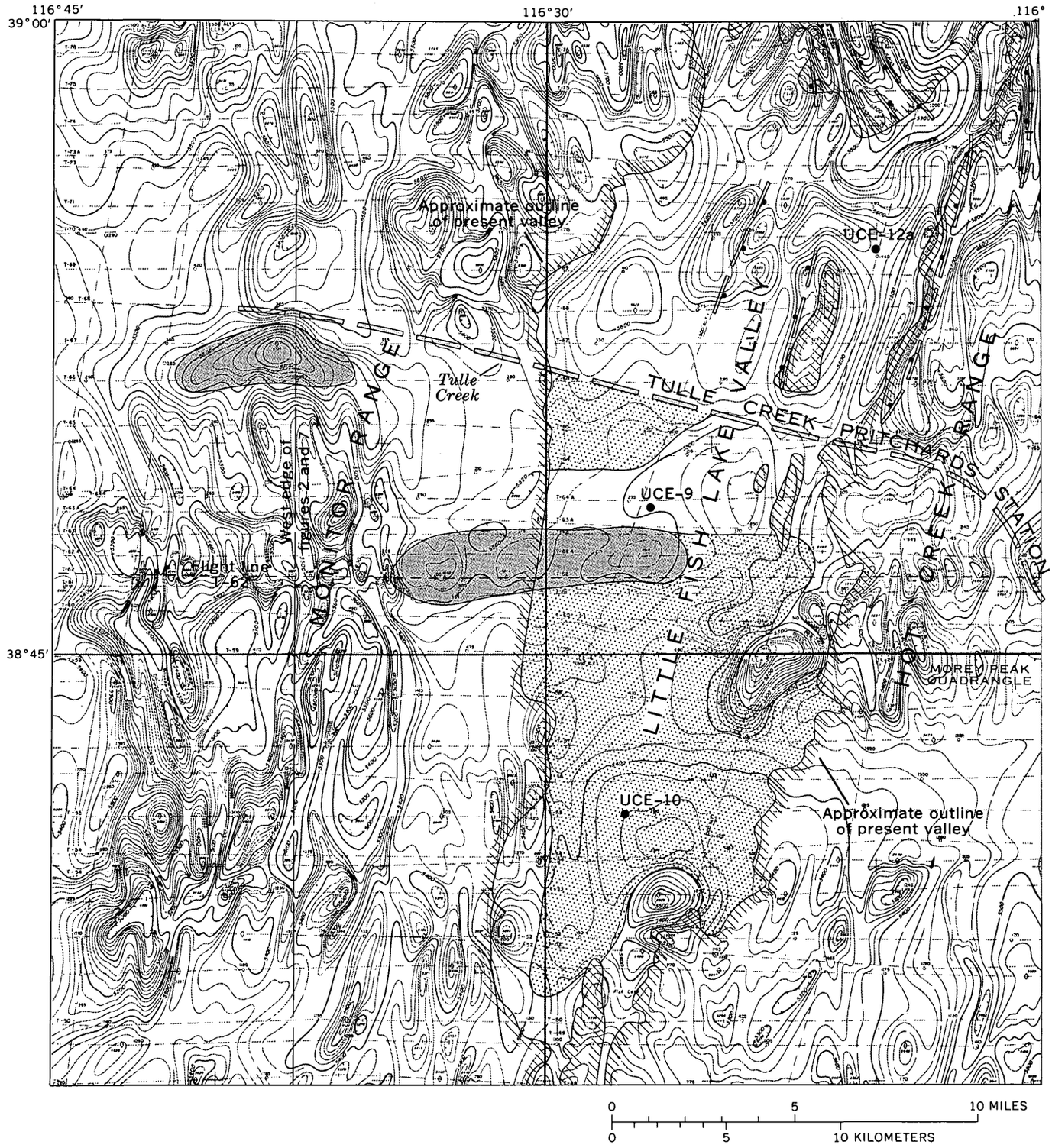

Figure 6.—Aeromagnetic map of Little Fish Lake Valley area, showing location of Tulle Creek-Pritchards Station lineament and alined edges

Contour interval 20 gammas. Magnetic contours from

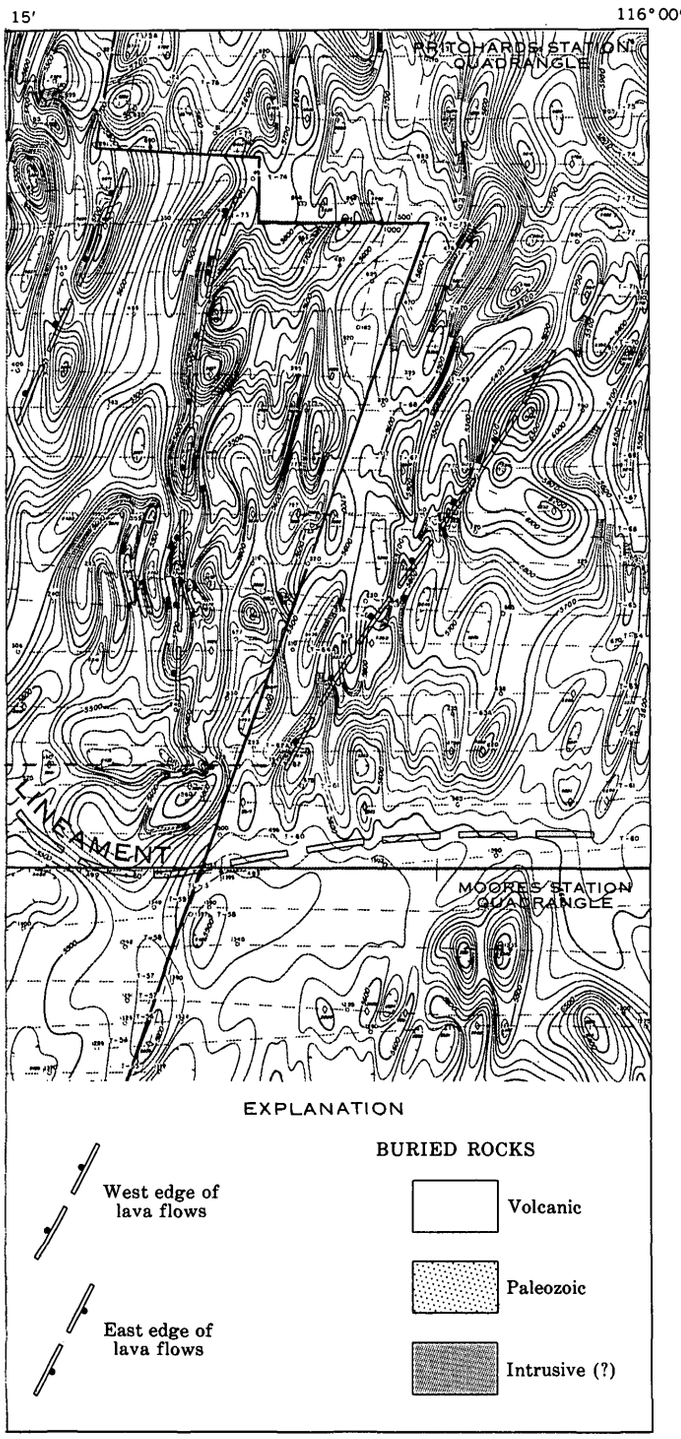

of lava flows, and showing inferred distribution of buried rocks.

U.S. Geological Survey (1968).

The beds in the upper plate include the Windous Butte Formation, the tuffs of Crested Wheat Ridge, and the Shingle Pass and Bates Mountain Tuffs. These are overlain by 61+ m (200+ ft) of stratified breccia (fig. 2) that dips 50° E. The breccia is composed of fragments of upper-plate rocks that range in size from less than 3 cm (1 in.) to large blocks 10 m or more long. Interbeds of nonwelded ash-fall tuff indicate that this breccia accumulated during a period when tuff vents were still active, probably in areas west of Little Fish Lake Valley. The north-trending fault plane is concealed by breccia debris, but judged from the positioning of breccia against the Paleozoic rocks the plane probably dips no steeper than about 40° W. The breccia must have been derived from broken upper-plate rocks that lay to the east, and it probably accumulated simultaneously with active thrusting. Upcanyon from locality E, thin latite lavas which are interbedded with tuffaceous conglomerate containing subrounded cobbles of intermediate lavas crop out. These strata dip 30° E. in the easternmost exposures but flatten to about 15° where they overlie Paleozoic rocks and rhyolite lava. The Windous Butte rests depositionally on these strata with a 10°–20° angular unconformity. The unconformity indicates that some tilting and erosion occurred after the extrusion of intermediate lavas and before the deposition of the Windous Butte. The base of the upper plate is believed to be below the canyon level in this area. On the south side of the canyon, a fault plane is exposed that dips 60° S. and displays slickensides ranging from vertical to horizontal. The fault drops the Windous Butte, Bates Mountain, and Shingle Pass Tuffs (fig. 2) against Paleozoic rocks near the upper end of the canyon, and near the lower end it swings northward to drop the younger tuffs against bedded conglomerate and the Windous Butte. The rocks in the downthrown block of this fault are badly fractured and in places completely brecciated. The degree of fracturing suggests that this fault is not a simple normal fault. Despite its curvature, it probably has an appreciable component of lateral displacement, and it separates an area to the south characterized by abundant normal faults (described above) from an area to the north that has few normal faults.

The Paleozoic rocks exposed south of the volcanic rocks (locs. A–C, fig. 2) are highly fractured in all exposures, and locally they are intensely brecciated. According to H. W. Dodge, Jr. (oral commun., 1972), the brecciation is compatible with shallow-depth deformation and the possibility exists, therefore, that the low-angle faults in the Palezoic rocks are Tertiary in age. If this is true, there is no evidence to indicate whether, or in what manner, such faults might be related to the deformation that affected the volcanic strata.

The aeromagnetic map (fig. 6) shows a pronounced discontinuity where the volcanic rocks abut Paleozoic strata to the south of the Tulle Creek-Pritchards Station lineament. This discontinuity coincides closely with the south edge of the upper plate. In this area, however, unaltered rhyolite lavas in the lower plate probably contribute to the magnetic anoma-

lies. The strong magnetic low at the edge of the valley is possibly caused by a thick pile of buried strongly reverse-magnetized quartz latitic lava that in surface exposures rests on the old rhyolite and was mapped with the rhyolite (fig. 2).

Between the southernmost discontinuity (fig. 6) and the Tulle Creek–Pritchards Station lineament is an east-trending anomalous zone characterized by a series of small highs and lows. These are almost entirely confined to a single flight line (T-62, fig. 6) and probably are due principally to a datum shift along that flight line. Along the east flank of the Monitor Range in the vicinity of Danville Canyon (fig. 6), however, and extending out into the valley, magnetic rocks are indicated by aeromagnetic data even where surface outcrops are either Paleozoic rocks or intensely altered tuffs that are almost nonmagnetic. In this vicinity and in the Green Monster Canyon area (fig. 6) the rocks are locally impregnated with copper sulfides and are intruded by a few thin dikes. The magnetic anomalies therefore could reflect a buried east-trending intrusive mass.

The fact that the Tulle Creek-Pritchards Station lineament virtually forms the south boundary of the intermediate lavas for a distance of at least 64 km (40 mi) (despite the fact that where the lineament surfaces no enormous lateral displacements are required to explain all the stratigraphic relationships) suggests that the lineament is a deep-seated structure which first served as a volcanic province boundary and then became an active strike-slip fault zone.

Valley configuration

Gravity data (fig. 7) define a symmetrical low which is centered on drill hole UCE-9 in the west half of Little Fish Lake Valley, and a smaller low centered on UCE-12a at the northeast end of the valley. The southern terminus of the low at UCE-12a is defined by the -225 mGal contour line that coincides fairly closely with the buried Tulle Creek-Pritchards Station lineament. The lineament serves not only as a terminus to the low at UCE-12a but also as a structural boundary that divides the valley into two parts that have decidedly different tectonic styles. North of the Tulle Creek-Pritchards Station aeromagnetic lineament, the valley is anticlinal, the Monitor Range dipping westward and the Hot Creek Range dipping eastward. South of the lineament, both ranges dip westward and the valley is synclinal; the strata exposed in fault blocks on the flanks of both ranges dip toward the valley.

Drill hole UCE-12a cut 450 m (1,500 ft) of alluvium, 15 m (50 ft) of Bates Mountain Tuff, 85 m (280 ft) of tuffs of Crested Wheat Ridge (Dixon and others, 1973), 400 m (1,300 ft) of Windous Butte Formation, and bottomed in andesite lava at a depth of 975 m (3,200 ft). A downdropped block exposed southwest of the drill hole (fig. 2) dips 15°–20° E. into a boundary fault or faults having about 1,520 m (5,000 ft) of stratigraphic displacement. This east-dipping block has the same attitude as the Hot Creek Range to the east. Similarly, on the western flank of the valley along section $A–A'$ (fig. 2), the buried blocks are inferred to dip west into western bounding faults. This interpretation is based on the character of the magnetic profiles over buried faulted blocks where "edges" develop as a result of faulting. Magnetic highs are positioned over the tilted normally magnetized lava on the upthrown blocks, and magnetic lows are positioned over the downthrown blocks. The profile resulting from a west-dipping fault block is a mirror image of the profile over an east-dipping block.

In the southern part of the valley in the vicinity of drill hole UCE-9, (section $B–B'$, fig. 2), where the deepest gravity low occurs in little Fish Lake Valley and, by inference, the thickest combined alluvial-volcanic fill is present, displacement at the west margin of the graben is distributed across several faults that are down to the east and have a combined throw of at least 1,820 m (6,000 ft). These faults include northeast-trending normal faults and a major younger north-trending fault that parallels the margin of the graben as defined by gravity data. One northeast-trending fault, however, projects out into the valley, as evidenced by a recent fault scarp in the alluvium. The upper unit of the Monitor Range on the downthrown block adjacent to the valley (section $B–B'$) dips about 30° toward the valley. The attitude of these blocks contrasts with the previously noted attitudes of the downthrown blocks along the flanks of the valley to the north (section $A–A'$). Along section $B–B'$, drill hole UCE-9 cut 850 m (2,800 ft) of alluvial fill and tuffaceous sediments underlain in turn by the Bates Mountain and Shingle Pass Tuffs. The latter two units together are only 75 m (250 ft) thick, a thickness comparable to that where they are preserved in the flanking ranges. The hole bottomed at a depth of 1,000 m (3,295 ft) in bedded tuff and tuffaceous sandstone which apparently correlate with bedded strata that crop out beneath the Shingle Pass Tuff adjacent to the mapped area on the south. In the vicinity of section $C–C'$ (fig. 2) and southward along the west flank of the valley, the downthrown fault blocks adjacent to the valley dip inward. This dip of volcanic rocks away from the ranges gives the deceptive appearance of younger volcanic rocks lapping up on older fault blocks.

Combined geologic and geophysical data indicate that the southern half of Little Fish Lake Valley is superimposed on a prevalley topographic high that either was never covered by volcanic rocks or was stripped of volcanic rocks by erosion before development of the valley. Gravity calculations based on densities of alluvium and volcanic rock that were obtained from geophysical logs (drill holes UCE-9, UCE-12a, UCE-10) indicate that Paleozoic rocks probably are within 1,460 m (4,800 ft) of the surface at drill hole UCE-9, or about 460 m (1,500 ft) below the hole bottom. The valley fill in a considerable area south of UCE-9 is probably underlain directly by Paleozoic rocks, as suggested by a strikingly featureless aeromagnetic configuration which extends from this area into Paleozoic outcrops in the Hot Creek Range and near locality D (fig. 2), about 5 m (3 mi) southeast of UCE-9.

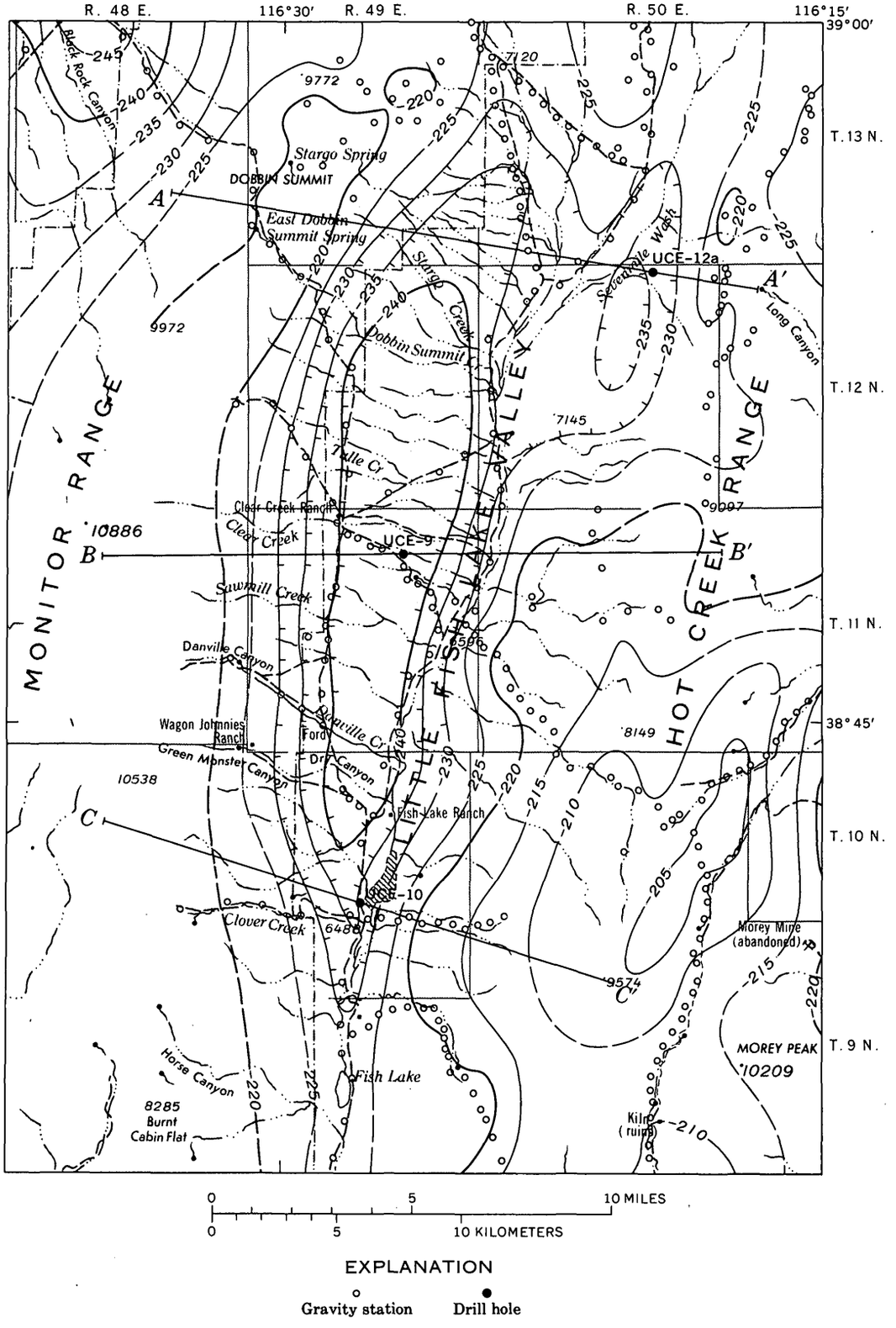

Figure 7.–Complete Bouguer gravity anomaly map of Little Fish Lake Valley area. Contours are dashed where approximately located; hachures indicate closed areas of lower gravity. Interval is 5 mGal. Contours by D. L. Healey. Base from U.S. Geological Survey, Tonopah 1:250,000 quadrangle, 1956–62.

That Paleozoic rocks directly underlie the valley fill in this area is confirmed by data from drill hole UCE-10, which bottomed in massive relatively unfractured dolomite of probable Devonian age at a depth of 903 m (2,963 ft) after cutting 810 m (2,660 ft) of valley-fill alluvium. The occurrence of valley-fill alluvium directly above Paleozoic strata in parts of the valley indicates that the valley is younger than the youngest ash-flow tuff, which was dated at about 23 m.y.

The data indicate that valley formation began in late Miocene or early Pliocene time, and it is inferred to have extended through Pliocene time. Late Miocene or early Pliocene valley formation is suggested by Gilluly and Masursky (1965) for valleys in the Cortez area to the north, by Noble, McKee, Smith, and Korringa (1970) for valleys in northwestern Nevada, by Ekren, Rogers, Anderson, and Orkild (1968) in the Nevada Test Site to the south-southeast, and by Anderson, Longwell, Armstrong, and Marvin (1972) and Anderson (1971a) for valleys in the Lake Mead area in the southern part of the Great Basin. We concur with Stewart (1971), who suggested that most basin-and-range structure in central Nevada is late Cenozoic in age and probably is younger than 17 m.y.

SUMMARY OF CENOZOIC EVENTS

Volcanism started in the Little Fish Lake Valley area in Oligocene time about 37 m.y. ago with the eruption of discontinuous piles of virtually aphyric rhyolite lava. Extensive sheets of intermediate lavas were then erupted north of a line that now corresponds to the Tulle Creek-Pritchards Station lineament, and we infer that this distribution conforms closely to the original distribution. Locally, eruption of the sheets was followed by tilting and erosion. About 33 m.y. ago eruption of ash-flow tuff started and it continued through about 23 m.y. ago. Some of these eruptions were from centers located marginal to Little Fish Lake Valley—the center closest to the valley is at Morey Peak. Left-lateral movement along the Tulle Creek-Pritchards Station lineament commenced after the deposition of the Bates Mountain Tuff (23 m.y. ago) but had ceased before the development of the Little Fish Lake Valley graben and the deposition of the earliest graben-filling sediments in late Miocene and early Pliocene time.

RELATIONSHIP OF LITTLE FISH LAKE VALLEY TO ORIGIN OF THE GREAT BASIN

An interrelationship must exist between the central location of Little Fish Lake Valley, the ancestral and present-day topographic and structural high, and the anticlinal symmetry of the Great Basin as reflected by range attitudes east and west of the valley. These features must be controlled by and must reflect the mechanism that gave rise to the basin-and-range province. The possibility that the central Great Basin was uplifted to form a north-trending anticline prior to block faulting seems remote for two reasons: (1) to establish a dip of even a few degrees on the flanks of the "anticline" would require an unrealistic central uplift of tens of thousands of meters, and such an uplift would have caused the erosion of much, if not all, of the volcanic strata along the axis of the uplift; and (2) the youngest ash flows found by drilling within the graben are also the youngest ash flows cropping out in broad areas on adjacent ranges. One fact seems inescapable, therefore: the block faulting and the east and west tilting of the ranges developed as a single process without an initial central uplift of large magnitude. The fact that Little Fish Lake Valley, however, remained relatively high until the graben actually formed and is topographically and structurally high today suggests that the central part of the Great Basin was constantly buoyed up during rifting of the province, possibly by the addition of new crustal material.

In Little Fish Lake Valley the rifting of the crust that gave rise to the present pattern of basins and ranges began several million years after the last ash-flow tuff was erupted, probably in late Miocene or early Pliocene time or about the same time inferred for basin-and-range development in other parts of the Great Basin. There apparently was no outward migration of basin-and-range faulting from a central area as suggested by Armstrong, Ekren, McKee, and Noble (1969). Certainly, no close time and space relationship exists between calc-alkaline ash-flow tuff volcanism in the central Great Basin and crustal rifting as expressed by the present pattern of basins and ranges. If, as postulated in this report, east-west magnetic lineaments were loci for strike-slip movements that predate the formation of grabens in the central Great Basin, then it is necessary to conclude that in parts of the Great Basin, transcurrent faulting has both preceded and developed concurrently with basin-and-range normal faulting (Shawe, 1965; Hamilton and Myers, 1966; Anderson, 1971a, b).

In the adjacent areas of the Great Basin the development of basins and ranges was accompanied by the eruption of rhyolite and basalt (McKee and Silberman, 1970; McKee, 1971). Christiansen and Lipman (1972) and Lipman, Prostka, and Christiansen (1972) related the inception of biomodal basalt-rhyolite volcanism and crustal extension with changes resulting from collision of the East Pacific Rise with a mid-Tertiary continental margin trench and the resulting direct contact of the American and eastern Pacific plates along a right-lateral transform fault system. McKee (1971) considered the possibility that the change in the type of volcanism noted above and the inception of basin-and-range faulting were caused by the East Pacific Rise reaching a position beneath the Great Basin 16 m.y. ago (see also Menard, 1964). Scholz, Barazangi, and Sbar (1971) postulated that the change was due to the termination of the early to middle Cenozoic west coast subduction zone about 25 m.y. ago, which released the compressive stress field and allowed extension to occur in the Great Basin. Whatever the reason for the development of the east-west zone of extension and the drastic change of volcanism that accompanied this development, any model of

plate tectonics must take into account the mounting evidence that the basins and ranges began to form at virtually the same time throughout the Great Basin.

ACKNOWLEDGMENTS

The Little Fish Lake Valley project was a multidisciplinary study that involved several geologists, geophysicists, and hydrologists who are not included herein as authors. Chief among these are F. J. Kleinhampl and J. I. Ziony, who mapped the Paleozoic rocks in the Monitor Range; K. A. Sargent and F. M. Byers, Jr., who mapped part of the volcanic rocks in the Monitor Range and supplied thin-section and chemical data; W. J. Carr, E. N. Hinrichs, H. W. Dodge, Jr., and F. M. Byers, Jr., who mapped part of the Hot Creek Range and east flank of Little Fish Lake Valley; D. L. Hoover, who supervised the exploratory drilling; and S. W. West, who supervised all hydrologic and related studies.

We acknowledge with gratitude and pleasure the thought-provoking ideas, constructive criticisms, and stimulating arguments offered by R. E. Anderson, R. C. Bucknam, and W. J. Carr.

REFERENCES CITED

Anderson, R. E., 1971a, Thin skin distension in Tertiary rocks of southeastern Nevada: Geol. Soc. America Bull., v. 82, no. 1, p. 43–58.

———1971b, Thin skin distension in Tertiary rocks of southeastern Nevada—Reply: Geol. Soc. America Bull., v. 82, no. 12, p. 3533–3536.

Anderson, R. E., Longwell, C. R., Armstrong, R. L., and Marvin, R. F., 1972, Significance of K-Ar ages of Tertiary rocks from the Lake Mead region, Nevada-Arizona: Geol. Soc. America Bull., v. 83, no. 2, p. 273–287.

Armstrong, R. L., Ekren, E. B., McKee, E. H., and Noble, D. C., 1969, Space-time relations of Cenozoic silicic volcanism in the Great Basin of the western United States: Am. Jour. Sci., v. 267, no. 4, p. 478–490.

Calkins, F. C., and Thayer, T. P., 1945, Preliminary geologic map of the Comstock Lode district, Nevada: U.S. Geol. Survey open-file rept.

Christiansen, R. L., and Lipman, P. W., 1972, Cenozoic volcanism and plate-tectonic evolution of the Western United States—[Pt.] 2. Late Cenozoic: Royal Soc. London Philos. Trans., v. 271, no. 1213, p. 249–284.

Cook, E. F., 1965, Stratigraphy of Tertiary volcanic rocks in eastern Nevada: Nevada Bur. Mines Rept. 11, 61 p.

Diment, W. H., Stewart, S. W., and Roller, J. C., 1961, Crustal structure from the Nevada Test Site to Kingman, Arizona, from seismic and gravity observations: Jour. Geophys. Research, v. 66, no. 1, p. 201–214.

Dixon, G. L., Hedlund, D. C. and Ekren, E. B., 1973, Geologic map of the Pritchards Station quadrangle, Nye County, Nevada: U.S. Geol. Survey Misc. Geol. Inv. Map I-728, scale 1:48,000.

Eaton, J. P., 1963, Crustal structure from San Francisco, California, to Eureka, Nevada, from seismic-refraction measurements: Jour. Geophys. Research, v. 68, no. 20, p. 5789–5806.

Ekren, E. B., Hinrichs, E. N., Quinlivan, W. D., and Hoover, D. L., 1973, Geologic map of the Moores Station quadrangle, Nye County, Nevada: U.S. Geol. Survey Misc. Geol. Inv. Map 1-756, scale 1:48,000. (In press.)

Ekren, E. B., Rogers, C. L., Anderson, R. E., and Orkild, P. P., 1968, Age of basin and range normal faults in Nevada Test Site and Nellis Air Force Range, Nevada, *in* Nevada Test Site: Geol. Soc. America Mem. 110, p. 247–250.

Gilluly, James, 1970, Crustal deformation in the western United States, *in* Johnson, Helgi, and Smith, B. L., eds., The megatectonics of continents and oceans: New Brunswick, N.J., Rutgers Univ. Press, p. 47–73.

Gilluly, James, and Masursky, Harold, 1965, Geology of the Cortez quadrangle, Nevada, with a section on Gravity and aeromagnetic surveys, by D. R. Mabey: U.S. Geol. Survey Bull. 1175, 117 p.

Grommé, C. S., McKee, E. H., and Blake, M. C., Jr., 1972, Paleomagnetic correlations and potassium-argon dating of middle Tertiary ash-flow sheets in the eastern Great Basin, Nevada and Utah: Geol. Soc. America Bull., v. 83, no. 6, p. 1619–1638.

Hamilton, Warren, and Myers, W. B., 1966, Cenozoic tectonics of the western United States, *in* The world rift system—Internat. Upper Mantle Comm., Symposium, Ottawa, 1965: Canada Geol. Survey Paper 66-14, p. 291–306; Rev. Geophysics, v. 4, no. 4, p. 509–549.

Hill, D. P., and Pakiser, L. C., 1966, Crustal structure between the Nevada Test Site and Boise, Idaho, from seismic-refraction measurements, *in* The earth beneath the continents—A volume of geophysical studies in honor of Merle A. Tuve: Am. Geophys. Union Mon. 10 (Natl. Acad. Sci.—Natl. Research Council Pub. 1467), p. 391–419.

Kleinhampl, F. J., and Ziony, J. I., 1967, Preliminary geologic map of northern Nye County, Nevada: U.S. Geol. Survey open-file map scale 1:200,000.

Lipman, P. W., Prostka, H. J., and Christiansen, R. L., 1972, Cenozoic volcanism and plate-tectonic evolution of the Western United States—[Pt.]1. Early and Middle Cenozoic: Royal Soc. London Philos. Trans., v. 271, no. 1213, p. 217–248.

Lowell, J. D., 1965, Lower and Middle Ordovician stratigraphy in the Hot Creek and Monitor Ranges, central Nevada: Geol. Soc. America Bull., v. 76, no. 2, p. 259–266.

Mabey, D. R., 1960, Regional gravity survey of part of the Basin and Range province, *in* Short papers in the geological sciences: U.S. Geol. Survey Prof. Paper 400-B, p. B283–B285.

Mackin, J. H., 1960, Structural significance of Tertiary volcanic rocks in southwestern Utah: Am. Jour. Sci., v. 258, no. 2, p. 81–131.

McKee, E. H., 1971, Tertiary igneous chronology of the Great Basin of western United States—Implications for tectonic models: Geol. Soc. America Bull., v. 82, no. 12, p. 3497–3501.

McKee, E. H., and Silberman, M. L., 1970, Geochronology of Tertiary igneous rocks in central Nevada: Geol. Soc. America Bull., v. 81, no. 8, p. 2317–2327.

Menard, H. W., 1964, Marine geology of the Pacific: New York, McGraw-Hill Inc., 271 p.

Merriam, C. W., 1963, Paleozoic rocks of Antelope Valley, Eureka and Nye Counties, Nevada: U.S. Geol. Survey Prof. Paper 423, 67 p.

Noble, D. C., McKee, E. H., Smith, J. G., and Korringa, M. K., 1970, Stratigraphy and geochronology of Miocene volcanic rocks in northwestern Nevada, *in* Geological Survey Research 1970: U.S. Geol. Survey Prof. Paper 700-D, p. D23–D32.

Nolan, T. B., Merriam, C. W., and Williams, J. S., 1956, The stratigraphic section in the vicinity of Eureka, Nevada: U.S. Geol. Survey Prof. Paper 276, 77 p.

Pakiser, L. C., 1963, Structure of the crust and upper mantle in the western United States: Jour. Geophys. Research, v. 68, no. 20, p. 5747–5756.

Prodehl, Claus, 1970, Seismic refraction study of crustal structure in the western United States: Geol. Soc. America Bull., v. 81, no. 9, p. 2629–2645.

Quinlivan, W. D., and Rogers, C. L., 1974, Geologic map of the Tybo quadrangle, Nye County, Nevada: U.S. Geol. Survey Misc. Geol. Inv. Map I-821, scale 1:48,000. (In press.)

Reid, J. A., 1911, The geomorphogeny of the Sierra Nevada northeast of Lake Tahoe [Nev.]: California Univ. Dept. Geology Bull. 6, p. 89–161, pl. 28, scale 1:125,000.

Sargent, K. A., and McKee, E. H., 1969, The Bates Mountain Tuff in northern Nye County, Nevada: U.S. Geol. Survey Bull. 1294-E, p. E1–E12.

Scholz, C. H., Barazangi, Muawia, and Sbar, M. L., 1971, Late Cenozoic evolution of the Great Basin, western United States, as an ensialic interarc basin: Geol. Soc. America Bull., v. 82, no. 11, p. 2979–2990.

Sharp, R. V., 1967, San Jacinto fault zone in the Peninsular Ranges of Southern California: Geol. Soc. America Bull., v. 78, no. 6, p. 705–729.

Shawe, D. R., 1965, Strike-slip control of Basin-Range structure indicated by historical faults in western Nevada: Geol. Soc. America Bull., v. 76, no. 12, p. 1361–1377.

Smith, D. T., 1904, The geology of the upper region of the main Walker River, Nevada: California Univ. Dept. Geology Bull., v. 4, p. 1–32.

Stewart, J. H., 1971, Basin and range structure—A system of horsts and grabens produced by deep-seated extension: Geol. Soc. America Bull., v. 82, no. 4, p. 1019–1043.

Stewart, J. H., and McKee, E. H., 1968, Geologic map of the Mount Callaghan quadrangle, Lander County, Nevada: U.S. Geol. Survey Geol. Quad. Map GQ-730, scale 1:62,500.

U.S. Geological Survey, 1968, Aeromagnetic map of the Hot Creek Range region, south-central Nevada: U.S. Geol. Survey Geophys. Inv. Map GP-637, scale 1:250,000.

——1970, Geological Survey research 1970: U.S. Geol. Survey Prof. Paper 700-A, 426 p.

Warren, D. H., 1968, Transcontinental geophysical survey (35°–39° N.) seismic refraction profiles of the crust and upper mantle from 112° W. longitude to the coast of California: U.S. Geol. Survey Misc. Geol. Inv. Map I-532-D, scale 1:1,000,000.

Winterer, E. L., and Murphy, M. A., 1960, Silurian reef complex and associated facies, central Nevada: Jour. Geology, v. 68, no. 2, p. 117-139.

Jour. Research U.S. Geol. Survey
Vol. 2, No. 1, Jan.-Feb. 1974, p. 119—123

RETENTION OF CHLORIDE IN THE UNSATURATED ZONE

By L. G. TOLER and S. J. POLLOCK, Boston, Mass.

Prepared in cooperation with Massachusetts Department of Public Works, Research and Materials Section

Abstract.—Some of the chloride from highway deicing salts (predominantly sodium chloride) that enters the ground is retained in the unsaturated zone. At a test site in sand and silt at Chelmsford, Mass., the amount of chloride retained in the unsaturated zone to a depth of 4.6 m (15 ft), ranged from 15 to 55 percent of the annual amount applied to the highways as sodium chloride from 1965 to 1969. Grain size of the soil materials, depth to the water table, and amount and seasonal distribution of precipitation control the amount of chloride retained in the unsaturated zone.

The use of sodium and calcium chloride salts for melting ice and snow on highways is common in the northern States. In Massachusetts, the statewide use of these salts—95 percent sodium chloride and 5 percent calcium chloride—on State-maintained highways, increased from about 23,600 metric tonnes, (26,000 tons) in 1954–55 to about 189,600 tonnes (209,000 tons) in 1970–71. An equal amount of salt is probably applied to streets by the cities and towns. Much of the salt applied to highways is plowed, along with snow, to the adjacent unpaved area. Melt water from the salt-laden snowbanks then flows overland to streams or percolates downward to the water table.

The dispersion of deicing salts applied to highways is of interest because of detrimental effects of salt on soils, vegetation, and water supplies (Coogan, 1971; Dowst, 1967; Lacasse and Rich, 1964; and Pollock and Toler, 1973). The amount retained above the water table is of further interest in assessing the lag in time between the application of salt to the highway and its appearance in ground water.

In 1965 the U.S. Geological Survey began monitoring the chloride content of ground water at 10 sites along arterial highways in Massachusetts. One site was selected for additional measurements that included continuous measurements of rainfall and ground-water level and periodic sampling of the chloride content of soil above the water table. Concentration of chloride in ground water at this site increased from less than 100 mg/l in 1965 to about 400 mg/l in 1971 (Pollock and Toler, 1973).

The Chelmsford test site, about 3 km (2 mi) south of Lowell (fig. 1), lies along the east side of U.S. Highway 3, a four-lane divided highway. The site is in a shallow roadcut on the crest of a small hill. The land surface slopes gently away from the road about 9.1 m (30 ft) to a shallow drainage ditch parallel to the highway. Salt and snow from two lanes of the highway are plowed toward the test site. Test wells for monitoring water level and changes in the chloride content of ground water at several depths are installed at 4.6 and 9.1 m (15 and 30 ft) from the edge of the pavement.

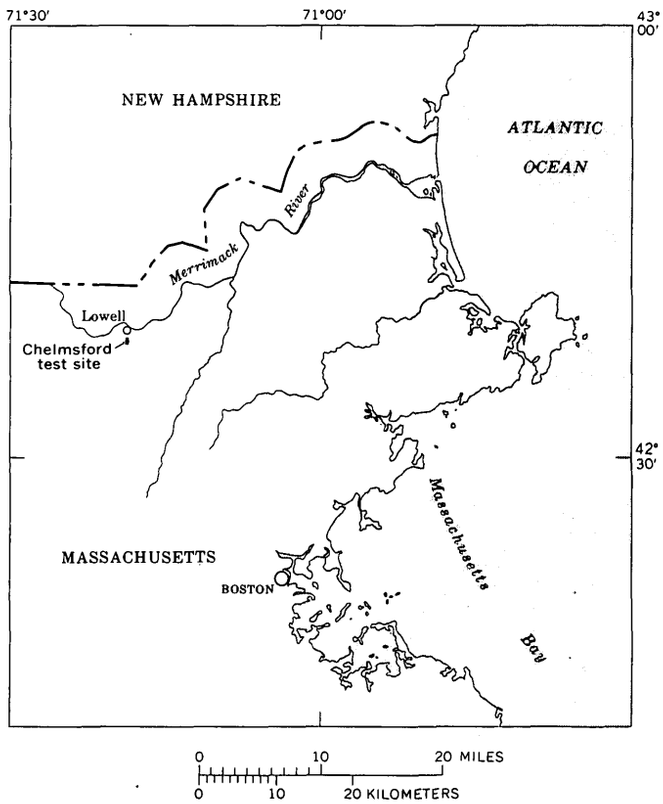

Figure 1.—Location of study area.

Logs of test borings show that the material that extends from land surface to glacial till, at a depth of 18.3 m (60 ft), consists of layers and lenses of fine to coarse sand and silt. In

general, the coarse sand is at the surface, allowing rapid infiltration of precipitation and snowmelt, and the sand grades with depth to fine sand and silt. During 1965 to 1969, the water table ranged from about 4.6 to 5.8 m, (15–19 ft) below land surface.

Soil samples were taken with a hand auger once or twice annually from 1965 to 1969 to determine the chloride content of the materials in the unsaturated zone (table 1). The augering sites are a few meters apart (fig. 2), and land-surface elevations for all holes are within a range of about 0.6 m (2 ft).

In 1965 and 1966 the augered materials were visually inspected, and sampled for chloride analyses where changes in grain size, color, or texture were observed. The concentration of chloride in each sample was weighted by the thickness of material it represented to obtain average chloride values in table 1.

From 1967 to 1969 the entire thickness of the unsaturated zone was sampled, each sample representing between about 3 and 15 cm (0.1–0.5 ft). All samples were air dried before 100 ml of distilled water was mixed with a representative 100-g part of each sample, stirred, allowed to stand overnight, decanted or filtered, and the filtrate analyzed for chloride. For samples collected from 1967 to 1969, the remainder of each sample—usually about 1 kg—was sieved through a stack of screens having 2.0-, 1.0-, 0.5-, 0.250-, 0.125-, and 0.0625-mm openings.

RESULTS

Chloride is a good tracer of water movement because it is affected little by physical or chemical interaction with soil materials. The chloride in the unsaturated zone is assumed to have been in solution in the pellicular water in the soil.

Concentration of chloride in materials from the unsaturated zone shows the same general distribution for all years, as illustrated by the chloride–concentration profiles (fig. 3) of sites 4 to 7 (fig. 2). Some of the offset in peak chloride concentrations for the four sites is caused by the difference in elevation of the sampling sites and probably by some lateral differences in grain-size distribution of the soil material.

Concentrations of chloride are higher near the bottom of the unsaturated zone and correspond to a general decrease in grain size of the materials or an increase in the percentage of the finer size fractions (fig. 3). This increase in chloride with a decrease in grain size is in accord with the assumption that the chloride is in solution in the pellicular water in the soil. The amount of pellicular water available before drying is a function

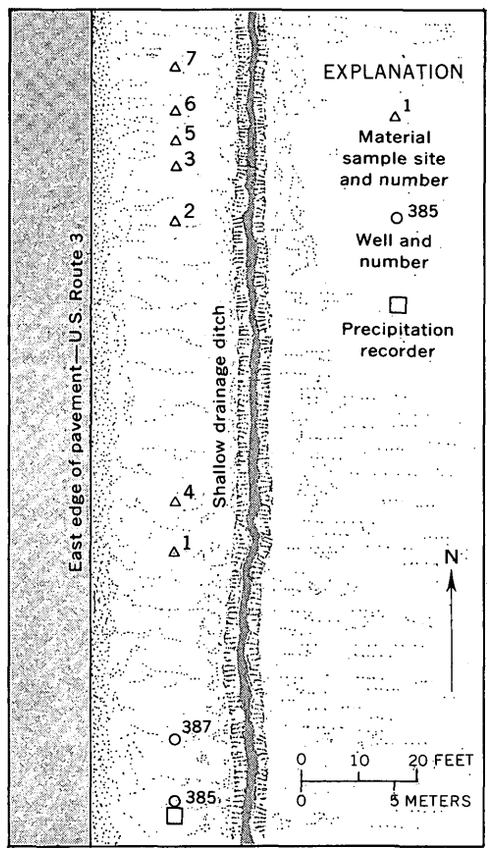

Figure 2.—Sketch map of test site.

Table 1.—*Sampling-site data*

Site No.	Date of collection	Depth of hole below land surface		Number of samples	Quantity of salt applied[1]		Quantity of chloride, as NaCl, in insaturated zone[2]	
		Meters	Feet		Tonnes	Tons	Tonnes	Tons
1	10-18-65	5.64	18.5	7	12.3	13.6	4.30	4.74
2	4-19-66	4.88	16.0	10	....	....	4.57	5.04
3	11- 7-66	4.88	16.0	17	8.3	9.2	4.63	5.10
4	11- 9-67	5.49	18.0	71	18.7	20.6	5.64	6.22
5	7- 1-68	4.66	15.3	49	....	....	6.43	7.09
6	10-16-68	4.78	15.7	51	31.8	35.0	4.72	5.20
7	10- 7-69	5.18	17.0	68	45.9	50.6	7.86	8.66

[1] Value is salt applied to 1.6 km (1 mi) of 2-lane highway during previous winter because two lanes of highway are plowed toward test site.
[2] Value is salt calculated to remain adjacent to the highway in a block 9.1 m (30 ft) wide, 4.5 m (15 ft) deep and 1.6 km (1 mi) long.

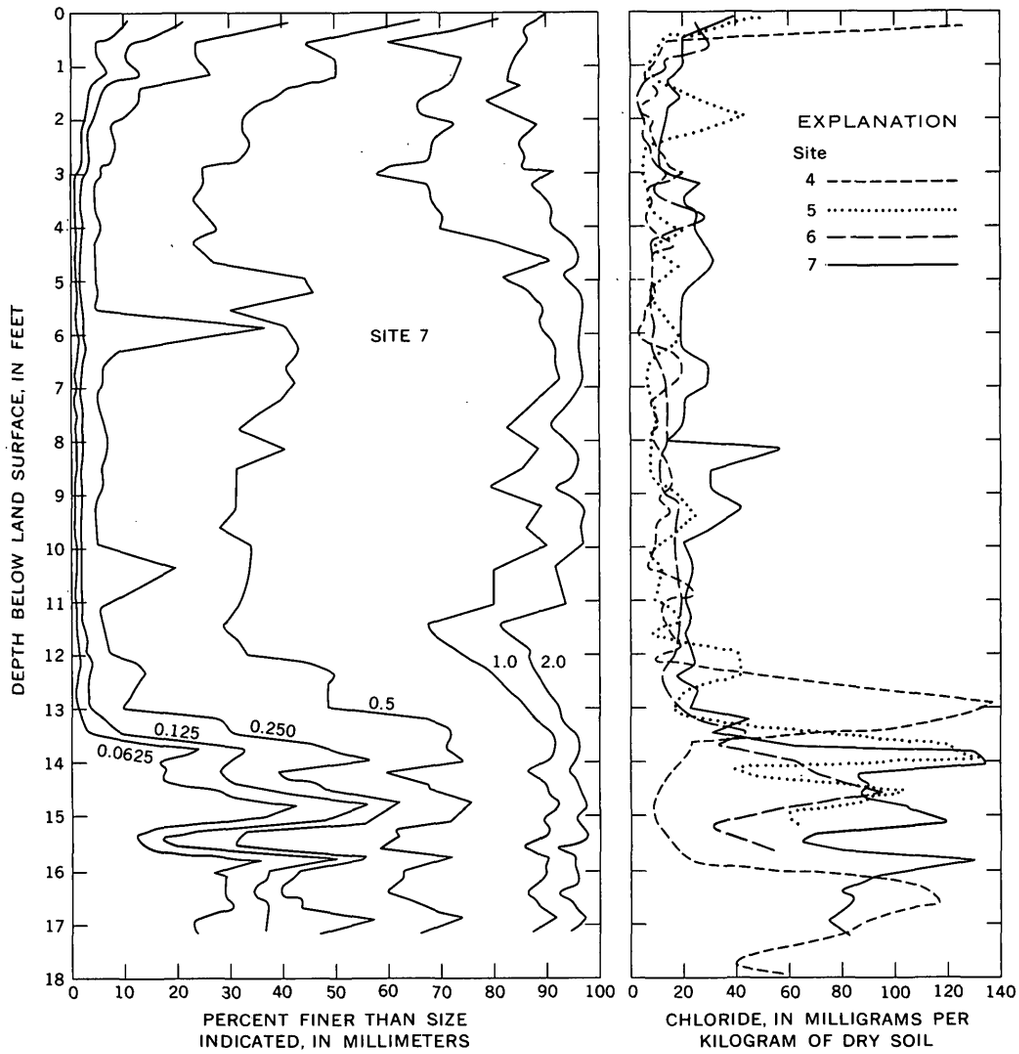

Figure 3.—Grain-size distribution and chloride content of materials in the unsaturated zone. (1 ft = 0.3048 m.)

of grain size because the surface area of a unit mass of grains increases with a decrease in average grain size. The surface area of 1 kg of each sample was calculated, assuming each size fraction to have an average grain diameter halfway between the diameter of the screen retaining the material and the next larger screen size and an average mineral grain density of 2.65 g/cm^3. Correlation between concentration of chloride and grain size is good when surface area is used as an index of grain size (fig. 4).

All four chloride profiles for which size analyses of the soil material are available show similar relations. The coefficient of correlation relating the concentration of chloride to the percentage of each size fraction is much higher for the smaller sizes (fig. 5) and gives the best results when calculated surface area is used as an index of grain size. The correlation with surface area might be improved if the size gradation of the fraction smaller than 0.0625 mm were determined. The surface area of samples containing a large percentage of material finer than 0.0625 mm could be greater than the calculated value because the average diameter of this fraction is probably less than the value of 0.031 mm used.

Data and graphs by Hutchinson (1966 and 1967) show high concentrations of sodium and chloride in soils adjacent to highways and decreasing concentrations with distance as much as 18.3 m (60 ft) from the highway. It seems from Hutchinson's work and from samples at 4.6 and 9.1 m (15 and 30 ft) from the highway collected during this study that most of the salt that percolates downward with ground-water recharge enters the ground within 9.1 m (30 ft) from the paved edge of the highway. The concentration of chloride in samples of the unsaturated zone 4.6 m (15 ft) from the highway should, therefore, approximate an average concentration of chloride in the unsaturated zone in the strip adjacent to the highway that is affected by highway deicing salts. On

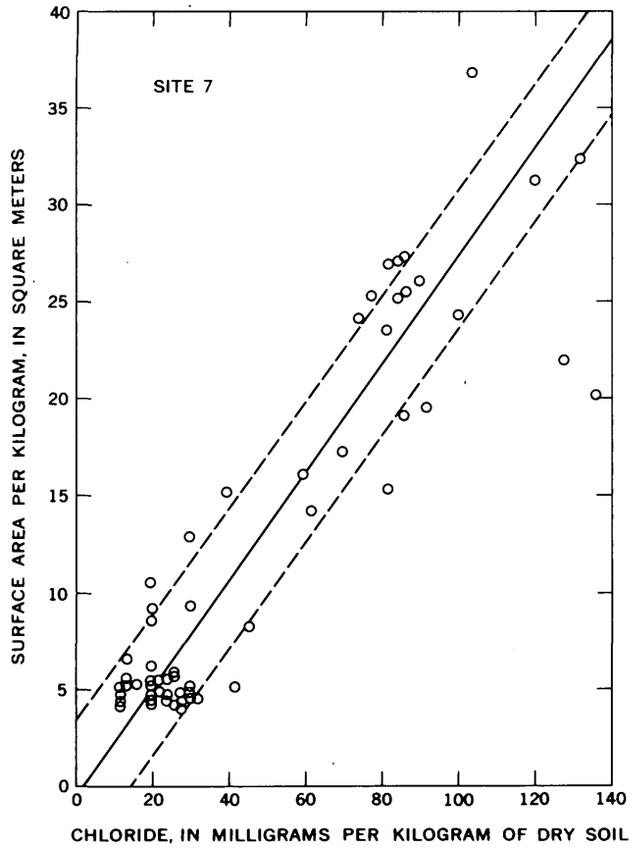

Figure 4.—Relation of chloride content to surface area of mineral grains in the unsaturated zone.

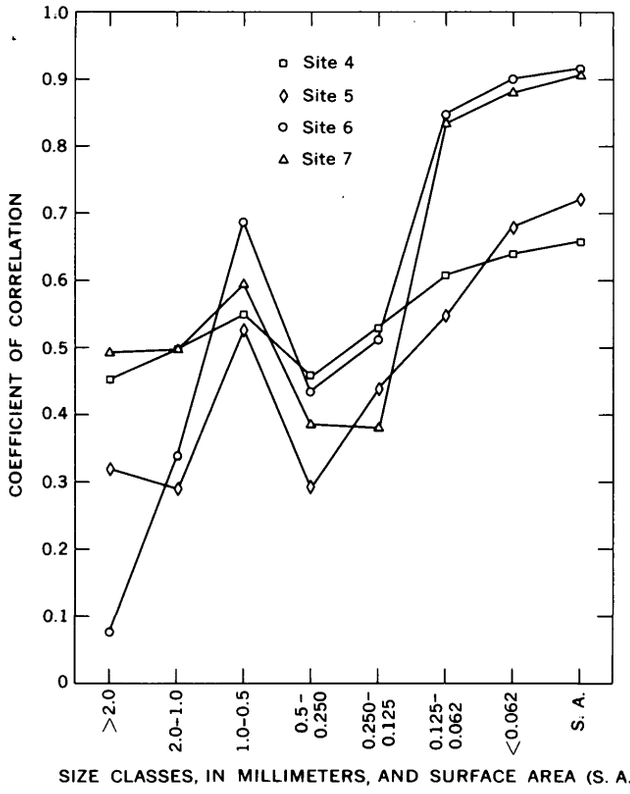

Figure 5.—Correlation coefficients for the relationship of chloride concentration to the percentage of material in each size fraction and of chloride concentration to surface area of material grains.

the basis of this assumption, the amount of chloride retained in the unsaturated zone to a depth of 4.6 m (15 ft) in an area 9.1 m (30 ft) wide and 1.6 km (1 mi) long adjacent to the highway should indicate the fraction of the annual amount of salt applied to the highway (table 1) that is retained in the unsaturated zone. The amount of chloride, as sodium chloride, retained in a block of the above dimensions was calculated from an assumed mineral grain density of 2.65 g/cm^3 and an average porosity of 20 percent and from the average concentration of chloride in the unsaturated zone 4.6 m (15 ft) from the highway. A depth of 4.6 m (15 ft) for the above block in the unsaturated zone was used because ground-water levels (fig. 6) show that the water table was below this depth during the investigation.

The amount of chloride retained in the unsaturated zone apparently reaches a plateau soon after the first salting season for the highway and does not increase significantly thereafter. Unlike the concentration of chloride in ground water (fig. 6), the concentration of chloride in the unsaturated zone does not change in response to the rate of deicing salt application. The amount of chloride, as sodium chloride, in the unsaturated zone in 1969 apparently increased because rainfall was not high (fig. 6) between the end of the application of deicing salt and the time of sampling, thereby resulting in lower than normal flushing of chloride from the unsaturated zone. All samples were taken after the spring period of maximum ground-water recharge, as indicated by peak ground-water levels, and before the next winter salting season. At the time of sampling, the previous season's salt has been flushed from the unsaturated zone to the ground-water body as completely as the spring and summer rainfall for that year permitted. The concentration of chloride in ground water (fig. 6) is responsive to the annual salt-application rate and indicates that most of the chloride reached the water table during mid-summer of each year.

Because salt and snow from two lanes of highway is plowed toward the sampling sites, the amount of salt available is twice that applied per lane mile. The amount of chloride, as sodium chloride, retained in the upper 4.6 m (15 ft) of unsaturated zone in autumn ranged from 15 to 55 percent of the amount of salt applied during the previous season of salt application.

CONCLUSIONS

Some of the salt applied to highways for snow and ice control is retained in the unsaturated zone. The amount of

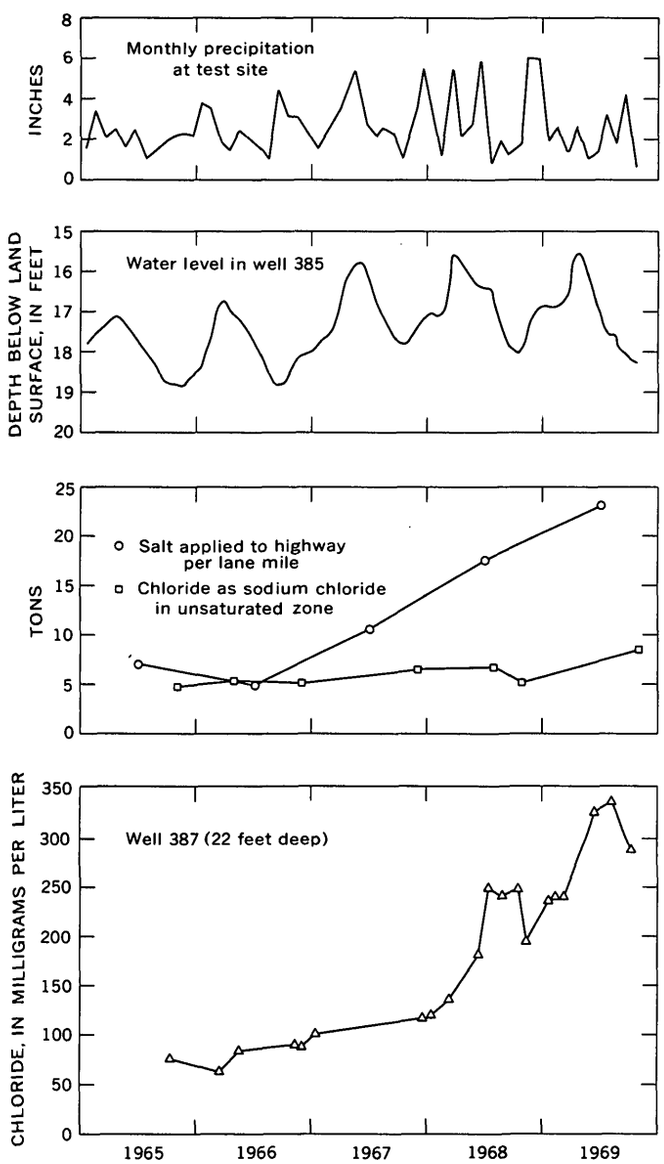

Figure 6.—Hydrographs of chloride and related parameters at Chelmsford test site. (1 in. = 2.54 cm, 1 ft = 0.348 m, 1 ton = 0.907 metric tonnes.)

chloride retained in the unsaturated zone apparently reaches relatively constant concentration soon after salt application begins and does not respond to changes in the annual rate of salt applied. The salt retained in the unsaturated zone at the Chelmsford test site, as measured by the concentration of chloride in air-dried soil samples, is inversely related to grain size and directly related to the surface area of the grains, probably because the small silt-size grains have a greater surface area per unit weight and volume and, therefore, are capable of retaining more pellicular water per unit weight and volume than the coarser sand grains. Salt in the unsaturated zone probably remains in solution in the soil moisture or is precipitated on grain surfaces as soil moisture decreases. The amount of chloride retained in the unsaturated zone from one salt season to the next also depends on depth to water table and the amount and seasonal distribution of precipitation.

The amount of chloride, as sodium chloride in autumn, in a block of the unsaturated zone adjacent to the highway and 9.1 m (30 ft) wide, 4.6 m (15 ft) deep, and 1.6 km (1 mi) long ranged from 15 to 55 percent of the amount of salt applied during the previous season of deicing salt application.

The concentration of chloride in ground water responds to the annual rate of salt application. This response and the lack of a chloride buildup in the unsaturated zone indicate that the increase in the concentration of chloride in ground water adjacent to the highway during the summer is attributable to the salt application of the previous winter.

This information will allow a better interpretation of the annual dispersion of chloride from deicing salts in the hydrologic system.

ACKNOWLEDGMENTS

We are indebted to Mr. Leo Stevens, Massachusetts Department of Public Works, Research and Materials Section, for grain-size and chloride analyses in this report. Mr. James Norcott, District 4 Snow and Ice Control Engineer, kindly compiled salt-application data for the test site.

REFERENCES CITED

Coogan, C. J., 1971, The increase in chloride experienced in Massachusetts water supplies: New England Water Works Assoc. Jour., v. 85, no. 2, p. 173–178.

Dowst, R. B., 1967, Highway chloride applications and their effects on water supplies: New England Water Works Assoc. Jour., v. 81, no. 1, p. 63–67.

Hutchinson, F. E., 1966, Accumulation of road salt ions in soils along Maine highways: Maine Farm Research, October 1966, p. 13–16.

——1967, The relationship of road salt applications to sodium and chloride ion levels in the soil bordering major highways: Washington, D.C., Highway Research Board, Highway Research Rec. 193, p. 1–7.

Lacasse, N. L., and Rich, A. E., 1964, Maple decline in New Hampshire: Phytopathology, v. 54, no. 9, p. 1071–1075.

Pollock, S. J., and Toler, L. G., 1973, Effects of highway deicing salts on ground water and water supplies in Massachusetts: Washington, D.C., Highway Research Board, Highway Research Rec. 425, p. 17–22.

Jour. Research U.S. Geol. Survey
Vol. 2, No. 1, Jan.-Feb. 1974, p. 125—131

USE OF BASE-RUNOFF RECESSION CURVES TO DETERMINE AREAL TRANSMISSIVITIES IN THE UPPER POTOMAC RIVER BASIN

By FRANK W. TRAINER and FRANK A. WATKINS, JR.,
Albuquerque, N.M., Winter Park, Fla.

Abstract.—The recession curve of base runoff is used in geohydrologic study of the upper Potomac River basin, a humid temperate region underlain by fractured rocks in which ground water is largely unconfined and feeds the streams. The slope of the recession curve, shown by Rorabaugh to be proportional to aquifer diffusivity (the ratio of transmissivity to storage coefficient), is used with other data to estimate average basin values for transmissivity from streamflow data. Two general recession curves characterize the tributary basins: (1) A continuous (simple) curve, approximately straight on a semilogarithmic plot, which represents a constant set of diffusivity values within a basin and (2) a discontinuous (compound) curve, composed of a steeper first segment and a gentler second segment. Simple curves represent basins underlain by sandstone, shale, or crystalline rock; by combinations of these rocks; or by carbonate rock. Compound curves, which represent basins underlain in part by carbonate rock and in part by noncarbonate rock, are believed to reflect seasonal changes in relative discharge of these unlike aquifers, with the carbonate rock providing most of the ground-water runoff during summer-autumn and during drought.

The recession curve of base runoff is a promising means of studying regional hydrology because it represents groundwater discharge to the streams in an entire drainage basin. This report describes recession curves in the upper Potomac River basin, a temperate humid region of complex geology.

The Potomac River drains part of the central Appalachian region in Pennsylvania, Maryland, Virginia, and West Virginia (fig. 1). The upper part of the Potomac basin, upstream from Washington, D.C., has an area of 11,560 mi^2 (about 29,940 km^2). This upper basin is underlain by crystalline rock and by sandstone, shale, and subordinate limestone in the Piedmont and the Blue Ridge physiographic provinces; by shale, carbonate rock, and sandstone in the Valley and Ridge province; and by sandstone and shale, with subordinate limestone and coal, in the Appalachian Plateaus province. Unconsolidated deposits consist of alluvium along stream courses and in fanlike features along several mountain bases and of regolith, which is commonly thin in the mountainous parts of the basin but is as thick as several tens of feet in much of the Piedmont region and in some wide valleys in the Blue Ridge and the Valley and Ridge provinces.

The climate of the Potomac River basin is temperate and humid. The summer and winter seasons are well defined, but precipitation is rather evenly distributed through the year. The average annual precipitation, most of which falls as rain, is about 38 in. (about 960 mm).

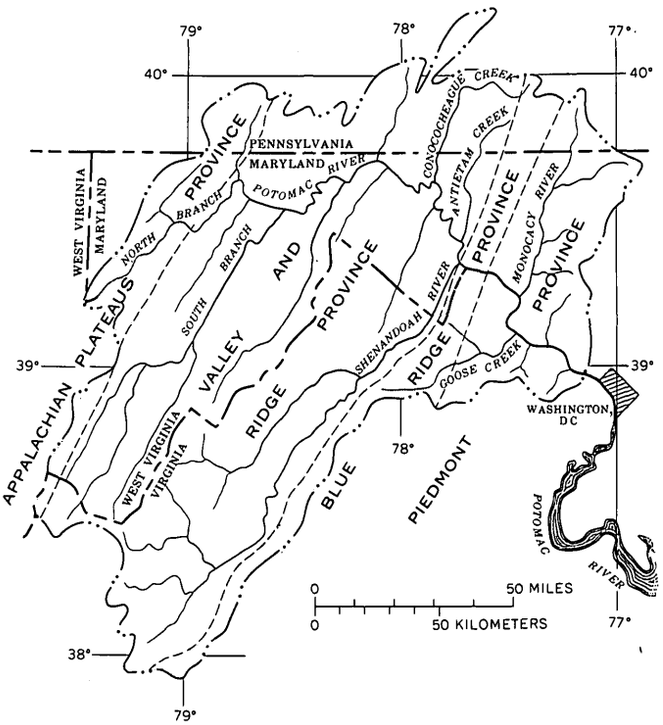

Figure 1.—Physiographic provinces of the upper Potomac River basin.

In much of the upper Potomac River basin the ground water is unconfined. However, because of the layered structure of the rocks and perhaps in places because of the clay content of regolith and alluvium, the ground water is confined or semiconfined, at least locally. In all the consolidated rocks the water is stored in and transmitted through fractures; in the carbonate rock some fractures have been extensively altered by solution. In the unconsolidated material and in part of the

sandstone, water is stored in and transmitted through intergranular pores. The streams are hydraulically connected with the ground-water reservoir; they are fed by ground-water discharge, which supplies all or most of their flow in dry weather and a substantial part of it in wet weather.

CONSTRUCTION OF THE RECESSION CURVE OF BASE RUNOFF

Base runoff—that is, the part of the streamflow provided largely or entirely by natural ground-water discharge—diminishes during dry weather as ground-water storage becomes depleted. Several methods have been used by hydrologists to construct a curve which defines this recession. In this investigation we constructed the recession curve by a graphical method (Horton, 1933, p. 449; Snyder, 1939, p. 728–730; Grundy, 1951, p. 215-216) which is simple and which, because one works directly with the stream hydrograph, helps focus attention on the record of base runoff. The recession curve is synthesized from many short segments of hydrograph, each of which is believed to represent a period when the stream was in or approaching the base-runoff regime. Many hydrologists have recognized that the recession limb of the hydrograph for a stream or spring approaches or follows a logarithmic law. Rorabaugh (1964, p. 434) found that once sufficient time has elapsed, after a period of recharge, for the shape of the water-table profile in a finite aquifer to stabilize, discharge from the aquifer can be represented on a semilogarithmic plot by a straight line. Accordingly, we used segments of the stream hydrograph which are straight or which are approaching a straight line on a semilogarithmic plot (fig. 2).

FACTORS WHICH AFFECT THE SLOPE OF THE RECESSION CURVE

Rorabaugh (1960, 1964) developed an equation which expresses the relation of the slope of the recession curve to the transmissivity and storage coefficient of the ground-water reservoir. The equation, derived from the exponent of an infinite series, expresses the slope of the hydrograph after the development of a stable water-level profile. An abbreviated form of the equation (Rorabaugh and Simons, 1966, p. 12) is

$$\frac{T}{a^2S} = \frac{0.933}{\Delta t/\text{cycle}}$$

where T is the transmissivity of the aquifer, S is the storage coefficient, a is the average distance from the stream to the hydrologic divide, and Δt is the time required for discharge to decline through one log cycle. (Taking change in time across one log cycle simplifies computations. It also provides a convenient standard for comparison of change in ground-water storage in several basins because decline through one log cycle represents depletion of 90 percent of the ground water in storage above stream level.) The numerical value for the ratio $T{:}a^2S$ can be used directly as a basin characteristic (Rorabaugh and Simons, 1966, p. 12) to describe geohydrologic conditions on the basis of the streamflow record; or, if a and either T or S are known or can be inferred from other studies, average (basin) values for S or T can be estimated.

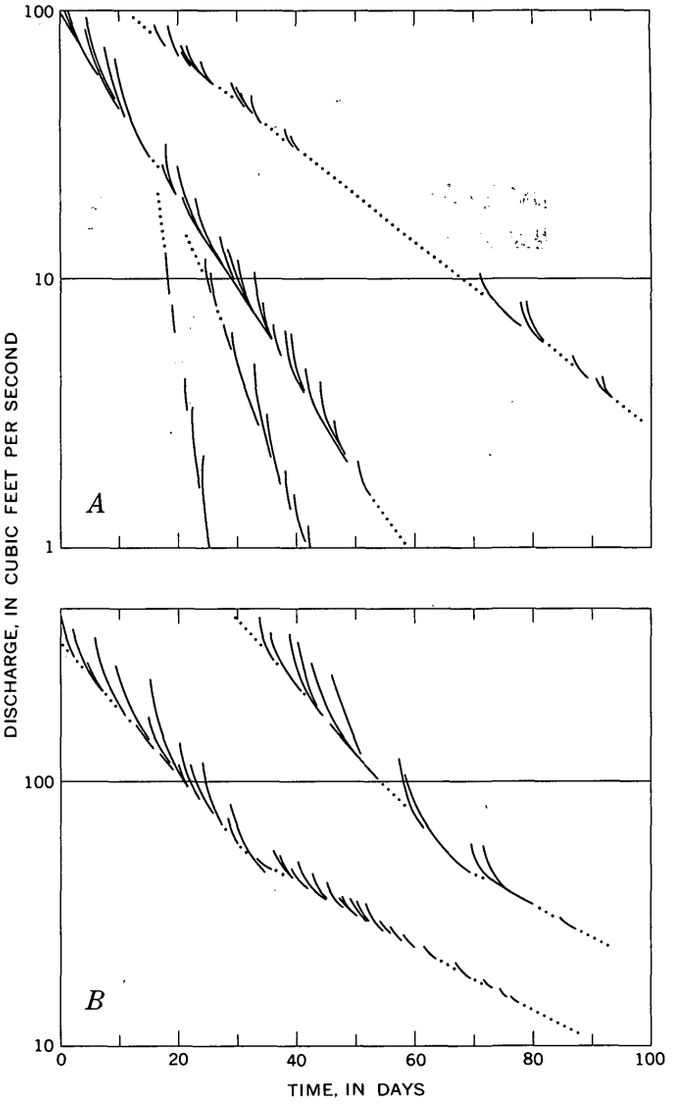

Figure 2.—Base-runoff recession curves (dotted lines) constructed from segments of stream hydrographs (solid lines). Absolute positions of times scales are arbitrary. *A*, Passage Creek at Buckton, Va.; winter curve (top) and examples of parts of summer curve (bottom). *B*, South Branch Potomac River at Franklin, W. Va.; generalized recession curve (left) and curve for 1953 (right).

Factors which affect the slope of the recession curve complicate its interpretation. These factors include the following: (1) The brevity of most recession episodes in this humid region makes it difficult to determine the slope of the recession curve precisely, (2) losses from ground water and

from streamflow, through evapotranspiration, distort the recession curve during much of the year, and (3) complexity of many recession curves may be related to nonhomogeneity of the aquifers or to the presence of multiple aquifers.

Effect of duration of streamflow recession

The abbreviated equation given above is valid only after sufficient time has elapsed for stabilization of the water-table profile after an episode of recharge. Rorabaugh (1964, p. 434) showed that the critical time for stabilization is about one-fifth of the period required for the straight-line recession curve to decline through one log cycle of discharge. For example, if the base-runoff recession curve for a given stream declines through one log cycle in 40 d, the semilogarithmic hydrograph should become a straight line after about 8 d of uninterrupted recession following a flood peak. On the other hand, if the time required is about 200 d per cycle, the straight-line form should be attained in about 40 d.

In the Potomac River basin, storms are frequent and periods of streamflow recession, between flood peaks, are therefore relatively short. There are several storms per month, on the average, and periods of a month or more without precipitation are rare. A recession curve which becomes linear on the semilogarithmic plot within 8 to 10 d after a flood peak can be determined readily if several annual hydrographs are available. On the other hand, the straight-line part of a curve which would become linear only after 30 or 40 d of uninterrupted recession can be determined only approximately without resort to rigorous analysis of the early part of the recession. A recession curve constructed from hydrograph segments which have not quite attained the straight-line form is somewhat steeper than the stable-profile curve, and it therefore overestimates the rate of decline of base runoff or leads to underestimation of the base runoff for a given period.

Effect of evapotranspiration

Many hydrologists have recognized seasonal ("winter" and "summer") forms of the recession curve. The winter curve is taken to represent recession which is little affected by evapotranspiration and hence to reflect the geohydrologic control of base runoff. In the Potomac River basin the winter curve can be recognized in many recession episodes during October-April, but its slope is difficult to determine because most of the recessions are brief. Our study suggests that, where we have recognized the winter recession curve, the tributary basin is characterized by one winter curve which approaches a straight line on a semilogarithmic plot.

Some recessions during the period October-April and most of them during the remainder of the year can be fitted by a summer curve which is nearly straight on a semilogarithmic plot but which slopes more steeply than the winter curve. However, in late summer and early autumn, particularly in basins underlain by relatively impermeable rocks and in which streamflow at that season is no more than a few cubic feet per second, the summer curve may become progressively steeper as the season advances (fig. 24). This curvature, which has been well shown by Riggs and Hanson (1969), reflects the increasingly large effect on the streamflow of evapotranspiration from ground water near the stream and from the stream itself. In part, however, it may also reflect decrease in transmissivity of the unconfined aquifer, a factor considered briefly in the next section of this report.

Where the recession curve is to be used in study of geohydrologic controls on base runoff, the winter curve should be used. Use of the summer curve for this purpose would result in an erroneously steep slope and a correspondingly high rate of decline in base runoff. On the other hand, if the analysis is intended for study of summer streamflow, as in some water-supply problems, the summer curve should be used because it reflects the rate of streamflow recession during dry weather in summer.

Nonhomogeneity of aquifers

It seems likely that both areal and vertical differences in characteristics of the unconfined aquifer contribute to the complexity of many recession curves.

The normal downward closure of rock joints causes downward decrease in porosity and hydraulic conductivity. We believe that in some fractured rocks these changes may be appreciable even within the zone of annual water-table fluctuation. During the late-summer period of low groundwater level, any resulting decrease in transmissivity and storage coefficient in these rocks would lead to increase in the rate of base-runoff recession, reinforcing the effect of evapotranspiration in causing the recession curve to become concave downward.

It appears that the presence of multiple aquifers within a tributary basin may also contribute to the complexity of the recession curves. This effect is discussed in the section of this report which describes the compound recession curve.

SIMPLE AND COMPOUND RECESSION CURVES

The simple recession curve

For many tributary streams in the upper Potomac River basin the winter recession curve becomes a single straight line on a semilogarithmic plot. This continuity through a considerable range in discharge implies that each of these tributary basins is relatively homogeneous in terms of transmissivity and storage coefficient. There may be areal differences in these aquifer characteristics within a given rock type or from one rock to another, but the ratio $T{:}a^2S$ is nearly constant within a given tributary basin. We term this single continuous curve a **simple** recession curve.

For some basins the simple recession curves exhibit a very narrow range in slope. For example, in 13 basins underlain by fractured rock with thin regolith (table 1) Δt, the number of

Table 1.—*Descriptor for slope of base-runoff recession curve, and base runoff during spring, for selected tributary basins in the upper Potomac River basin.*

[To convert base runoff to $m^3\ s^{-1}\ km^{-2}$, multiply value given in $ft^3\ s^{-1}\ mi^{-2}$ by $10^{-2} \times 1.09$]

Station[1]	Tributary basin	Δt (d/cycle)	Base runoff ($ft^3\ s^{-1}\ mi^{-2}$)
	Basins underlain by fractured rock with thin regolith		
1-5965	Savage River near Barton, Md	56	0.82
5970	Crabtree Creek near Swanton, Md	52	1.02
6045	Patterson Creek near Headsville, W. Va	63	.36
6075	South Fork South Branch Potomac River at Brandywine, W. Va	59	.59
6140	Back Creek near Jones Springs, W. Va	56	.44
6205	North River near Stokesville, Va	45	1.27
6320	North Fork Shenandoah River at Cootes Store, Va	54	.46
6345	Cedar Creek near Winchester, Va	60	.61
6355	Passage Creek at Buckton, Va	57	.57
6362.1	Happy Creek at Front Royal, Va	45	.87
6405	Owens Creek at Lantz, Md	57	1.48
6410	Hunting Creek at Jimtown, Md	57	1.26
6415	Fishing Creek near Lewistown, Md.	55	1.71
	Basins underlain by fractured rock with thick regolith		
1-6375	Catoctin Creek near Middletown, Md	46	0.88
6390	Monocacy River at Bridgeport, Md	35	.45
6395	Big Pipe Creek at Bruceville, Md	94	.85
6425	Linganore Creek near Frederick, Md	105	.92
6440	Goose Creek near Leesburg, Va	71	.66
6450	Seneca Creek at Dawsonville, Md	127	.87
6460	Difficult Run near Great Falls, Va	90	.86
	Basins underlain in substantial part by carbonate rock[2]		
1-6145	Conococheague Creek at Fairview, Md.	111	1.24
6150	Opequon Creek near Berryville, Va	84	.21
6165	Opequon Creek near Martinsburg, W. Va	155	.60
6170	Tuscarora Creek above Martinsburg, W. Va	100	1.08
6195	Antietam Creek near Sharpsburg, Md	216	1.26
6220	North River near Burketown, Va	293	.98
6250	Middle River near Grottoes, Va	184	.89
6260	South River near Waynesboro, Va	299	1.46
6285	South Fork Shenandoah River near Lynnwood, Va	242	1.11
6310	South Fork Shenandoah River at Front Royal, Va.	540	1.08
6330	North Fork Shenandoah River at Mount Jackson, Va	58	.46
6340	North Fork Shenandoah River near Strasburg, Va	108	70
6365	Shenandoah River at Millville, W. Va	229	.80

[1] Stream-discharge station, U.S. Geological Survey.

[2] Δt given for second segment of compound recession curve. Base runoff computed, using probable value of discharge from noncarbonate rock.

days per cycle, ranges from 45 to 63 d and averages about 55 d. These basins are underlain by shale, tight sandstone, or crystalline rock; they are in the Blue Ridge, Valley and Ridge, and Appalachian Plateaus provinces. The range in slope is much greater in other basins underlain by fractured (mostly noncarbonate) rock with thick regolith. Seven of these basins, in which Δt ranges from 35 to 127 d, are underlain by a wide spectrum of rock types—gneiss, schist, sandstone, shale, subordinate carbonate rock, and diabase. Nonetheless, each of these tributary basins studied (which may be underlain by several of these rock types) is characterized by one simple winter recession curve of base runoff.

The compound recession curve

The recession curves in figure 2*B* differ from those in figure 2A in being concave upward. Generalized recession curves for many tributary streams in the Potomac basin, each based on data from several or many annual hydrographs, show this concave-upward form. The steeper first segment of each of these curves occurs in winter and spring. The more gently sloping second segment begins in spring or summer and commonly defines base runoff from then into the following autumn or early winter. This concave-upward curve differs markedly from the simple recession curve described earlier. The downward concavity of the simple curve is believed to be due principally to evapotranspiration. The other curve must also be affected by evapotranspiration, but its concavity, being of opposite sense, occurs despite evapotranspiration rather than because of it. Riggs (1964, p. 353–354) used a hypothetical example to show how the combined runoff from two very unlike aquifers in a single drainage basin might yield a recession curve having two regions of very different slope. Following this reasoning, we believe that the concave-upward recession curve reflects runoff from two aquifers for which the ratio $T{:}a^2S$ is markedly different. We term this curve a **compound** recession curve.

The points of inflection in the generalized compound curves occur at different magnitudes of streamflow (in terms of discharge per unit drainage area) in different tributary basins, and at somewhat different magnitudes in a given basin during different years. Recession curves for some basins, constructed from single annual hydrographs, show that the first and second segments of the curve join in a transitional segment (fig. 2*B*, right curve) rather than in the single point obtained by extrapolation in construction of the generalized recession curve.

Among the compound curves we have constructed, Δt for the first segment is commonly in the range from 30 to 70 d per log cycle; Δt for the second segment ranges from 50 to several hundred days per cycle (table 1). In many instances winter forms of the recession curve were not recognized among the first segments of these curves; the second segments listed in table 1 are summer curves.

The higher values of Δt for second segments of compound curves are at best approximations because the brevity of most recession episodes precludes determination of precise values.

In some basins the slope of the recession curve has been affected by regulation—the streamflow is regulated slightly, but sufficiently to affect very low flows. On the other hand, all the tributary basins for which we found compound curves are underlain in part by carbonate rock and in part by sandstone, shale, or crystalline rock. In the Potomac basin, carbonate rock is commonly a much more productive aquifer than the noncarbonate rocks, and streamflow measurements (not included in this report) show that its average base runoff is higher than that from the noncarbonate rocks. Moreover, many of the carbonate-rock basins characterized by recession curves (second segments) of gentle slope are in part underlain by thick regolith and by alluvial-fan deposits whose drainage may help sustain base runoff. We believe that long values for Δt (low slopes of recession curves) are valid for these second segments. Precise slopes cannot be determined, however, nor can the quantitative significance of the several geologic (terrain) factors which influence these slopes yet be determined.

We believe that the compound recession curve reflects a seasonal sequence of change in the proportions of base runoff provided by two aquifers in the basin. Where each aquifer underlies an appreciable part of the basin, each may provide a substantial part of the total ground-water runoff during early spring. During late spring and summer, however, the aquifer with greater diffusivity provides a progressively lesser part of the total base runoff, and eventually the aquifer with lesser diffusivity provides most or nearly all of it. By this hypothesis the first segment of the recession curve represents the combined effects of both aquifers, while the second segment is very nearly the summer recession curve for the aquifer with lesser diffusivity.

This hypothesis is of particular interest for its bearing on water supply from streamflow during summer and autumn and during drought: the compound recession curve serves to identify basins whose low flows are relatively well sustained during long-continued dry weather, whereas the simple recession curve identifies basins whose low flows are less well sustained over long dry periods.

Segmented recession curves have been reported from regions of carbonate rock in France, North Africa, and the Near East by Henri Schoeller, his students, and other geohydrologists (for example, Schoeller, 1948, 1962, p. 211–214, 1967; Mijatović, 1968). Using empirical equations developed by Boussinesq (1904 and earlier papers) and used by Maillet (1905 and earlier papers) to study spring discharge and streamflow, these investigators found that some recession segments can be fitted by equations for turbulent flow and some by equations for laminar flow. Recession curves which consist of as many as three or four segments were therefore interpreted in terms of a sequence of turbulent and laminar flow regimes. The question arises: Why are these recession curves more complex than the curves reported in the present study? We believe that the two sets of curves do not represent comparable parts of the recession. In our effort to exclude the effect of surface runoff, we also excluded the effect of early ground-water flow, including much of the turbulent flow through cavernous openings in the carbonate rock. On the other hand, early parts of some hydrographs and recession curves of Schoeller and other writers may include some surface runoff. Hall (1968, p. 974) noted that the French term source is probably best translated as an area of natural discharge, including springs and seeps; it seems likely that some of these areas receive surface runoff during and shortly after storms. A third explanation of the disparity in interpretation lies in the possibility that the drainage areas of some of the springs studied by Schoeller and other writers are underlain in part by noncarbonate rocks (see, for example, Flandrin and Paloc, 1969, pl. 2) which differ markedly, in their hydrology, from the carbonate rock. We tentatively conclude that our second segment corresponds to the last segment found by Schoeller and other investigators.

ESTIMATES OF AQUIFER CHARACTERISTICS

Ranges in slope of the base-runoff recession curve, with other hydrologic data, show that the consolidated rocks in the upper Potomac River basin can be classified in three groups, each of which is characterized by typical geohydrologic conditions. These three terrains are (1) fractured rock which has a thin regolith or mantle of weathered material, (2) fractured rock which has a relatively thick regolith, and (3) carbonate rock. The first terrain, in which the storage and transmission of water depend largely or almost entirely on fractures, consists of tight shale and sandstone in the Valley and Ridge province and of crystalline rock in the Blue Ridge. The second terrain, in which regolith provides a strong control on ground-water storage, underlies the Piedmont and the lowland part of the Blue Ridge province; the bedrock is metamorphic rock and Triassic sedimentary and igneous rock. The carbonate rock which makes up the third terrain owes its geohydrologic character to regolith and to the selective solutional enlargement of fractures. This terrain occurs in the Appalachian Valley and in parts of other valleys in the Valley and Ridge and the Piedmont provinces.

The values for Δt and for base runoff given in table 1 were used with the abbreviated form of Rorabaugh's equation to estimate average aquifer characteristics for the three terrains. Base runoff during the spring season of low evapotranspiration was used because we are concerned with the geohydrologic controls on base runoff. Base runoff during spring was determined as follows: Streamflow records for the upper Potomac River basin were searched for recession episodes that occurred in all parts of the basin following basin-wide storms. Four such episodes, during February, March, or April, were found in the period 1950–66. Discharge in each tributary basin, just before interruption of recession by a new flood peak, was averaged for the four episodes. These averages,

expressed on a unit-area basis, are taken for the purpose of this comparative study as relative values for base runoff from the respective tributary basins during spring. (These average values are believed to be larger than long-term averages for spring base runoff and should not be taken as absolute values.)

An average value for aquifer diffusivity (T:S) in the fractured rocks which lack thick regolith was computed using representative average values for Δt (55 d) and a (1,350 ft or 411 m). (Distance a was determined from the relation $A=2aL$, where A is basin area, a is average distance from stream to divide, and L is total length of streams in the basin. A and L were measured on topographic maps.)

$$\frac{T}{(0.9)(1.8\times 10^6\ \text{ft}^2)\,S}=\frac{1}{55\ \text{d}},$$

$$\frac{T}{S}=\frac{1.6\times 10^6\ \text{ft}^2}{55\text{d}}=29{,}000\ \text{ft}^2/\text{d}\ (2{,}700\ \text{m}^2/\text{d}).$$

It is possible to estimate T or S from the diffusivity, given a value for S or T. We assumed S (because it appears to fall in a narrower range of values in the upper Potomac River basin than does T) and computed T. Seven values for S, provided by pumping tests, range from 0.002 to 0.02; the median value is 0.006. Four values for gravity yield (which approximates the storage coefficient), determined by a method described by Olmsted and Hely (1962, p. A16–A17), range from 0.003 to 0.016, with a median value of 0.004. Assuming S to average 0.005, we computed the average T in these basins to be 140 ft^2/d (13 m^2/d). This computed value appears to be of the correct order of magnitude; 25 values for T provided by pumping tests range from 3 to 2,000 ft^2/d (0.28–190m^2/d), and the median value is 170 ft^2/d (16 m^2/d).

In similar fashion T:S was computed for fractured rocks covered by thick regolith. Taking a as 1,250 ft (380 m) and Δt as 80 d, we obtained an average value for T:S of 18,000 ft^2/d (1,670 m^2/d). The median value for S, from five pumping tests, is 0.004. Five values for gravity yield range from 0.007 to 0.014, with a median of 0.01. We believe these values to be more representative of the entire ground-water reservoir than those provided by the pumping tests. Assuming an average S of 0.01, we computed an average transmissivity of 180 ft^2/d (17 m^2/d). Seven values for T, from pumping tests, range from 60 to 7,000 ft^2/d (5.6–650 m^2/d); the median value is 670 ft^2/d (62 m^2/d). The computed value appears to be of the correct order of magnitude, but it agrees with the pumping-test values less closely than does the value computed for fractured rock with thin regolith.

The ratio T:S was also computed for the carbonate-rock aquifer. An average value for a, 1,800 ft (550 m), was estimated from measurements of A and L on topographic maps. The average Δt was taken as 180 d (see table 1). The computed ratio T:S is 16,000 ft^2/d (1,500 m^2/d). The median of three values for S, from pumping tests, is 0.04. Assuming this value for S we computed an average T of 640 ft^2/d (60 m^2/d). Eleven pumping tests in the carbonate rock provide transmissivity values which range from 1 to about 27,000 ft^2/d(0.1–2,500 m^2/d); the median value is 1,740 ft^2/d (160 m^2/d).

Several factors bear on evaluation of the validity of transmissivities computed from the recession data. If values determined by pumping tests are used as a standard of comparison, the agreement of computed and test values is better with a large number of tests than with a small one. A large sample of test values is, of course, more likely to provide a reliable median or average than a small sample. This would be true in relatively homogeneous terrains, but it is even more so where the rocks are far from homogeneous. Thus, agreement is better where the fractured rock has been little affected by weathering, and poorer where the rock has been modified by solution and soil formation. The fractured rock with thin regolith is of generally low permeability, while the other terrains have been more affected by solution and possess both a greater areal variability in hydrologic character and a greater range in permeability. Aside from this effect of the intrinsic geohydrologic character of the rocks, bias is introduced by selection of wells to be tested by pumping: Many of the wells tested by pumping had already been shown by bailing to be relatively productive, while relatively unproductive wells were not tested by pumping. Thus, pumping tests tend to be made in the more permeable rocks of a given type, and high transmissivities are the result. Because of the greater range in permeability and the much greater maximum permeabilities in the carbonate rock and the rock with thick regolith, the bias in transmissivity values is much greater in these terrains than in the rocks with thin regolith.

The three average transmissivities estimated from the streamflow-recession data appear to be ranked in their correct relative order. On the basis of the results and discussion in the preceding paragraphs, we conclude that they are also of reasonable absolute magnitudes. Streamflow data thus appear to be potentially valuable in estimating transmissivity where the ground-water reservoir is both unconfined and hydraulically connected with the streams. Provided reasonable estimates of the storage coefficient can be made, the method may therefore be useful in regions where well data are scanty. Because these transmissivity values are basin averages, they cannot be used in estimating potential yields of wells. They should, however, be useful where regional estimates of transmissivity are needed, as in preliminary ground-water modeling of drainage basins before the range and areal distribution of transmissivity have been determined in useful detail.

ACKNOWLEDGMENTS

We gratefully acknowledge the helpful and stimulating comments and discussion of the following colleagues during the course of this study: R. R. Bennett, H. H. Cooper, Jr., J.

F. Daniel, J. G. Ferris, F. H. Olmsted, H. C. Riggs, and M. I. Rorabaugh.

REFERENCES CITED

Boussinesq, J., 1904, Recherches théoriques sur l'écoulement des nappes d'eau infiltrées dans le sol et sur le débit des sources: Jour. Math. Pures et Appl., v. 10, ser. 5, p. 5–78, 363–394.

Flandrin, J., and Paloc, H., 1969, Contribution a la connaissance du reservoir aquifere de la Fontaine du Vaucluse; resultats des études effectuces en 1967 et 1968: Bur. de Recherches Géol. et Minières, Mem. 76, p. 611–643.

Grundy, F., 1951, The ground-water depletion curve, its construction and uses: Internat. Assoc. Sci. Hydrology Pub. 33, p. 213–217.

Hall, F. R., 1968, Base-flow recessions—a review: Water Resources Research, v. 4, no. 5, p. 973–983.

Horton, R. E., 1933, The role of infiltration in the hydrologic cycle: Am. Geophys. Union Trans., v. 14, p. 446–460.

Maillet, E., 1905, Essais d'hydraulique souterraine et fluviale: Paris, Hermann, 218 p.

Mijatović, B. F., 1968, A method of studying the hydrodynamic regime of karst aquifers by analysis of the discharge curve and level fluctuations during recession: Inst. Geol. and Geophys. Research [Belgrade], Eng. Geology and Hydrogeology Bull., ser. B, no. 8, p. 41–74; English translation of Inzenjerska Geologija i Hidrogeologija, Vesnik.

Olmsted, F. H., and Hely, A. G., 1962, Relation between ground water and surface water in Brandywine Creek basin, Pennsylvania: U.S. Geol. Survey Prof. Paper 417-A, 21 p.

Riggs, H. C., 1964, The base-flow recession curve as an indicator of ground water: Internat. Assoc. Sci. Hydrology Pub. 63, p. 352–363.

Riggs, H. C., and Hanson, R. L., 1969, Seasonal low-flow forecasting, *in* Hydrological Forecasting: World Meteorol. Organization, Tech. Note 92, Geneva, Switzerland.

Rorabaugh, M. I., 1960, Use of water levels in estimating aquifer constants in a finite aquifer: Internat. Assoc. Sci. Hydrology Pub. 52, p. 314–323.

——1964, Estimating changes in bank storage as ground-water contribution to streamflow: Internat. Assoc. Sci. Hydrology Pub. 63, p. 432–441.

Rorabaugh, M. I., and Simons, W. D., 1966, Exploration of methods of relating ground water to surface water, Columbia River basin—Second phase: U.S. Geol. Survey open-file rept., 62 p.

Schoeller, Henri, 1948, Le regime hydro-géologique des calcaires éocènes du synclinal du Dyr el Kef (Tunisie): Soc. Géol. France Bull., ser. 5, v. 18, p. 167–180.

——1962, Les eaux souterraines: Paris, Masson et Cie, 642 p.

——1967, Hydrodynamique dans le karst (écoulement et emmagasinement): Internat. Assoc. Sci. Hydrology Pub. 73, p. 3–20.

Snyder, F. F., 1939, A conception of runoff-phenomena: Am. Geophys. Union Trans., v. 20, p. 725–738.

☆ U.S. Government Printing Office: 1974—0-543-465/3

RECENT PUBLICATIONS OF THE U.S. GEOLOGICAL SURVEY

(Books may be ordered from the Superintendent of Documents, Government Printing Office, Washington, DC 20402, to whom remittances should be sent by check or money order. Give series number, title, stock number shown in parentheses in this list, and catalog number shown in brackets)

Professional Papers

433-L. Distribution of radionuclides in bottom sediments of the Columbia River estuary, by D. W. Hubbell and J. L. Glenn. 1973. p. L1-L63; plates in pocket. $2. (2401-00247) [I 19:16:433-L]

793. Geology of the South Pass area, Fremont County, Wyo., by R. W. Bayley, P. D. Proctor, and K. C. Condie. 1973. 39 p.; plate in pocket. $1.10. (2401-02398) [I 19:16:793]

803. X-ray mineralogy of the Parachute Creek Member, Green River Formation, in the northern Piceance Creek basin, Colorado, by D. A. Brobst and J. D. Tucker. 1973. 53 p. $1. (2401-00336) [I 19:16:803]

Bulletins

1374. Placer deposits of Alaska, by E. H. Cobb. 1973. 213 p.; plate in pocket. $3.10. (2401-02369) [I 19:3:1374]

1391-A. Mineral resources of an area near the Popo Agie Primitive Area, Fremont County, Wyo., by R. C. Pearson, L. L. Patten, and D. L. Gaskill. 1973. 18 p.; plate in pocket. $1.30. (2401-02403) [I 19:3:1391-A]

Water-Supply Papers

2026. Characteristics of water quality and streamflow, Passaic River basin above Little Falls, N. J., by P. W. Anderson and S. D. Faust. 1973. 80 p. 70¢. (2401-02371) [I 19:13:2026]

2090. Ground-water levels in the United States, 1967-71—North-central States. 1973. 114 p. 80¢. (2401-00324) [I 19:13:2090]

2092. Quality of surface waters of the United States, 1968—Part 2, South Atlantic slope and Eastern Gulf of Mexico basins. 1973. 373 p. $2.35. (2401-02385) [I 19:13:2092]

2093. Quality of surface waters of the United States, 1968—Part 3, Ohio River basin. 1973. 309 p. $2.10. (2401-02384) [I 19:13:2093]

2094. Quality of surface waters of the United States, 1968—Parts 4 and 5, St. Lawrence River basin, and Hudson Bay and Upper Mississippi River basins. 1973. 293 p. $2.10. (2401-02380) [I 19:13:2094]

2095. Quality of surface waters of the United States, 1968—Part 6, Missouri River basin. 1973. 394 p. $2.35. (2401-02383) [I 19:13:2095]

2110. Surface water supply of the United States, 1966-70—Part 3, Ohio River basin—Volume 4, Ohio River basin below Wabash River. 1973. 806 p. $3.70. (2401-02386) [I 19:13:2110]

2115. Surface water supply of the United States, 1966-70—Part 5, Hudson Bay and Upper Mississippi River basins—Volume 3, Upper Mississippi River basin below Keokuk, Iowa. 1973. 607 p. $3.20. (2401-02376) [I 19:13:2115]

2117. Surface water supply of the United States, 1966-70—Part 6, Missouri River basin—Volume 2, Missouri River basin from Williston, North Dakota, to Sioux City, Iowa. 1973. 612 p. $3.20. (2401-02382) [I 19:13:2117]

2118. Surface water supply of the United States, 1966-70—Part 6. Missouri River basin—Volume 3, Missouri River basin from Sioux City, Iowa, to Nebraska City, Nebr. 1973. 710 p. $3.45. (2401-02377) [I 19:13:2118]

2124. Surface water supply of the United States, 1966-70—Part 9, Colorado River basin—Volume 1, Colorado River basin above Green River. 1973. 543 p. $2.95. (2401-02375) [I 19:13:2124]

2125. Surface water supply of the United States 1966-70—Part 9, Colorado River basin—Volume 2, Colorado River basin from Green River to Compact Point. 1973. 634 p. $3.20. (2401-02381) [I 19:13:2125]

Miscellaneous Investigations Series

I-850. Resource and land information for South Dade County, Florida. 1973. 66 p. $2.45. (2401-02693) [I 1.2:D12]